SEISMIC ASSESSMENT OF UNREINFORCED MASONRY BUILDINGS IN CANADA

by

Gilbert Bélec

Thesis submitted to the
Faculty of Graduate and Postdoctoral Studies
In the partial fulfillment of the requirements for the degree of

Master of Applied Science

In Civil Engineering

Under the auspices of the Ottawa-Carleton Institute for Civil Engineering

uOttawa

University of Ottawa
January 2016

Abstract

Unreinforced masonry (URM) structures have shown to be susceptible to significant damage during strong earthquakes. Vulnerability assessment of URM buildings is needed so that appropriate mitigation strategies can be implemented. The existing Canadian practice consists of rapid seismic screening of buildings to assign priorities for further and more refined assessments, followed by refined analysis of individual critical buildings. The current seismic screening procedure, from 1992, is based on qualitative observations of seismic vulnerability, enabling the assignment of seismic priority indices, quantified on the basis of expert opinion and experience. More refined tools are needed for seismic vulnerability assessment of URM buildings in Canada, based on the current Canadian seismic hazard values. The objective of the research project is to fulfill these needs by developing fragility curves that provide a probabilistic assessment of different levels of building performance under different intensities of eastern and western seismicity.

Using an inventory of over 50,000 structures, a seismic assessment of typical low-rise and mid-rise URM structures located in eastern and western Canada was carried out. The required analyses were done using applied element method software which effectively modeled the in-plane and out-of-plane behaviour of masonry walls. Using incremental dynamic analysis, fragility curves were developed to reflect the capacity of URM structures with a wide variety of selected structural and ground motion parameters. The results were verified against available fragility information in the literature. They show the significance of selected parameters, while providing effective tools for seismic vulnerability assessment of URM buildings in eastern and western Canada.

Résumé

Les bâtiments en maçonnerie non-renforcée (URM) ont démontré au cours des années qu'ils sont susceptibles de subir des dommages importants. L'estimation des dégâts peut se faire avec une évaluation de la vulnérabilité sismique et pourrait contribuer à des stratégies d'atténuation lors de séismes futurs. La pratique courante au Canada se limite à des évaluations rapides par des experts ainsi qu'à quelques évaluations de structures individuelles. Des outils plus adaptés sont nécessaires afin d'évaluer les risques aux bâtiments URM, considérant les nouveaux standards Canadiens. L'objectif de cet ouvrage est de développer des courbes de fragilité qui permettront de relier les risques aux structures en fonction de leurs caractéristiques.

À l'aide d'une banque de donnée de plus de 50,000 structures, une évaluation sismique pour des bâtiments URM typiques de deux et trois étages a été menée à bout. Les analyses nécessaires à cet ouvrage ont été performées à l'aide d'un logiciel utilisant la méthode des éléments appliqués, permettant ainsi de modéliser adéquatement les comportements de la maçonnerie parallèle et perpendiculaire aux murs de maçonnerie. À l'aide d'une analyse dynamique incrémentale, des courbes de fragilité ont été développées afin de représenter la capacité de structures URM avec une variété de paramètres. Les résultats ont été comparés à des ouvrages similaires dans la littérature. Ils démontrent l'importance des paramètres sélectionnés tout en apportant un outil efficace pour l'évaluation sismique des risques pour les bâtiments URM pour l'est et l'ouest du Canada.

Acknowledgments

I would like to take this small space to thank my supervisor, Dr. Murat Saatcioglu. Without his guidance, vast knowledge and invaluable input, this work would not be. Furthermore, his financial support gave me the opportunity to dedicate as much time as I could to my research.

Similar thanks are made to the University of Ottawa and the Ontario Ministry of Training for their financial support. The faculty, staff and colleagues at the department of Civil Engineering were very supportive through my years of study.

Many thanks also go to Dr. Michael Sawada, Mr. Jocelyn Paquette and Dr. Najif Ismail who did not hesitate to share results from their works.

Special thanks to my sources of motivation through the many long nights of reading, analysis and writing: Berlioz, Brahms, Shostakovich and Wagner to name a few.

Mais surtout, merci à MP.

Table of contents

Abstract .... **ii**

Résumé .... **iii**

Acknowledgments .... **iv**

List of tables .... **ix**

List of figures .... **xii**

List of abbreviations .... **xx**

1 Introduction **1**

1.1 Research Needs 1

1.2 Scope and objective 3

2 Literature review **5**

2.1 Introduction 5

2.2 Masonry structures 6

2.2.1. URM building stock and selection 6

2.2.2. URM structural configurations 11

2.3 Properties of masonry and modeling 15

2.3.1. Mechanical properties of masonry 15

2.3.2. Modelling of masonry 17

2.4 Seismic demand 20

2.5 Damage assessment and its representation 23

2.5.1. Failure mechanisms of masonry 23

2.5.2. Damage estimation 23

2.5.3. Damage assessment of structures 24

2.6 Existing research 27

2.6.1. Seismic assessment in Canada 27

2.6.2. Seismic assessment in the world 33

3 Selection of structural and ground motion parameters 35

3.1 Building inventory 35

3.2 Typical URM buildings 38

3.2.1. Visual inspection 38

3.2.2. URM characteristics 39

3.2.3. Model information 42

3.3 Ground motions 44

3.4 Data collection 48

3.4.1. Damage measure 48

3.4.2. Generation and display of results 50

4 Results and fragility curves 52

4.1 Application of incremental dynamic analysis 52

4.1.1. Hunt and fill algorithm 52

4.1.2. Identification of immediate occupancy 57

4.1.3. Identification of collapse prevention 57

4.1.4. Identification of life safety 58

4.1.5. Local failures as indicators 59

4.2 Summary of incremental dynamic analysis 63

4.2.1. Mid-rise URM – Eastern Canada 64

4.2.2. Mid-rise URM – Western Canada 72

4.2.3. Low-rise URM – Eastern Canada 80

4.2.4. Low-rise URM – Western Canada 84

4.3 Development of fragility curves 88

4.3.1. Mid-Rise URM – Eastern Canada 89

4.3.2. Mid-rise URM – Western Canada 93

4.3.3. Low-rise URM – Eastern Canada 97

4.3.4. Low-rise URM – Western Canada 99

5 Discussion of results 101

5.1.1. Normality check of limit states 101

5.1.2. Verification of the damage measure 106

5.2 Observed damage and behaviour 108

5.2.1. In-plane mechanisms 109

5.2.2. Out-of-plane damage 111

5.3 Comparison with existing works 113

5.3.1. Karbassi (2010) 113

5.3.2. Park et al. (2009) 115

5.3.3. Frankie (2010) ... 117

5.3.4. Hazus-MH ... 119

5.4 Effect of parameters on building fragility ... 120

5.4.1. Year of construction ... 120

5.4.2. Openings size ... 122

5.4.3. Number of storeys ... 123

5.4.4. Geology ... 125

5.4.5. Earthquake duration ... 126

5.4.6. Intensity measure ... 128

6 Summary and Conclusions ... 130

6.1 Summary ... 130

6.2 Conclusions ... 131

6.3 Recommendations for future research ... 133

References ... 134

A Model validation ... 144

B Accelerograms ... 154

C Effect of openings on stiffness ... 177

List of tables

Table 2-1: URM classification in New Zealand 8

Table 2-2: Hazus-MH building occupancy classes 10

Table 2-3: Mechanical properties and correlations of masonry 15

Table 2-4: Mechanical properties and correlations of mortar 16

Table 3-1: Average and median values of characteristics in the structure sample 39

Table 3-2: Material properties used 41

Table 3-4: Comparison of structural periods for analytical models 43

Table 3-5: Acceptance criteria for limit states 48

Table 4-1: Mid-rise, pre-code, large openings limit states (E) 65

Table 4-2: Mid-rise, pre-code, small openings limit states (E) 67

Table 4-3: Mid-rise, low-code, large openings limit states (E) 69

Table 4-4: Mid-rise, low-code, small openings limit states (E) 71

Table 4-5: Mid-rise, pre-code, large openings limit states (W) 73

Table 4-6: Mid-rise, pre-code, small openings limit states (W) 75

Table 4-7: Mid-rise, low-code, large openings limit states (W) 77

Table 4-8: Mid-rise, low-code, small openings limit states (W) 79

Table 4-9: Low-rise, pre-code, large openings limit states (E) 81

Table 4-10: Low-rise, pre-code, small openings limit states (E) 83

Table 4-11: Low-rise, pre-code, large openings limit states (W) 85

Table 4-12: Low-rise, pre-code, small openings limit states (W) 87

Table 4-13: Mid-rise, pre-code, large openings fragility parameters (E) 89

Table 4-14: Mid-rise, pre-code, small openings fragility parameters (E) 90

Table 4-15: Mid-rise, low-code, large openings fragility parameters (E) 91

Table 4-16: Mid-rise, low-code, small openings fragility parameters (E) 92

Table 4-17: Mid-rise, pre-code, large openings fragility parameters (W) 93

Table 4-18: Mid-rise, pre-code, small openings fragility parameters (W) 94

Table 4-19: Mid-rise, low-code, large openings fragility parameters (W) 95

Table 4-20: Mid-rise, low-code, small openings fragility parameters (W) 96

Table 4-21: Low-rise, pre-code, large openings fragility parameters (E) 97

Table 4-22: Low-rise, pre-code, small openings fragility parameters (E) 98

Table 4-23: Low-rise, low-code, large openings fragility parameters (W) 99

Table 4-24: Low-rise, pre-code, small openings fragility parameters (W) 100

Table 5-1: Example of expected Z-score of fragility parameters at CP level 103

Table 5-2: Coefficients of determination for limit state levels 105

Table 5-3: Proportional standard error of the mean for damage measure 107

Table 5-4: Deviation to median ratio of fragility parameters 129

Table B-1: URMM accelerogram data (E) 154

Table B-2: URMM accelerogram data (W) 165

Table B-3: URML accelerogram data 176

Table C-1: Piers data for worked example 187

Table C-2: Combined wall sections for worked example..187

List of figures

Figure 1-1: Damage to URM after the 2015 Gorkha earthquake.. 1

Figure 1-2: Damage to URM after the 2011 Christchurch earthquake................................ 2

Figure 1-3: Damage sustained to URM in Canada 3

Figure 2-1: Seismic assessment procedure 6

Figure 2-2: Industrial URM construction 7

Figure 2-3: (a) Building group with corner structures shaded, (b) individual regular, (c) individual irregular 8

Figure 2-4: Structural damageability as a function of storeys 12

Figure 2-5: Fragility curves based on number of storeys 12

Figure 2-6: Variations in openings 13

Figure 2-7: Damage to bricks near openings 13

Figure 2-8: Effects of unit and mortar properties on masonry prisms 17

Figure 2-9: Three-dimensional masonry model 17

Figure 2-10: Modeling philosophies for masonry 18

Figure 2-11: Equivalent masonry frame using TREMURI 18

Figure 2-12: Discretization of masonry assembly in AEM 19

Figure 2-13: Springs at element interfaces in AEM. 20

Figure 2-14: Effects of accelerogram rotation 22

Figure 2-15: In-plane failures of URM (a) rocking (b) diagonal tension (c) sliding (d) stair-stepped 23

Figure 2-16: Fragility curve concept 25

Figure 2-17: Multi-record IDA 26

Figure 2-18: Structural response to scaled and unscaled records 27

Figure 2-19: Industrial URM structure used for seismic assessment of Karbassi (2010) ... 28

Figure 2-20: Increase in seismic demand interactivity 30

Figure 2-21: Evaluation of damage to Christchurch URM structures 30

Figure 2-22: Damage probability matrix 31

Figure 2-23: Seismic design levels based on year of construction 32

Figure 2-24: Capacity diagram of URM inventory 33

Figure 2-25: Spring model of URM low-rise 34

Figure 3-1: Structures part of GIS database by Sawada et al. (2014) 36

Figure 3-2: Information available in building inventory 37

Figure 3-3: Masonry in good condition (left) and poor condition (right) 39

Table 3-3: First-mode of vibration periods of typical structures considered in seconds 41

Figure 3-4: Alfred P. Murrah building simulation (left) and actual (right) state after blast 44

Figure 3-5: Prevalence of URM structures in Vancouver 45

Figure 3-6: Relative seismic risk in urban areas of Canada 45

Figure 3-7: Spectra of scaled ground motions for Ottawa 47

Figure 3-8: Spectra of scaled ground motions for Vancouver 47

Figure 3-9: Parameters required for interstorey drift calculation 49

Figure 3-10: Parameters required for local pier failure calculation 50

Figure 3-11: Various in-planed failure mechanisms of masonry 50

Figure 4-1: Base accelerogram for IDA 54

Figure 4-3: Mid-rise second storey response to E6c1_1 55

Figure 4-4: Structural resurrection IDA 55

Figure 4-5: Base IDA curve, E6c1_1 56

Figure 4-6: IDA curve for E6c2_1 59

Figure 4-7: Rocking of individual pier at CP level 60

Figure 4-8: Relative drift of individual pier at CP level 61

Figure 4-9: Rocking of individual pier at LS level 61

Figure 4-10: Relative drift of individual pier at LS level 62

Figure 4-11: Mid-rise, pre-code, large openings IDA curve (E) 64

Figure 4-12: Mid-rise, pre-code, small openings IDA curve (E) 66

Figure 4-13: Mid-rise, low-code, large openings IDA curve (E) 68

Figure 4-14: Mid-rise, low-code, small openings IDA curve (E) 70

Figure 4-15: Mid-rise, pre-code, large openings IDA curve (W) 72

Figure 4-16: Mid-rise, pre-code, small openings IDA curve (W) 74

Figure 4-17: Mid-rise, low-code, large openings IDA curve (W) 76

Figure 4-18: Mid-rise, low-code, small openings IDA curve (W) 78

Figure 4-19: Low-rise, pre-code, large openings IDA curve (E) 80

Figure 4-20: Low-rise, pre-code, small openings IDA curve (E) 82

Figure 4-21: Low-rise, pre-code, large openings IDA curve (W) 84

Figure 4-22: Low-rise, pre-code, small openings IDA curve (W) 86

Figure 4-23: Mid-rise, pre-code, large openings fragility curves (E) 89

Figure 4-24: Mid-rise, pre-code, small openings fragility curves (E).................................. 90

Figure 4-25: Mid-rise, low-code, large openings fragility curves (E) 91

Figure 4-26: Mid-rise, low-code, small openings fragility curves (E) 92

Figure 4-27: Mid-rise, pre-code, large openings fragility curves (W) 93

Figure 4-28: Mid-rise, pre-code, small openings fragility curves (W) 94

Figure 4-29: Mid-rise, low-code, large openings fragility curves (W)................................. 95

Figure 4-30: Mid-rise, low-code, small openings fragility curves (W) 96

Figure 4-31: Low-rise, pre-code, large openings fragility curves (E) 97

Figure 4-32: Low-rise, pre-code, small openings fragility curves (E) 98

Figure 4-33: Low-rise, pre-code, large openings fragility curves (W)................................. 99

Figure 4-34: Low-rise, pre-code, small openings fragility curves (W) 100

Figure 5-1: Standard normal distribution with evenly distributed population 102

Figure 5-2: Expected value of a standard normal distribution 102

Figure 5-3: Example of expected Z-score of fragility parameters at CP level...................104

Figure 5-4: Expected Z-score of mid-rise, pre-code, small openings at CP level (W).......106

Figure 5-5: Typical failures due to shear (red), bending (blue) and out-of-plane failures (green) 108

Figure 5-6: Typical crack patterns observed (red) at the end of ground shaking.............109

Figure 5-7: Pier rocking and toe crushing (red) observed during ground shaking............110

Figure 5-8: Residual sliding observed at the end of ground shaking................................110

Figure 5-9: Out-of-plane damage of low-code URML 112

Figure 5-10: Revised slenderness ratios for stiff or flexible diaphragms...........................112

Figure 5-11: Fragility comparison with Karbassi (2010), “long direction” 114

Figure 5-12: Fragility comparison with Karbassi (2010), “short direction”......................115

Figure 5-13: Fragility comparison with Park et al. (2009), “case 3” 116

Figure 5-14: Ground motion intensities from Park et al. (2009) 117

Figure 5-15: Fragility comparison with Frankie (2010), “3-storey uplands” 118

Figure 5-16: Fragility comparison with Hazus-MH (NIBS, 2003a), “URMM pre-code”...119

Figure 5-17: Year of construction effect on fragility 121

Figure 5-18: Openings effect on fragility...123

Figure 5-19: Effect of number of storeys on fragility 124

Figure 5-20: Crust rebound due to glaciers...125

Figure 5-21: Effect of geology on fragility...126

Figure 5-22: Effect of accelerogram length on fragility 128

Figure A-1: Test structure 145

Figure A-2: Analytical model in ELS, east wall focus 145

Figure A-3: Comparison of hysteretic loop and displacement-based force relationship....147

Figure A-4: Comparison of hysteretic loop envelope and displacement-based force relationship...147

Figure A-5: Experimentally observed cracks on east wall 149

Figure A-6: Location of cracks formed on east wall of ELS model, positive loading........149

Figure A-7: Wall model showing tendon location 151

Figure A-8: Force-displacement comparison of experimental (black) and analytical (red) cyclic out-of-plane loading..152

Figure B-1: E6c1_1 accelerogram 155

Figure B-2: E6c1_2 accelerogram 155

Figure B-3: E6c1_3 accelerogram 156

Figure B-4: E6c1_4 accelerogram 156

Figure B-5: E6c1_5 accelerogram 157

Figure B-6: E6c2_1 accelerogram 157

Figure B-7: E6c2_2 accelerogram 158

Figure B-8: E6c2_3 accelerogram 158

Figure B-9: E6c2_4 accelerogram 159

Figure B-10: E6c2_5 accelerogram 159

Figure B-11: E7c1_1 accelerogram 160

Figure B-12: E7c1_2 accelerogram 160

Figure B-13: E7c1_3 accelerogram 161

Figure B-14: E7c1_4 accelerogram 161

Figure B-15: E7c1_5 accelerogram 162

Figure B-16: E7c2_1 accelerogram 162

Figure B-17: E7c2_2 accelerogram 163

Figure B-18: E7c2_3 accelerogram 163

Figure B-19: E7c2_4 accelerogram 164

Figure B-20: E7c2_5 accelerogram 164

Figure B-21: W6c1_1 accelerogram 166

Figure B-22: W6c1_2 accelerogram 166

Figure B-23: W6c1_3 accelerogram 167

Figure B-24: W6c1_4 accelerogram 167

Figure B-25: W6c1_5 accelerogram 168

Figure B-26: W6c2_1 accelerogram 168

Figure B-27: W6c2_2 accelerogram 169

Figure B-28: W6c2_3 accelerogram 169

Figure B-29: W6c2_4 accelerogram 170

Figure B-30: W6c2_5 accelerogram 170

Figure B-31: W7c1_1 accelerogram 171

Figure B-32: W7c1_2 accelerogram 171

Figure B-33: W7c1_3 accelerogram 172

Figure B-34: W7c1_4 accelerogram 172

Figure B-35: W7c1_5 accelerogram 173

Figure B-36: W7c2_1 accelerogram 173

Figure B-37: W7c2_2 accelerogram 174

Figure B-38: W7c2_3 accelerogram 174

Figure B-39: W7c2_4 accelerogram 175

Figure B-40: W7c2_5 accelerogram 175

Figure C-1: Cantilever wall dimensions 178

Figure C-2: Springs in parallel 179

Figure C-3: Springs in series 179

Figure C-4: Effects of opening location on identical walls, side opening (left) and central opening (right) 180

Figure C-5: Effective stiffness as a function of single opening placement 182

Figure C-6: Springs representation of URM building 182

Figure C-7: Wall with openings for evaluation of effective stiffness 184

Figure C-8: Solid wall representation 184

Figure C-9: Opening strip o1 185

Figure C-10: Partial wall p1 and pier 1 185

Figure C-11: Remaining pier contributions to be considered 186

List of abbreviations

AEM	Applied element method
ASCE	American Society of Civil Engineers
ASI	Applied Sciences International
CDF	Cumulative density function
cm	Centimeter
CP	Collapse prevention
FEMA	Federal Emergency Management Agency
g	Gravity unit; 9.81 m/s^2
GIS	Geographic information system
IDA	Incremental dynamic analysis
IO	Immediate occupancy
LS	Life safety
m	Meter
MPa	Megapascal
NBCC	National Building Code of Canada
NIBS	National Institute of Building Sciences
NRCC	National Research Council Canada
PGA	Peak ground acceleration
s	Second
SA	Spectral acceleration
URM	Unreinforced masonry
d	Damage level
D	Performance level threshold

E_m	Modulus of elasticity of masonry assembly
E_{mo}	Modulus of elasticity of mortar
E_{mu}	Modulus of elasticity of brick units
F	Fragility curve function
f'_m	Compressive strength of masonry assembly
f'_{mo}	Compressive strength of mortar
f'_{tmo}	Tensile strength of mortar
f'_{tn}	Tensile strength of masonry assembly
f'_u	Compressive strength of brick units
G_m	Shear modulus of masonry assembly
G_{mo}	Shear modulus of mortar
G_u	Shear modulus of brick units
	Height of wall
$_{eff}$	Effective height of pier
P	Probability of exceeding a given performance level
t	Thickness of wall
X	Intensity measure
x	Ground acceleration
Δ	Displacement of diaphragm
Δ_{bot}	Displacement at the bottom of pier
Δ_{top}	Displacement at the top of pier
θ	Interstorey drift
θ_L	Local pier drift
μ	Median
σ	Standard deviation

ϕ	Normal distribution
$=$	Parallel direction
$\top$	Perpendicular direction
(E)	Eastern Canada
(W)	Western Canada

Chapter 1

Introduction

1.1 Research Needs

Poor seismic performance of unreinforced masonry (URM) structures heightened awareness once again in 2015. The disaster that struck Nepal attracted media attention to the region of Kathmandu where a high concentration of URM highlighted the material's poor ability to withstand the effects of strong ground motions. Partial or complete collapse occurred in a large number of URM structures as shown in Figure 1-1, resulting in over 9000 human casualties and a significant economic impact equivalent to 25% of the Nepalese GDP (The Economist, 2015). Bloomberg (2015) noted that the construction standards and the building code used in Nepal, as well as their implementation and enforcement were not up to par.

Figure 1-1: Damage to URM after the 2015 Gorkha earthquake, from A. Abdullah (2015)

While the structures in Nepal may have been susceptible to this kind of disaster due to poor standards of construction, this is not the case in New-Zealand which has one of the world's most advanced seismic codes. However, the 2011 Christchurch Earthquake in New Zealand resulted in considerable damage in masonry buildings, as seen in Figure 1-2.

Figure 1-2: Damage to URM after the 2011 Christchurch earthquake, from Wikimedia Foundation by Schwede66 (2011)

The above two recent examples demonstrate that similar damage can occur in seismically active regions of Canada. In addition to the brittle nature of URM construction and lack of proper seismic design practices in pre-1970s buildings in Canada, Drysdale (2002) indicated that the first proper mention of "engineered masonry" occurred in 1965. Bruneau and Lamontagne (1994) confirmed several instances of highly damaged URM structures in eastern Canada during the 20th century. Furthermore, some of the existing URM structures are simply in poor condition, and bricks may fall out even without seismic activity, as shown in Figure 1-3. While seismic assessments of Canadian URM structures already exist (Abo-El-Ezz et al., 2013; Elsabbagh, 2013; Karbassi, 2010; Onur, 2001), Karantoni et al. (2012) found that these assessments are often limited to areas of similar material characteristics and structures. The authors further explained that empirical work based on either judgment or data collected after earthquakes may not be suitable. Some of the existing studies in Canada do indeed focus on specific characteristics (e.g. stone masonry, industrial structures) or are based on rapid assessments which require user input and thus subjectivity. An improved seismic assessment can be done if fragility relationships are established for buildings, providing probability of exceedance of selected performance limits. Mebarki et al. (2013) indicated that the accuracy of seismic assessment using this approach depends directly on the quality of the fragility curves. Currently, comprehensive fragility curves for URM buildings in eastern and western Canada do not exist. Therefore there is need for conducting rigorous seismic assessment of URM structures for buildings that are most typical of the building stock in Canada, by developing seismic fragility curves.

Figure 1-3: Damage sustained to URM in Canada due to progressive spalling, from G. Bélec (2015)

1.2 Scope and objective

The main objective of this thesis is to perform seismic assessment of unreinforced masonry structures in Canada by analytical means and to develop fragility curves for URM buildings in eastern and western Canada. In order to achieve this objective, a thorough process is undertaken in order to review the URM structures that are most typical to

Canada by consulting existing structures. This information will be crucial to save on computational time and will allow the consideration of a larger extent of characteristics.

In order to provide for results that are easily accessible for future mitigation purposes, the results will be processed through statistical means. Bélec et al. (2015) present this eloquently by the following: “once a structure is known to be deficient and susceptible to damage, its rehabilitation is easier to justify for all parties involved”.

As this Chapter comes to a close, it is worth introducing the remaining contents of the thesis:

- Chapter 2 presents a literature review of existing research on seismic assessment as well as the means used to perform them.
- Chapter 3 describes the methodology used for the analysis phase of the research.
- Chapter 4 details the methodology to some extent before presenting the results of the analysis phase.
- Chapter 5 is meant to verify the results through statistical means as well as by comparison with similar works. It will further present observations made during the analysis phase as well as observations made through the results of the seismic assessment.
- Chapter 6 summarizes the conclusions found during this research and provides some recommendations for future work on seismic assessment of URM structures.
- Appendixes are included as supplementary information and for validation of the theoretical models used for the analysis phase.

Chapter 2

Literature review

2.1 Introduction

Seismic risk assessment is the intersection of seismic hazard, building vulnerability and risk to assets that are subjected to ground motions (Bostrom et al., 2008). In the present research, consequence of damage in terms of human casualties and/or economic losses is not included, hence the focus is placed on building damage likely to be sustained during an earthquake – see Figure 2-1. Once the vulnerability and hazard are determined, it becomes useful to combine them together to obtain a statistically representative function that links ground motion to likely building damage.

The current chapter provides a brief summary of the aforementioned topics as currently exist in scientific literature, focusing specifically on URM. Building vulnerability is covered in Sections 2.2 and 2.3; seismic hazard is covered in Section 2.4; estimation of building damage in Section 2.5. Finally, Section 2.6 provides a brief overview of research related to seismic assessment of unreinforced masonry buildings.

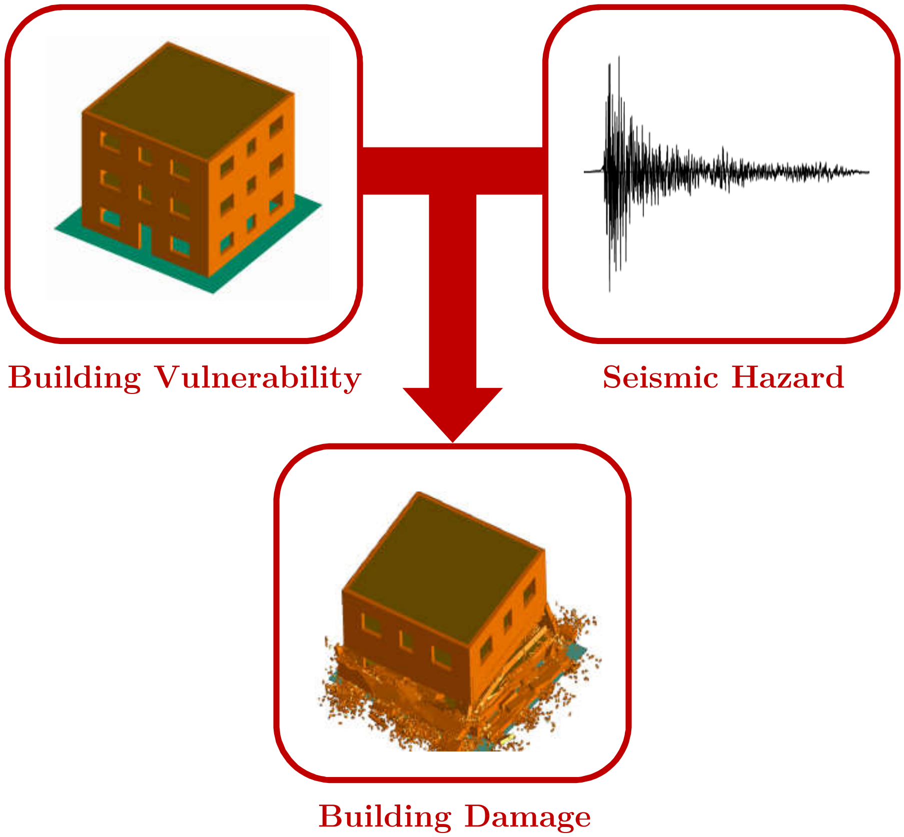

Figure 2-1: Seismic Assessment Procedure

2.2 Masonry structures

2.2.1. URM building stock and selection

Unreinforced masonry structures come in many configurations and sizes. The majority of masonry buildings in Canada were built mainly in the first half of the twentieth century (Brzev, 2010), and more precisely, before the 1940s (NRCC, 1993). Ventura et al. (2005) states that it remained as a common construction type in Canada up until 1973, when the National Building Code of Canada (NBCC) instituted a change that prevented the construction of masonry without reinforcement. The modern seismic design provisions of the NBCC had not been in effect during this period. Therefore, there was no difference among the design and construction practices of URM buildings based on seismic hazard as dictated by seismic regionalization. In other words, no parameter accounted for higher seismic activity in any given region. This makes it difficult to make seismic assessment of URM buildings on a regional scale. Hence, it is common to classify and group URM structures on the basis of their structural and architectural configurations to reduce the amount of evaluations to a reasonable number. This is also advantageous because of the past observations of URM building behaviour during previous earthquakes, which indicate that the building configuration plays an important role in the seismic performance of URM structures (Elsabbagh, 2013).

The Canadian Manual for Screening of Buildings for Seismic Investigation (NRCC, 1993) recognizes the variety of URM structures built in Canada, noting that the building height ranges between one to six storeys. It further notes that construction practices vary based on their use; for instance, residential URM structures tend to have light wood floors and interior loadbearing partitions while industrial URM may have reinforced concrete floors and interior columns as seen in Figure 2-2. However, the Manual fails to give clear configurations of the latter construction type. Therefore, the review of URM construction practices outside of Canada is necessary to properly categorize the URM construction.

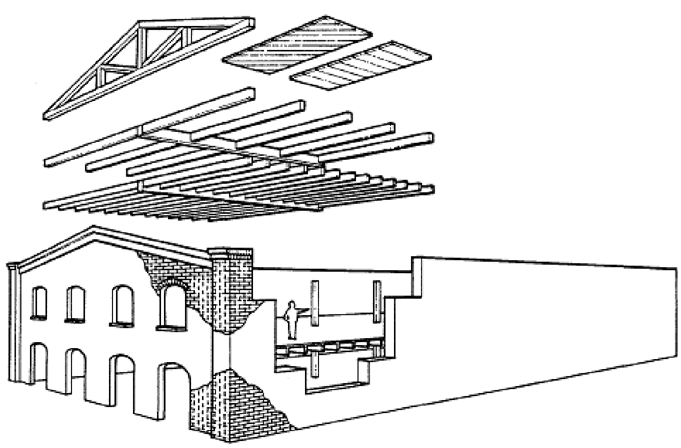

Figure 2-2: Industrial URM construction (NRCC, 1993)

Lang (2002) and Barrantes (2012) identified two main characteristics that categorize URM buildings: individual structure or building group; regular or irregular structure. The latter makes a further distinction for the group URM with regards to their location on an edge/corner or in between other buildings. This is to account for observation from previous earthquakes where it was seen that the proximity of structures could lead to pounding damage under ground excitations. The irregularity, or lack thereof, of structures may refer to the plan configuration (for instance reintrant corners), orthogonality of load-bearing walls and openings arrangement. Some of these various categories are illustrated in plan view in Figure 2-3, although all combinations are naturally possible.

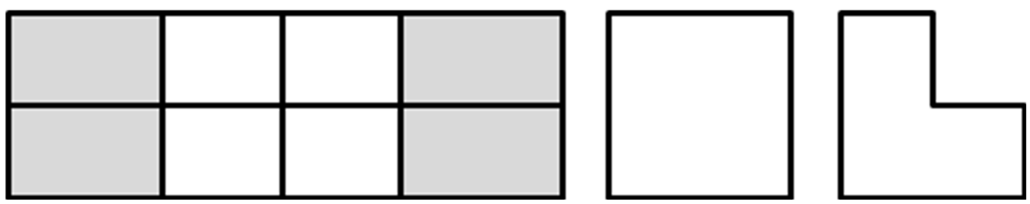

(a) (b) (c)

Figure 2-3: (a) Building group with corner structures shaded, (b) individual regular, (c) individual irregular

A similar classification is used by Russel and Ingham (2010b). Classifications were identified based on the number of storeys (one, two, three and more), row or isolated and another category for URM not meeting these criteria. Thus, a URM can be placed in one of seven classes as shown below in Table 2-1.

Table 2-1: URM classification in New Zealand (Russel and Ingham, 2010b)

One storey		Two storey		Three storeys and more		Others
Isolated	Row	Isolated	Row	Isolated	Row	

In the United States, the Hazus-MH (NIBS, 1997) tool was developed in order to assess the effects of natural hazards, including earthquakes. Using Geographic Information Systems, the tool allows users to estimate losses in a given region based on the intensity of the hazard. In order to consider structures adequately, they are divided based on their construction material and arrangement, such as concrete shear walls. In the case of URM, it distinguishes between 2 categories of bearing walls: low-rise and mid-rise. Low-rise structures, abbreviated as URML, range from one to two storeys whereas mid-rise structures, abbreviated as URMM, represent the remainder of the structures, i.e., three storeys and more. Typical overall heights of URM are also suggested, although this is not necessarily useful given the varying number of storeys. The building stock is further divided into occupancy classes to group structures with similar use. The Hazus occupancy classes are summarized in Table 2-2. Ulmi et al. (2014) extended the Hazus-MH tool to Canada for the earthquake module, as part of a Geological Survey of Canada project. This work is further discussed in Section 2.6.

Another approach for seismic risk assessment is to take a sample inventory of structures in a given region and defining either a representative structure or a few typologies which best portray the overall building stock in the region. These types of representative structures have been used to assess either single structures or entire regions. D'Ayala and Speranza (2003) studied four municipalities in Italy and identified common typologies for each of them. Despite some differences among the municipalities, the study noted that the approach was useful for comparing vulnerability of structures constructed under the same building tradition; that is, with the same practice but with some differences in characteristics. Grubbs et al. (2007) focused on essential facilities in central and eastern United States. This led them to choose two firehouses of typical construction prior to 1950.

While this type of structure is quite unique in itself, the authors argued that the chosen structures shared several characteristics with other types of URM structures. They concluded that "the case studies provided insight into the seismic performance and rehabilitation needs for other similar URM buildings."

Table 2-2: Hazus-MH building occupancy classes

Occupancy	Label	Description
Residential	RES1	Single family dwelling
	RES2	Manufactured housing
	RES3	Multi family dwelling
	RES4	Temporary lodging
	RES5	Institutional dormitory
	RES6	Nursing home
Commercial	COM1	Retail trade
	COM2	Wholesale trade
	COM3	Personal and repair services
	COM4	Professional/technical/business services
	COM5	Banks
	COM6	Hospital
	COM7	Medical office/clinic
	COM8	Entertainment and recreation
	COM9	Theaters
	COM10	Parking
Industrial	IND1	Heavy factories
	IND2	Light factories
	IND3	Food/drugs/chemicals
	IND4	Metals/minerals processing
	IND5	High technology
	IND6	Construction
Agricultural	AGR1	Agriculture
Religious	REL1	Church
Governmental	GOV1	General services
	GOV2	Emergency response
Educational	EDU1	Schools/libraries
	EDU2	Colleges/universities

Tarque Ruiz (2008) used a building inventory from a survey conducted by the Peruvian Instituto Nacional de Estadística e Informática. Thirty buildings were chosen to be assessed and their parameters (dimensions, height, wall thickness, etc.) were defined in order to obtain their mean and standard deviation. This allowed a reduction in the amount of analysis to be performed in order to assess structures in the region of Cusco, Peru. Karantoni et al. (2012) used a single structure with varying parameters (number of storeys, openings, wall thickness, etc.) which led to 216 typologies representing URM buildings in Greece.

2.2.2. URM structural configurations

The number of storeys of URM structures has shown to be an important factor in their seismic response and is often included as an important parameter of seismic assessment (NIBS, 2003a; Frankie, 2010; Derakhshan, 2011; Barrantes, 2012; Elsabbagh, 2013; Penner, 2014). While it is difficult to generalize that all structures with the same number of storeys will behave in a similar manner, there is a clear tendency for damageability to increase as the number of storeys increases as seen in Figure 2-4. As mentioned in the previous subsection, low-rise structures are grouped in the Hazus-MH tool as one and two storey buildings, and three storeys and higher structures are classified as mid-rise. The general trend can be observed in Figure 2-4, however the fragility curves shown in Figure 2-5 indicate a difference in behaviour between one and two storey buildings. While there is a higher likelihood of damage for two-storey buildings than one-storey low-rise buildings, the increase in the likelihood damage is much smaller moving from a mid-rise to a low-rise. Considering two storey structures as representative of URML will therefore yield a conservative estimate of the low-rise category as a whole.

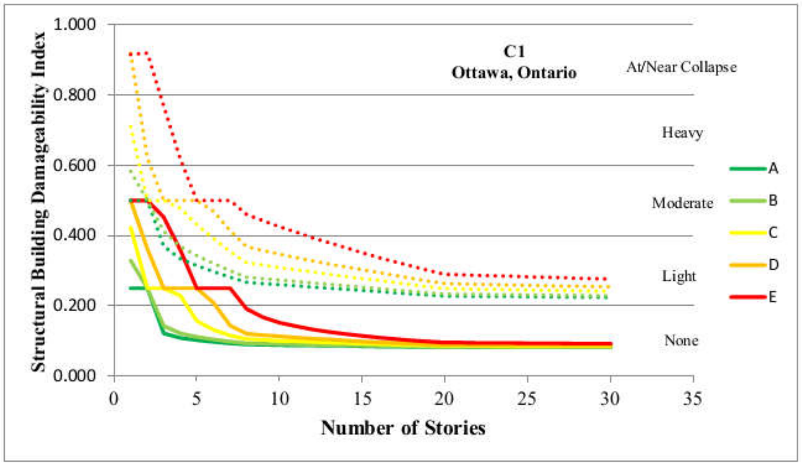

Figure 2-4: Structural damageability as a function of storeys, from Elsabbagh (2013)

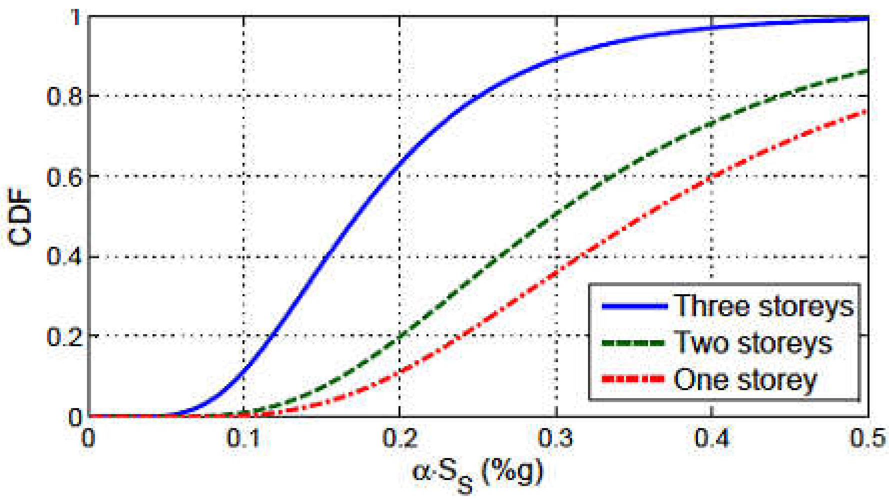

Figure 2-5: Fragility curves based on number of storeys, from Barrantes (2012)

The presence of openings and their placement may greatly affect the capacity of walls as will be illustrated later in Appendix C. Some of the defining criteria used by Frankie (2010) depend on the size of piers and spandrels which are defined on the basis of the location and size of openings in URM walls. The author notes that large piers (small openings) typically respond very well to seismic excitations even under varying material properties. Elsabbagh (2013) as well as Parisi and Augenti (2012) cite the number of openings in a wall and their location as a possible source of irregularity which lead to lower wall capacity. Karbassi (2010) found that having a greater number of openings could severely weaken the capacity of mid-rise URM but could provide more ductility. The presence of more or larger openings also facilitates the appearance of diagonal cracks in the wall, as could be observed in the 2002 Molise earthquake (Parisi and Augenti, 2013) or the 2011 Christchurch earthquake (Ingham and Griffith, 2011a), as shown in Figure 2-7.

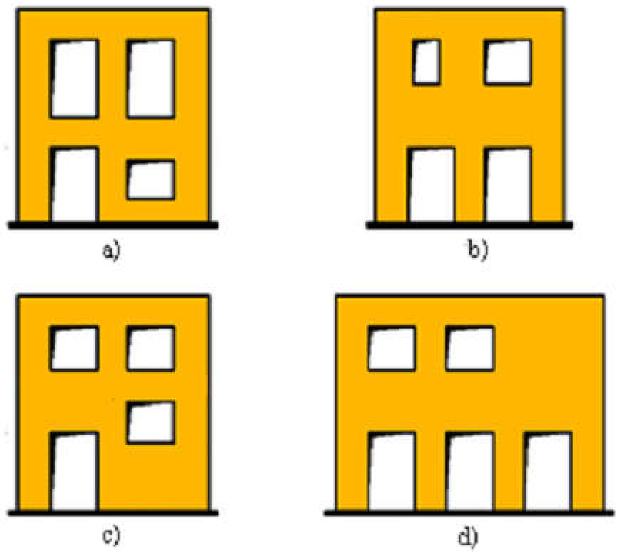

Figure 2-6: Variations in openings, adapted from Parisi and Augenti (2012)

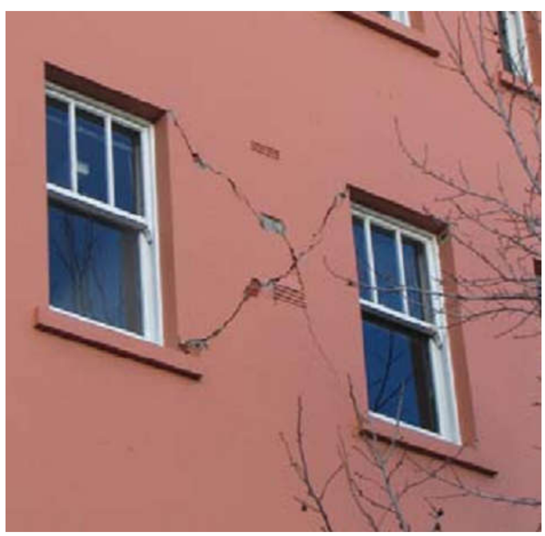

Figure 2-7: Damage to bricks near openings, from Ingham and Griffith (2011a)

In terms of wall dimensions, wall thickness is a parameter worth investigating. While it has a direct effect on in-plane wall stiffness, it is most often considered as a parameter for out-of-plane failure mechanisms where the slenderness of the walls leads to failures between half to two-thirds of the wall's height (Turek, 2002; Erberik, 2008; Derakshan, 2010; Penner, 2014). Although the ASCE 41 slenderness limit $/t \geq 9$ is often used to explore the in-plane failure mechanisms of unreinforced masonry, some researchers consider two or three-wythe thickness as a criterion (Turek, 2002; Paquette and Bruneau, 2003; Karbassi, 2010; Erberik and Ceran, 2012). It should be noted that these limits were developed with 50% probability of survival as a goal (Bruneau, 1994).

Structural irregularities can be responsible for a large portion of structural damage observed in previous earthquakes; these are defined by FEMA 454 and include re-entrant corners, torsional irregularity, non-parallel walls, soft walls, and vertical irregularities, amongst others. Bruneau and Lamontagne (1994) investigated damage to unreinforced masonry structures in Canada during the 20th century and found that while out-of-plane failure was the most common type of observed damage, the presence of weak storeys (due to large openings) and re-entrant corners could lead to severe in-plane cracks. The observed out-of-plane damage was generally more visible but the building's structural integrity would usually not be compromised. Lang (2002) mentioned that effective analysis of irregular structures requires a more in-depth approach. When irregular structures are concerned, selecting a representative structure may not give the best portrait of the situation. In such cases, it may prove advantageous to use a rapid assessment method such as that developed by Elsabbagh (2013) which may be used to quickly estimate the capacity of the structure before determining whether a complete analysis is required.

2.3 Properties of masonry and modeling

2.3.1. Mechanical properties of masonry

The mechanical properties of masonry have been shown to vary greatly from one building to another and from one country to another (Lefevbre, 2004; Dizhur et al., (2010); Lefevbre 2012; Lumantarna, 2012; Lumantarna et al., 2012a; Lumantarna et al., 2012b; Lumantarna, 2014). A brief review of literature provides the values and correlations shown in Table 2-3 for bricks and their assembly. As the table shows, there is a very wide range of values, which makes assessment of regional URM difficult without selecting combinations of several mechanical properties. Doing so would result in a greater compatibility for seismic assessments, but increases computational requirements.

Table 2-3: Mechanical properties and correlations of masonry

<table>
<tr><th></th><th>Source</th><th>Region</th><th>Period or condition</th><th>f'_u / f'_m (MPa)</th><th>f'_{tu}/ f'_{tn} (MPa)</th><th>E_u / E_m (MPa)</th><th>G_u / G_m (MPa)</th></tr>
<tr><td rowspan="7">Single Units</td><td>Drysdale and Hamid (2005)</td><td>Canada</td><td>Late 20th c.</td><td>20.7</td><td>$0.10f'_m$</td><td>$700f'_m$</td><td>–</td></tr>
<tr><td>Zardini (2006)</td><td>Canada</td><td>1947</td><td>37.9</td><td>–</td><td>–</td><td>–</td></tr>
<tr><td>Karbassi (2010)</td><td>Canada</td><td>1900~1950</td><td>10</td><td>1</td><td>14,000</td><td>–</td></tr>
<tr><td>Lefebvre (2004)</td><td>Canada</td><td>19th c.</td><td>0.46 ~ 0.82</td><td>0</td><td>220 ~ 3,600</td><td>–</td></tr>
<tr><td>Lefebvre (2012)</td><td>Canada</td><td>1934</td><td>35</td><td>2</td><td>14,000</td><td>–</td></tr>
<tr><td>Lumantarna (2012a, 2012b)</td><td>New-Zealand</td><td>1940~1950</td><td>17.7 ~ 28.9</td><td>$0.12f'_m$</td><td>$294f'_m$</td><td>–</td></tr>
<tr><td>Lumantarna et al. (2014)</td><td>New-Zealand</td><td>1930s
1940s
1946</td><td>27.3
17.1
21.1</td><td>–</td><td>–</td><td>–</td></tr>
<tr><td rowspan="3">Assembly</td><td>FEMA 356</td><td>USA</td><td>Poor
Fair
Good</td><td>2.7
5.4
8.1</td><td>0
0.09
0.18</td><td>$423f'_m$</td><td>$0.4E_m$</td></tr>
<tr><td>AS 3826-1998 (1998)</td><td>Australia</td><td>20th c.</td><td>3</td><td>0</td><td>$700f'_m$</td><td>$300f'_m$</td></tr>
<tr><td>OPCM 3431 (2005)</td><td>Italy</td><td>20th c.</td><td>1.8 ~ 2.8</td><td>–</td><td>1,800 ~ 2,400</td><td>300 ~ 400</td></tr>
</table>

A similar review as above was conducted with a focus on the mechanical properties of mortar, as shown in Table 2-4. The information regarding some of these characteristics is not typically measured as evidenced by the many incomplete cells in the table. This may be in part due to the manner in which masonry is modelled in the industry, with more focus on masonry as a continuum. This is discussed in detail in the next sub-section. It is however possible to have a good idea on the mechanical properties of masonry prisms by correlating the compressive strength of masonry units and the mortar, as shown in Figure 2-8, which is based on the many correlations available in Table 2-3.

Table 2-4: Mechanical properties and correlations of mortar

Source	Region	Period or condition	f'_{mo} (MPa)	f'_{tmo} (MPa)	E_{mo} (MPa)	G_{mo} (MPa)
Drysdale and Hamid (2005)	Canada	Late 20th c.	3.5	–	–	–
Karbassi (2010)	Canada	Early 20th c.	1	0.5	500	–
Lefebvre (2012)	Canada	1934	4	0.2	500	–
Lumantarna (2012a, 2012b)	New-Zealand	1940~1950	2.62 ~ 6.65	–	–	–
Lumantarna et al. (2014)	New-Zealand	1930s 1940s 1946	6.65 2.62 5.92	–	–	–
Bureau of Standards (1924)	USA	1925	1.4	–	–	–
Davison et al.	USA	20th c.	0.5 ~ 5.1	–	–	–
Grimm (2000)	USA	20th c.	–	–	$464f'_m$	$186f'_m$

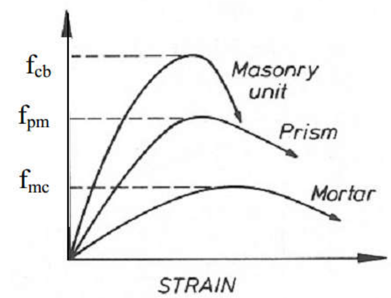

Figure 2-8: Effects of unit and mortar properties on masonry prisms, from Wijanto (2007)

2.3.2. Modelling of masonry

As computational power has increased over the years, the ability to develop more complex models has also increased, given that analysis time has become shorter. While the models once used were in the form of simplified truss models (e.g. Taghdi et al., 2000), nowadays models may account for element separation and fully three-dimensional behaviour (e.g. Bakeer, 2009), as seen in Figure 2-9, or rely on computational power to perform several thousands of numerical models using a Monte-Carlo algorithm (e.g. Barrantes, 2012).

Figure 2-9: Three-dimensional masonry model, from Bakeer (2009)

Bakeer (2009) and Pantazopoulou (2013) defined different contemporary design approaches that are commonly used for masonry. As seen in Figure 2-10, the masonry material may be discretized as a continuum element where the overall assembly properties are considered. The resulting homogeneous material will present capacities similar to those seen Figure 2-8, where the actual properties do not match those of the individual materials. This may be used, for instance, to develop simplified frame models such as in TREMURI (Lagomarsino et al., 2013), as presented in Figure 2-11, or more complex finite element models (e.g. Frankie, 2010; Pasticier et al., 2008). Bakeer (2009) further argued that the finite element method may also be used in this way or in a micro modelling fashion to include discrete functions such as element separation, provided that sufficient input is provided by users.

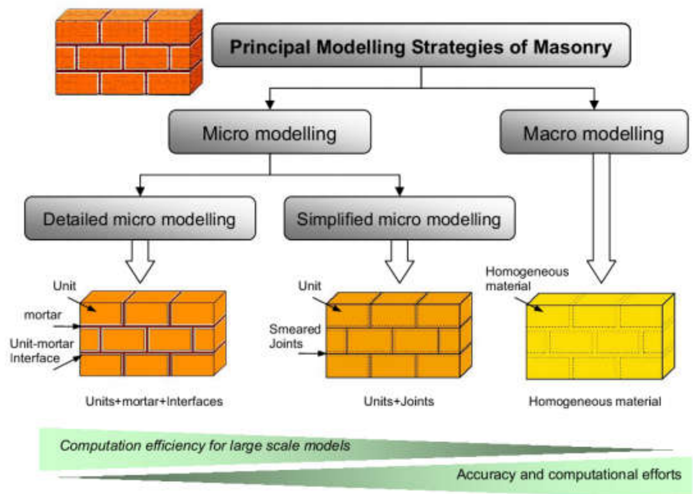

Figure 2-10: Modeling philosophies for masonry, from Bakeer (2009)

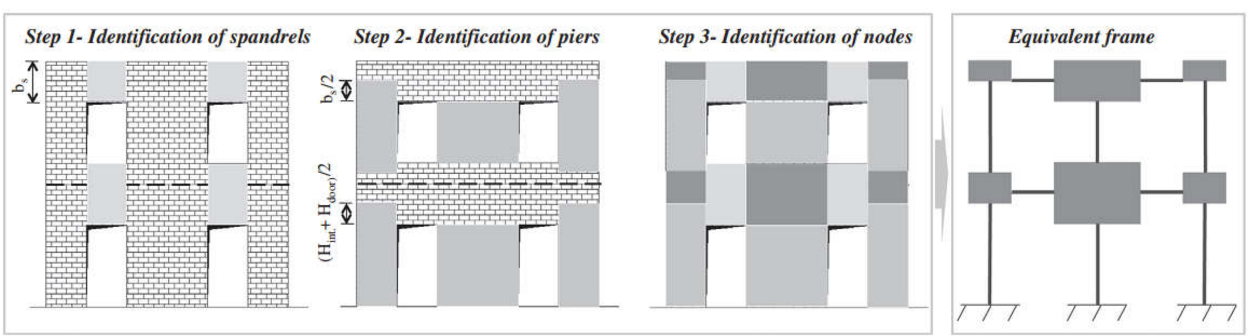

Figure 2-11: Equivalent masonry frame using TREMURI, from Lagomarsino et al (2013)

At the other end of the spectrum, there is discrete modelling using a detailed representation of individual material properties that form the assembly. Such models have potentials to provide very accurate results, but are often computationally expensive. The applied element method (AEM) developed by Meguro et al. (1999) aims to provide this discrete element modelling accuracy while avoiding the pitfall of increasing computational time exponentially. Tagel-Din (2008) explains that by keeping individual elements rigid and allowing their movement in 6 directions (3 translations and 3 rotations), six degrees of freedom are generated by each element compared to 24 degrees of freedom for a similar element in finite element analysis. As shown in Figure 2-12 and Figure 2-13, masonry is not considered homogeneous and springs are generated in between various elements such that their properties remain quite distinct. As the inner workings of AEM are not the goal of this subsection, the reader is referred to ASI (2010a, 2010b, 2010c, 2013) for further details.

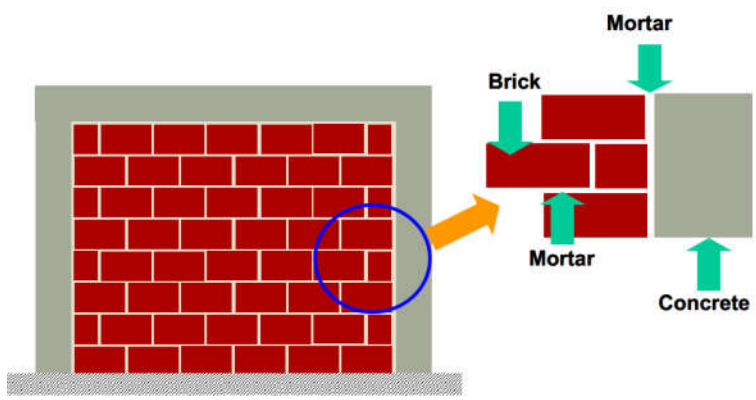

Figure 2-12: Discretization of masonry assembly in AEM, from Tagel-Din (2008)

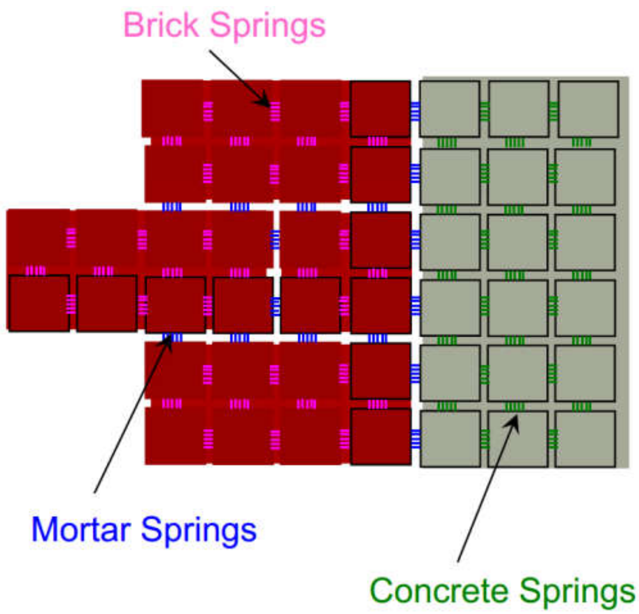

Figure 2-13: Springs at element interfaces in AEM, from Tagel-Din (2008)

2.4 Seismic demand

The estimation of seismic forces in Canada has considerably advanced since the introduction of seismic engineering in the NBCC (Mitchell et al., 2010). The first considerations of seismic forces were as a percentage of the structure's weight with no consideration for the remaining factors. This type of simplification led to the static analysis of structures undergoing ground motions, and would typically be limited to elastic analysis, with inelastic effects is introduced subsequently, often empirically. The recent versions of the NBCC since 2005 favor the use of dynamic analysis over a static approach. Estimation of seismic demand is better represented through time-history analysis under recorded ground motions (Frankie, 2010). Many research papers are available on the topic in the literature. The ground motion records, or accelerograms, may also be synthetically generated. Such work was performed by Atkinson and Beresnev (1998) and Atkinson (2009), resulting in NBCC compatible records to be used in Canada.

The use of synthetic accelerograms is often disputed in the literature; Lin et al. (2013) found that records from previous earthquakes are able to generate greater deformations in structures than their synthetic counterparts at equivalent intensities. Nonetheless, they conclude that, where insufficient information is available, simulated accelerograms can be used. In eastern Canada there have been a limited number of strong earthquakes that have been recorded (Bruneau and Lamontagne, 1994). Therefore, researchers, such as Karbassi (2010), used synthetic accelerograms in their time history analyses. By the arguments presented above, comparing synthetic and real accelerograms may skew results; therefore the use of only synthetic or real ground motions may be preferable. In the case of research focusing on Canada, the use of synthetic ground motions is therefore perfectly justified.

ASCE 41 recommends the use of bi-directional accelerograms (neglecting the vertical component) in the assessment of structures. Beyer and Bommer (2007) warn against the "30%-rule" which is a common practice where the orthogonal component of the ground motion represents 30% of the main direction's intensity. Given that the accelerations will vary, the angle of incidence of the main action of the earthquake may rotate and no longer be parallel to the axis of consideration. In Figure 2-14, the authors used a bi-directional accelerogram which was rotated by increments of 1^{o} to calculate the spectral acceleration effect on a structure. In this figure, the outer circle represents the maximum intensity, the thick line represents the angle of the principal axes and the remaining lines represent a measure of the two components. They argued that in order to identify the maximum response due to two accelerograms (and its direction of action), it is required to test the accelerograms at all angles, with a sufficiently small angle of rotation. This creates a very large number of analyses required to verify the intensity measures. On the other hand, uni-directional accelerograms are easy to calculate and orient according to the axis of analysis.

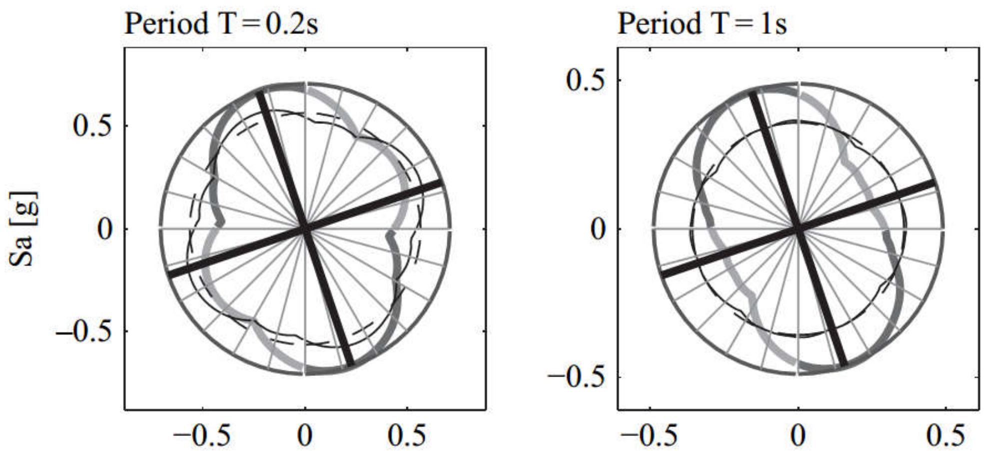

Figure 2-14: Effects of accelerogram rotation, from Beyer and Bommer (2007)

The amount of accelerograms used to adequately test structures varies greatly but is often within an interval of 10 to 20 records (Karbassi, 2010; Frankie, 2010; Bothara et al., 2009; Park et. al, 2009) although some may use fewer (Rota et al., 2010; Bakeer, 2009). Ghorbanie-Asl (2007) indicates that the selection of at least 20 ground motions usually provides satisfactory results in representing all of the earthquake source characteristics. Naturally, when more accelerograms are used, it is less likely to miss the larger responses that the structure may undergo at a given intensity. Furthermore, any error present will be statistically diminished by the increased number of accelerograms.

When dealing with unreinforced masonry, the use of spectral acceleration is suggested as intensity measure due to the first mode of vibration usually being the dominant response (Karbassi, 2010). This is typically true of short-period structures such as URM whose fundamental period ranges somewhere from 0.10 to 0.50 s (Mouyiannou et al., 2014; Pantazopoulou, 2013; Ingham and Griffith, 2011b). This period interval should therefore be suitable when selecting scaled accelerograms.

2.5 Damage assessment and its representation

2.5.1. Failure mechanisms of masonry

There are two main categories of structural damage likely to be sustained by URM structures: in-plane and out-of-plane. The latter has been shown to be a function of slenderness (height to thickness ratio) and of the overburden load on the wall (Penner, 2014; Derakhshan, 2011; Ismail et al., 2011; Lazzarini, 2009; Meisl, 2006).

For the in-plane failures, Figure 2-15 shows the possible modes. It is also possible that several of these mechanisms act simultaneously (Parisi and Augenti, 2013). Further information regarding typical damage indicators and their thresholds will be presented in Chapter 3.

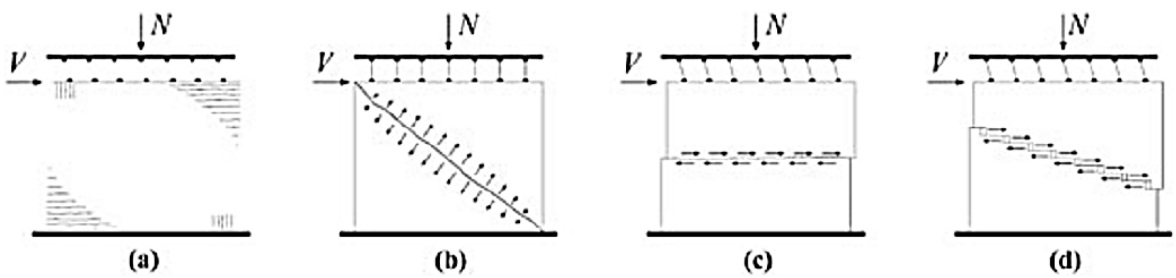

Figure 2-15: In-plane failures of URM (a) rocking (b) diagonal tension (c) sliding (d) stair-stepped, from Parisi and Augenti (2013)

2.5.2. Damage estimation

The evaluation of damage and capacity in URM structures has been the object of many studies, with it being as one of the oldest building materials while being very poorly understood (Abrams, 2001). Indeed, many definitions exist to quantify the likely damage sustained by URM structures; Hill and Rossetto (2008) performed a comparison on twelve different damage scales being used in Europe. Of these, the most common in Canada are the Hazus-MH and FEMA 356 terminologies. These works present vastly different limits for damage in URM, although this is explained by the different goals of each: Hazus-MH is a tool used to estimate seismic risk and therefore the damage definitions presented serve for seismic loss estimation. On the other hand, FEMA 356's (also used in ASCE 41) goals are performance-based evaluation of structures. The recent trend for masonry is closely tied to performance-based design (Hill and Rossetto, 2008; Sabatino and Rizzano, 2011). The performance limits from FEMA 356 are immediate occupancy, life safety and collapse prevention; their definitions follow. In terms of engineering, a measure is selected, such as roof displacement or drift, to represent these performance limits.

"**Immediate occupancy**: Minor (< 1/8" width) cracking of veneers. Minor spalling in veneers at a few corner openings. No observable out-of-plane offsets.

Life safety: Extensive cracking. Noticeable in-plane offsets of masonry and minor out-of-plane offsets.

Collapse prevention: Extensive cracking; face course and veneer may peel off. Noticeable in-plane and out-of-plane offsets."

Distinction should be made between target performance levels and acceptance criteria for existing buildings. The former applies to newer structures or to rehabilitated ones. In the case of seismic assessment of structures as they currently stand, the acceptance criteria should be used. Further information will be presented in Section 3.4.

2.5.3. Damage assessment of structures

In order to assess the vulnerability of structures due to various levels of ground motion intensity, various methods have been used over the years. Perhaps the most widely used technique in the current state of research, as evidenced by the number of research in the area (e.g. Abo-El-Ezz et al., 2013; Barrantes, 2012; Karbassi and Lestuzzi, 2012; Frankie, 2010; Bothara et al., 2009; Onur, 2001) is fragility curves, which provide a direct relationship between the ground motion intensity and the damage probability. Fragility curves assume that the range of damage to a structure, based on events of equal intensity, follows a log-normal distribution as can be seen in Figure 2-16.

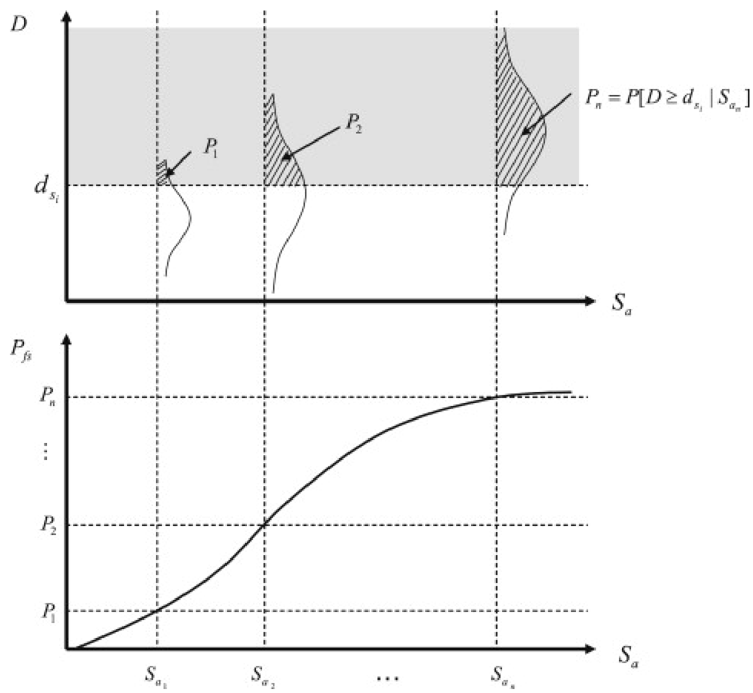

Figure 2-16: Fragility curve concept, from Park et al. (2008)

In other words, two earthquakes of the same spectral acceleration for a given period of vibration will not necessarily create the same damage to a structure. Fragility curves help determine the likelihood of the structure to sustain damage should an earthquake of the same intensity occur. Equation 2-1 shows the equation governing fragility curves.

$$F(X) = P(d > D) = \phi\left[\frac{\ln(X) \quad \mu}{\sigma}\right] \tag{2-1}$$

In this equation, X is the intensity measure, P is the probability of exceeding a given performance level, d is the damage level, D is the performance level limit, ϕ is the normal distribution function, μ is the median of earthquake intensities and σ is their standard deviation. As seen in Equation 2-1, one requires ground motions and an intensity measure (Section 2.4), damage estimate measures or performance levels (Subsection 2.5.2) and a method linking them together in order to generate fragility curves. Frankie (2010) gives examples of these methods: pushover analysis method and capacity spectrum method. Another method was introduced by Vamvatsikos and Cornell (2004): the incremental dynamic analysis (IDA). According to the authors, the IDA is "a series of dynamic nonlinear runs performed under scaled accelerograms, whose intensity measures are selected to cover the whole range from elastic to nonlinear and finally to collapse of the structure". In other words, one may use a single accelerogram to cover the whole behavioural state of the structure by appropriately scaling the ground motion. Furthermore, the use of several ground motions is also possible, leading to a multi-record IDA as is shown in Figure 2-17. Combined with the fragility curve concept shown in Figure 2-16, the IDA brings all the necessary tools to perform seismic assessment of structures.

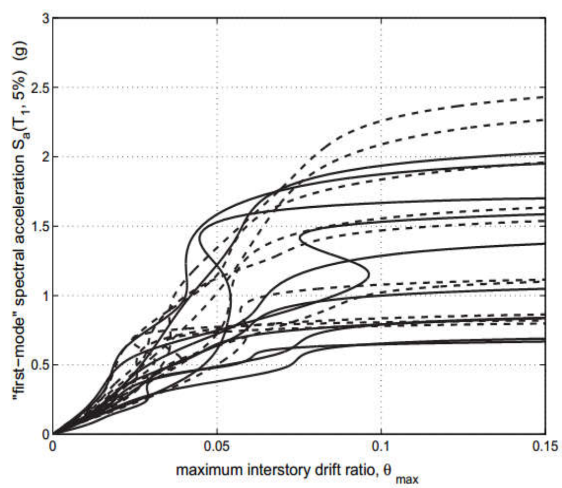

Figure 2-17: Multi-record IDA, from Vamvatsikos and Cornell (2002)

Regarding the validity of record scaling in terms of the resulting damage when compared to natural records of that intensity, the authors cite several works on the topic suggesting that there is little difference between the two. For instance, the work of Bazzuro et al. (1998) in Figure 2-18 is presented. In this figure, a regression analysis was performed to compare the damage measure of unscaled records compared to that of scaled records. The authors only plotted one of these regressions, explaining that the proximity between the two curves was such that they only felt the need to plot one of them.

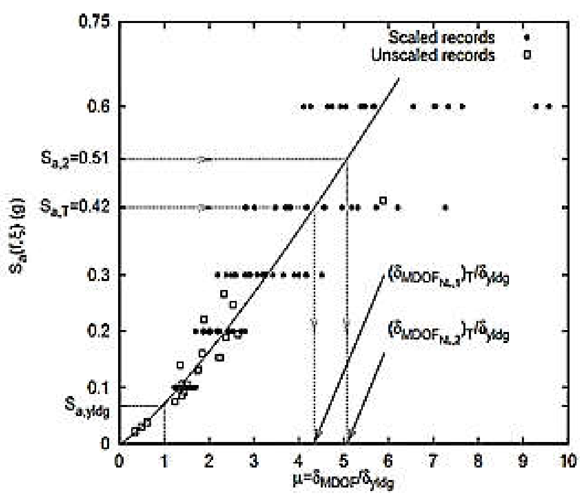

Figure 2-18: Structural response to scaled and unscaled records, from Bazzuro et al. (1998)

2.6 Existing research

2.6.1. Seismic assessment in Canada

Karbassi (2010), using a building inventory compiled by Lefebvre (2004), performed a seismic assessment of early 20th century industrial URM structures in Montréal. This was done through a performance based seismic vulnerability evaluation on a six storey URM structure with large openings as shown in Figure 2-19. This building, located at 1015 William St. in Montréal, was constructed in 1905 in the target area of Lefebvre (2004)'s inventory. The seismic force resisting system was determined to be masonry walls while gravity systems also included columns and beams of steel and wood. The construction material of the floors was made of wood. As can be seen from Figure 2-19, the structure presents a large amount of openings in both directions; the difference being that the “longer direction” features more piers overall than the “shorter direction”. A direct consequence of this is seen in the two first modes of vibration which are respectively 0.38s and 0.69s. Karbassi (2010) used an incremental dynamic analysis with fourteen synthetic and real ground motion records using the applied element method.

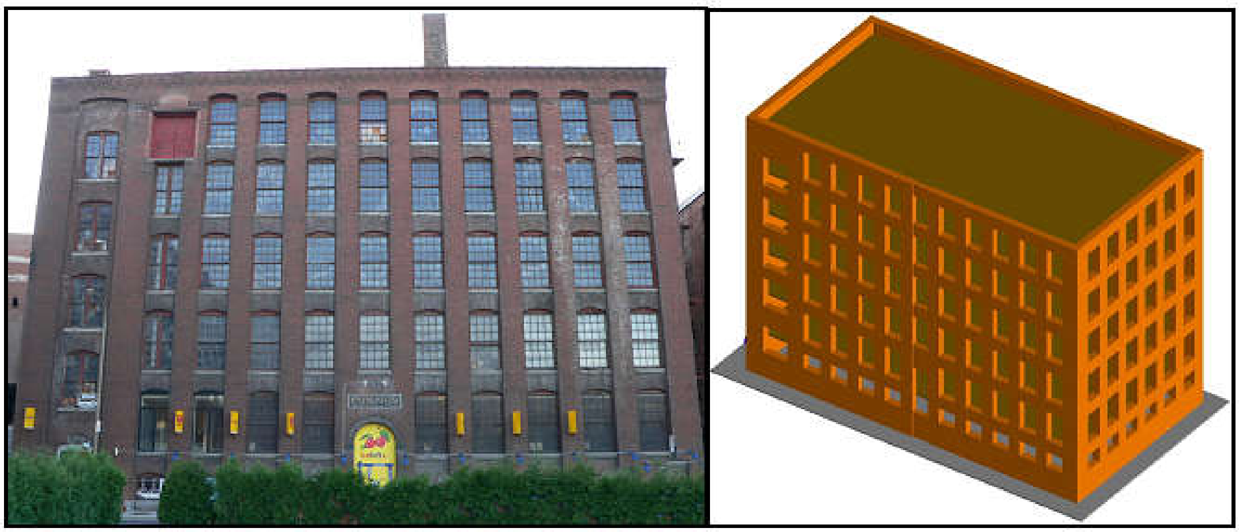

Figure 2-19: Industrial URM structure used for seismic assessment of Karbassi (2010)

The selected damage measure used the ASCE 41’s definition of performance levels: immediate occupancy, life safety and collapse prevention. Inter-storey drift was picked as the damage measure since it relates well to indicators such as local and global collapse. The thresholds were respectively 0.1%, 0.3% and 0.4% while the intensity measure for the ground motion was selected as spectral acceleration. The reasoning from Karbassi (2010) for this selection was that URM structures are “sensitive to the power of the frequency content near the first-mode”. This finding is further corroborated by Silva et al. (2013). The resulting fragility curves for in-plane failures were compared to those of Hazus-MH and found to be more vulnerable. The author argued that his results show that the structure considered is less ductile than the ones by Hazus-MH due to its height and weight. Furthermore, Karbassi further noted that Hazus doesn't provide parameters of six-storey URM buildings which contribute greatly to the discrepancy of the fragility curves from both works.

Elsabbagh (2013) conducted a seismic risk assessment of URM structures in Canada, with a focus on structures in the city of Ottawa. The assessment of vulnerability was done through user input and fuzzy logic. This provided the means to perform rapid evaluation of structures based on the structural factors of URM buildings, such as the number of storeys, year of construction and vertical irregularities. The fuzzy logic concept also allowed the interaction of various parameters acting together as seen in Figure 2-20. The visualization of likely damage sustained by structures was done by inputting the user evaluation of structural liabilities into the CanRisk program which then evaluates the damage state of the current structure to a code-level earthquake with 2% probability of exceedance in 50 years. The output data from the software presents the damage state as defined by ATC-13: none, slight, light, moderate, heavy, major or destroyed. The methodology was verified by comparing with 15 structures that were damaged during the Christchurch 2011 earthquake and showed to be consistent with the evaluation done on the field, as shown in Figure 2-21.

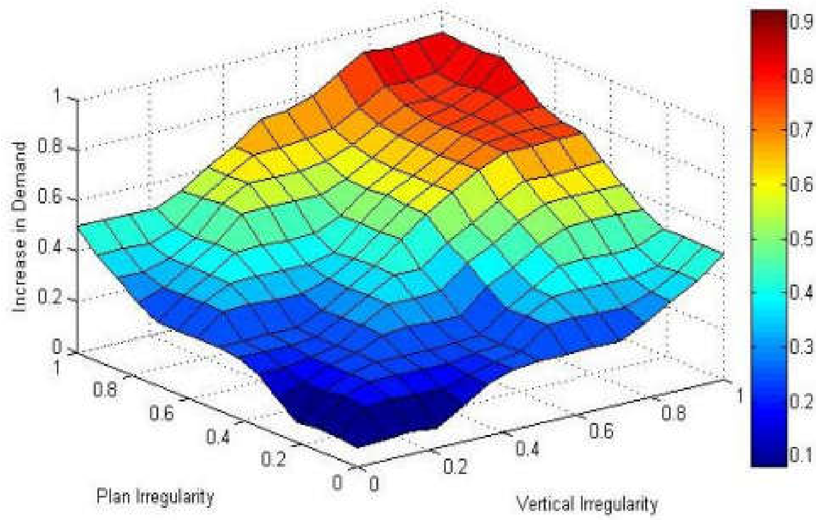

Figure 2-20: Increase in seismic demand interactivity, from Elsabbagh (2013)

Building Number	Building Address	Configuration	Number of Stories	Vertical Irregularity	Plan Irregularity	Spectral Acceleration	Distance from epicenter (km)	Construction Quality	Year of Construction	Structural Damageability Index (I^{BD})	Structural Damageability (CanRisk)	ATC-13 Damage State
1	623-629 Colombo St	Row-Middle	2	M	VL	0.65	7.48	AVG	1890 (retrofit A)	0.61	Heavy	Heavy
2	603-615 Colombo St	Row-Middle	2	H	L	0.65	7.45	AVG	1906	0.72	Heavy	Major
3	208 Hereford St	Stand-alone	2	VL	VL	0.65	7.41	AVG	1865	0.65	Heavy	Major
4	287 Manchester St	Row-End	1	L	VL	0.52	7.87	GD	unknown	0.4	Light	Light
5	107A Cambridge Terrace	Row-End	1	VL	M	0.52	7.98	PR	1875 (retrofit A)	0.47	Moderate	Moderate
6	222 St Asaph St	Row-Middle	1	L	VL	0.52	7.22	AVG	unknown (retrofit A)	0.43	Moderate	Moderate
7	80 Lichfield St	Row-End	3	L	VL	0.77	7.44	AVG	1881	0.84	At/Near Collapse	Major
8	1-3 Hereford St	Row-Middle	3	VL	VL	0.77	8.22	GD	1910	0.78	Heavy	Heavy
9	116 Lichfield St	Row-End	3	H	M	0.77	7.39	PR	unknown	0.92	At/Near Collapse	Destroyed
10	116 Madras St	Stand-alone	2	VL	VL	0.52	7.09	GD	1876 (retrofit A&B)	0.33	Light	Light
11	84 Lichfield St	Row-End	3	VL	VL	0.77	7.45	AVG	1890 (retrofit A)	0.84	At/Near Collapse	Destroyed
12	141 Lichfield St	Row-End	1	VL	M	0.52	7.26	PR	1903 (retrofit A)	0.53	Moderate	Moderate
13	146 Kilmore St	Stand-alone	2	L	L	0.65	8.05	PR	1929	0.72	Heavy	Major
14	644 Colombo St	Row-Middle	2	L	M	0.65	7.5	AVG	unknown (retrofit A&B)	0.6	Moderate	Light
15	270 St Asaph St	Stand-alone	2	L	L	0.65	7.06	AVG	unknown (retrofit A&B)	0.61	Heavy	Heavy

Figure 2-21: Evaluation of damage to Christchurch URM structures, from Elsabbagh (2013)

The strength of this work resides in its reliability, its capacity to evaluate any URM structure, including irregularities, and its swiftness in producing estimates of damage. However, it is also reliant on user input and thus subjectivity: two users may not consider the same degree of importance for a given structural irregularity. Furthermore, no information can be obtained for earthquakes of intensity different from the code level. In other words, if a relatively low intensity earthquake occurs, the tool would not yield an accurate overview of the likely damage sustained by URM structures.

Onur (2001) is another example of seismic assessment based on expert judgement; 71 earthquake engineers provided estimates of damage to structures which was then fit as a Beta distribution based on intensity as shown in Figure 2-22 using the damage probability matrix. Fragility curves were also produced using the capacity spectrum method with moment magnitude intensity and spectral displacement as ground motion intensity measures. The structures used for this portion of the work were built in the United States and were considered similar enough in construction practice in order to evaluate Canadian URM buildings.

Central DF	Modified Mercalli Intensity						
	VI	VII	VIII	IX	X	XI	XII
Wood Frame – Low Rise							
0	3.7	***	***	***	***	***	***
0.5	68.5	26.8	1.6	***	***	***	***
5	27.8	73.2	94.9	62.4	11.5	1.8	***
20	***	***	3.5	37.6	76.0	75.1	24.8
45	***	***	***	***	12.5	23.1	73.5
80	***	***	***	***	***	***	1.7
100	***	***	***	***	***	***	***

Figure 2-22: Damage probability matrix, from Onur (2001)

Ulmi et al. (2014) have begun the daunting task of adapting the Hazus-MH (NIBS, 1997) tool to Canada, effectively creating Hazus Canada. The original tool has proved invaluable in evaluating risks associated with earthquakes, tsunamis and other natural disasters. However it was not calibrated to Canada. In order to remedy this issue, the existing data from Hazus-MH was matched to Canadian data by using databases such as Statistics Canada. Local data for provinces were adapted based on states with similar occupancy. For instance, Ontario is matched to Michigan while Québec is matched to Massachusetts. The included fragility curves are based on expert opinion (Abo-El-Ezz et al., 2013; Karbassi, 2010; Park et al., 2008) and are matched to the building classes presented in Table 2-2. Several characteristics of building are reprised from NIBS (2003a) as shown in Figure 2-23.

	Year Built				
Building Type	**2005-Onward**	**1990-2004**	**1970-1989**	**1941-1969**	**Pre-1941**
Wood, Steel, or Concrete		**HS** (Special High-Code)	**MS** (Special Moderate-Code)	**LS** (Special Low-Code)	
Masonry, Mobile, Others		**HC** (High-Code)	**MC** (Moderate-Code)	**LC** (Low-Code)	
All Building Types	**HS** (Special High-Code)				**PC** (Pre-Code)

Figure 2-23: Seismic design levels based on year of construction, from Ulmi et al. (2014)

The tool helps users in their mitigation efforts, preparedness and response to future events. Ulmi et al. (2014) state that no modifications were done to assumptions regarding damage estimates or to the fragility curves. As a result of this, the fragility curves still represent American practice and are not tuned to Canadian building codes or differences in materials used. While the tool is still being developed, the reader is referred to NIBS (2003a, 2003b, 2003c) in order to get a full picture of its functioning.

2.6.2. Seismic assessment in the world

Frankie (2010) and Park et al. (2008) both developed fragility curves for URM buildings in central and eastern United States. The former used the capacity-spectrum method to assess the vulnerability of structures with the Hazus-MH limit states by using a database of previously tested structures as shown in Figure 2-24. These structures were later divided by storey height and code level compliance (low, medium, high) as well as the ground conditions on which they were constructed. The author mentioned the variability of openings in buildings but no distinction was made in the available fragility parameters.

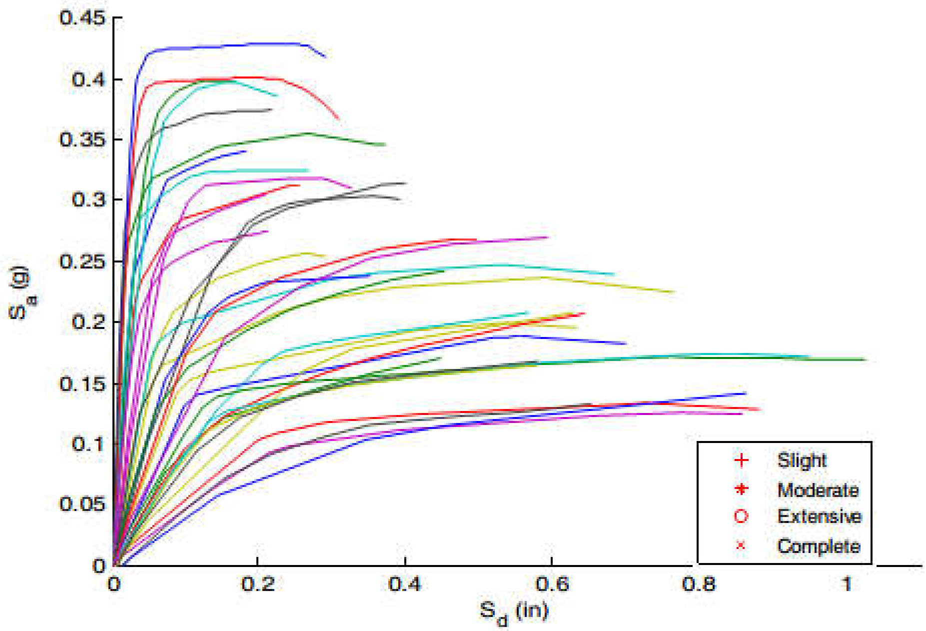

Figure 2-24: Capacity diagram of URM inventory, from Frankie (2010)

Park et al. (2008) used a typical two-storey URM building to generate in-plane fragility curves. A composite model was used by representing piers in the structure by springs. As such, each pier was investigated to determine its governing behaviour, stiffness and strength and the model springs could represent the full three-dimensional response of the structure as is shown in Figure 2-25. The authors considered three levels of connection between the in-plane and out-of-plane walls: i) zero contribution, ii) fixed at the top and bottom iii) and fixed along the entire perimeter. The results showed that the out-of-plane connection contributed greatly in the overall capacity and that the ensuing fragility curves were much less vulnerable when a sound connection of the out-of-plane walls was present, and should therefore not be ignored as is often done.

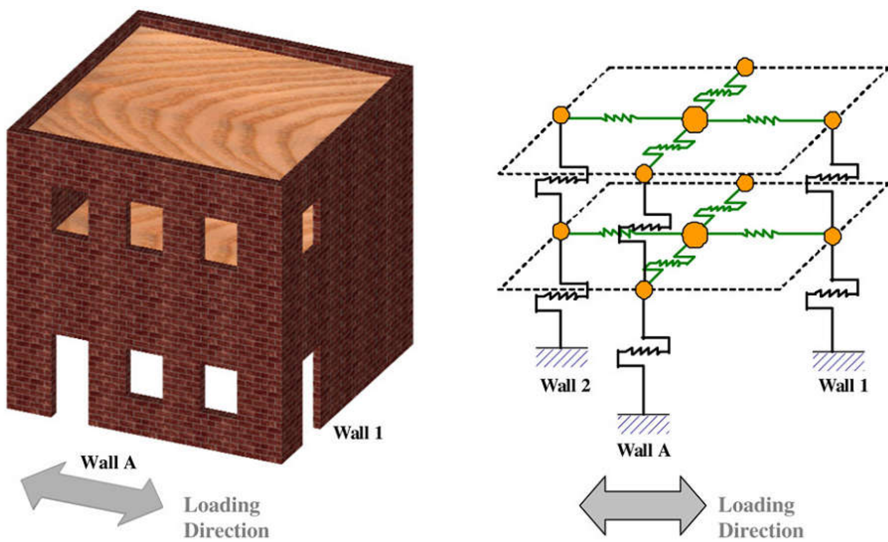

Figure 2-25: Spring model of URM low-rise, from Park et al. (2008)

Seismic risk assessment is not limited to North America. Many works are published from around the world (e.g. Bilgin, 2013; Ceran and Erberik, 2013; Barrantes, 2012; Karbassi and Lestuzzi, 2012; Derakhshan, 2011; Kafle et al., 2011; Rota et al., 2010; Bakeer, 2009; Bothara et al., 2009 Lang, 2002) as more and more engineers start focusing on mitigation efforts in the hopes of reducing seismic risk in the future.

Chapter 3

Selection of structural and ground motion parameters

This chapter describes the details of structural and ground motion parameters selected for constructing the analytical models of buildings used in dynamic inelastic time history analysis required for computing fragility relationships. Structural parameters also include the selection of damage indicators for use in seismic fragility curves.

The primary elements of seismic vulnerability assessment were presented and reviewed in Chapter 2 for URM buildings in Canada. These can be grouped under three categories as outlined by Frankie (2010). Accordingly, the elements of seismic vulnerability assessment require the characteristics of building inventory, seismic hazard, and the resulting fragility relationships. Sections 3.1 and 3.2 cover the selection of typical URM buildings that form the building inventory. Seismic hazard, as reflected by ground motions is discussed in Section 3.3. Fragility relationships, including damage indicators, are discussed in Sections 3.4 and 3.5.

3.1 Building inventory

The proper assessment of buildings in a given region requires sufficient knowledge of building inventory, for which a survey of existing buildings is of great asset (Onur, 2001). Onur (2001) indicates that the quality of an inventory is a function of the amount of time available, as it allows for a more comprehensible overview of structures in the region. One of the most time-consuming processes of a robust seismic assessment process is therefore the collection of data required to build the inventory. The elements that make a robust inventory includes: street address, occupancy, construction material and structural system, year of construction and number of stories (Onur 2011). For buildings in the Ottawa area, Sawada et al. (2014) collected information for over 50,000 building structures in the national capital region and assembled an inventory. The locations of structure in the inventory were recorded using latitude and longitude so that they could be input in a geographic information system (GIS), as depicted in Figure 3-1. The information collected for each building is compatible with Hazus-MH. The construction type, building occupancy, number of stories, irregularities and year of construction, as well as other structural and non-structural details have been compiled, as shown in Figure 3-2.

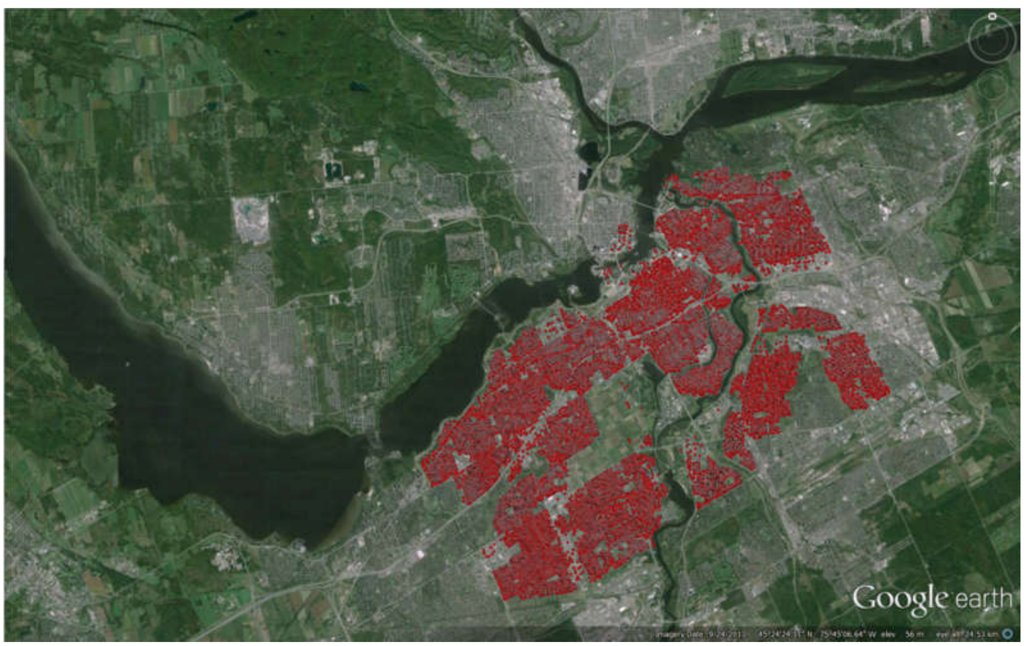

Figure 3-1: Structures part of GIS database by Sawada et al. (2014)

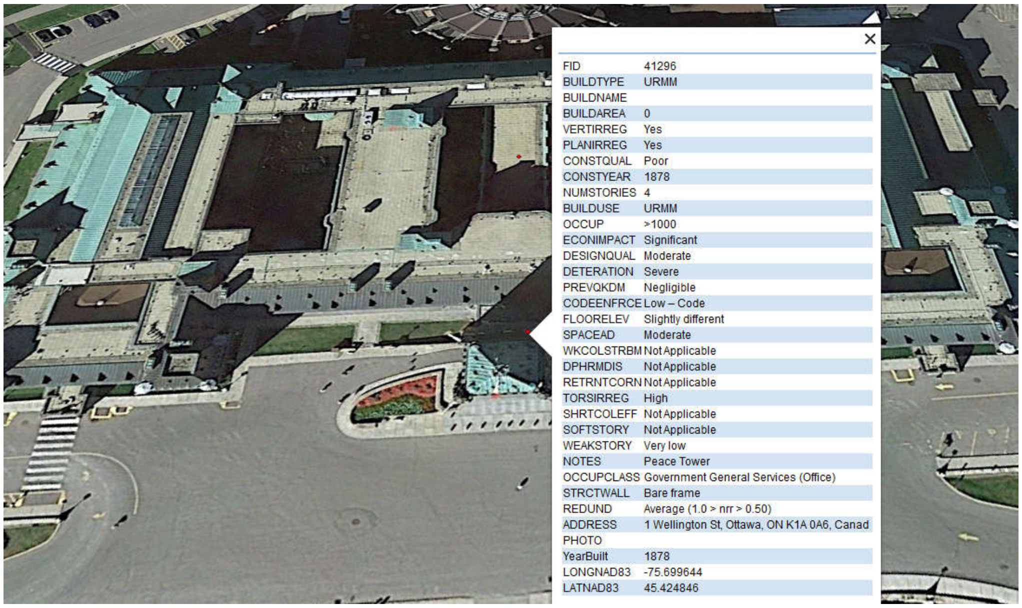

Figure 3-2: Information available in building inventory

This information was collected by trained personnel who conducted on-site appraisal of each building structure in the inventory. Year of construction, which is not typically available on site, was obtained through municipal databases or through educated guess based on the construction practice or keystone markings (Sawada et al., 2014).

Bélec et al. (2015) used this inventory to extract information relevant to URM structures. Of the 50,000 structures, slightly more than 4% were flagged as URM. Almost 50% of the URM buildings were two-storeys high; over 30% were three storeys high and around 15% had a single storey. The remaining structures over three storeys high accounted for less than 5% of all URM structures. Of the URM structures in the inventory, 82% were found to be built before 1945, and 97% before 1970. The buildings presented very few irregularities. Out of a scale of ascending order of severity, the irregularities were listed as; i) not applicable, ii) negligible, iii) low, iv) moderate, v) high, and vi) very high. Of the buildings in the inventory, 66% did not feature re-entrant corners and 91% had low or negligible irregularities. Furthermore, 93% of the buildings did not present signs of any torsional irregularity; 93% did not have soft storeys; 98% did not have weak storeys; and 96% had the same storey height.

3.2 Typical URM buildings

3.2.1. Visual inspection

Since the building inventory did not contain the dimensional data, a visual inspection of all URM buildings was carried out using the GIS database within Google Earth to confirm the information presented in the inventory. A sample of 20 URM building structures was selected with characteristics that were representatives of the building inventory presented in Section 3.1. For these structures, dimensions were estimated using the city of Ottawa zoning map application, which was available at the city of Ottawa website. On-site visits were also performed to observe the number of wythes in masonry walls; confirm the building classification as unreinforced masonry; gather information about openings; evaluate the storey height; and assess the condition of the masonry as seen in Figure 3-3. Using the relevant information about openings and the dimensions of the structures, the effective stiffnesses of buildings in the sample could be evaluated. Information about the effective stiffness is available in Appendix C. Table 3-1 shows the average and median values obtained from the selected sample. Because the number of openings and their effect varied greatly, lower-half and upper-half averages and medians are also included (first and third quartile). Each structure provided dimensions and effective stiffnesses in each orthogonal wall. In all cases, the number of bricks forming the masonry wall thickness was found to be three. The height of each storey was estimated to be very close to approximately 3 meters in each building. The most variable parameter was found to be the effective stiffness as illustrated in Table 3-1.

Figure 3-3: Masonry in good condition (left) and poor condition (right)

Table 3-1: Average and median values of characteristics in the structure sample

	Dimensions (m)	Effective stiffness (%)
Lower-half average	8.5	32
Lower-half median	8.5	24
Overall average	10.6	48.5
Overall median	10	53
Upper-half average	12.7	81
Upper-half median	12.5	83

3.2.2. URM characteristics

From the collected data in the previous subsection, as well as the review of literature on masonry properties, two typical structures with representative characteristics were selected to carry out the dynamic analysis task of current research. Two-storey low-rise and three-storey mid-rise buildings were selected due to their predominance in the inventory. One-storey buildings were not selected because of the reported similarities in behaviour between single and two-storey structures (Barrantes, 2012). The plan dimensions were selected to be 9 m x10 m. This is consistent with the dimensions reported in Table 3-1.

Since most buildings in the inventory were built prior to 1945, low strength materials, representative of pre-code era were used. To account for the remaining structures, a material more reminiscent of materials in good condition was used, using an approximate construction year of 1970 as reference to represent the latest URM constructions allowed without reinforcement (Ventura, 2005). The data presented in Table 3-2 is taken from Chapter 2 and the sources therein. For the wood diaphragm, a single set of data was selected from Karbassi and Nollet (2013) as the weathering effects are typically not as severe and aging is not as much of a factor, often leaving the diaphragm to behave in an "infinitely linear" manner during seismic response, even in historic URM buildings (Ingham et al., 2011; Wilson et al., 2011; Paquette and Bruneau, 2006). The first-mode periods of all buildings considered are shown in Table 3-3. As can be seen, the impact of openings is small in low-rise buildings' structural period.

With regards to the openings; the first and the third cases in Table 3-1 with corresponding stiffness values were selected, i.e., 24% (large openings) and 83% (small openings). The out-of-plane failure mechanisms were controlled by the ASCE 41 slenderness ratio limit of 9 that was discussed in Chapter 2. This was justified in view of the relatively thick walls observed (having 3 wythes). Consideration of the out-of-plane thickness as a separate wall parameter would require a significant increase in the number of analyses to be run, though it would be preferable to combine in-plane fragility curves with out-of-plane fragility curves, and use a combination of the two to create lower-bound fragility parameters.

Table 3-2: Material properties used

Material	Property	Pre-code	Low-code
Brick units	Compressive strength, f'_m (MPa)	10	21
	Tensile strength (MPa)	1	2.1
	Modulus of elasticity, E (MPa)	7000	14700
	Shear modulus (MPa)	2800	5880
Mortar	Compressive strength, f'_m (MPa)	1	3.5
	Tensile strength (MPa)	0.5	1.5
	Modulus of elasticity (MPa)	464	1624
	Shear modulus (MPa)	186	651
Wood diaphragm	Compressive strength (MPa)	36.2 (=) 3.2 ($\top$)	
	Tensile strength (MPa)	3.2	
	Modulus of elasticity (MPa)	8900	
	Shear modulus (MPa)	3600	

Table 3-3: First-mode of vibration periods of typical structures considered in seconds

		Pre-code	Low-code
Mid-rise	Large openings	0.271	0.214
	Small openings	0.173	0.136
Low-rise	Large openings	0.145	0.136
	Small openings	0.113	0.107

A summary of the above cases discussed in this Subsection is shown in Figure 3-4 below.

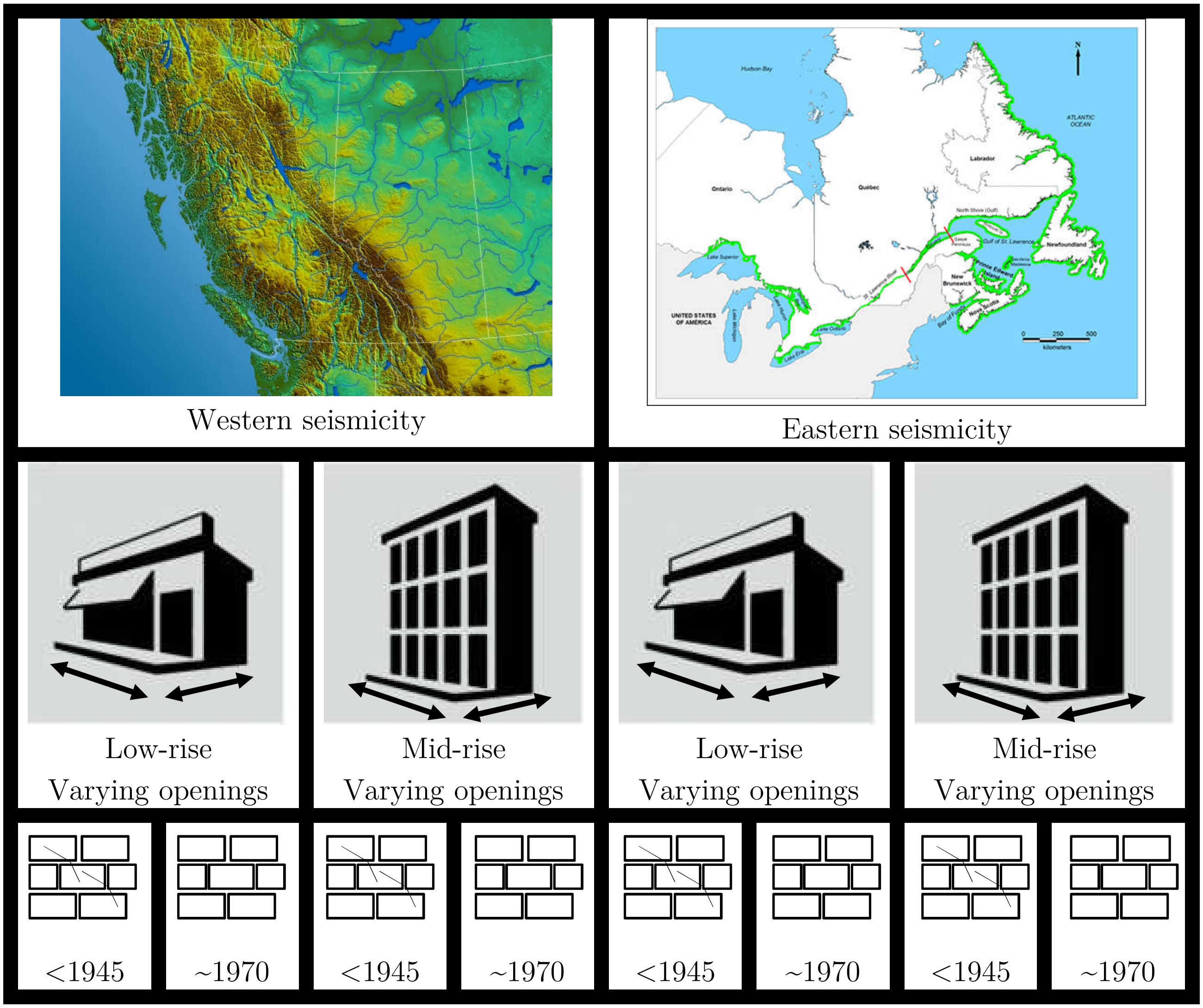

Figure 3-4: Summary of parameters considered in dynamic analysis

3.2.3. Model information

The analytical models were developed with the applied element software Extreme Loading® for Structures by Applied Science International. The software incorporates a material model for masonry which contains masonry meshing. This type of meshing allows separation of units as well as generation of springs featuring the physical properties of the mortar and brick units as shown in Figure 2-13. Regular meshing of elements would instead result in the mortar and brick unit properties to be averaged and thus creating a homogeneous material (ASI, 2013).

The above buildings were represented by three-dimensional models, and were analysed with a 1:1 brick to element ratio – that is, each brick in the real-size structure was individually represented by a corresponding element in the analytical model. Subsequently, a simpler model was used to reduce the computer time. It was verified that the simpler models behaved adequately. This validation was performed with a single accelerogram at 100% scale. The structural periods for the first 3 modes obtained from full and reduced models are shown in Table 3-4 with sufficiently close correlations.

Table 3-4: Comparison of structural periods for analytical models

Pre-code model	Mid-rise		Low-rise	
Structural Period	Full-size	Reduced	Full-size	Reduced
First-mode (s)	0.280	0.278	0.146	0.150
Second-mode (s)	0.241	0.243	0.136	0.140
Third-mode (s)	0.169	0.170	0.109	0.110

Like finite element analysis, the applied element method utilizes the principles of energy (ASI, 2013) with increasing number of elements resulting in more life-like behaviour of the model. The full-size mid-rise model contained over 85,000 elements while the final reduced model had slightly less than 5,000 elements. A similar ratio was obtained for the low-rise buildings: 51,000 elements for the full-size model and 3,100 for the reduced version. These quantities of elements correlate well with similar studies using the same software. Karbassi (2010) developed a model for a six-storey URM of larger proportions using approximately 10,000 elements. ASI (2004) recreated the eight-storey Alfred P. Murrah building in Oklahoma City to investigate the structural cause of the 1995 partial collapse using a model with 7,000 elements and was able to generate results in very good agreement with the final state of the structure shown in Figure 3-6.

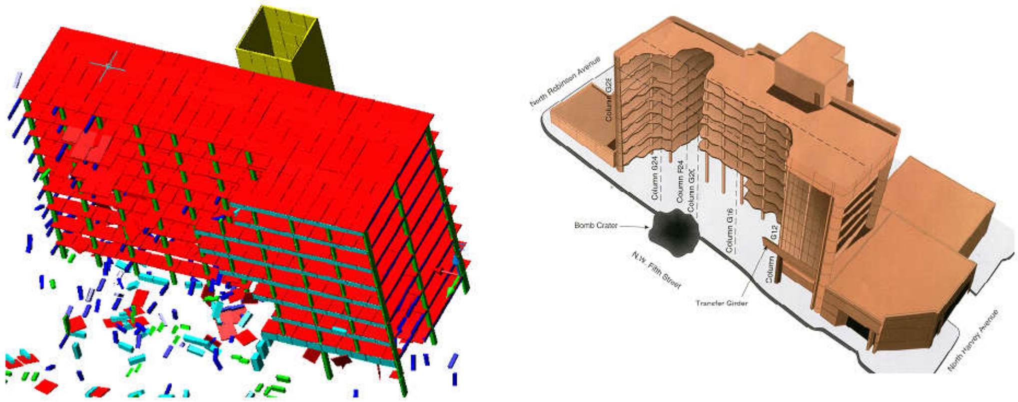

Figure 3-4: Alfred P. Murrah building simulation (left) and actual (right) state after blast, from ASI (2004)

3.3 Ground motions

In light of the factors discussed in Chapter 2; 20 synthetic ground motions were selected to represent seismic hazard in each of the two cities considered in the analyses; i.e., Ottawa and Vancouver. For reasons discussed in Section 2.4., the accelerograms were uni-directional and were applied in each orthogonal direction. The selection of the city of Ottawa is only appropriate as the building inventory used was obtained from Ottawa. The hazard values (uniform hazard spectra) for Ottawa and Montréal are almost the same in the 2010 NBCC. As a result, selecting Ottawa hazard values provides insight into a vast number of URM structures in eastern Canada, located in zones of moderate seismicity. On the other hand, the selection of the city of Vancouver was based on its high seismic hazard values and dense population, resulting in a high-risk region. Onur (2001) conducted a survey of 20,000 structures in the city of Vancouver and found approximately 1900 URM structures; of these, 88% were categorized as low-rise. An example of the repartitioning of structures is shown in Figure 3-5. Furthermore, the city of Vancouver has been identified by Adams et al. (2002) as being of the highest relative seismic risk in

Canada, as depicted in Figure 3-6. For these reasons, the selection of Ottawa and Vancouver aims to cover most of the seismic risk in Canada.

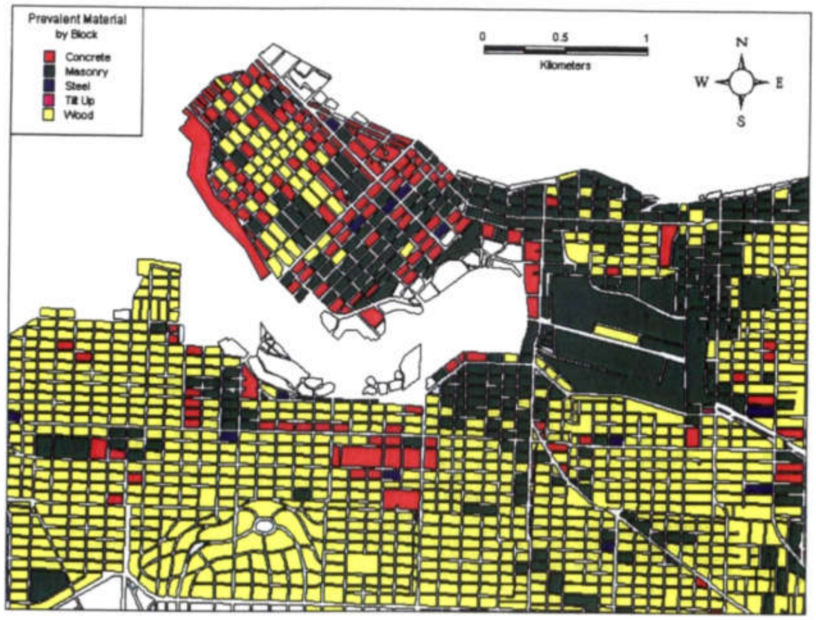

Figure 3-5: Prevalence of URM structures in Vancouver, from Onur (2001)

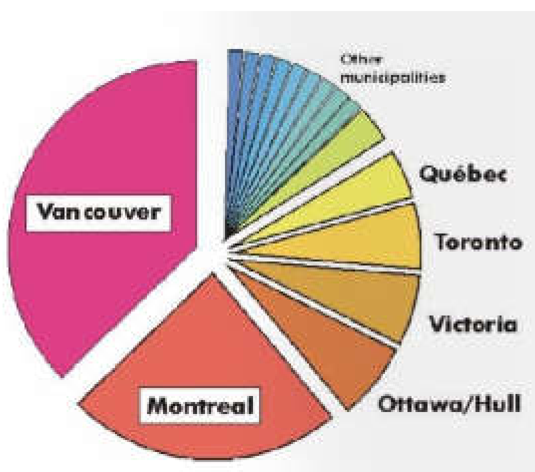

Figure 3-6: Relative seismic risk in urban areas of Canada, from Adams et al. (2002)

The work of Atkinson (2009) allowed the selection of ground motions that best fit the requirements presented in Section 2.4 for Ottawa and Vancouver. The selection of accelerograms was also based on the following criteria:

- 40 accelerograms in total, 20 for eastern Canada and 20 for western Canada.

  As discussed in Section 2.4; 20 ground motions is on the higher end of the range considered by previous researchers, and provides a good ratio of computational time to reduction of errors.

- Scaling period range of interest is 0.10 to 0.50 seconds for mid-rise and 0.10 to 0.30 seconds for low-rise buildings.

  As discussed in Section 2.4 and Subsection 3.2.2, these are typical ranges for fundamental period of URM structures. A smaller interval was selected for low-rise buildings as the first-mode periods considered are considerably lower.

- 5 accelerograms from each magnitude-distance category (Magnitude 6 or 7 and radius 20 or 70 km for both eastern and western ground motions) on reference soil class C.

  The goal is to include as much diversity in the nature of earthquakes while ensuring that compatibility is maintained with ongoing research at the University of Ottawa. Soil class C is also used as base reference in Ulmi et al. (2014).

- Scaling procedure suggested by Atkinson (2009).

  For reasons discussed by the author, the selection of ground motions that match a given uniform hazard spectrum should be based on the smallest possible deviation between the 2 spectra while also maintaining a scaling factor within the [0.5, 2] interval.

The average spectra for selected accelerograms for the mid-rise building are compared with the target spectra for Ottawa and Vancouver in Figure 3-7 and Figure 3-8. Further information regarding these ground motions is available in Appendix B.

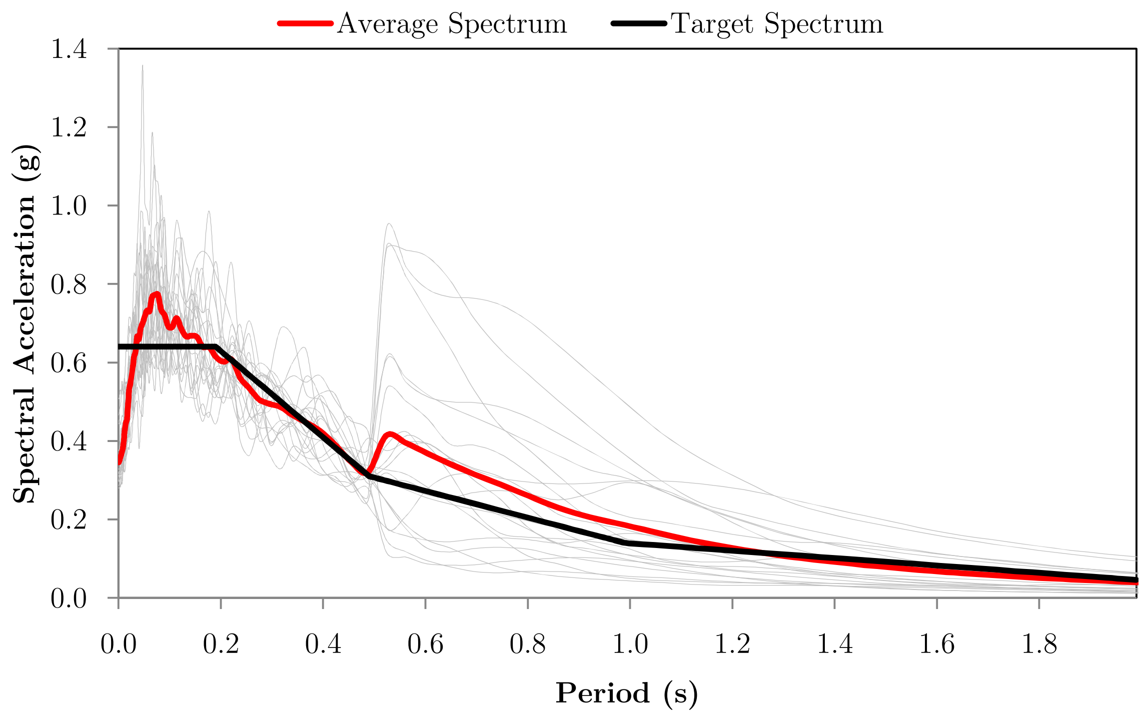

Figure 3-7: Spectra of scaled ground motions for Ottawa

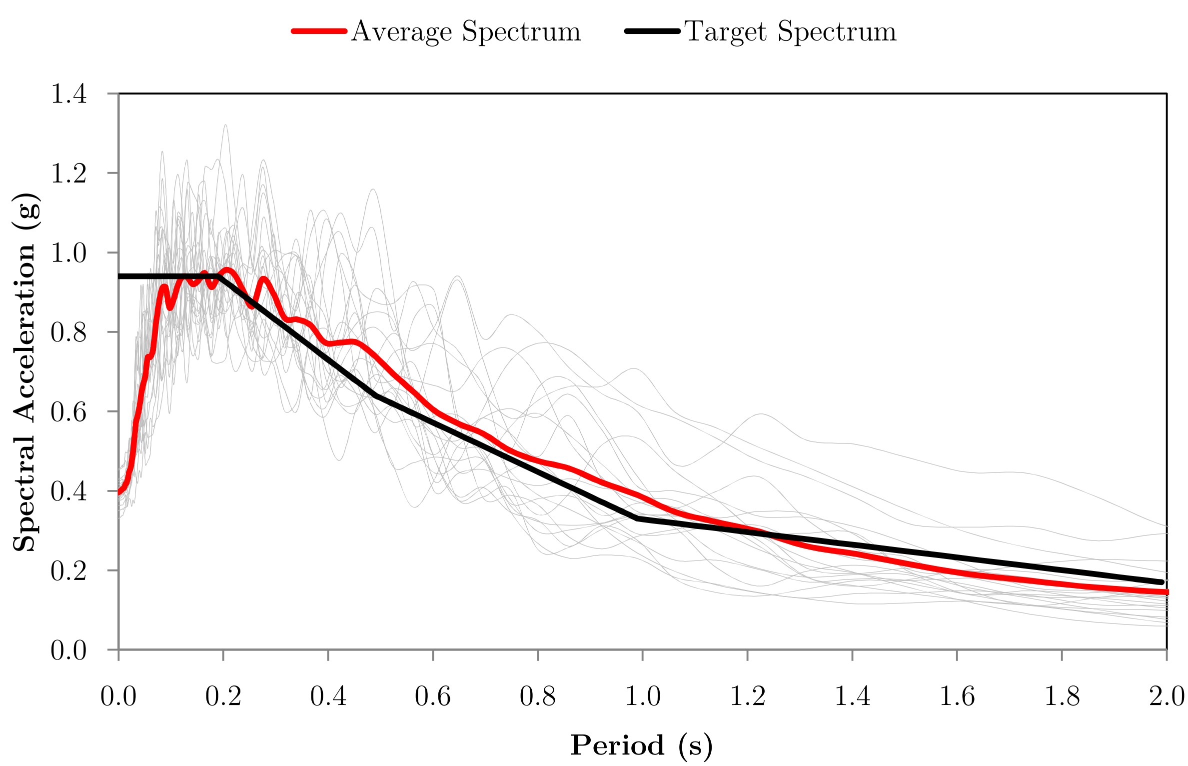

Figure 3-8: Spectra of scaled ground motions for Vancouver

The sudden jump observed at 0.5s in Figure 3-7 is explained by Atkinson's intention in providing a rich content to longer-period structures in set 7c2. No apparent differences were observed during the analysis phase between this set and the other sets which were not skewed so.

3.4 Data collection

3.4.1. Damage measure

Performance-based assessment was selected for reasons explained in Section 2.5, as well as to preserve compatibility with similar work currently in progress at the University of Ottawa for reinforced concrete buildings. D'ayala et al., (1997) have shown that limit states analysis with storey drift as a damage indicator correlates well with observed damage. These are the same damage indicators used by Karbassi (2010) who used the same applied element software with relatively similar parameters as detailed in Section 2.6. The acceptance criteria for unreinforced masonry thresholds as defined by Abrams (2001) and ASCE 41 are shown in Table 3-5. The reasons explaining the inclusion of the local failure of piers will be presented in Chapter 4.

Table 3-5: Acceptance criteria for limit states

Acceptance criteria			
Drift	Immediate occupancy (%)	Life safety (%)	Collapse prevention (%)
Piers (θ_L)	0.1	0.3 $_{eff}/L$	0.4 $_{eff}/L$
Inter-storey (θ)	0.1	0.3	0.4

The damage indicators, interstorey drift (θ) and local pier drift (θ_L), can be obtained by using Equation 3-1 and Equation 3-2. The parameters shown in Table 3-5 and Equation 3-1 and Equation 3-2 are defined in Figure 3-9 and Figure 3-10.

$$\theta = \frac{\Delta}{} \tag{3-1}$$

$$\theta_L = \frac{\Delta_{top} \qquad \Delta_{bot}}{{}_{eff}} \tag{3-2}$$

Interstorey drift and local drift are able to capture the in-plane failure mechanisms of masonry which are shown in Figure 3-11. These damage measures have proven to be a reliable indicator of damage sustained by URM structures even though larger displacements and drifts may be developed without collapse of the structure (Priestley et al., 2007). Magenes (July 2010) also indicates that significant damage may be obtained in the range of 0.4 to 0.53% drift. They also proved to be consistent with the results that are presented in Chapter 4.

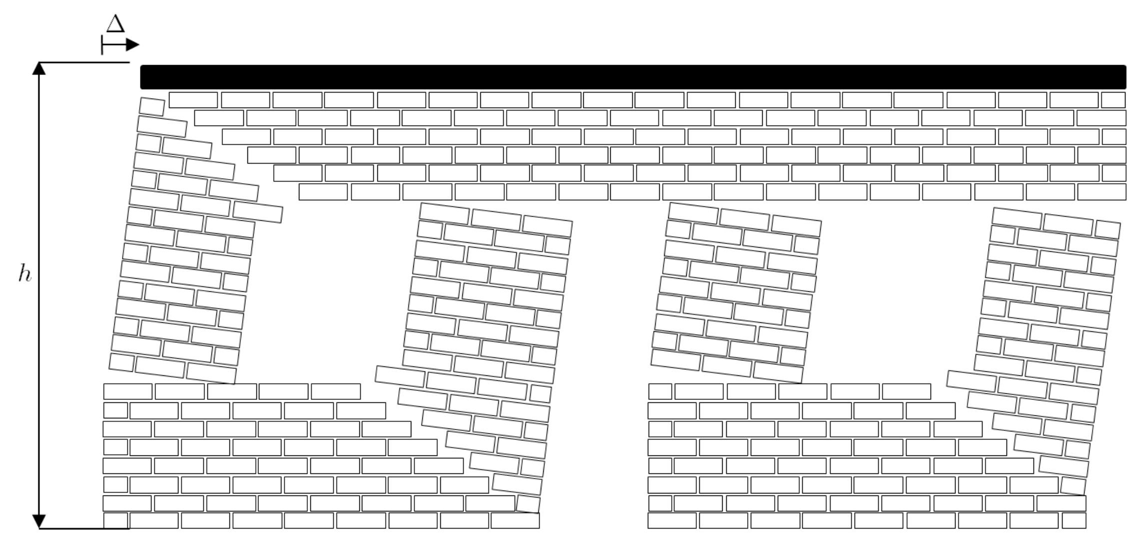

Figure 3-9: Parameters required for interstorey drift calculation

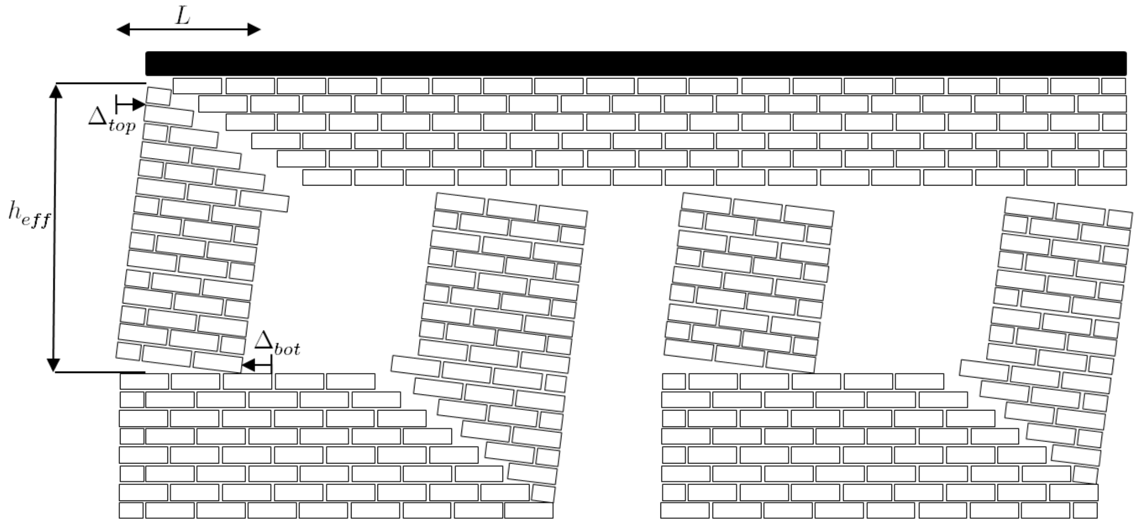

Figure 3-10: Parameters required for local pier failure calculation

(PARISI 2013)

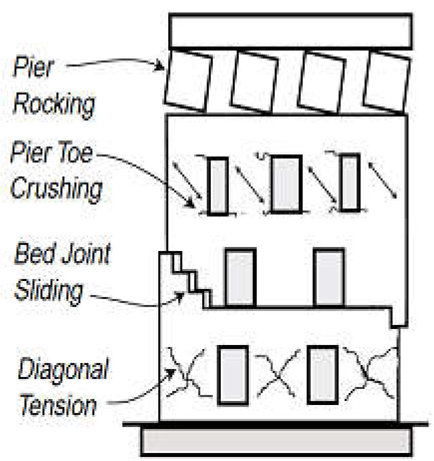

Figure 3-11: Various in-planed failure mechanisms of masonry, from Parisi and Augenti (2013)

3.4.2. Generation and display of results

In the spirit of keeping with recent trends, ongoing research at the University of Ottawa and due to their versatility, fragility curves were selected for representation of likely damage to be sustained by URM structures. The parameters required for the generation of fragility curves are obtained through incremental dynamic analysis (IDA). While the general concepts of the fragility curves and IDA were introduced in Section 2.5, the algorithm used to investigate the response of the structure was not. As presented by Vamvatsikos and Cornell (2002), the hunt and fill algorithm is useful in the quest to identify the various limit states of a given structure. The sequence of the process followed is indicated below:

Hunt

1. Increase the intensity measure (spectral acceleration in this work) by a certain step;
2. Run analysis and extract damage measures;
3. Increase the intensity measure step and repeat as required;
4. If the damage measure indicates collapse, select a spectral acceleration using bisection between the largest intensity measure that maintains the structure's stability and the smallest intensity measure creating instability until the interval size is satisfactory;

Fill

1. Select intensity measure at the middle of the widest gap of the intensity measure in the IDA curve;
2. Run analysis and extract damage measures;
3. Repeat as required.

Examples of the hunt and fill algorithm as well as advantages of the algorithm are provided in Section 4.1.

Chapter 4

Results and fragility curves

This Chapter presents the results obtained from the analytical procedure described in Chapter 3. Moreover, the means by which they were obtained are detailed. Due to the size of the investigation, the focus is placed on a single branch of the study – the others follow the same procedure.

The discussion in Sections 4.1 and 4.2 pertain to data originated from the first category of buildings presented in Section 3.6, i.e., a mid-rise URM building built in pre-code era with large openings, situated in the city of Ottawa. The ground motion used is E6c1_1. Other relevant information is available in Appendix B.

4.1 Application of incremental dynamic analysis

The ground motion records are scaled up and down to conduct incremental dynamic analysis, as explained in Section 3.5, providing reasonably accurate response of the structure compared to that resulting from an actual earthquake of similar intensity. In this case, the accelerogram that matches the 2010 NBCC UHS for the city of Ottawa is selected as ground motion to represent the intensity measure of the earthquake. The accelerogram and its response spectra are shown in Figure 4-1 and 4-2. The procedure described in the following subsections is used to construct the fragility curves.

4.1.1. Hunt and fill algorithm

In order to use the hunt and fill procedure described by Vamvatsikos and Cornell (2002), the accelerogram is first scaled down to investigate the structure's response at the lower levels of intensity measures (spectral acceleration or peak ground acceleration). The ensuing scaled accelerogram is then used to excite the structure and calculate the interstorey drifts, which was selected as the damage measure in this study. The results for the second storey are shown in Figure 4-3 where the left y-axis shows the displacement in millimeters while the right y-axis shows the equivalent drift as a percentage of the second storey height. For this intensity level, the largest relative displacement occurred at the second storey and hence was selected for this figure; the other two storeys are not shown to enhance clarity. At higher levels of intensity, where the damage approached collapse, the critical inter-storey drift was exclusively at the first storey level, indicating that the first mode of response governed collapse. However, immediate occupancy performance level was often reached at the second floor which shows that the second and third mode response certainly have an important contribution in the damage sustained by the mid-rise structure.

The maximum response is determined to be 0.24% for the second storey at 21.44 sec, which coincides with the large impulse of the ground motion seen in Figure 4-1. Because this drift level appear is in between the immediate occupancy and life safety levels defined in Section 3.5, the next step requires scaling the accelerogram at a slightly higher/lower level and repeating the steps up until this point. This process is repeated a minimum of 10 times (when the structural response is within acceptable range without local or global failure) for each accelerogram and parametric combination to ensure that there is no so-called structural resurrection as can be seen in Figure 4-4. Even if all performance levels appear to be identified prior to the 10 different scaled intensities of the ground motion, the objective of the hunt and fill algorithm is to eliminate potential situations where a mathematical setup is able to keep the analytical structure standing by reversing the loading with sufficient impulse, preventing collapse that would occur at a lower level of ground motion from the same accelerogram. This case of false stability is called structural resurrection; in order to avoid missing critical instability of the structure, more attention is required in the hunt and fill algorithm in the higher damage measure range. An example of this phenomenon can be observed at around 0.70g in Figure 4-4 below. The exact number of runs to be performed for a given accelerogram is decided based on the behavior of the IDA curve and the necessity to fill in the gaps in between the various intensities that were investigated up until then.

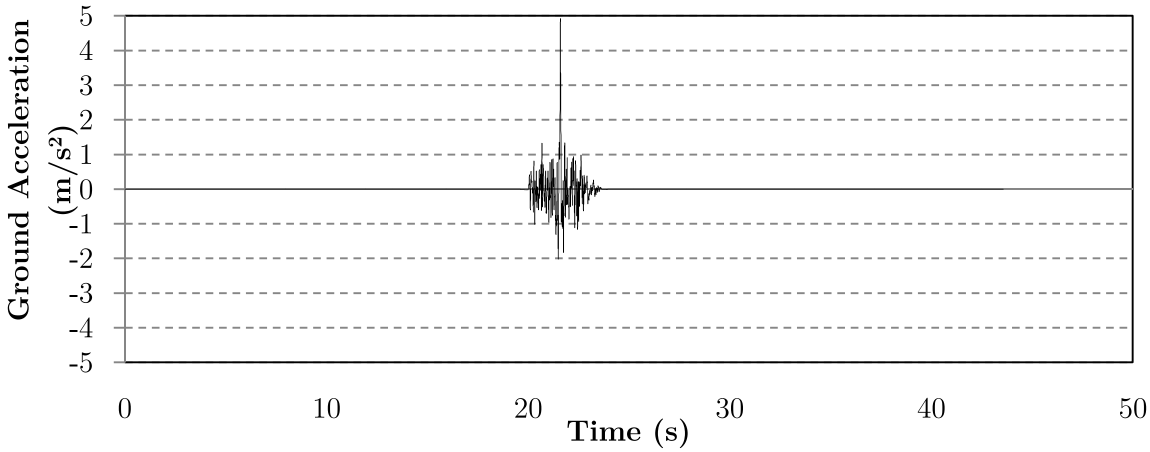

Figure 4-1: Base accelerogram for IDA

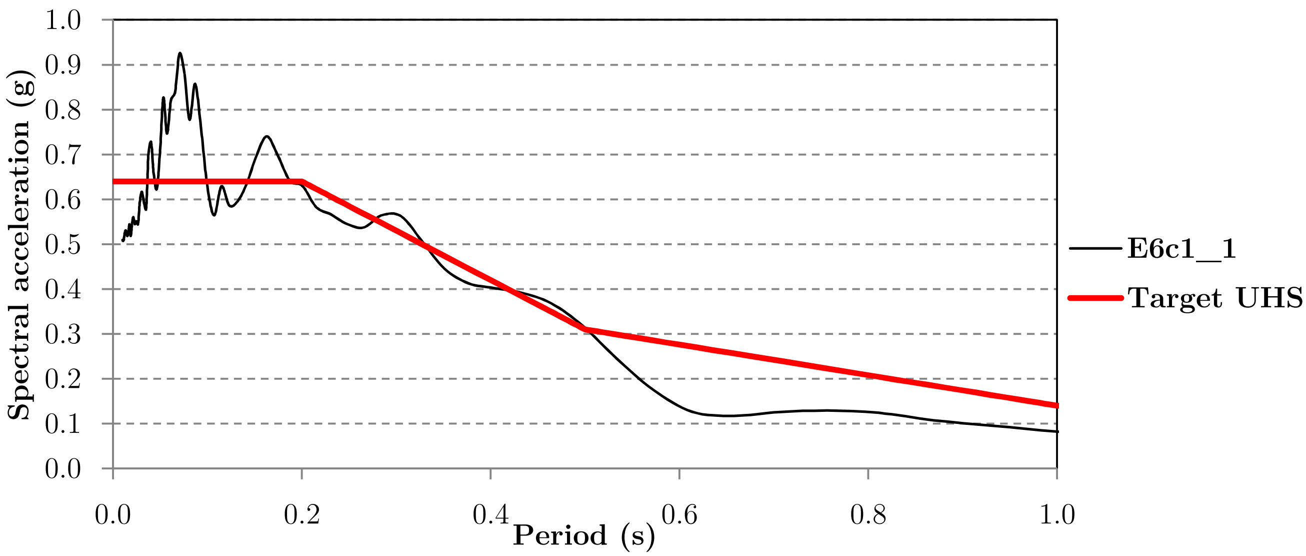

Figure 4-2: Response spectra of base accelerogram for IDA

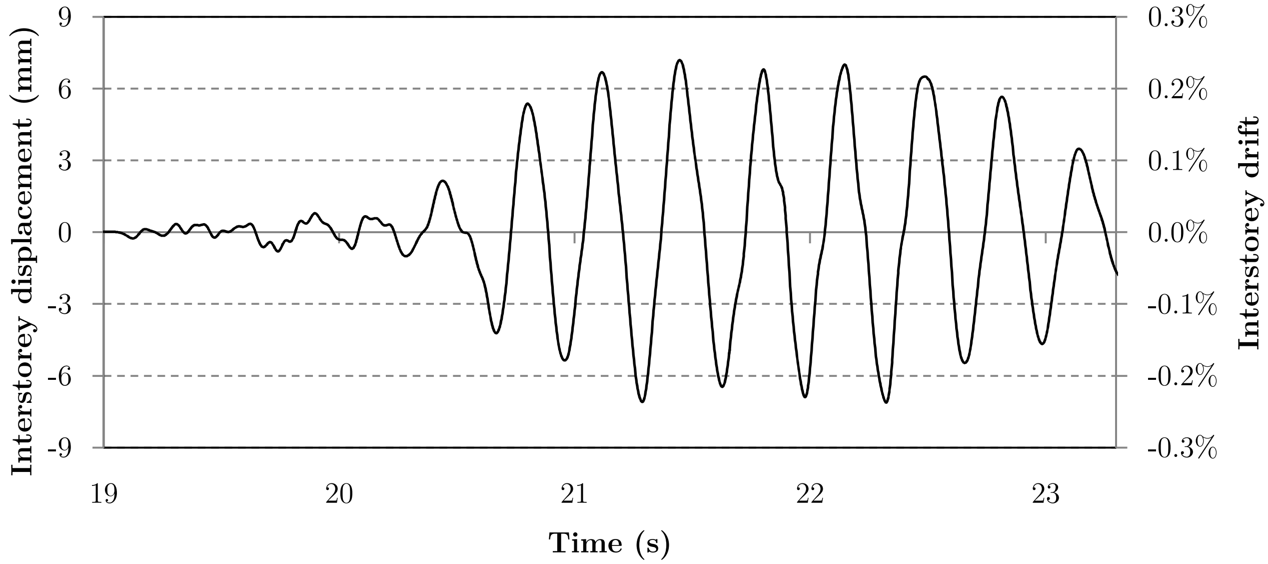

Figure 4-3: Mid-rise second storey response to E6c1_1

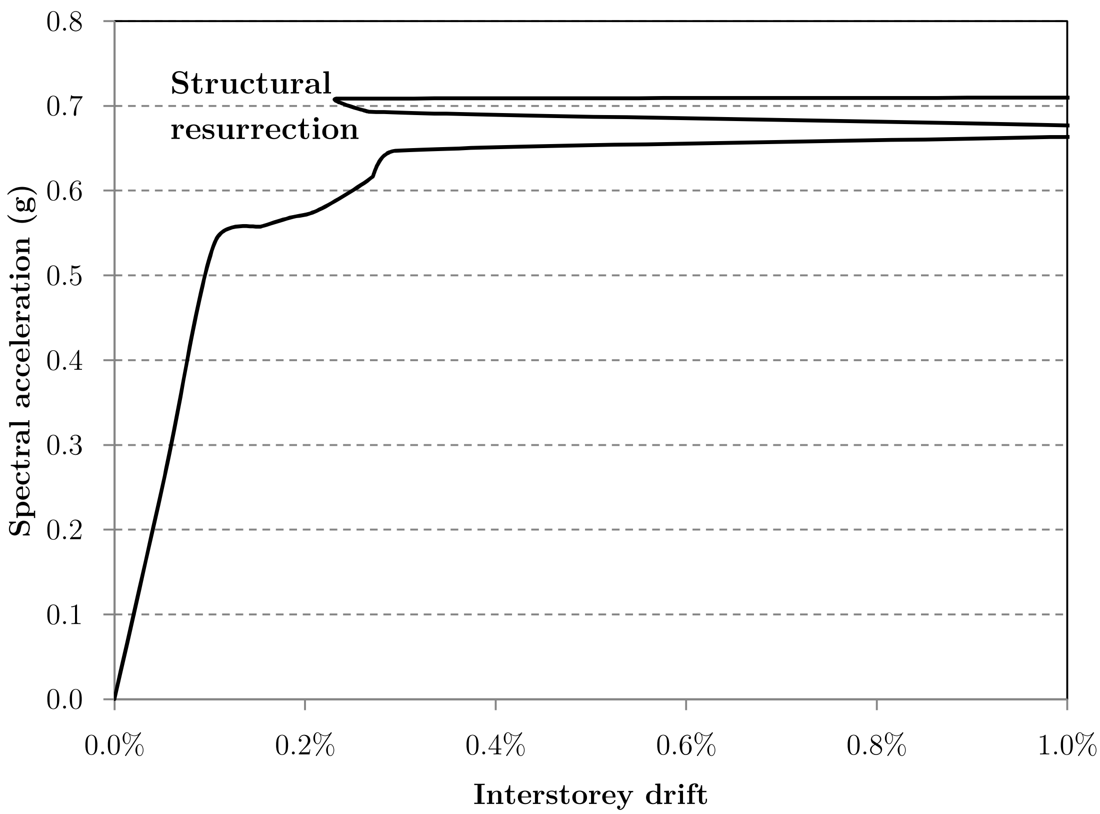

Figure 4-4: Structural resurrection IDA

In the case of this accelerogram and the parameter combinations, structural resurrection was not an issue and a relatively continuous curve was obtained. The curve showed progressively increasing collapse drift through larger and larger displacements as the intensity measure was scaled upwards. A total of 15 intensities were used in generating Figure 4-5. The last step consisted of determining the appropriate performance levels that were defined in Section 3.4. While the general interstorey drift levels of 0.1%, 0.3% and 0.4% are used as a guide for immediate occupancy, life safety and collapse prevention limit states, the actual behaviour of the structure may necessitate the adjustment of this criterion for the collapse prevention limit state as structural instability may occur before or after its 0.4% interstorey drift limit. In Figure 4-5, a tendency for structural instability is not clear. At around 0.80g, there is slight flattening of the curve, but observation of the simulation does not indicate instability. As a result, the steps identified in the following subsections were used to determine the intensity corresponding to each performance level.

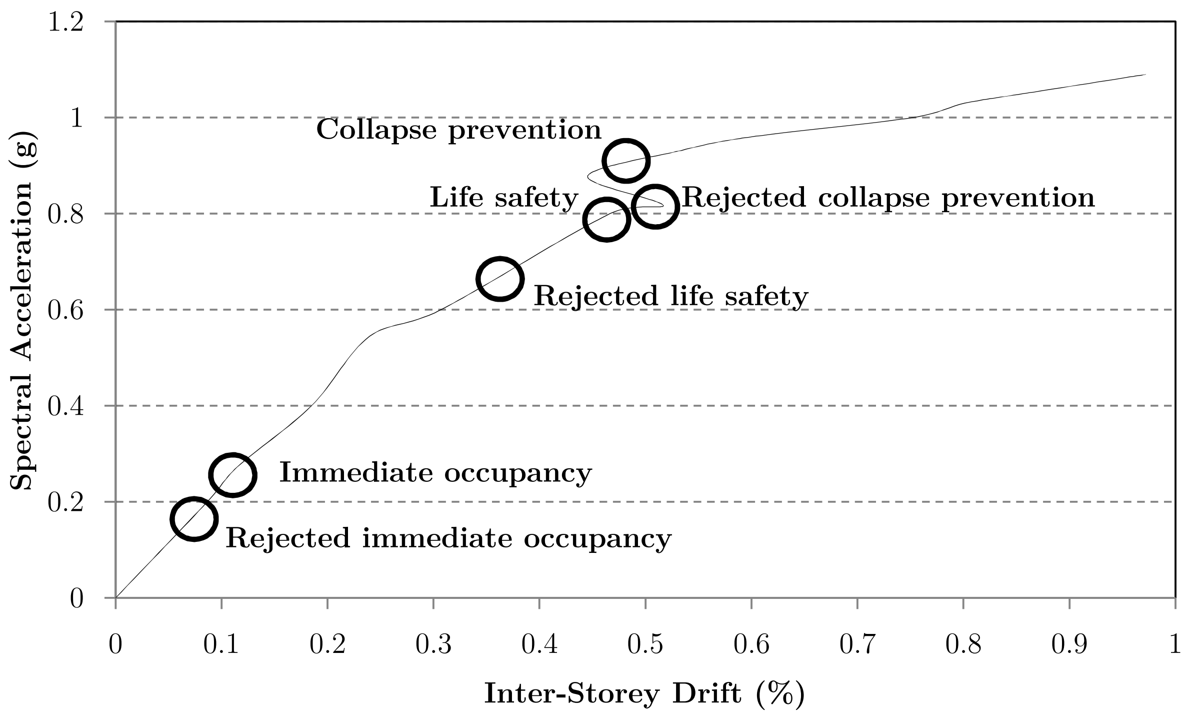

Figure 4-5: Base IDA curve, E6c1_1

4.1.2. Identification of immediate occupancy

In the case of immediate occupancy, the general guideline of 0.1% drift holds true most of the time based on the observed physical behaviour of masonry. When it does not, the definition from FEMA 356 is used to interpret the intensity, which more or less corresponds to the start of the non-linear portion of the IDA curve: "Minor cracking of veneers (less than 1/8" width); minor spalling in veneers at a few corner openings; no observable out-of-plane offsets."

Prior to yielding, as indicated by a change in slope of the IDA curve, cracking was not observed in the analysis. Once the initial secant of the IDA curve starts wearing off, the immediate occupancy performance level is identified. In Figure 4-5, the initial secant wavers slightly before 0.09% drift at 0.20g. However, the change is rather insignificant and the structure starts showing the effects of non-linearity at around 0.27g at an interstorey drift level of 0.115%.

4.1.3. Identification of collapse prevention

Before moving on to life safety, it is beneficial to first cover the collapse prevention (CP) performance level due to the fact that life safety is typically defined as a function of CP for URM. In Section 3.4, CP was defined as interstorey drift of 0.4%. The FEMA 356 definition suggests that veneer and face course may peel off which eventually leads to falling hazards and risks of eventual collapse and loss of lives. This can be clearly identified by the flattening of the curves to indicate structural instability (Vamvatsikos and Cornell, 2002). Another method suggested by the same authors is to use the FEMA 350 rule which suggests taking the last point on the IDA curve from where on the slope is equal to less than 20% of the initial elastic tangent. This can be useful when an IDA curve does not soften immediately but shows hardening and weaving behaviours as is the case of the IDA in Figure 4-5. Care must be exercised to ensure that a local flattening is not prematurely identified as structural instability and higher intensities should be evaluated to confirm whether to reject such points as a performance limit. In the case of Figure 4-5, a local flattening was observed slightly above 0.80g, but further investigation shows that the structure is not in immediate risk of collapse. As a result, this point is rejected as CP level and the next intensity featuring a slope less than 20% of the initial secant is chosen as collapse prevention limit at 0.88g and a drift of 0.45%. While the structure has not yet collapsed and does not do so before a spectral acceleration of 1.1g, inspection of the simulated earthquake showed extensive cracking, major permanent offsets and some peeling in the opening corners at the chosen intensity as well as subsequent ones. This was considered to have met all the criteria required for collapse prevention and was identified as the CP limit because the risk to human life became significant.

4.1.4. Identification of life safety

Life safety (LS) performance level is not very well defined in the literature and concern exists on the distance between LS and the other two performance levels (ASCE 41; Priestley, 2000). As a result, uncertainty remains when dealing with this limit. By default, it is defined as 75% of the collapse prevention deformation level as shown in Section 3.4 where LS is defined as 0.3% compared to the 0.4% of the CP limit. As a supplement, engineering sense may be used when a clear demarcation can be identified, for instance the onset of greater damage prior to the appearance of structural instability which would indicate the collapse prevention level. In Figure 4-5, the 0.3% drift definition seems inadequate when the CP limit was chosen as 0.45% with an intensity of 0.88g. 75% of the CP limit would be more revealing with a drift of 0.33% and intensity of 0.66g. However, looking slightly further along the curve, the onset of greater damage can be seen at an intensity of 0.80g, before the rejected collapse prevention limit. As a result, a decision was made to define the LS point at that intensity rather than the typical definitions mentioned earlier.

The examples provided in Subsections 4.1.2, 4.1.3 and 4.1.4 are meant to showcase how poorly behaving IDA curves are handled. In most cases, the definitions of the limit states provided in Section 3.4 proved to be adequate in identifying the IO, LS and CP levels.

4.1.5. Local failures as indicators

In addition to the previous discussion, local failure of piers is considered as described in Section 3.4. This approach is useful in confirming the selection of limit states when they are difficult to identify through the IDA curve. For the given IDA curve of Figure 4-5, local failure of piers was not necessary to identify the limits but it was used to confirm them. In order to explore this method, a different accelerogram is selected and its IDA curve is shown in Figure 4-6.

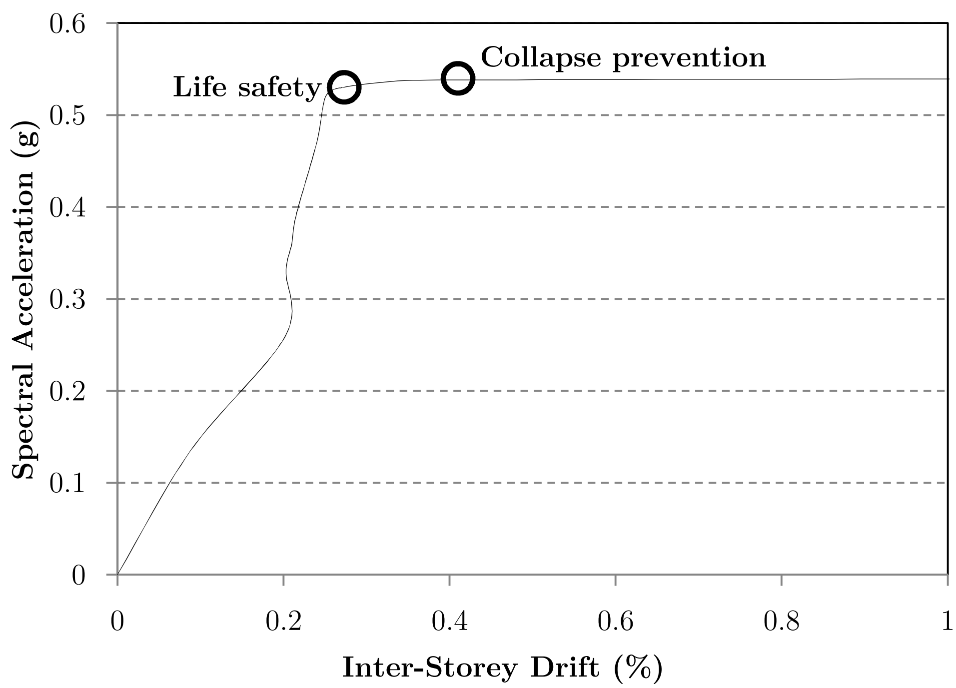

Figure 4-6: IDA curve for E6c2_1

For this ground motion, it was found that the LS and CP levels differ only slightly at spectral accelerations 0.52g and 0.54g, respectively. This initially suggested that the 75% displacement rule was not producing a representative evaluation of the structural damage, however a closer look at the state of individual piers for each of the two intensities revealed a significant difference between the two. Displacement and relative drift of one of these piers is shown Figure 4-7 and Figure 4-8 for CP level as well as in Figure 4-9 and Figure 4-10 for LS level.

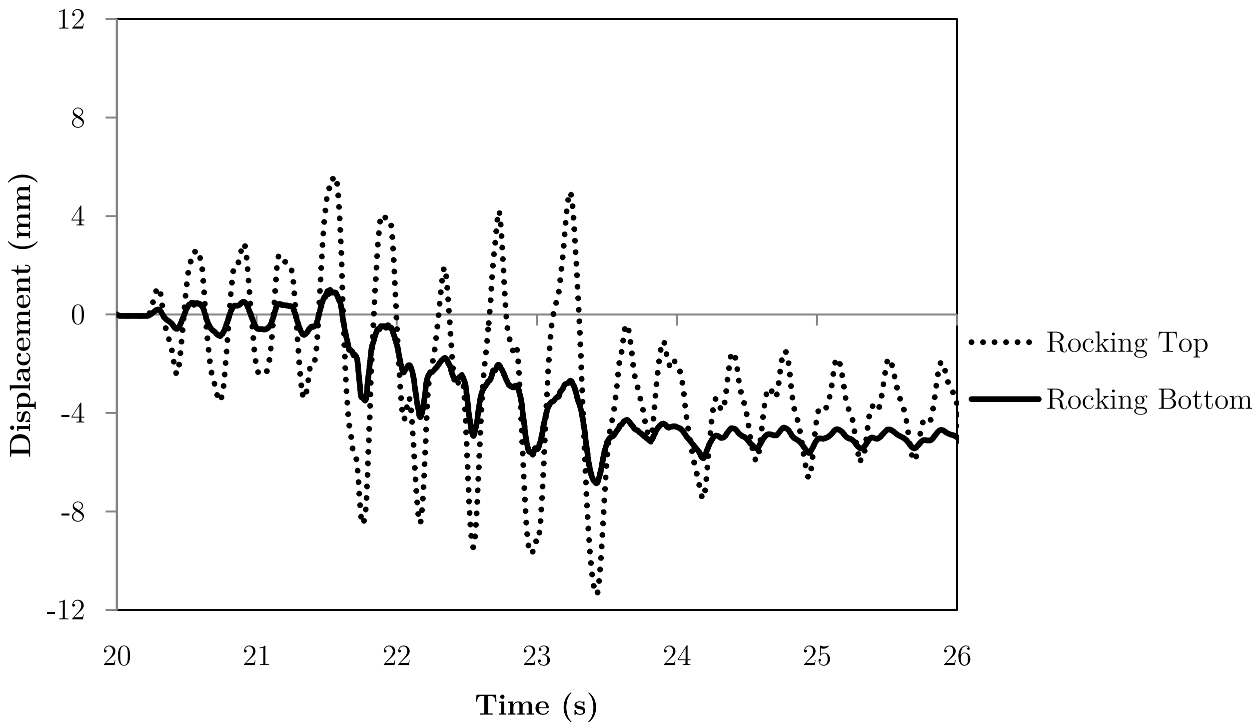

Figure 4-7: Rocking of individual pier at CP level

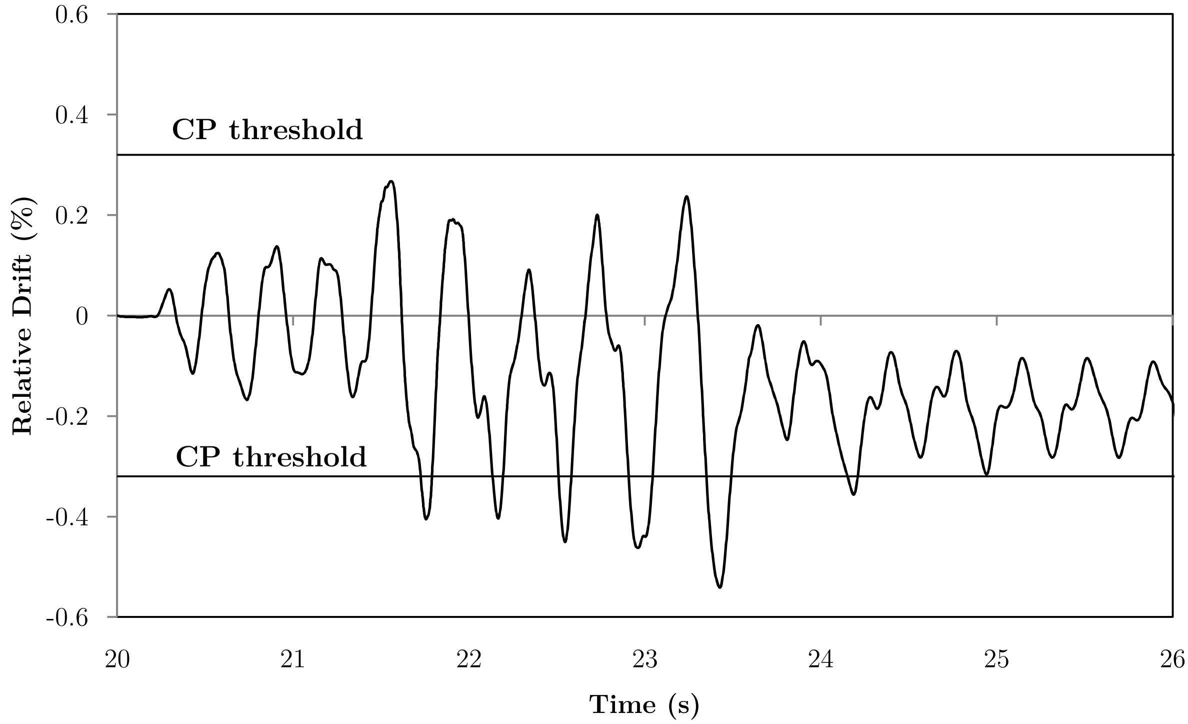

Figure 4-8: Relative drift of individual pier at CP level

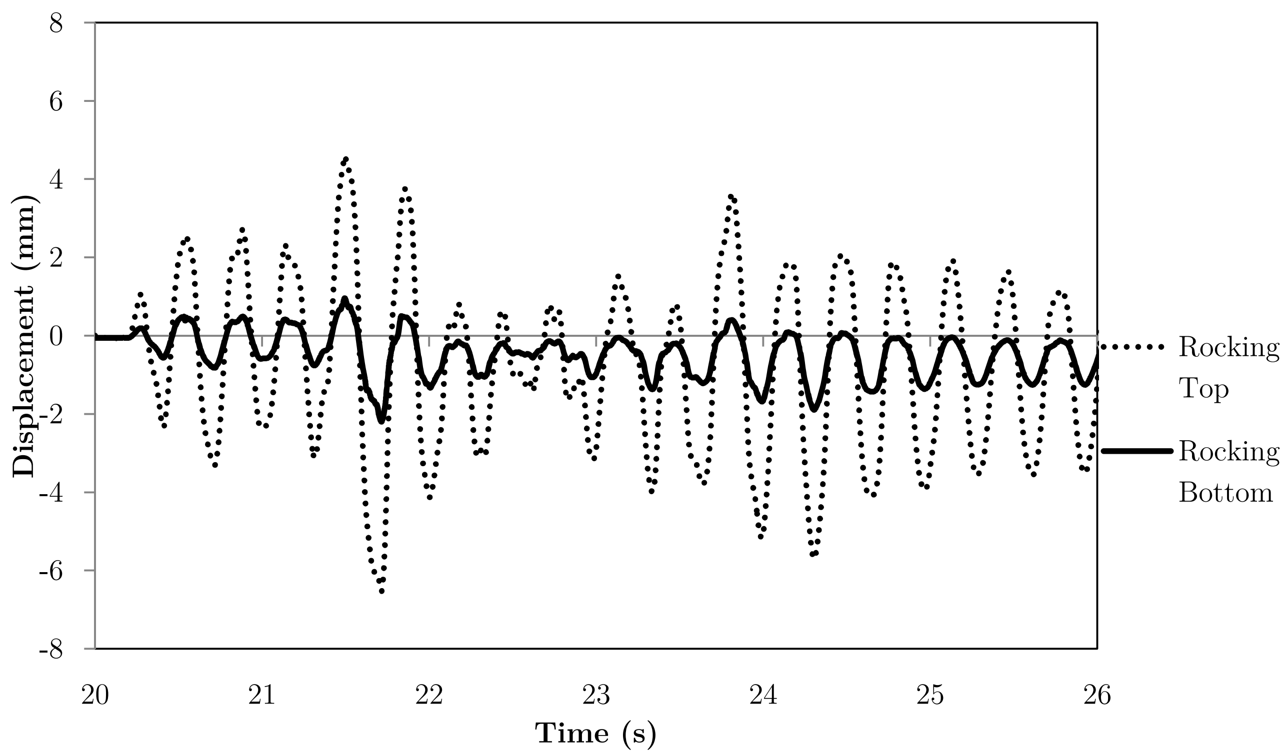

Figure 4-9: Rocking of individual pier at LS level

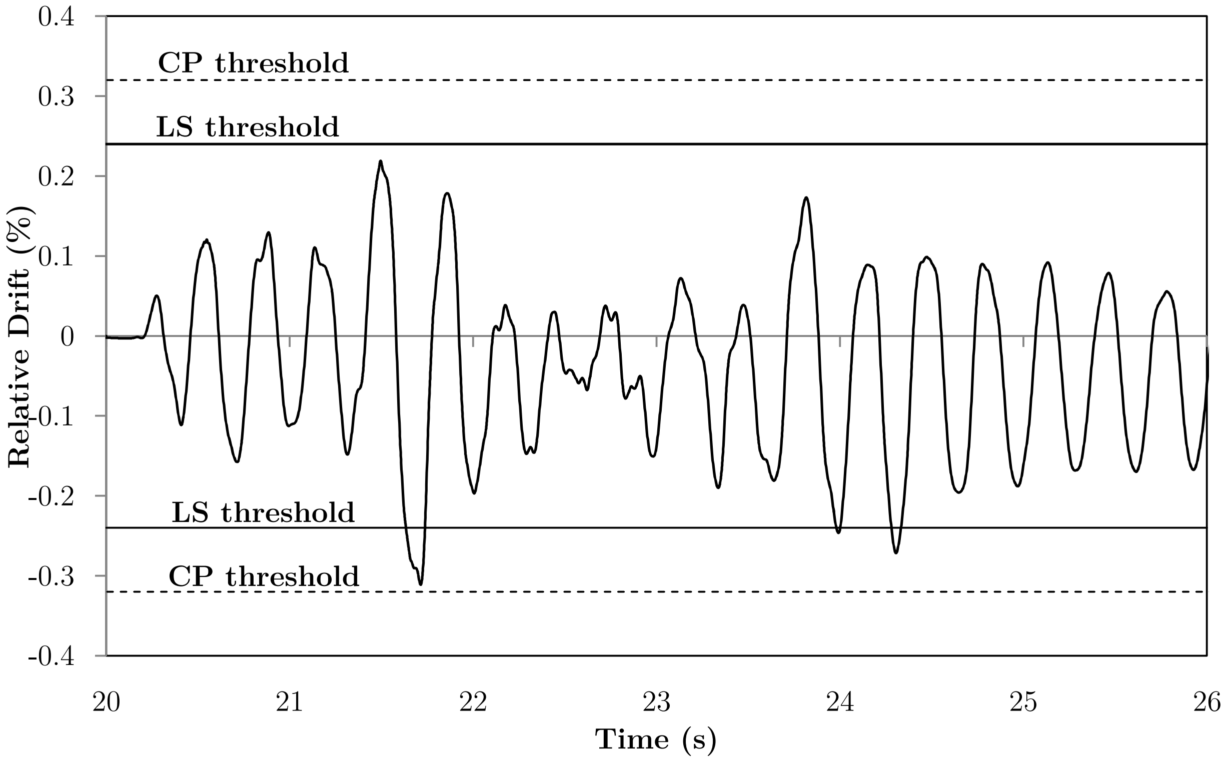

Figure 4-10: Relative drift of individual pier at LS level

While inspecting the differences between Figure 4-8 and Figure 4-10, it is clear that the behavior of the pier at the selected LS level exhibits great damage since it comes very close to the CP threshold, once the ground motion recedes, the pier rocking slowly diminishes under free vibration and the permanent drift becomes very small. On the other hand, the pier at the CP limit crosses the threshold on multiple occasions and the permanent drift remains at a level approaching the LS threshold. The structure remains intact after the earthquake, yet Figure 4-6 clearly shows that a slight intensity increase will make it collapse as the IDA curve becomes completely linear. These thresholds were also verified for lower intensities than the selected LS limit. While some of the piers would cross the LS threshold, the majority remained under the limit and moreover, the interstorey drift of the structure did not meet the 75% displacement rule of the collapse prevention performance level.

4.2 Summary of incremental dynamic analysis

Overall, the entire process presented in Section 4.1 was repeated for all the parameter combinations and for each of the 20 accelerograms associated with each case, for a total of over 3000 time history runs. Due to the magnitude of information this represents, the results are presented through the multiple-record IDA curves associated with each parameter, as well as their corresponding limit states. Discussion of results is presented in Chapter 5.

During the course of the analysis, it was observed that low-rise structures of more recent construction, referred to as low-code, were susceptible to out-of-plane failures prior to in-plane failures. This was contrary to the modeling objectives of the current research. Therefore, the results are not presented here, as extensive research focused on the topic exists in the literature. Nonetheless, the observed phenomenon is discussed in Chapter 5.

4.2.1. Mid-rise URM – Eastern Canada

Pre-code and large openings

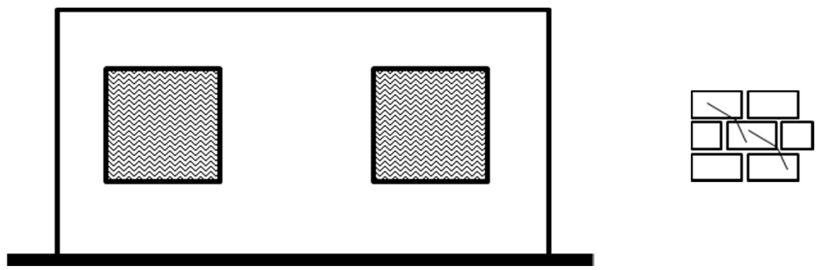

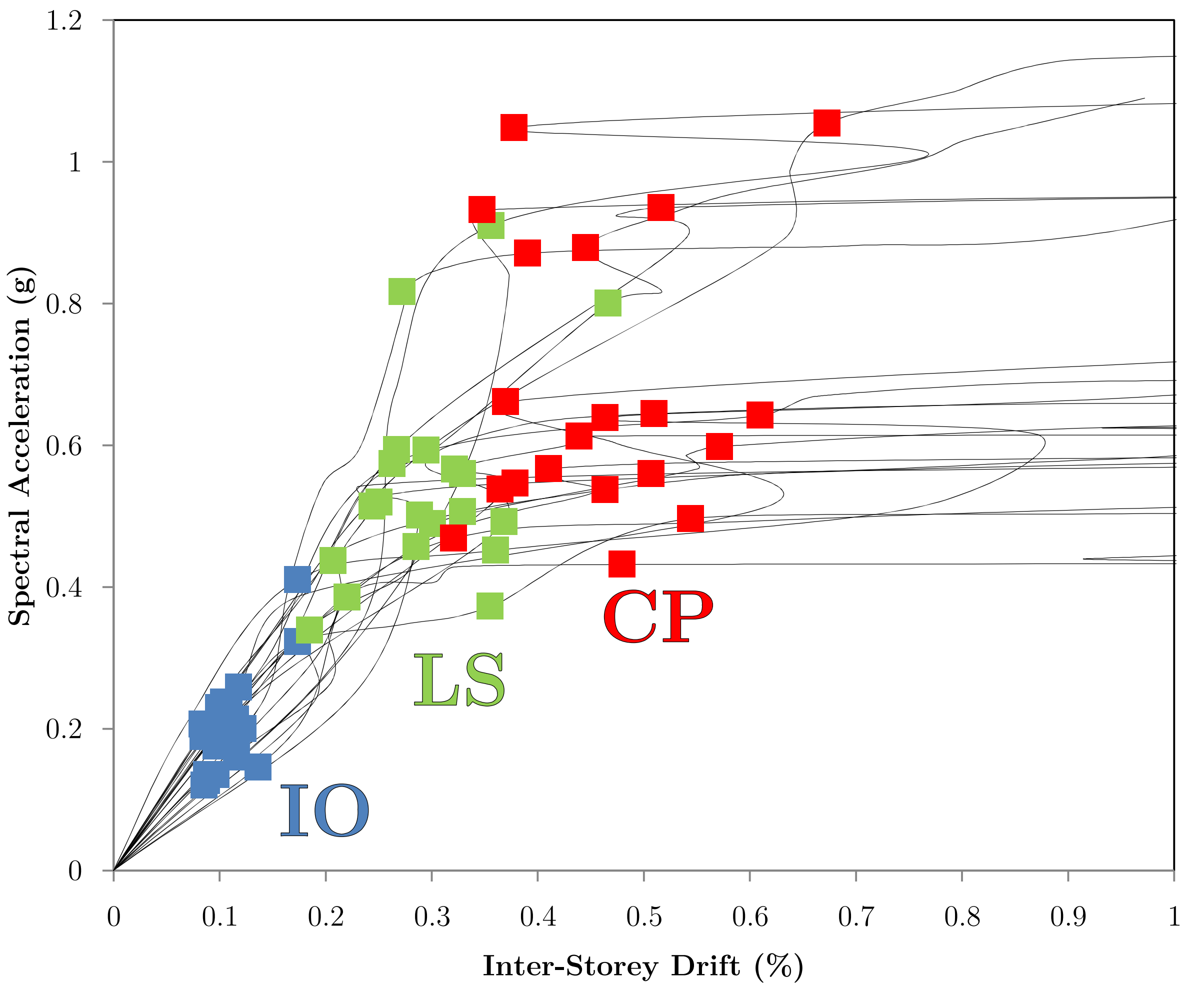

Figure 4-11: Mid-rise, pre-code, large openings IDA curve (E)

Table 4-1: Mid-rise, pre-code, large openings limit states (E)

	IO			**LS**			**CP**		
	Sa (g)	PGA (g)	ISD (%)	Sa (g)	PGA (g)	ISD (%)	Sa (g)	PGA (g)	ISD (%)
e6c1_1	0.200	0.184	0.086	0.800	0.737	0.467	0.878	0.809	0.445
e6c1_2	0.229	0.185	0.099	0.506	0.407	0.329	0.537	0.432	0.464
e6c1_3	0.200	0.169	0.122	0.816	0.690	0.272	0.871	0.736	0.391
e6c1_4	0.206	0.130	0.084	0.574	0.362	0.263	0.642	0.406	0.610
e6c1_5	0.237	0.173	0.104	0.593	0.432	0.295	0.890	0.648	0.631
e6c2_1	0.135	0.081	0.088	0.520	0.313	0.251	0.538	0.324	0.365
e6c2_2	0.175	0.075	0.097	0.910	0.391	0.356	1.048	0.450	0.378
e6c2_3	0.411	0.311	0.174	0.452	0.342	0.360	0.639	0.483	0.464
e6c2_4	0.214	0.117	0.115	0.594	0.324	0.267	0.935	0.510	0.517
e6c2_5	0.145	0.527	0.136	0.559	0.310	0.329	0.932	0.516	0.348
e7c1_1	0.182	0.109	0.116	0.492	0.293	0.369	0.645	0.384	0.510
e7c1_2	0.259	0.153	0.118	0.437	0.259	0.207	0.661	0.391	0.370
e7c1_3	0.135	0.107	0.097	0.386	0.305	0.220	0.432	0.341	0.480
e7c1_4	0.229	0.166	0.109	0.457	0.332	0.286	0.567	0.412	0.410
e7c1_5	0.189	0.104	0.085	0.490	0.270	0.301	0.598	0.330	0.571
e7c2_1	0.204	0.107	0.111	0.566	0.297	0.321	0.613	0.322	0.439
e7c2_2	0.120	0.081	0.085	0.501	0.339	0.289	0.546	0.370	0.379
e7c2_3	0.127	0.075	0.088	0.339	0.199	0.185	0.469	0.276	0.321
e7c2_4	0.323	0.220	0.174	0.372	0.254	0.355	0.497	0.339	0.544
e7c2_5	0.160	0.083	0.117	0.514	0.267	0.244	0.559	0.291	0.507

Pre-code and small openings

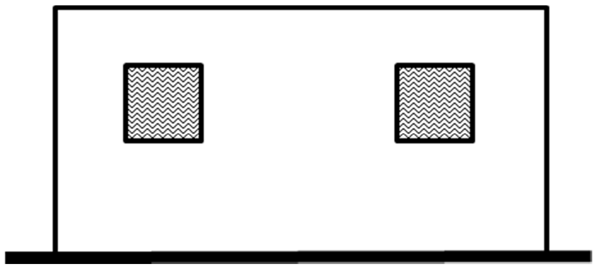

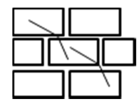

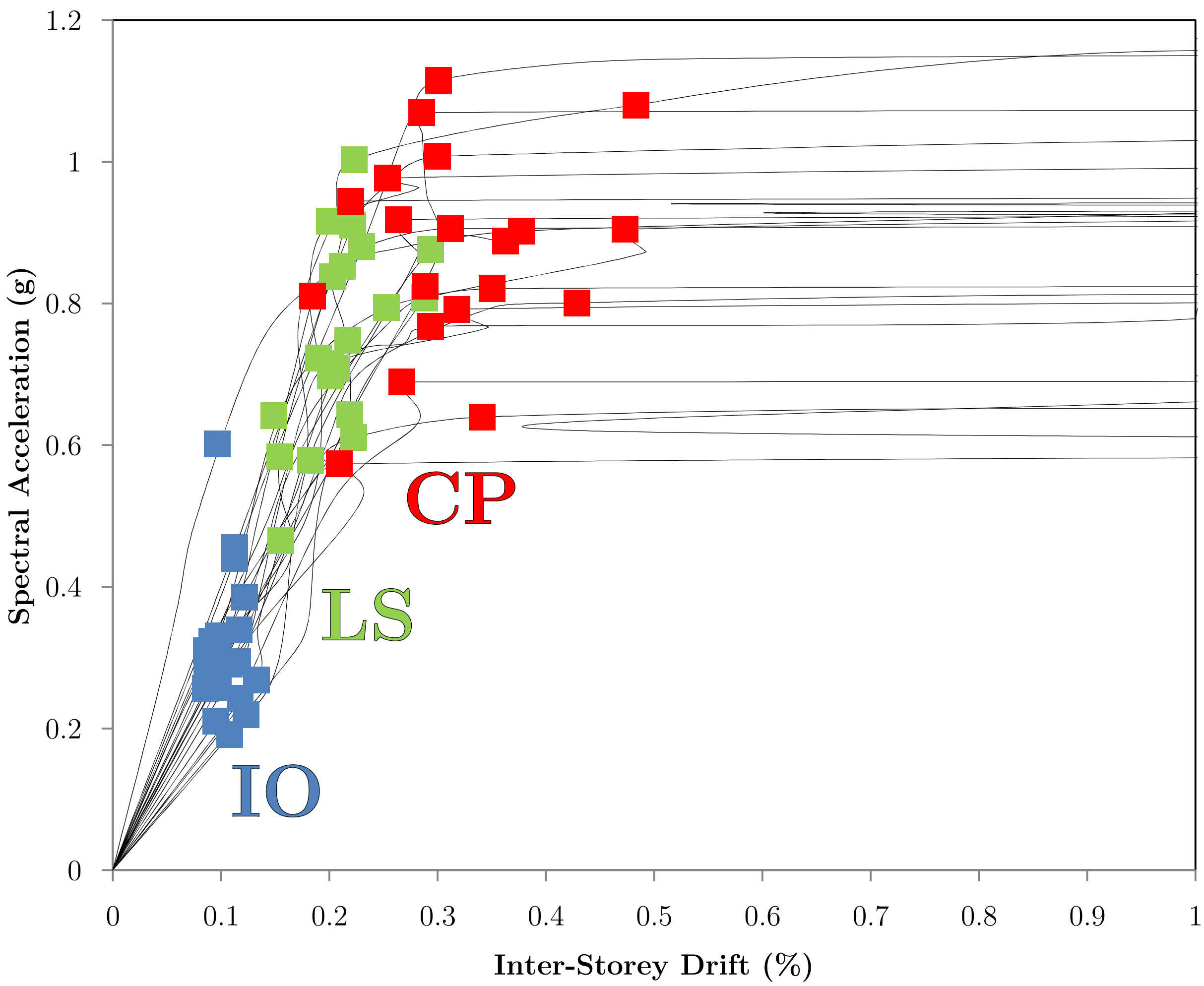

Figure 4-12: Mid-rise, pre-code, small openings IDA curve (E)

Table 4-2: Mid-rise, pre-code, small openings limit states (E)

	IO			LS			CP		
	Sa (g)	PGA (g)	ISD (%)	Sa (g)	PGA (g)	ISD (%)	Sa (g)	PGA (g)	ISD (%)
e6c1_1	0.440	0.376	0.113	0.880	0.753	0.230	1.115	0.953	0.301
e6c1_2	0.455	0.277	0.113	0.911	0.554	0.222	1.008	0.613	0.300
e6c1_3	0.386	0.230	0.122	1.003	0.598	0.223	1.080	0.644	0.484
e6c1_4	0.292	0.181	0.101	0.643	0.399	0.219	0.825	0.511	0.289
e6c1_5	0.292	0.216	0.103	0.876	0.648	0.294	0.888	0.656	0.363
e6c2_1	0.257	0.157	0.086	0.641	0.392	0.149	0.811	0.495	0.185
e6c2_2	0.292	0.145	0.087	0.583	0.289	0.155	0.945	0.469	0.220
e6c2_3	0.323	0.155	0.092	0.808	0.388	0.288	0.905	0.435	0.473
e6c2_4	0.602	0.389	0.097	0.852	0.551	0.212	0.902	0.583	0.378
e6c2_5	0.258	0.155	0.098	0.465	0.279	0.155	0.573	0.344	0.210
e7c1_1	0.339	0.147	0.117	0.916	0.396	0.201	0.977	0.422	0.254
e7c1_2	0.310	0.153	0.087	0.837	0.413	0.203	0.906	0.447	0.312
e7c1_3	0.192	0.101	0.108	0.698	0.366	0.202	0.919	0.482	0.264
e7c1_4	0.331	0.166	0.098	0.794	0.399	0.253	0.821	0.412	0.351
e7c1_5	0.269	0.132	0.133	0.708	0.348	0.207	0.768	0.377	0.294
e7c2_1	0.294	0.141	0.116	0.748	0.358	0.217	0.801	0.383	0.429
e7c2_2	0.220	0.129	0.124	0.723	0.424	0.191	1.069	0.628	0.286
e7c2_3	0.210	0.110	0.096	0.579	0.304	0.183	0.689	0.362	0.267
e7c2_4	0.291	0.169	0.108	0.611	0.356	0.223	0.640	0.373	0.342
e7c2_5	0.243	0.113	0.118	0.715	0.332	0.202	0.792	0.368	0.318

Low-code and large openings

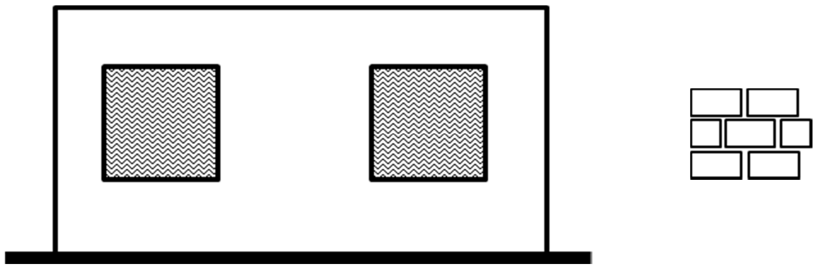

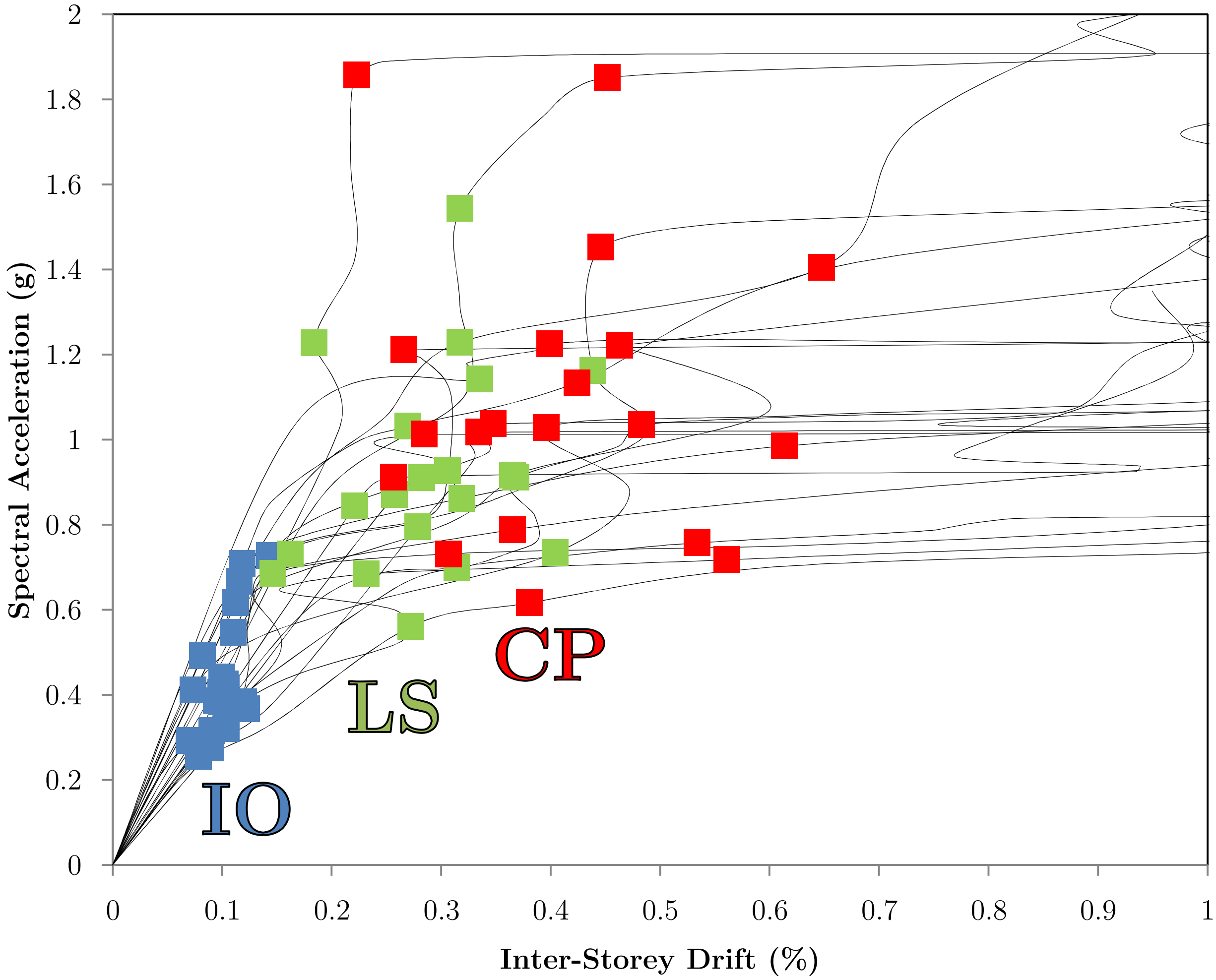

Figure 4-13: Mid-rise, low-code, large openings IDA curve (E)

Table 4-3: Mid-rise, low-code, large openings limit states (E)

	IO			LS			CP		
	Sa (g)	PGA (g)	ISD (%)	Sa (g)	PGA (g)	ISD (%)	Sa (g)	PGA (g)	ISD (%)
e6c1_1	0.492	0.351	0.082	1.229	0.879	0.317	1.404	1.004	0.648
e6c1_2	0.425	0.258	0.103	0.910	0.554	0.283	1.037	0.631	0.348
e6c1_3	0.441	0.230	0.100	1.543	0.805	0.317	1.851	0.966	0.452
e6c1_4	0.726	0.453	0.143	1.162	0.724	0.439	1.452	0.905	0.446
e6c1_5	0.616	0.540	0.113	0.862	0.756	0.319	0.985	0.864	0.614
e6c2_1	0.366	0.188	0.123	0.916	0.470	0.365	1.221	0.626	0.463
e6c2_2	0.405	0.173	0.099	0.843	0.361	0.222	0.911	0.390	0.257
e6c2_3	0.320	0.218	0.104	0.685	0.467	0.146	0.731	0.498	0.307
e6c2_4	0.708	0.405	0.118	1.031	0.590	0.270	1.133	0.648	0.424
e6c2_5	0.415	0.155	0.104	1.142	0.426	0.336	1.225	0.457	0.399
e7c1_1	0.411	0.205	0.074	0.734	0.366	0.404	1.027	0.513	0.396
e7c1_2	0.384	0.144	0.095	1.227	0.459	0.184	1.857	0.695	0.223
e7c1_3	0.383	0.168	0.100	0.870	0.381	0.258	1.012	0.444	0.285
e7c1_4	0.291	0.166	0.070	0.699	0.398	0.315	0.757	0.432	0.534
e7c1_5	0.275	0.171	0.090	0.560	0.348	0.273	0.616	0.383	0.381
e7c2_1	0.315	0.141	0.091	0.731	0.327	0.163	0.788	0.353	0.366
e7c2_2	0.254	0.136	0.079	0.795	0.424	0.279	1.017	0.542	0.335
e7c2_3	0.383	0.221	0.120	0.684	0.395	0.232	0.717	0.414	0.561
e7c2_4	0.546	0.254	0.110	0.911	0.424	0.369	1.035	0.481	0.484
e7c2_5	0.667	0.267	0.116	0.926	0.371	0.306	1.211	0.485	0.266

<u>Low-code and small openings</u>

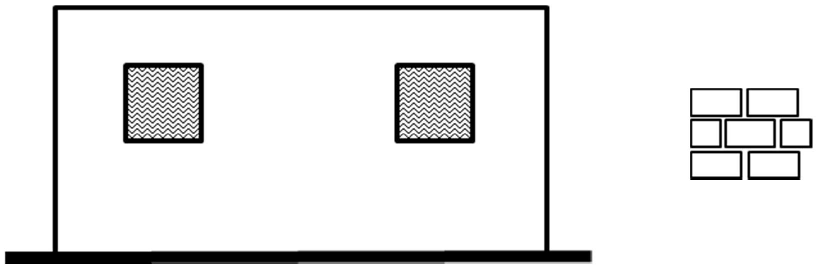

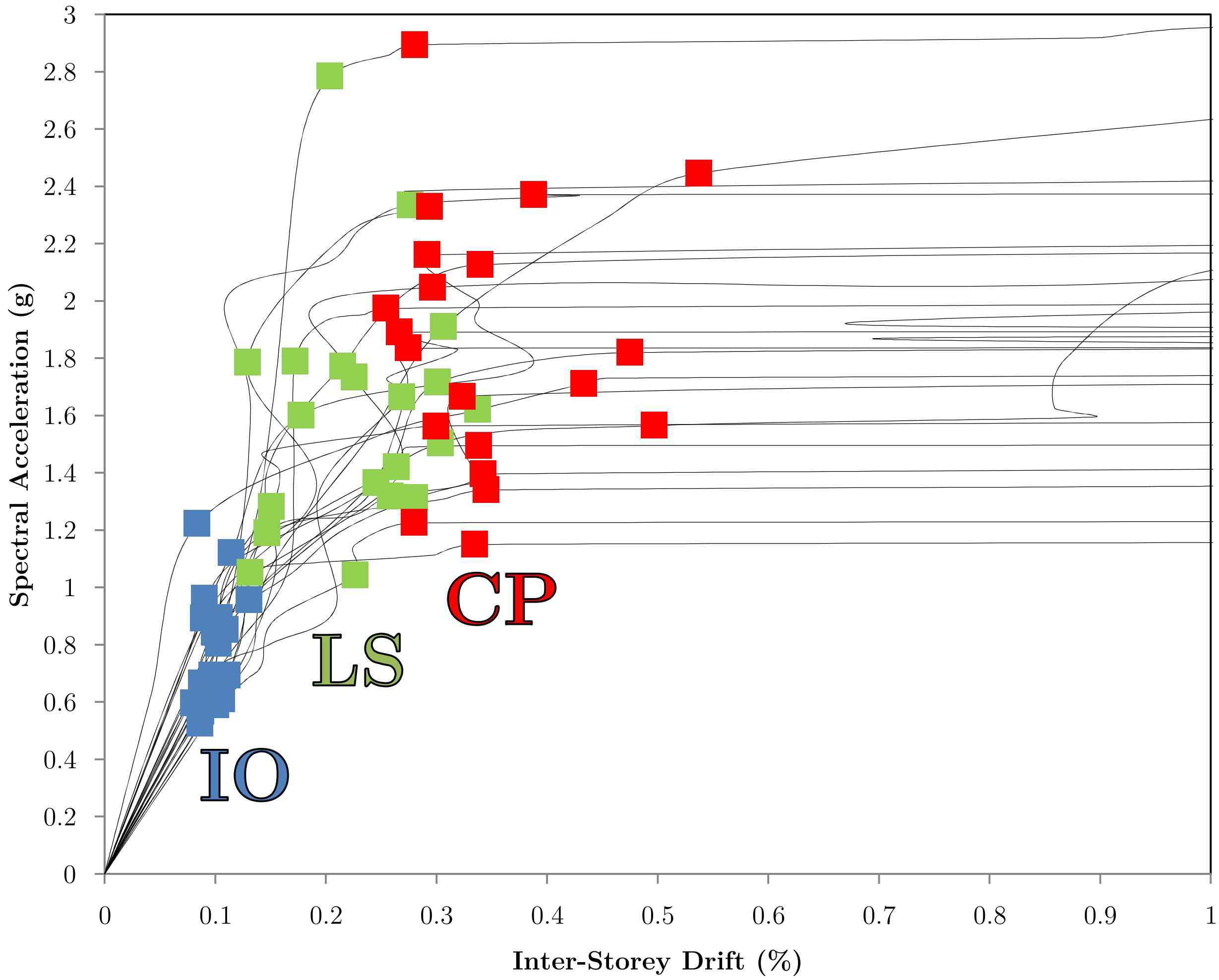

Figure 4-14: Mid-rise, low-code, small openings IDA curve (E)

Table 4-4: Mid-rise, low-code, small openings limit states (E)

	IO			LS			CP		
	Sa (g)	PGA (g)	ISD (%)	Sa (g)	PGA (g)	ISD (%)	Sa (g)	PGA (g)	ISD (%)
e6c1_1	1.223	1.004	0.084	1.620	1.330	0.338	1.712	1.406	0.433
e6c1_2	0.844	0.369	0.099	2.784	1.218	0.204	2.894	1.266	0.280
e6c1_3	0.961	0.644	0.090	1.716	1.150	0.301	1.819	1.219	0.475
e6c1_4	0.805	0.362	0.103	2.336	1.050	0.277	2.371	1.066	0.388
e6c1_5	0.694	0.432	0.097	1.735	1.080	0.226	2.047	1.274	0.297
e6c2_1	0.567	0.250	0.087	1.772	0.783	0.216	2.126	0.939	0.339
e6c2_2	0.595	0.289	0.080	1.191	0.578	0.147	1.340	0.650	0.345
e6c2_3	0.842	0.435	0.100	1.504	0.778	0.304	1.565	0.809	0.497
e6c2_4	0.612	0.259	0.106	1.911	0.810	0.307	2.446	1.037	0.537
e6c2_5	0.955	0.434	0.130	1.364	0.620	0.245	1.835	0.834	0.275
e7c1_1	0.641	0.293	0.093	1.281	0.586	0.151	1.563	0.715	0.300
e7c1_2	0.895	0.459	0.104	1.312	0.673	0.281	1.396	0.716	0.342
e7c1_3	0.694	0.305	0.111	1.319	0.580	0.258	1.667	0.732	0.323
e7c1_4	0.525	0.332	0.086	1.050	0.664	0.132	1.150	0.727	0.335
e7c1_5	0.853	0.522	0.109	1.421	0.870	0.264	1.495	0.915	0.338
e7c2_1	0.688	0.282	0.099	1.788	0.733	0.172	1.974	0.809	0.254
e7c2_2	1.121	0.475	0.114	1.601	0.678	0.178	2.161	0.915	0.292
e7c2_3	0.893	0.276	0.090	1.785	0.552	0.129	2.330	0.720	0.294
e7c2_4	0.589	0.383	0.101	1.043	0.678	0.226	1.226	0.797	0.280
e7c2_5	0.666	0.297	0.088	1.665	0.743	0.269	1.891	0.843	0.267

4.2.2. Mid-rise URM – Western Canada

Pre-code and large openings

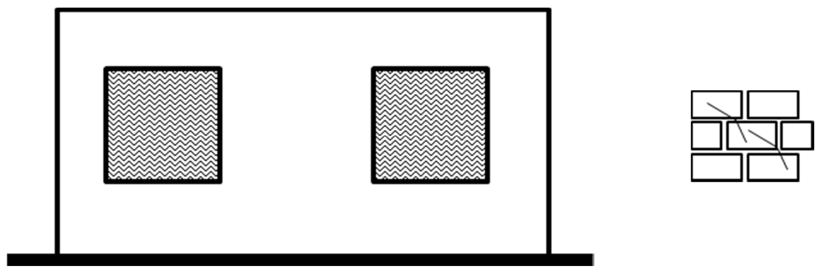

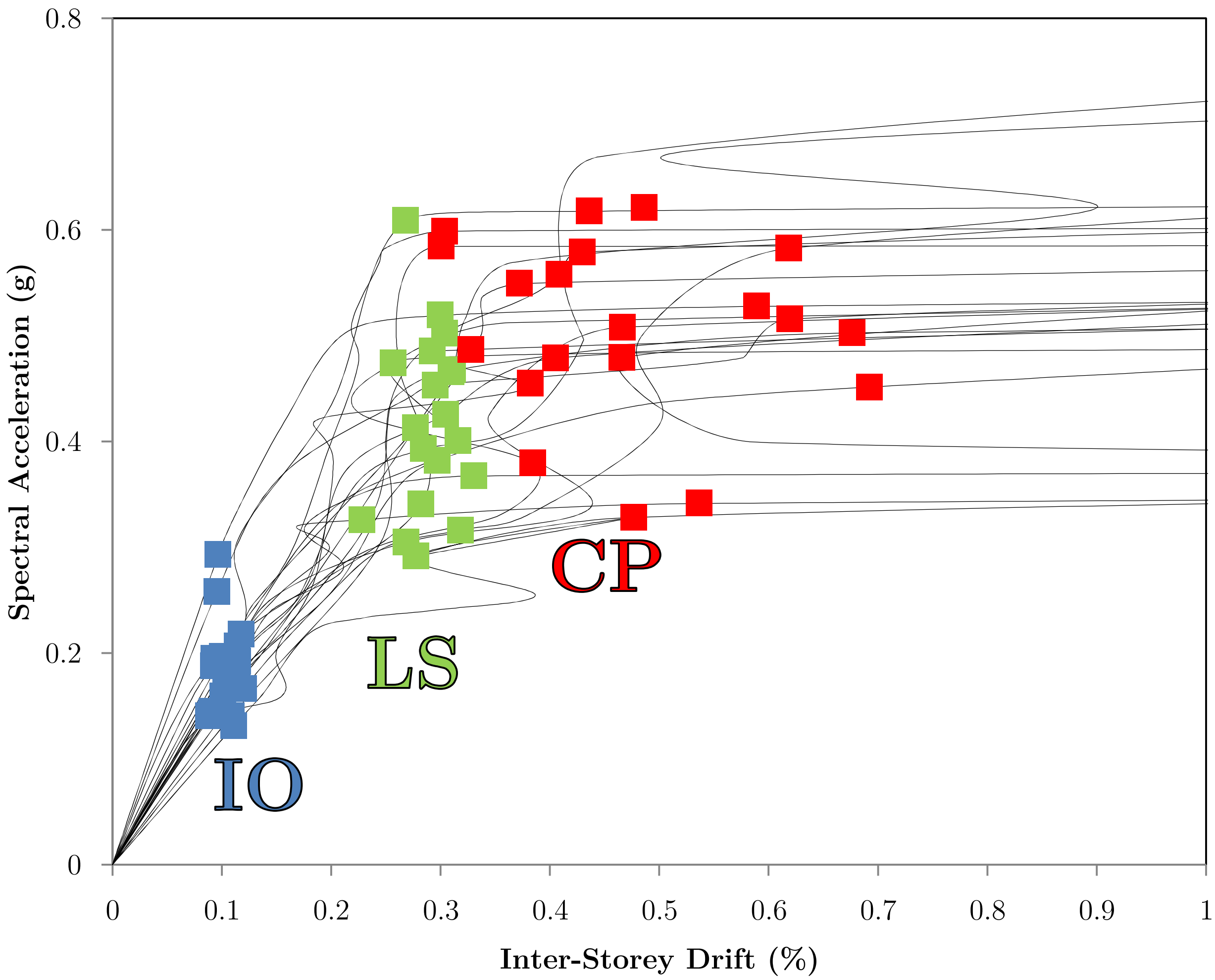

Figure 4-15: Mid-rise, pre-code, large openings IDA curve (W)

Table 4-5: Mid-rise, pre-code, large openings limit states (W)

	IO			LS			CP		
	Sa (g)	PGA (g)	ISD (%)	Sa (g)	PGA (g)	ISD (%)	Sa (g)	PGA (g)	ISD (%)
e6c1_1	0.293	0.143	0.097	0.519	0.253	0.300	0.528	0.257	0.589
e6c1_2	0.145	0.063	0.091	0.466	0.204	0.310	0.621	0.271	0.486
e6c1_3	0.258	0.148	0.095	0.453	0.260	0.295	0.516	0.296	0.619
e6c1_4	0.190	0.101	0.110	0.485	0.259	0.293	0.455	0.243	0.382
e6c1_5	0.166	0.066	0.120	0.316	0.125	0.319	0.582	0.231	0.619
e6c2_1	0.142	0.059	0.090	0.474	0.198	0.257	0.379	0.158	0.384
e6c2_2	0.174	0.083	0.114	0.382	0.183	0.297	0.452	0.216	0.692
e6c2_3	0.206	0.099	0.114	0.413	0.197	0.277	0.549	0.262	0.373
e6c2_4	0.218	0.091	0.118	0.609	0.254	0.268	0.618	0.257	0.436
e6c2_5	0.192	0.093	0.115	0.367	0.178	0.331	0.479	0.232	0.466
e7c1_1	0.167	0.060	0.104	0.502	0.180	0.304	0.558	0.200	0.409
e7c1_2	0.141	0.064	0.088	0.393	0.179	0.284	0.579	0.264	0.430
e7c1_3	0.186	0.088	0.104	0.305	0.145	0.269	0.508	0.241	0.467
e7c1_4	0.160	0.068	0.101	0.426	0.182	0.305	0.479	0.205	0.406
e7c1_5	0.197	0.095	0.101	0.599	0.289	0.304	0.599	0.289	0.304
e7c2_1	0.131	0.067	0.111	0.292	0.150	0.278	0.328	0.168	0.477
e7c2_2	0.188	0.088	0.092	0.326	0.152	0.228	0.341	0.160	0.537
e7c2_3	0.191	0.086	0.104	0.401	0.180	0.316	0.487	0.219	0.328
e7c2_4	0.195	0.077	0.093	0.341	0.135	0.283	0.584	0.232	0.301
e7c2_5	0.141	0.049	0.109	0.467	0.163	0.311	0.503	0.175	0.677

Pre-code and small openings

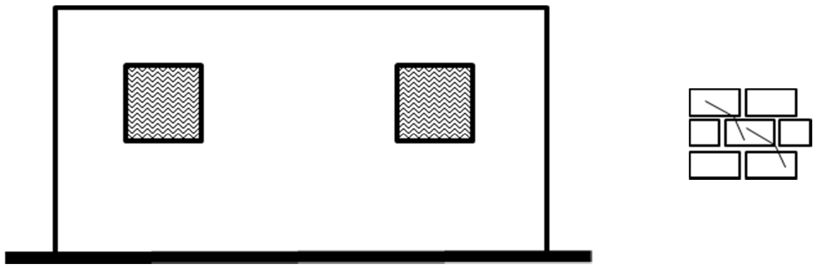

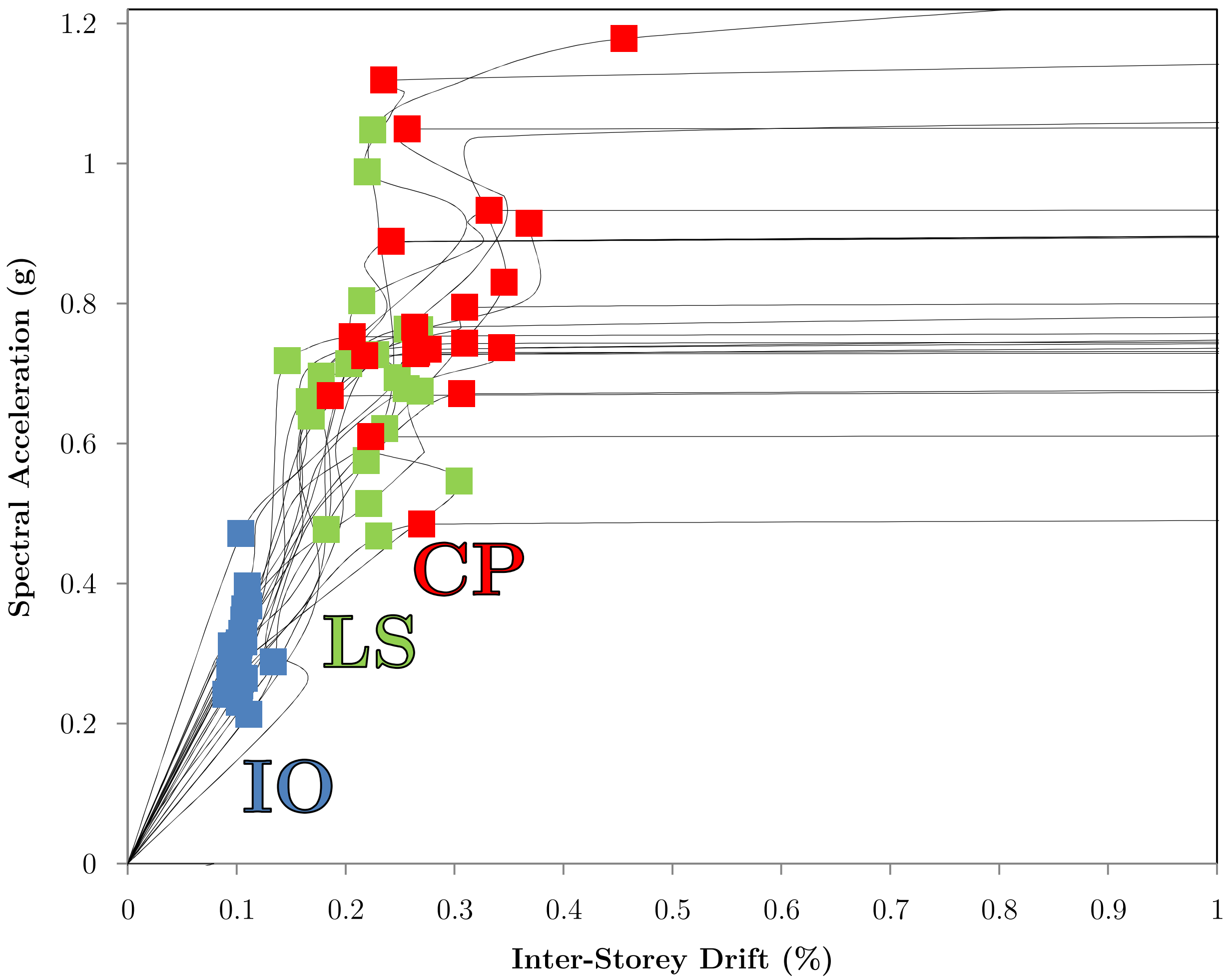

Figure 4-16: Mid-rise, pre-code, small openings IDA curve (W)

Table 4-6: Mid-rise, pre-code, small openings limit states (W)

	IO			LS			CP		
	Sa (g)	PGA (g)	ISD (%)	Sa (g)	PGA (g)	ISD (%)	Sa (g)	PGA (g)	ISD (%)
e6c1_1	0.311	0.143	0.095	0.728	0.335	0.264	0.728	0.335	0.264
e6c1_2	0.367	0.226	0.111	0.514	0.317	0.221	0.735	0.452	0.276
e6c1_3	0.363	0.159	0.108	0.678	0.296	0.256	0.736	0.321	0.344
e6c1_4	0.288	0.089	0.134	1.047	0.324	0.225	1.178	0.365	0.456
e6c1_5	0.311	0.099	0.102	0.674	0.214	0.269	0.830	0.264	0.346
e6c2_1	0.213	0.087	0.111	0.726	0.297	0.228	0.794	0.324	0.310
e6c2_2	0.316	0.154	0.107	0.718	0.349	0.147	0.752	0.365	0.206
e6c2_3	0.296	0.142	0.102	0.987	0.473	0.220	1.119	0.536	0.235
e6c2_4	0.264	0.094	0.107	0.762	0.272	0.268	0.914	0.326	0.369
e6c2_5	0.471	0.193	0.104	0.659	0.271	0.167	0.725	0.298	0.218
e7c1_1	0.328	0.144	0.105	0.639	0.280	0.169	0.730	0.320	0.265
e7c1_2	0.348	0.113	0.106	0.696	0.226	0.178	0.765	0.249	0.263
e7c1_3	0.396	0.161	0.110	0.693	0.281	0.247	0.743	0.301	0.309
e7c1_4	0.315	0.150	0.103	0.763	0.364	0.257	1.049	0.501	0.256
e7c1_5	0.241	0.114	0.090	0.804	0.380	0.215	0.933	0.440	0.332
e7c2_1	0.254	0.090	0.103	0.714	0.253	0.203	0.888	0.314	0.242
e7c2_2	0.230	0.096	0.102	0.575	0.239	0.219	0.671	0.279	0.307
e7c2_3	0.273	0.129	0.094	0.546	0.258	0.304	0.609	0.288	0.223
e7c2_4	0.286	0.116	0.095	0.477	0.193	0.183	0.668	0.271	0.186
e7c2_5	0.255	0.105	0.101	0.468	0.193	0.231	0.485	0.200	0.270

Low-code and large openings

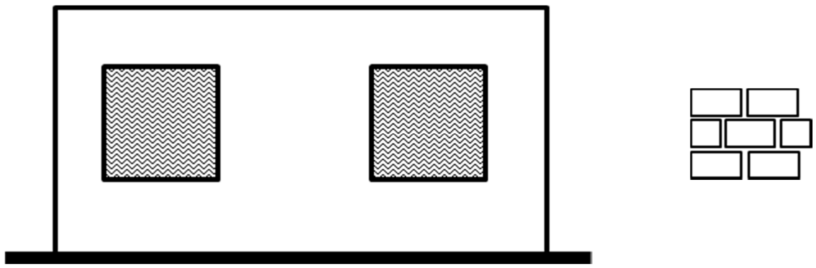

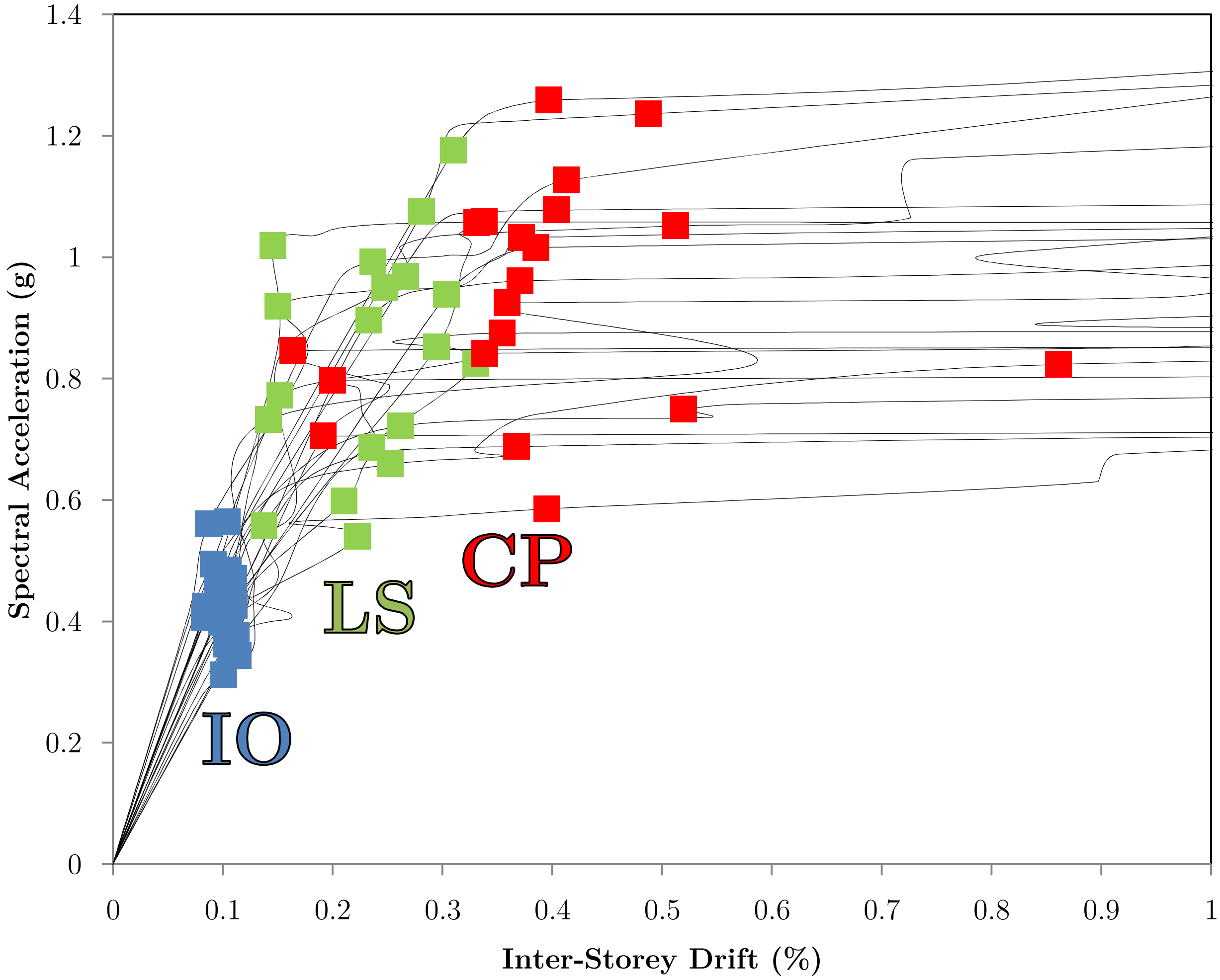

Figure 4-17: Mid-rise, low-code, large openings IDA curve (W)

Table 4-7: Mid-rise, low-code, large openings limit states (W)

	IO			LS			CP		
	Sa (g)	PGA (g)	ISD (%)	Sa (g)	PGA (g)	ISD (%)	Sa (g)	PGA (g)	ISD (%)
e6c1_1	0.429	0.204	0.098	0.773	0.367	0.153	0.842	0.400	0.339
e6c1_2	0.560	0.303	0.087	0.919	0.498	0.151	0.961	0.520	0.371
e6c1_3	0.425	0.211	0.085	1.019	0.508	0.146	1.058	0.527	0.339
e6c1_4	0.563	0.203	0.105	0.991	0.357	0.237	1.127	0.405	0.413
e6c1_5	0.422	0.148	0.087	0.938	0.330	0.304	1.032	0.363	0.372
e6c2_1	0.398	0.158	0.099	0.896	0.356	0.233	1.016	0.403	0.385
e6c2_2	0.311	0.141	0.101	0.732	0.332	0.142	0.924	0.419	0.359
e6c2_3	0.484	0.177	0.101	1.075	0.394	0.282	1.236	0.453	0.488
e6c2_4	0.426	0.181	0.111	0.852	0.362	0.295	1.056	0.449	0.332
e6c2_5	0.348	0.147	0.108	0.824	0.348	0.331	0.875	0.369	0.355
e7c1_1	0.451	0.200	0.095	0.722	0.320	0.262	0.749	0.332	0.520
e7c1_2	0.463	0.147	0.108	0.950	0.301	0.248	1.077	0.342	0.404
e7c1_3	0.484	0.201	0.106	0.968	0.402	0.267	1.051	0.436	0.513
e7c1_4	0.494	0.273	0.092	0.659	0.364	0.253	0.823	0.455	0.861
e7c1_5	0.470	0.152	0.110	1.176	0.380	0.310	1.258	0.406	0.397
e7c2_1	0.362	0.150	0.104	0.597	0.247	0.211	0.688	0.284	0.368
e7c2_2	0.343	0.148	0.114	0.557	0.239	0.138	0.705	0.303	0.192
e7c2_3	0.405	0.193	0.084	0.540	0.258	0.223	0.585	0.279	0.396
e7c2_4	0.413	0.193	0.106	0.686	0.321	0.236	0.797	0.373	0.201
e7c2_5	0.376	0.140	0.113	0.705	0.263	0.192	0.846	0.315	0.164

Low-code and small openings

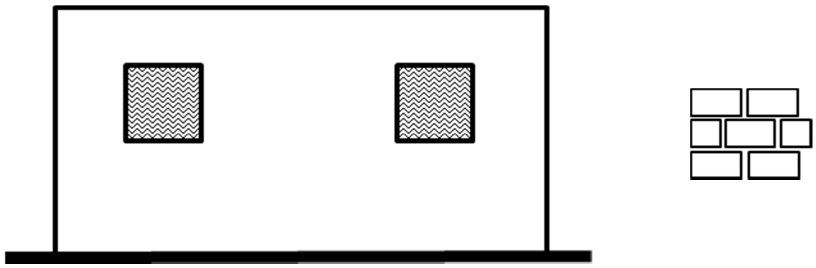

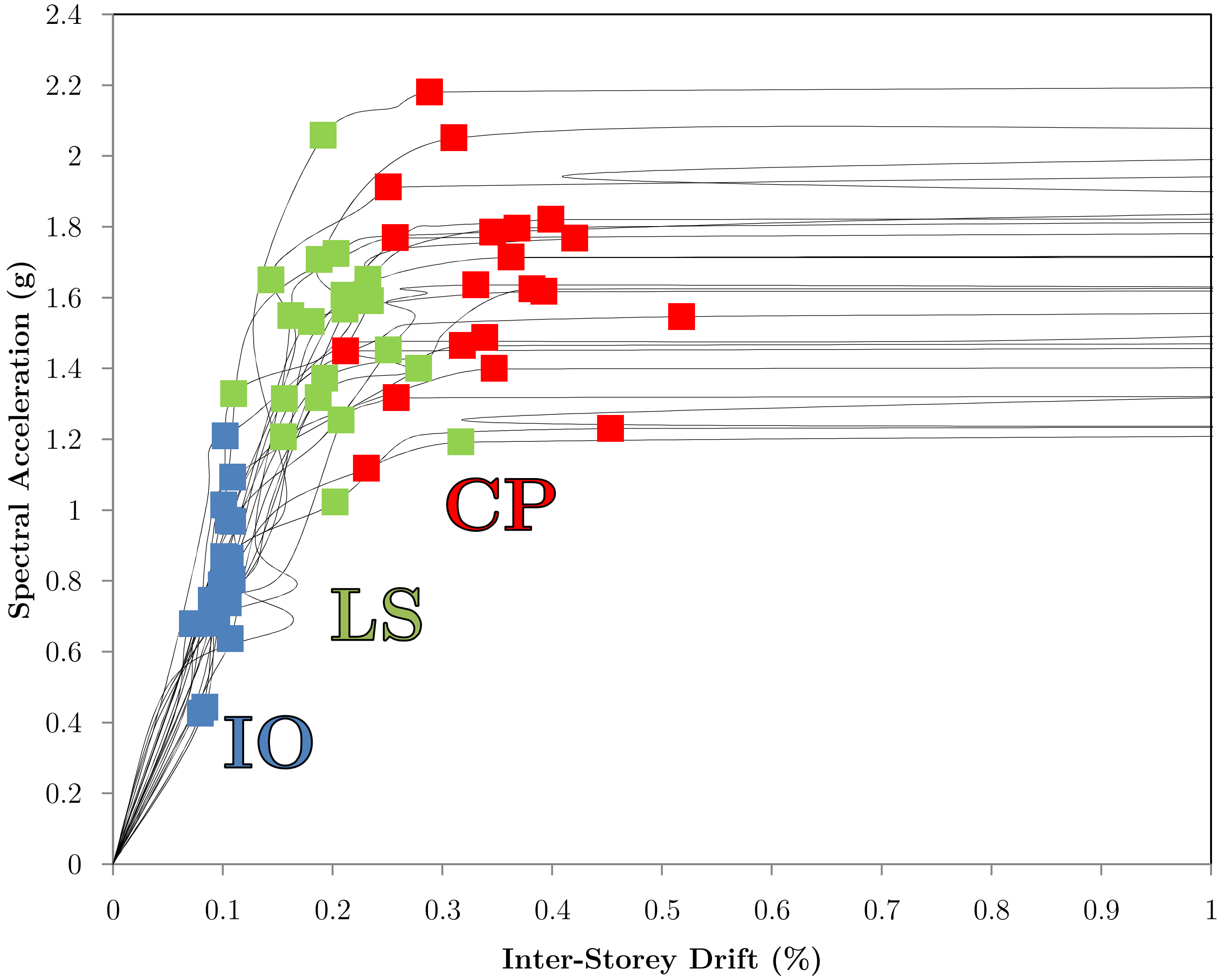

Figure 4-18: Mid-rise, low-code, small openings IDA curve (W)

Table 4-8: Mid-rise, low-code, small openings limit states (W)

	IO			LS			CP		
	Sa (g)	PGA (g)	ISD (%)	Sa (g)	PGA (g)	ISD (%)	Sa (g)	PGA (g)	ISD (%)
e6c1_1	0.680	0.286	0.095	1.651	0.694	0.233	1.796	0.755	0.369
e6c1_2	0.869	0.330	0.101	1.606	0.611	0.211	1.820	0.692	0.399
e6c1_3	1.014	0.423	0.101	1.724	0.719	0.204	1.784	0.744	0.346
e6c1_4	0.738	0.341	0.105	1.317	0.608	0.187	1.449	0.669	0.212
e6c1_5	1.209	0.389	0.103	1.708	0.550	0.188	2.050	0.660	0.311
e6c2_1	0.788	0.356	0.099	1.314	0.593	0.156	1.546	0.698	0.518
e6c2_2	0.443	0.208	0.084	1.328	0.623	0.110	1.487	0.698	0.339
e6c2_3	0.970	0.394	0.105	1.650	0.670	0.144	1.912	0.776	0.251
e6c2_4	0.636	0.217	0.107	1.591	0.544	0.235	1.767	0.604	0.421
e6c2_5	1.092	0.452	0.109	1.400	0.580	0.279	1.624	0.673	0.382
e7c1_1	0.864	0.336	0.107	2.057	0.799	0.192	2.181	0.847	0.289
e7c1_2	0.720	0.297	0.094	1.549	0.640	0.162	1.768	0.730	0.258
e7c1_3	0.426	0.201	0.080	1.022	0.482	0.202	1.230	0.580	0.453
e7c1_4	0.745	0.455	0.090	1.191	0.729	0.317	1.117	0.683	0.231
e7c1_5	0.804	0.380	0.109	1.206	0.570	0.155	1.399	0.661	0.348
e7c2_1	0.679	0.243	0.073	1.567	0.561	0.212	1.713	0.614	0.363
e7c2_2	0.769	0.335	0.101	1.372	0.598	0.193	1.464	0.638	0.319
e7c2_3	0.753	0.386	0.105	1.254	0.644	0.208	1.317	0.676	0.259
e7c2_4	0.851	0.387	0.102	1.532	0.696	0.181	1.617	0.735	0.393
e7c2_5	0.968	0.350	0.109	1.452	0.525	0.251	1.636	0.592	0.331

4.2.3. Low-rise URM – Eastern Canada

<u>Pre-code and large openings</u>

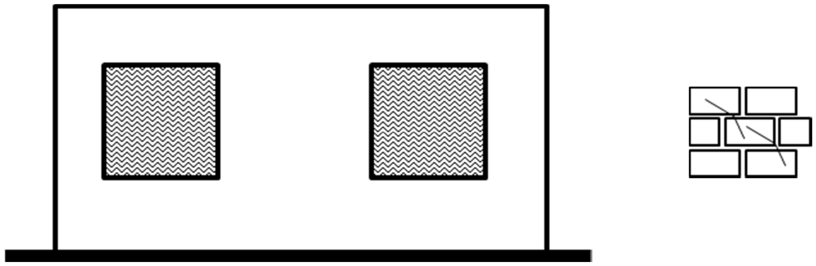

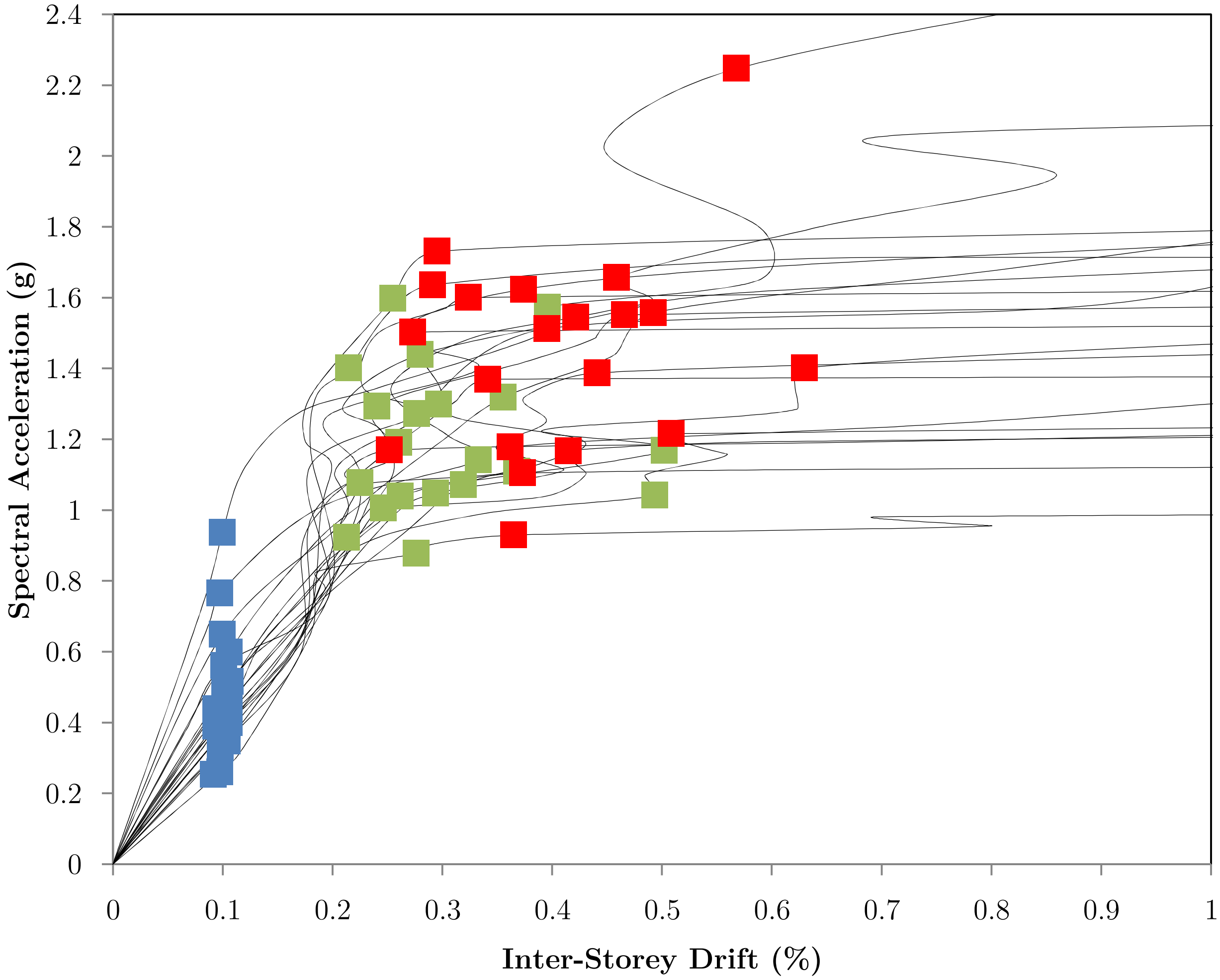

Figure 4-19: Low-rise, pre-code, large openings IDA curve (E)

Table 4-9: Low-rise, pre-code, large openings limit states (E)

	IO			LS			CP		
	Sa (g)	PGA (g)	ISD (%)	Sa (g)	PGA (g)	ISD (%)	Sa (g)	PGA (g)	ISD (%)
e6c1_1	0.649	0.323	0.100	1.299	0.646	0.297	1.624	0.807	0.374
e6c1_2	0.599	0.460	0.106	1.318	1.012	0.356	1.557	1.196	0.492
e6c1_3	0.504	0.205	0.106	1.440	0.586	0.280	1.656	0.674	0.459
e6c1_4	0.399	0.210	0.106	1.597	0.841	0.255	1.731	0.912	0.296
e6c1_5	0.936	0.378	0.100	1.573	0.635	0.396	2.247	0.907	0.568
e6c2_1	0.504	0.242	0.102	1.071	0.514	0.319	1.512	0.726	0.396
e6c2_2	0.254	0.112	0.092	1.078	0.476	0.225	1.503	0.664	0.273
e6c2_3	0.420	0.188	0.103	1.293	0.578	0.240	1.551	0.694	0.466
e6c2_4	0.766	0.334	0.098	1.142	0.499	0.333	1.545	0.675	0.422
e6c2_5	0.438	0.235	0.094	1.168	0.626	0.502	1.401	0.751	0.630
e7c1_1	0.260	0.124	0.098	1.039	0.498	0.262	1.104	0.529	0.373
e7c1_2	0.516	0.335	0.107	0.878	0.569	0.276	0.930	0.603	0.365
e7c1_3	0.458	0.212	0.106	1.047	0.484	0.294	1.178	0.544	0.362
e7c1_4	0.389	0.177	0.094	1.005	0.457	0.246	1.167	0.531	0.415
e7c1_5	0.328	0.168	0.098	1.191	0.610	0.261	1.370	0.702	0.342
e7c2_1	0.400	0.185	0.098	0.923	0.426	0.213	1.169	0.540	0.252
e7c2_2	0.350	0.115	0.103	1.402	0.459	0.215	1.636	0.535	0.291
e7c2_3	0.347	0.146	0.104	1.110	0.467	0.368	1.388	0.584	0.441
e7c2_4	0.382	0.215	0.099	1.042	0.587	0.494	1.216	0.685	0.508
e7c2_5	0.561	0.250	0.101	1.271	0.567	0.277	1.600	0.713	0.324

Pre-code and small openings

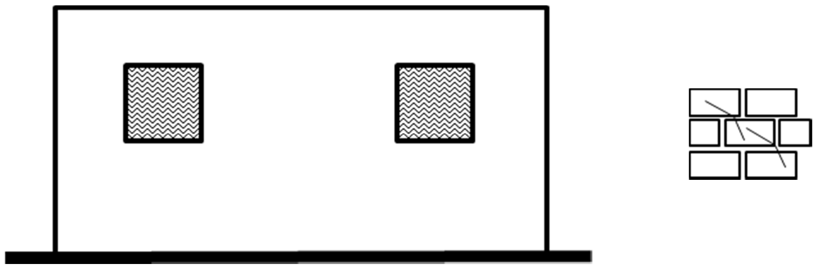

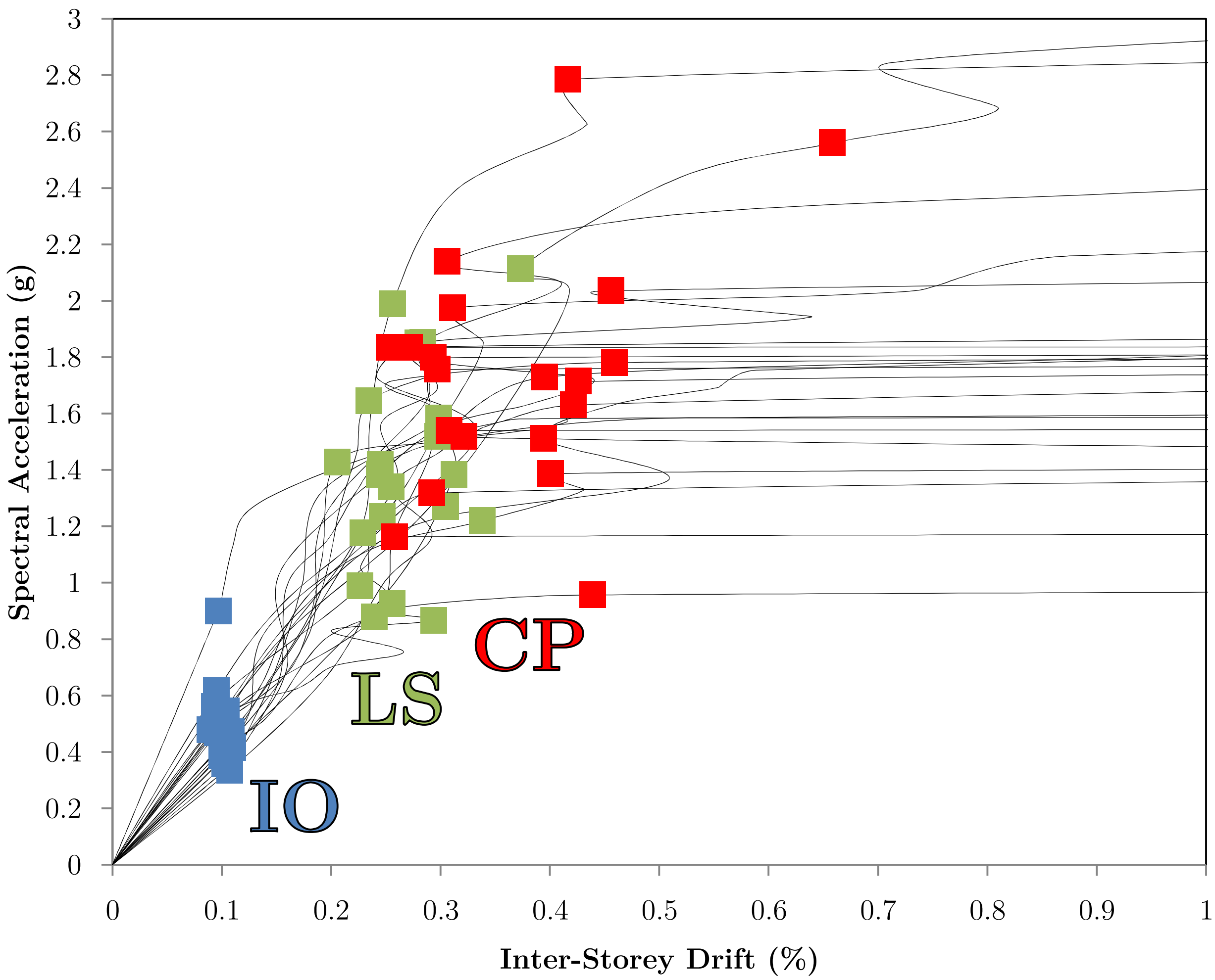

Figure 4-20: Low-rise, pre-code, small openings IDA curve (E)

Table 4-10: Low-rise, pre-code, small openings limit states (E)

	IO			LS			CP		
	Sa (g)	PGA (g)	ISD (%)	Sa (g)	PGA (g)	ISD (%)	Sa (g)	PGA (g)	ISD (%)
e6c1_1	0.617	0.323	0.095	1.234	0.646	0.247	1.974	1.033	0.311
e6c1_2	0.899	0.736	0.097	1.517	1.243	0.297	1.630	1.335	0.422
e6c1_3	0.524	0.249	0.098	1.850	0.879	0.280	2.035	0.967	0.456
e6c1_4	0.477	0.210	0.089	1.989	0.876	0.256	2.785	1.227	0.417
e6c1_5	0.488	0.181	0.095	2.113	0.786	0.373	2.559	0.953	0.659
e6c2_1	0.399	0.218	0.107	1.220	0.665	0.338	1.386	0.756	0.401
e6c2_2	0.411	0.182	0.100	1.644	0.729	0.235	1.834	0.813	0.254
e6c2_3	0.350	0.153	0.107	1.583	0.694	0.298	1.781	0.781	0.459
e6c2_4	0.387	0.164	0.100	1.383	0.587	0.313	1.729	0.733	0.395
e6c2_5	0.544	0.282	0.105	1.270	0.657	0.305	1.512	0.782	0.395
e7c1_1	0.500	0.218	0.102	1.428	0.622	0.206	1.714	0.747	0.426
e7c1_2	0.428	0.271	0.104	0.925	0.586	0.256	1.163	0.737	0.258
e7c1_3	0.356	0.163	0.103	1.419	0.650	0.246	1.518	0.695	0.322
e7c1_4	0.335	0.147	0.107	1.339	0.590	0.255	1.540	0.678	0.308
e7c1_5	0.468	0.244	0.096	0.878	0.458	0.240	1.756	0.915	0.297
e7c2_1	0.415	0.171	0.110	1.383	0.568	0.244	1.798	0.739	0.293
e7c2_2	0.411	0.127	0.103	1.851	0.574	0.284	2.139	0.663	0.306
e7c2_3	0.560	0.248	0.094	0.988	0.438	0.227	1.317	0.584	0.292
e7c2_4	0.504	0.326	0.097	0.866	0.561	0.294	0.957	0.620	0.439
e7c2_5	0.470	0.200	0.109	1.176	0.500	0.229	1.834	0.780	0.272

4.2.4. Low-rise URM – Western Canada

Pre-code and large openings

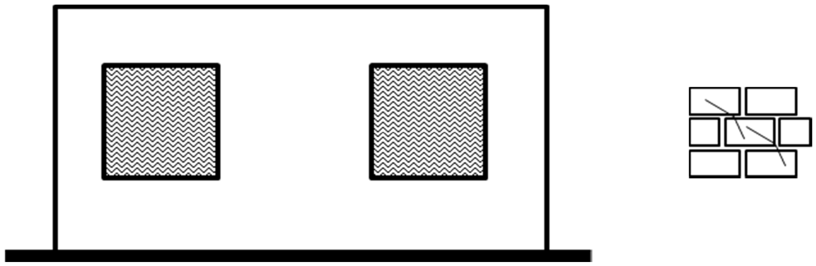

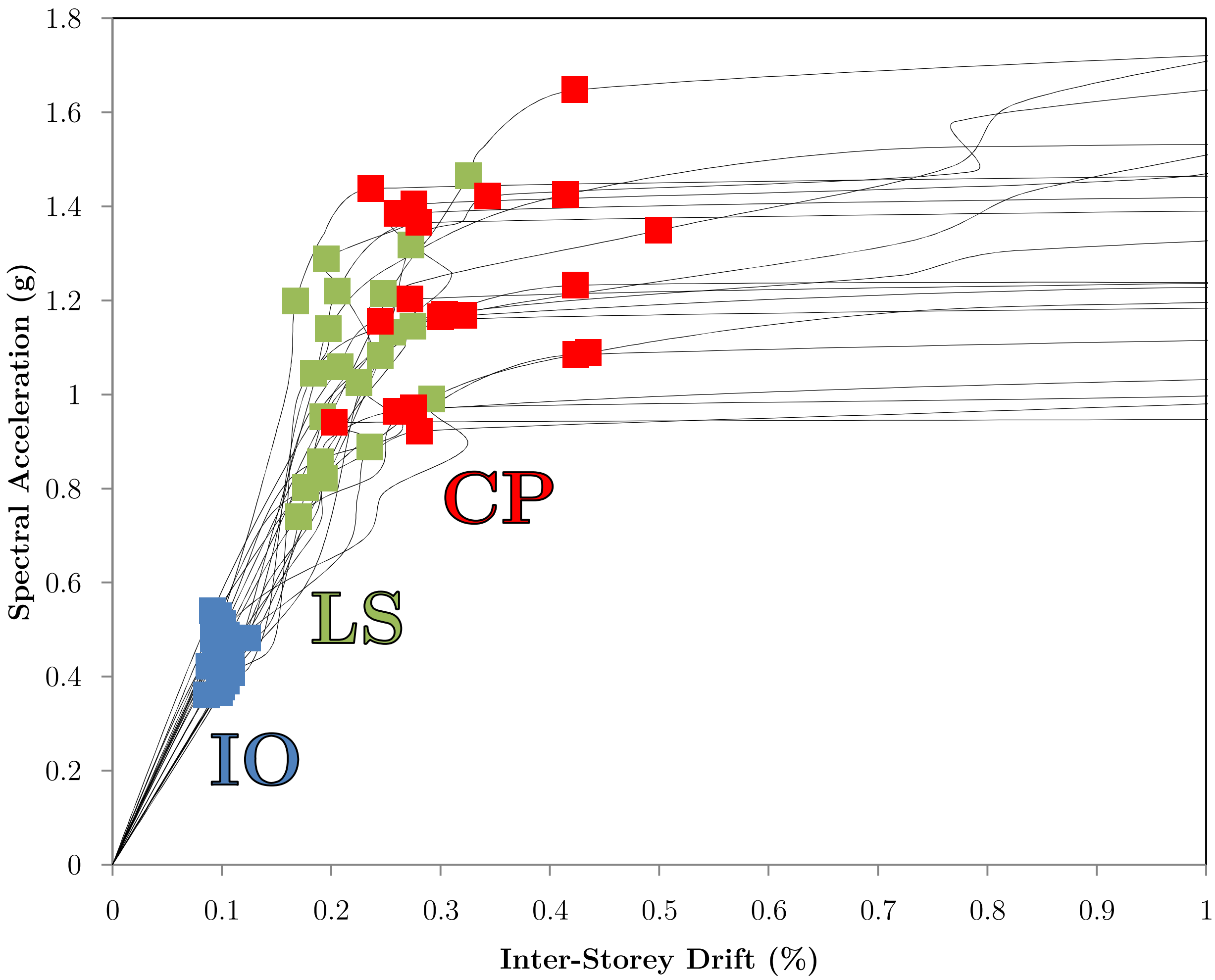

Figure 4-21: Low-rise, pre-code, large openings IDA curve (W)

Table 4-11: Low-rise, pre-code, large openings limit states (W)

	IO			LS			CP		
	Sa (g)	PGA (g)	ISD (%)	Sa (g)	PGA (g)	ISD (%)	Sa (g)	PGA (g)	ISD (%)
e6c1_1	0.488	0.191	0.104	1.464	0.573	0.326	1.647	0.644	0.423
e6c1_2	0.488	0.227	0.099	1.288	0.599	0.196	1.405	0.654	0.276
e6c1_3	0.528	0.290	0.093	1.144	0.627	0.275	1.232	0.676	0.424
e6c1_4	0.481	0.263	0.124	1.059	0.578	0.209	1.155	0.631	0.245
e6c1_5	0.421	0.208	0.089	1.317	0.651	0.273	1.422	0.703	0.343
e6c2_1	0.540	0.208	0.092	1.214	0.469	0.248	1.349	0.521	0.500
e6c2_2	0.407	0.177	0.110	1.140	0.497	0.198	1.425	0.621	0.414
e6c2_3	0.366	0.152	0.098	1.045	0.436	0.184	1.170	0.488	0.304
e6c2_4	0.462	0.233	0.101	0.739	0.373	0.170	0.970	0.490	0.275
e6c2_5	0.423	0.164	0.094	0.953	0.369	0.193	1.164	0.451	0.300
e7c1_1	0.479	0.212	0.093	1.198	0.530	0.168	1.438	0.636	0.236
e7c1_2	0.390	0.162	0.105	1.219	0.506	0.206	1.365	0.566	0.280
e7c1_3	0.512	0.219	0.101	1.024	0.438	0.226	1.168	0.499	0.322
e7c1_4	0.495	0.220	0.101	0.990	0.441	0.292	1.089	0.485	0.435
e7c1_5	0.529	0.319	0.097	0.802	0.483	0.177	0.922	0.555	0.281
e7c2_1	0.456	0.231	0.109	0.822	0.416	0.194	0.940	0.476	0.203
e7c2_2	0.444	0.218	0.097	0.887	0.437	0.236	1.085	0.534	0.424
e7c2_3	0.377	0.121	0.100	1.132	0.363	0.257	1.384	0.444	0.261
e7c2_4	0.385	0.187	0.100	0.857	0.416	0.190	0.964	0.468	0.260
e7c2_5	0.361	0.125	0.086	1.082	0.375	0.245	1.202	0.417	0.272

Pre-code and small openings

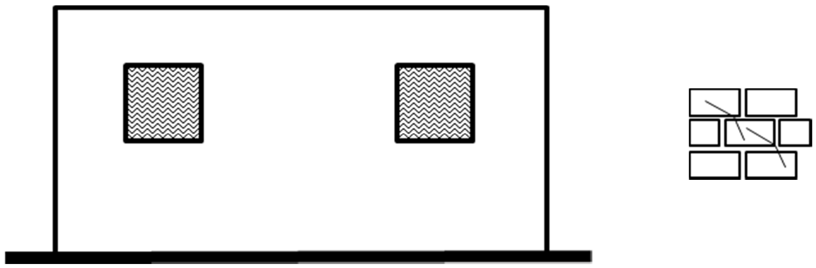

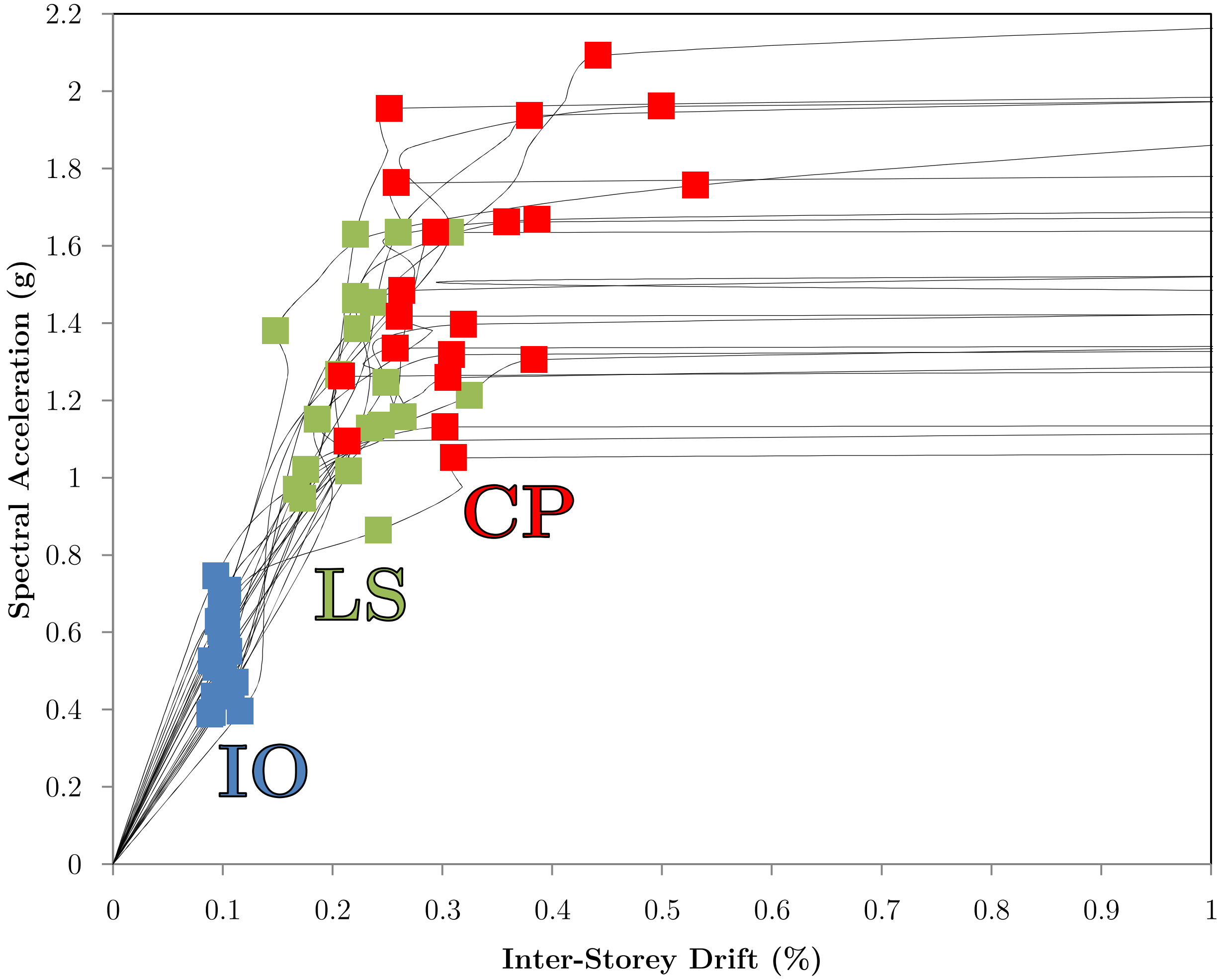

Figure 4-22: Low-rise, pre-code, small openings IDA curve (W)

Table 4-12: Low-rise, pre-code, small openings limit states (W)

	IO			LS			CP		
	Sa (g)	PGA (g)	ISD (%)	Sa (g)	PGA (g)	ISD (%)	Sa (g)	PGA (g)	ISD (%)
e6c1_1	0.629	0.239	0.098	1.634	0.620	0.260	1.936	0.735	0.380
e6c1_2	0.460	0.227	0.108	1.151	0.568	0.186	1.418	0.699	0.261
e6c1_3	0.521	0.241	0.102	1.459	0.676	0.221	1.668	0.772	0.386
e6c1_4	0.658	0.342	0.104	1.266	0.657	0.206	1.661	0.862	0.359
e6c1_5	0.465	0.208	0.102	1.453	0.651	0.238	2.092	0.937	0.442
e6c2_1	0.627	0.260	0.096	1.380	0.573	0.148	1.756	0.729	0.531
e6c2_2	0.708	0.288	0.105	1.634	0.665	0.308	1.961	0.799	0.500
e6c2_3	0.388	0.174	0.089	0.970	0.436	0.167	1.396	0.627	0.319
e6c2_4	0.396	0.187	0.116	1.385	0.653	0.222	1.484	0.700	0.263
e6c2_5	0.598	0.246	0.104	1.245	0.512	0.249	1.335	0.549	0.257
e7c1_1	0.434	0.169	0.093	1.629	0.636	0.221	1.955	0.763	0.252
e7c1_2	0.392	0.162	0.091	1.469	0.607	0.221	1.762	0.728	0.259
e7c1_3	0.746	0.350	0.094	1.212	0.569	0.325	1.306	0.613	0.384
e7c1_4	0.469	0.220	0.111	1.127	0.529	0.234	1.258	0.591	0.305
e7c1_5	0.550	0.338	0.106	1.021	0.628	0.176	1.131	0.695	0.303
e7c2_1	0.526	0.231	0.090	0.947	0.416	0.173	1.094	0.480	0.214
e7c2_2	0.601	0.388	0.098	0.863	0.558	0.242	1.051	0.679	0.311
e7c2_3	0.681	0.242	0.099	1.135	0.404	0.245	1.634	0.581	0.294
e7c2_4	0.509	0.260	0.094	1.018	0.520	0.215	1.262	0.645	0.208
e7c2_5	0.578	0.208	0.100	1.156	0.417	0.264	1.318	0.475	0.308

4.3 Development of fragility curves

In order to produce log-normal fragility curves, the natural logarithm of the limit states' intensity measures determined in Section 4.2 are taken to calculate the median and standard deviation for each combination and performance level. The curves are available under both spectral acceleration and peak ground acceleration intensity measures in this section. Furthermore, the data associated with each curve's generation are presented in tables accompanying the fragility curves. The tables also contain the associated demand spectrum parameters as a function spectral displacement (SD), in centimeters, which can be used to generate fragility curves compatible with various tools such as Hazus-MH.

Chapter 5 provides further discussion on the fragility curves, comparisons with existing works and statistical verification of the accuracy of the results.

4.3.1. Mid-Rise URM – Eastern Canada

Pre-code and large openings

Table 4-13: Mid-rise, pre-code, large openings fragility parameters (E)

	SA (g)		PGA (g)		SD (cm)	
	Median	Deviation	Median	Deviation	Median	Deviation
IO	-1.609	0.302	-2.091	0.492	-1.008	0.302
LS	-0.674	0.247	-1.144	0.303	-0.072	0.247
CP	-0.469	0.252	-0.920	0.288	0.133	0.252

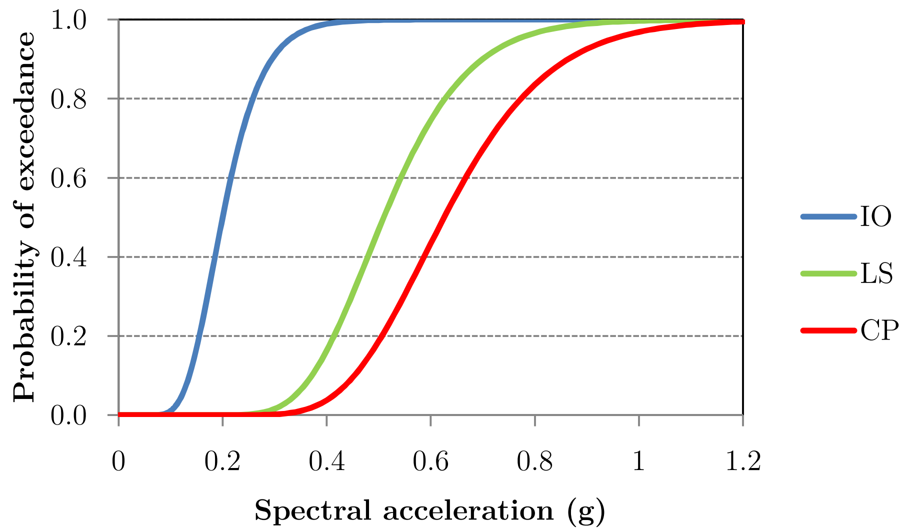

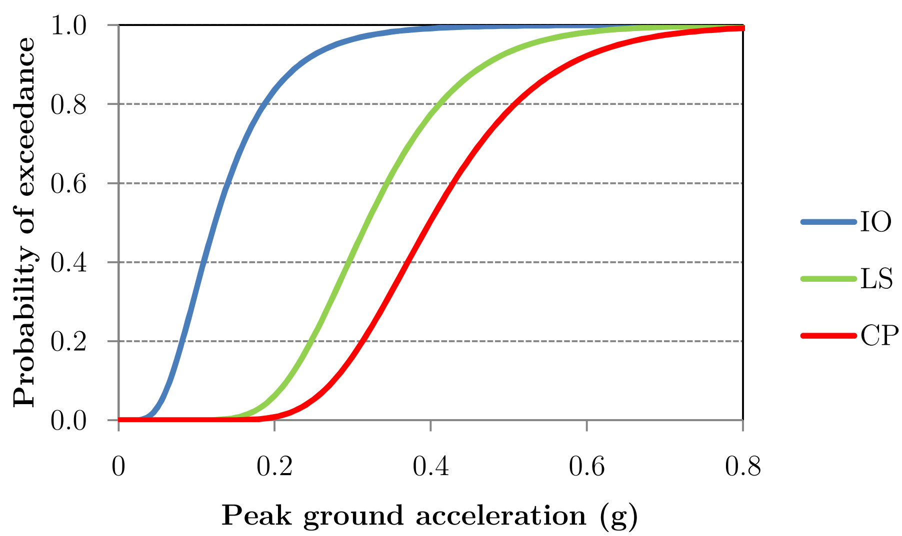

Figure 4-23: Mid-rise, pre-code, large openings fragility curves (E)

Pre-code and small openings

Table 4-14: Mid-rise, pre-code, small openings fragility parameters (E)

	SA (g)		PGA (g)		SD (cm)	
	Median	Deviation	Median	Deviation	Median	Deviation
IO	-1.230	0.267	-1.864	0.360	-1.101	0.267
LS	-0.308	0.188	-0.932	0.264	-0.178	0.188
CP	-0.111	0.168	-0.781	0.257	0.018	0.168

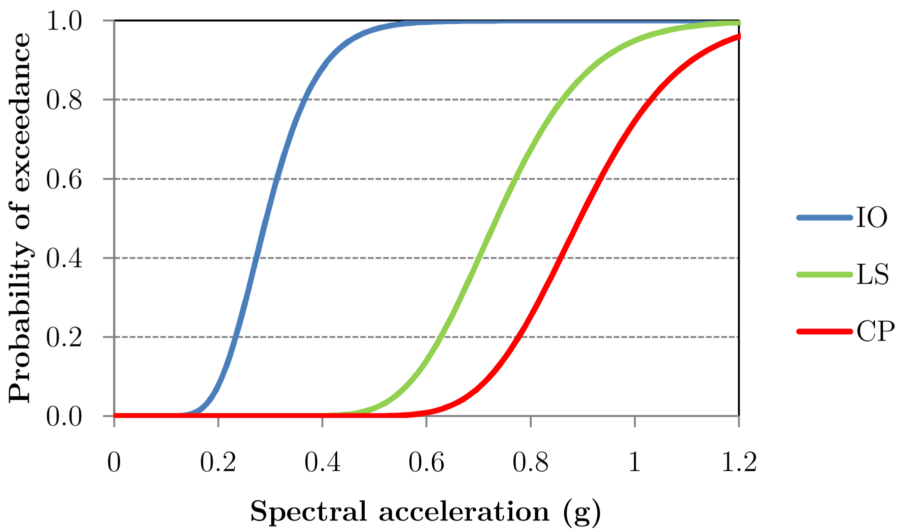

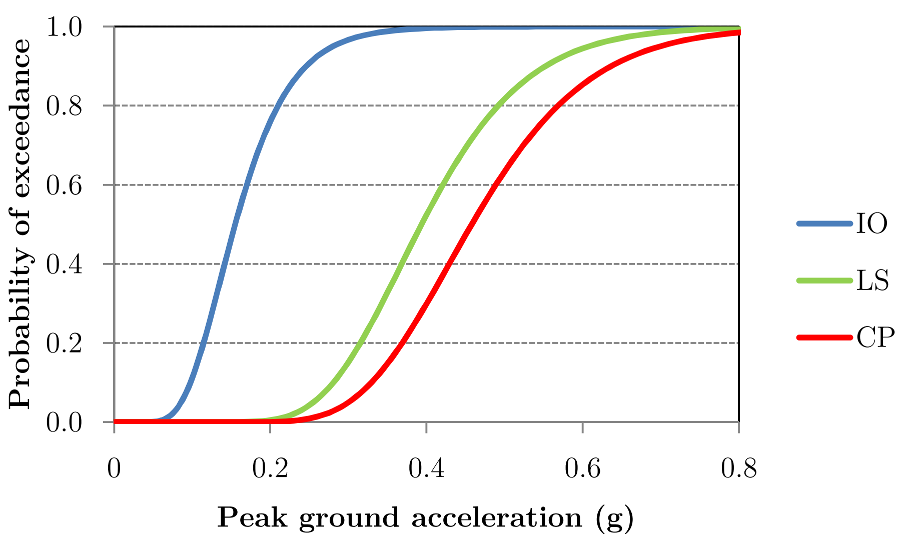

Figure 4-24: Mid-rise, pre-code, small openings fragility curves (E)

Low-code and large openings

Table 4-15: Mid-rise, low-code, large openings fragility parameters (E)

	SA (g)		PGA (g)		SD (cm)	
	Median	Deviation	Median	Deviation	Median	Deviation
IO	-0.897	0.300	-1.554	0.390	-1.189	0.300
LS	-0.117	0.254	-0.856	0.294	-0.409	0.254
CP	0.030	0.290	-0.683	0.313	-0.262	0.290

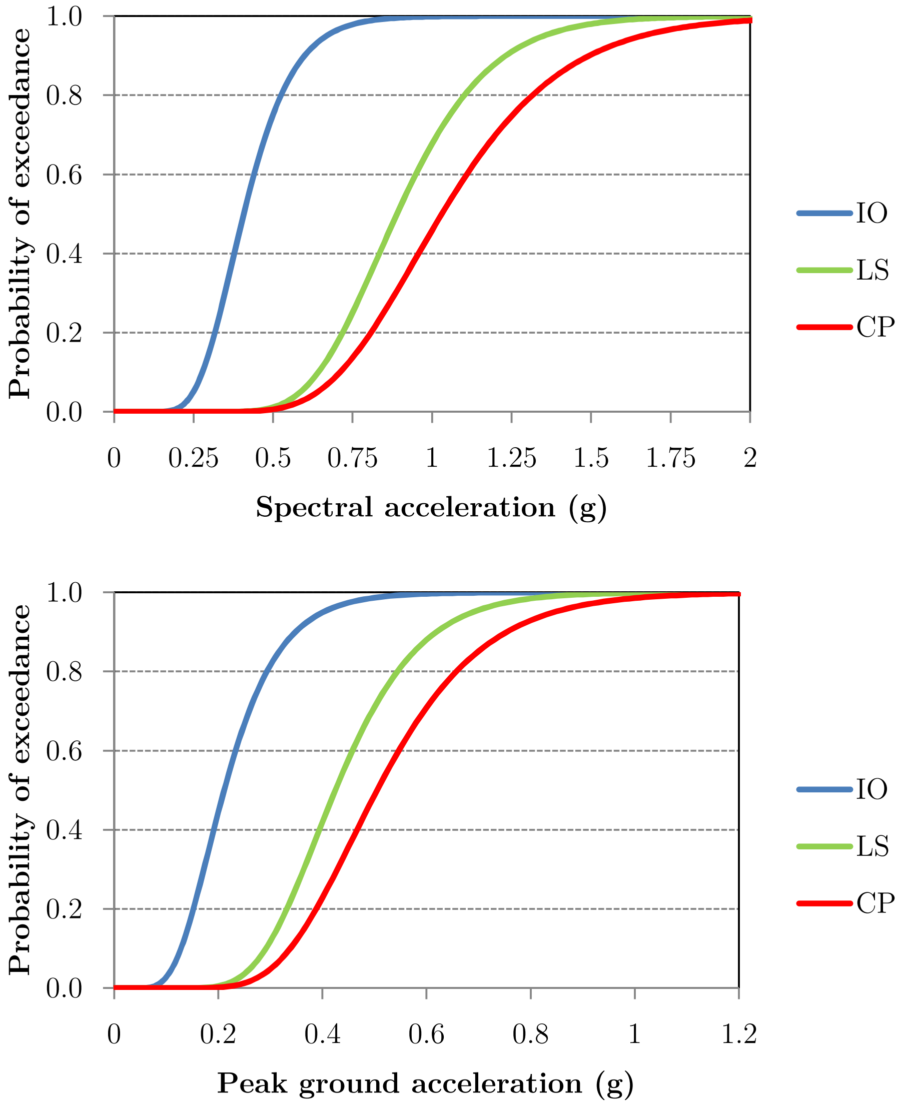

Figure 4-25: Mid-rise, low-code, large openings fragility curves (E)

Low-code and small openings

Table 4-16: Mid-rise, low-code, small openings fragility parameters (E)

	SA (g)		PGA (g)		SD (cm)	
	Median	Deviation	Median	Deviation	Median	Deviation
IO	-0.288	0.228	-1.006	0.335	-1.069	0.228
LS	0.476	0.238	-0.304	0.261	-0.302	0.238
CP	0.603	0.238	-0.176	0.221	-0.176	0.238

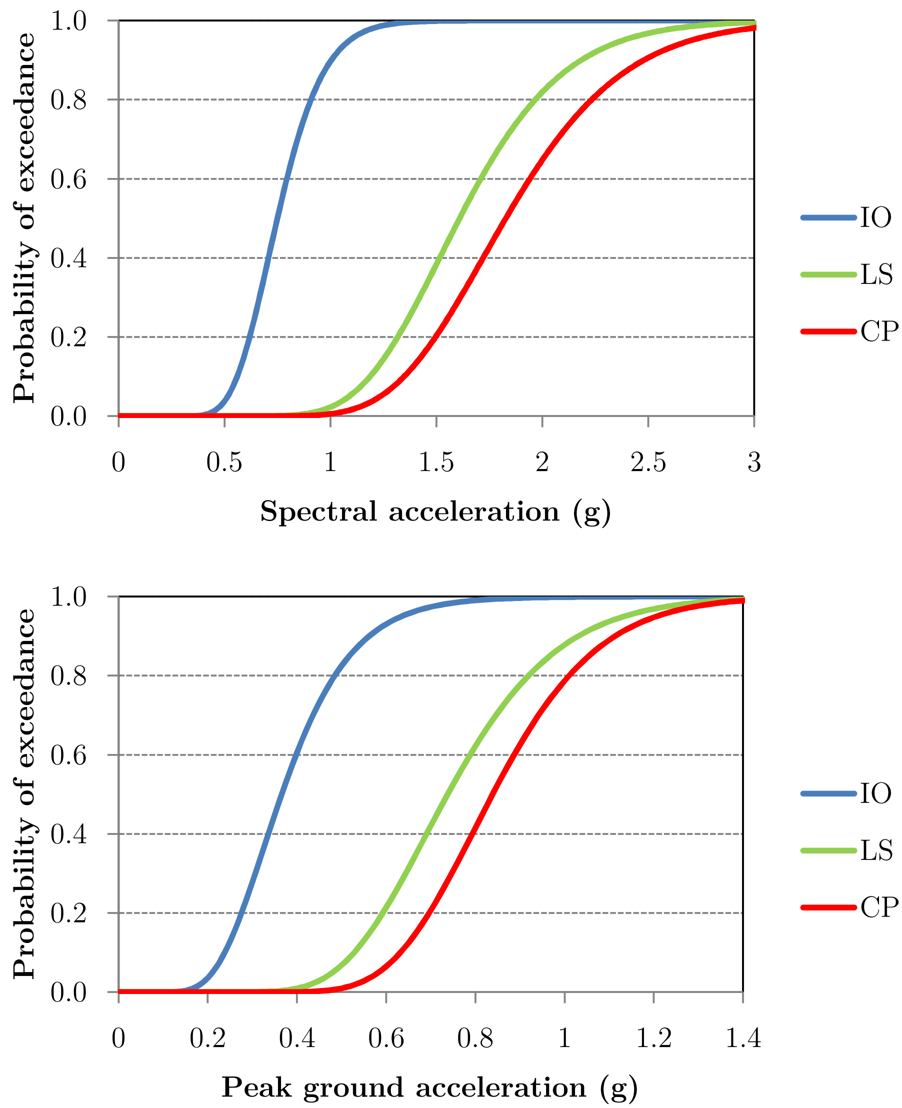

Figure 4-26: Mid-rise, low-code, small openings fragility curves (E)

4.3.2. Mid-rise URM – Western Canada

Pre-code and large openings

Table 4-17: Mid-rise, pre-code, large openings fragility parameters (W)

	SA (g)		PGA (g)		SD (cm)	
	Median	Deviation	Median	Deviation	Median	Deviation
IO	-1.677	0.200	-2.471	0.275	-1.075	0.200
LS	-0.869	0.227	-1.708	0.242	-0.268	0.227
CP	-0.670	0.185	-1.461	0.190	-0.068	0.185

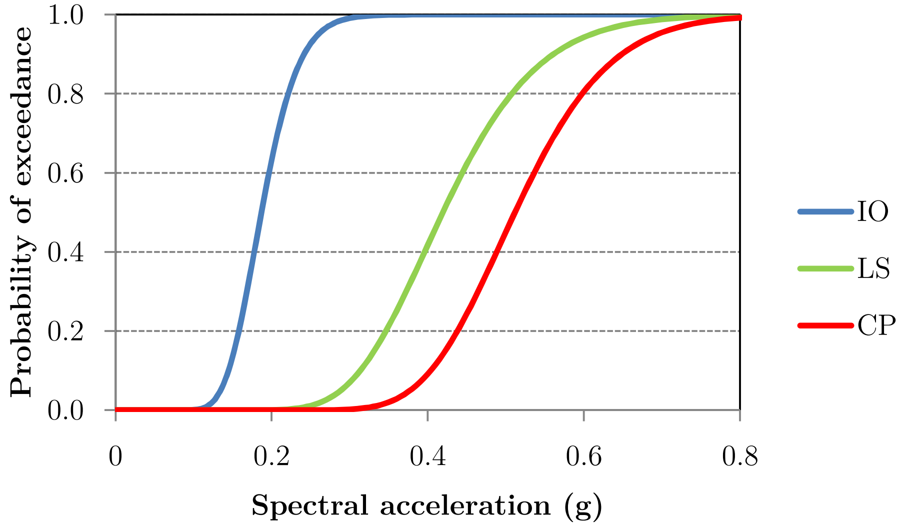

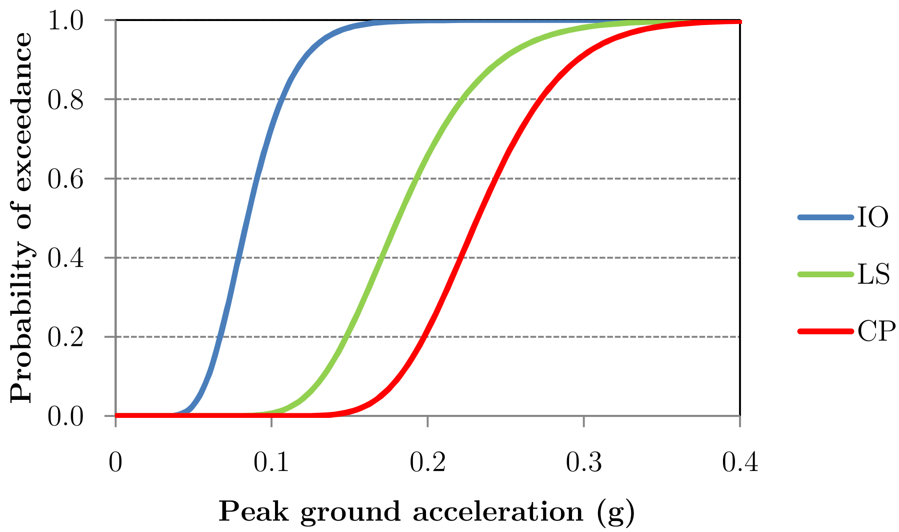

Figure 4-27: Mid-rise, pre-code, large openings fragility curves (W)

Pre-code and small openings

Table 4-18: Mid-rise, pre-code, small openings fragility parameters (W)

	SA (g)		PGA (g)		SD (cm)	
	Median	Deviation	Median	Deviation	Median	Deviation
IO	-1.193	0.189	-2.100	0.265	-1.064	0.189
LS	-0.364	0.203	-1.271	0.223	-0.235	0.203
CP	-0.291	0.203	-1.138	0.235	-0.162	0.203

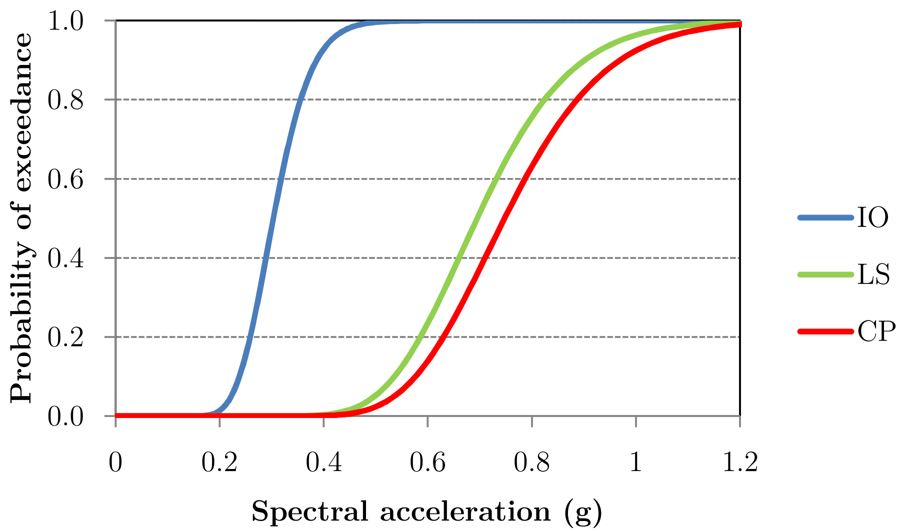

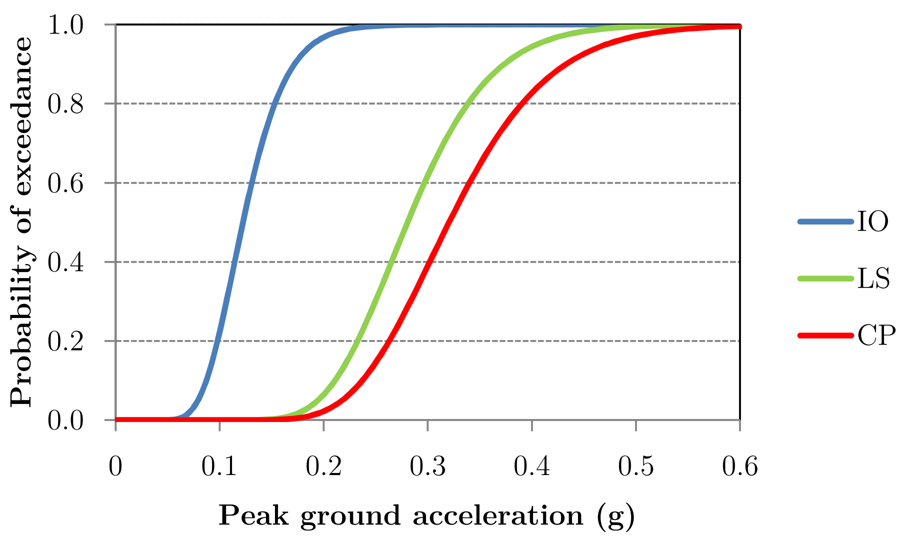

Figure 4-28: Mid-rise, pre-code, small openings fragility curves (W)

Low-code and large openings

Table 4-19: Mid-rise, low-code, large openings fragility parameters (W)

	SA (g)		PGA (g)		SD (cm)	
	Median	Deviation	Median	Deviation	Median	Deviation
IO	-0.855	0.152	-1.719	0.212	-1.147	0.152
LS	-0.177	0.216	-1.044	0.197	-0.469	0.216
CP	-0.059	0.198	-0.912	0.178	-0.351	0.198

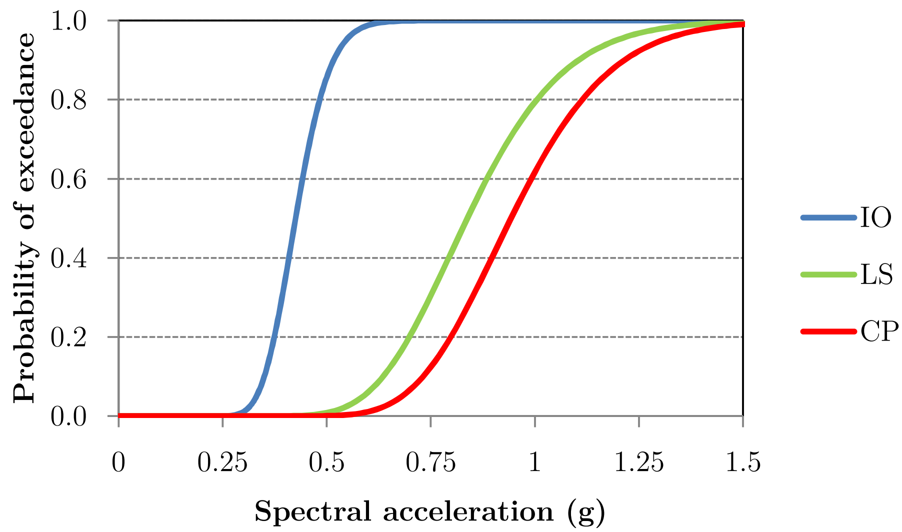

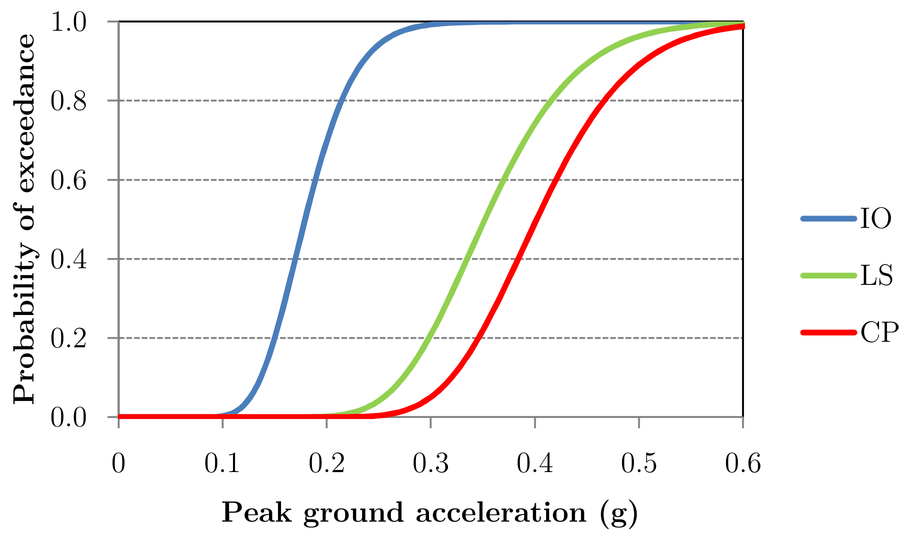

Figure 4-29: Mid-rise, low-code, large openings fragility curves (W)

Low-code and small openings

Table 4-20: Mid-rise, low-code, small openings fragility parameters (W)

	SA (g)		PGA (g)		SD (cm)	
	Median	Deviation	Median	Deviation	Median	Deviation
IO	-0.250	0.253	-1.063	0.241	-1.029	0.253
LS	0.400	0.157	-0.495	0.121	-0.379	0.157
CP	0.489	0.163	-0.386	0.093	-0.290	0.163

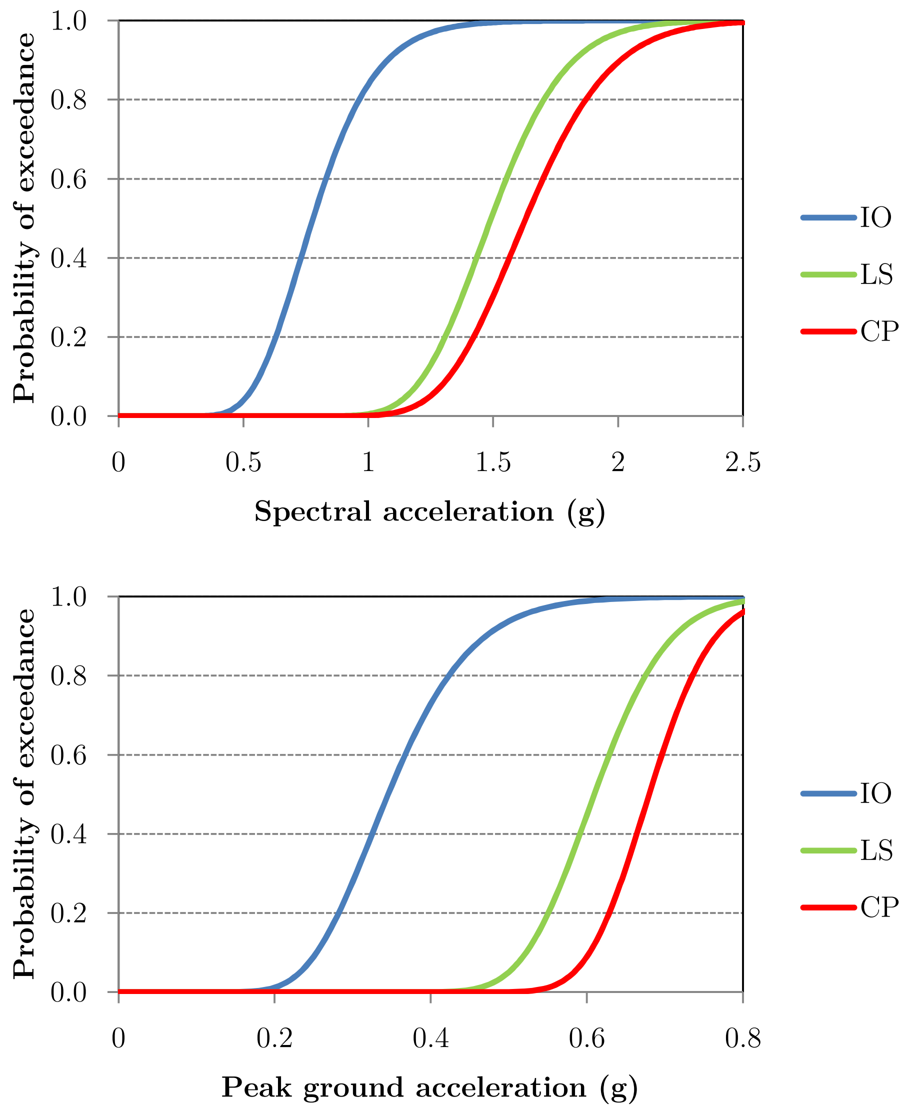

Figure 4-30: Mid-rise, low-code, small openings fragility curves (W)

4.3.3. Low-rise URM – Eastern Canada

Pre-code and large openings

Table 4-21: Low-rise, pre-code, large openings fragility parameters (E)

	SA (g)		PGA (g)		SD (cm)	
	Median	Deviation	Median	Deviation	Median	Deviation
IO	-0.846	0.322	-1.556	0.381	-1.500	0.322
LS	0.144	0.161	-0.566	0.206	-0.510	0.161
CP	0.410	0.192	-0.386	0.207	-0.243	0.192

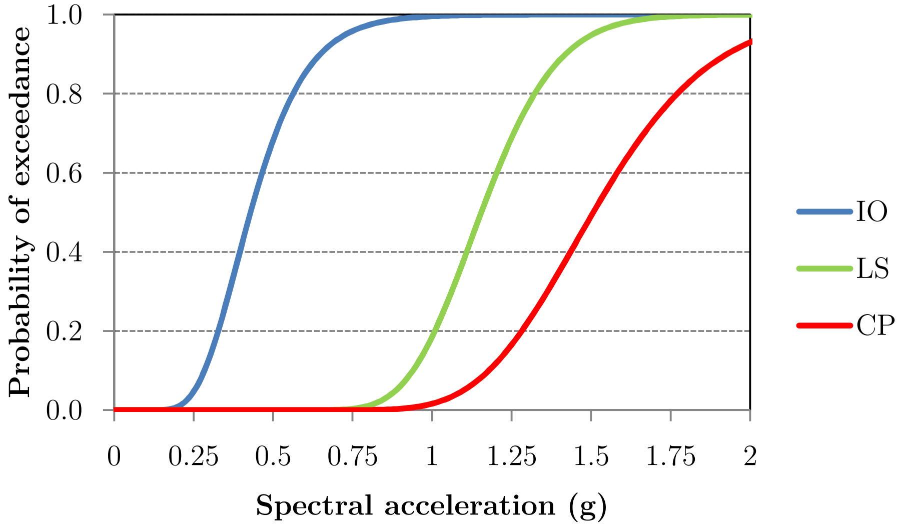

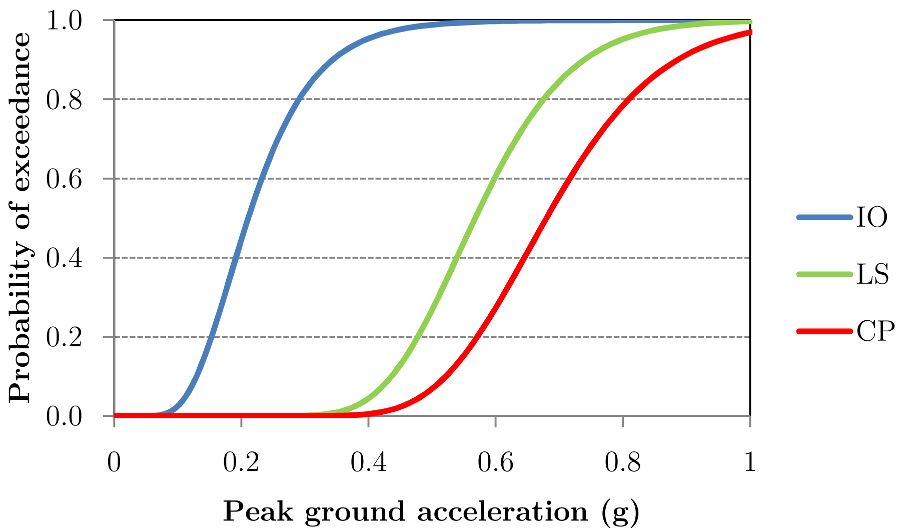

Figure 4-31: Low-rise, pre-code, large openings fragility curves (E)

Pre-code and small openings

Table 4-22: Low-rise, pre-code, small openings fragility parameters (E)

	SA (g)		PGA (g)		SD (cm)	
	Median	Deviation	Median	Deviation	Median	Deviation
IO	-0.756	0.220	-1.542	0.375	-1.530	0.220
LS	0.324	0.255	-0.456	0.233	-0.449	0.255
CP	0.555	0.240	-0.264	0.209	-0.218	0.240

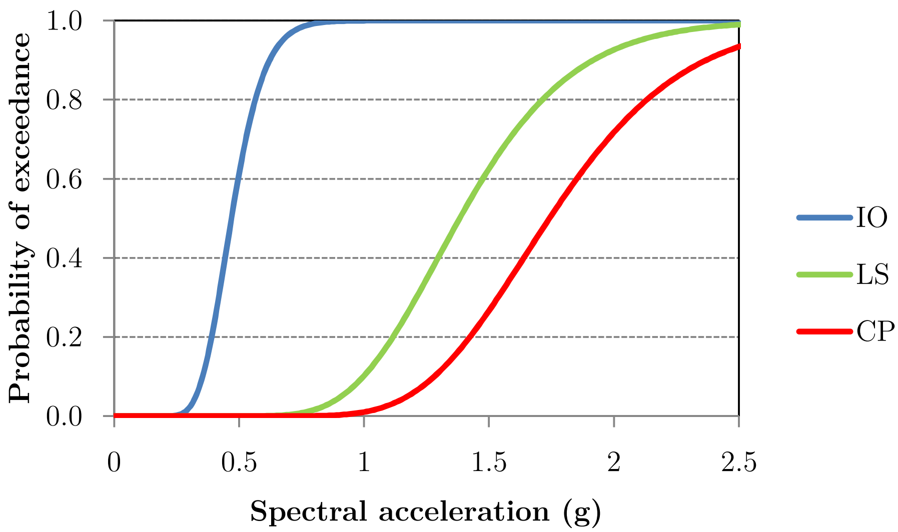

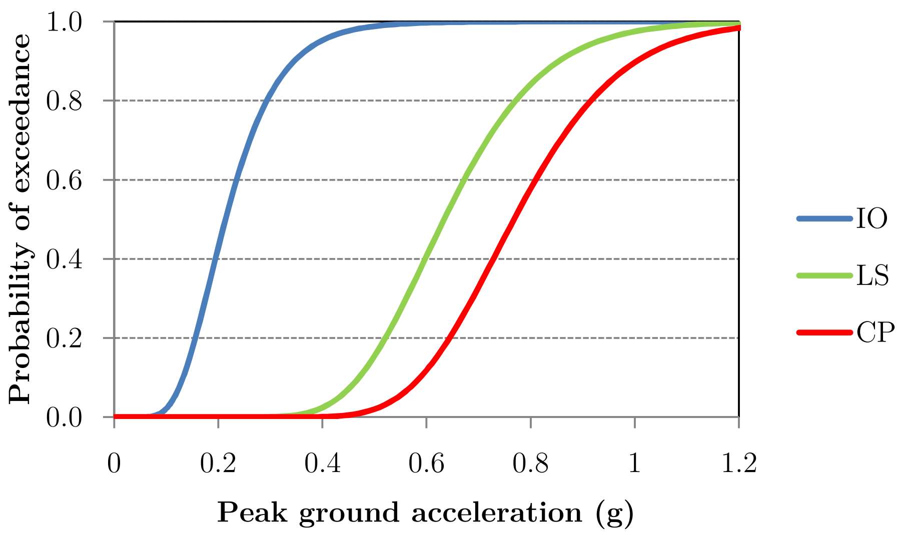

Figure 4-32: Low-rise, pre-code, small openings fragility curves (E)

4.3.4. Low-rise URM – Western Canada

Pre-code and large openings

Table 4-23: Low-rise, low-code, large openings fragility parameters (W)

	SA (g)		PGA (g)		SD (cm)	
	Median	Deviation	Median	Deviation	Median	Deviation
IO	-0.778	0.126	-1.560	0.242	-1.432	0.126
LS	0.068	0.177	-0.788	0.178	-0.585	0.177
CP	0.171	0.160	-0.640	0.154	-0.483	0.160

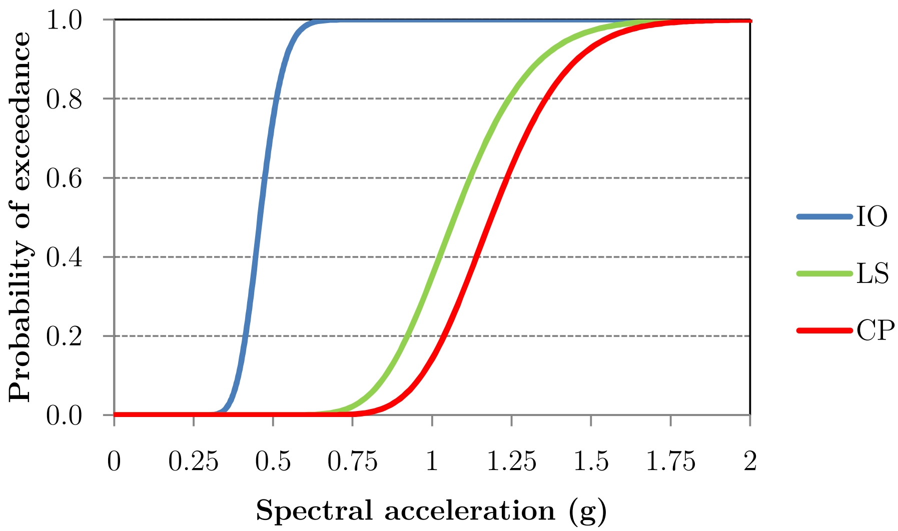

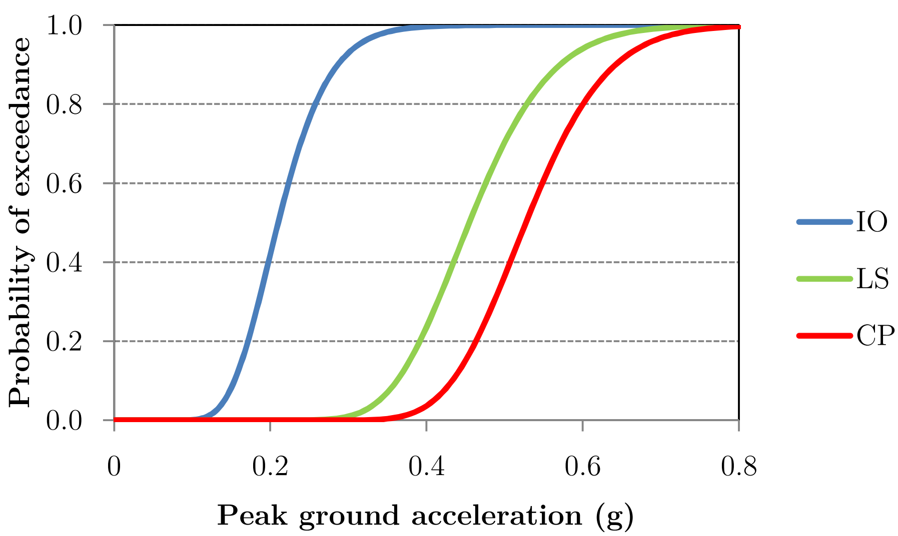

Figure 4-33: Low-rise, pre-code, large openings fragility curves (W)

Pre-code and small openings

Table 4-24: Low-rise, pre-code, small openings fragility parameters (W)

	SA (g)		PGA (g)		SD (cm)	
	Median	Deviation	Median	Deviation	Median	Deviation
IO	-0.620	0.196	-1.427	0.241	-1.394	0.196
LS	0.206	0.187	-0.560	0.165	-0.567	0.187
CP	0.372	0.203	-0.360	0.172	-0.402	0.203

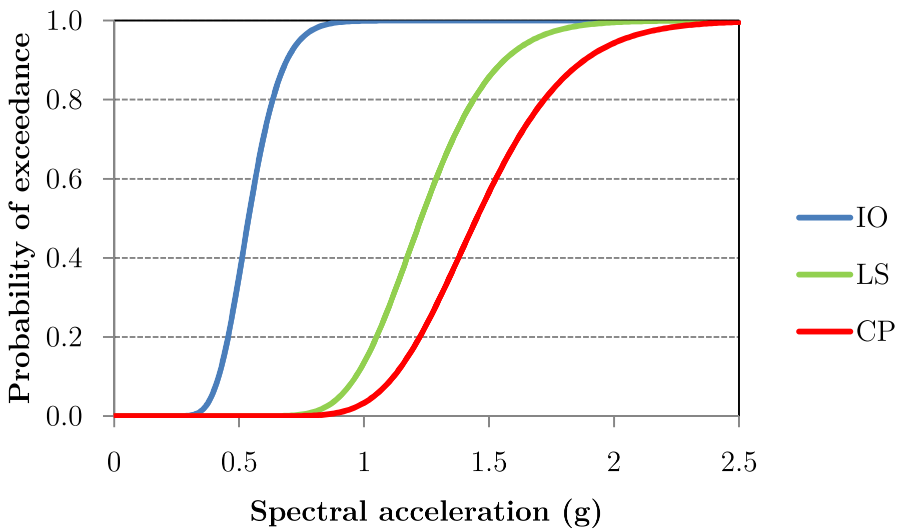

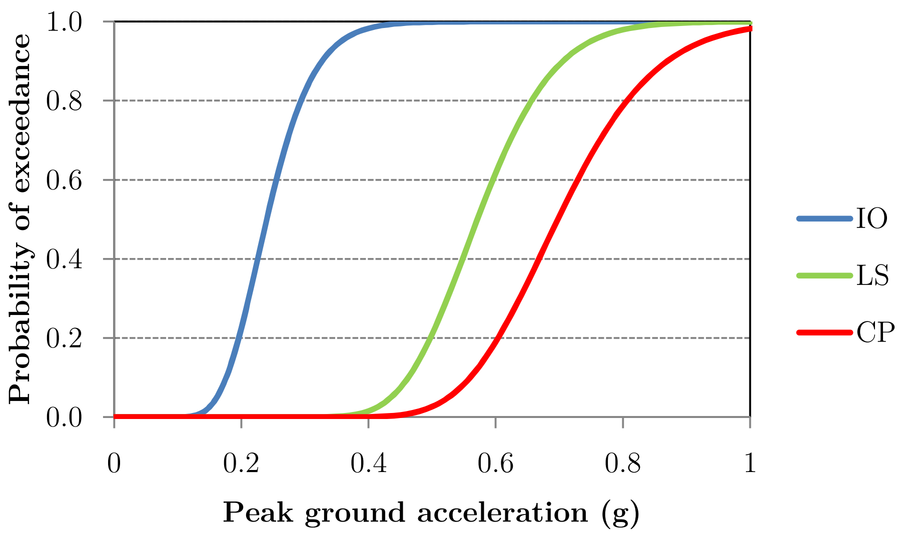

Figure 4-34: Low-rise, pre-code, small openings fragility curves (W)

Chapter 5

Discussion of results

In this chapter, the validity of the results will be verified through various means such as statistical verification of the fragility parameters. Consideration will be given to the characteristics of structures and their effects on the likelihood of damage to be sustained during an earthquake. The goal is to illustrate high variability of URM response; some prone to sustaining significant damage.

5.1.1. Normality check of limit states

One of the assumptions made in this work is that the fragility curves are spread based on a log-normal distribution. A relatively simple, yet telling way to verify this assumption is to plot the data obtained against expected log-normal distribution. In a perfectly distributed normal distribution, the population is expected to be spread continuously so that the percentage of data between any two points is equal. An illustration of this is visible in Figure 5-1. While this figure is not immediately informative, plotting the same data against its expected score value is more telling and allows one to calculate the coefficient of determination of a regression, R^2. The expected scores should follow a linear relationship as is shown in Figure 5-2. In this case, a perfect sample was generated and the coefficient of determination shows no error, $R^2 = 1$.

The same process will be applied to the fragility parameters obtained in Chapter 4, based on their respective medians and standard deviations.

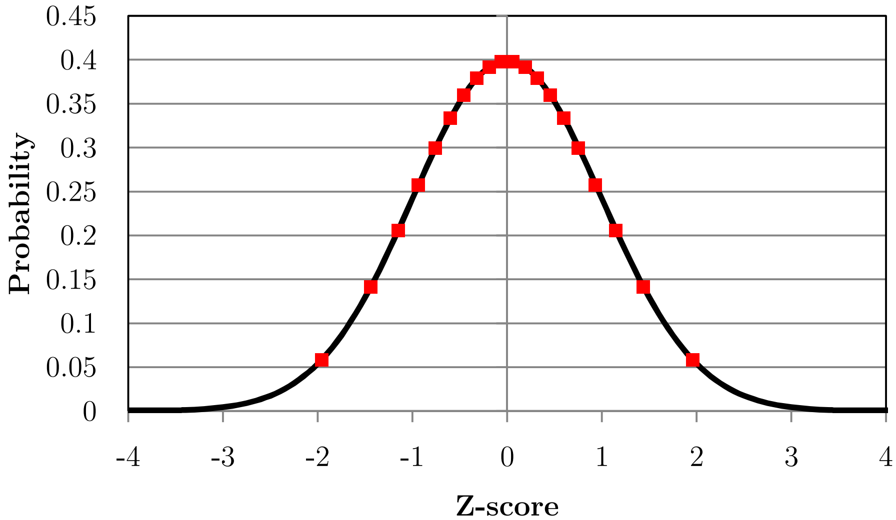

Figure 5-1: Standard normal distribution with evenly distributed population

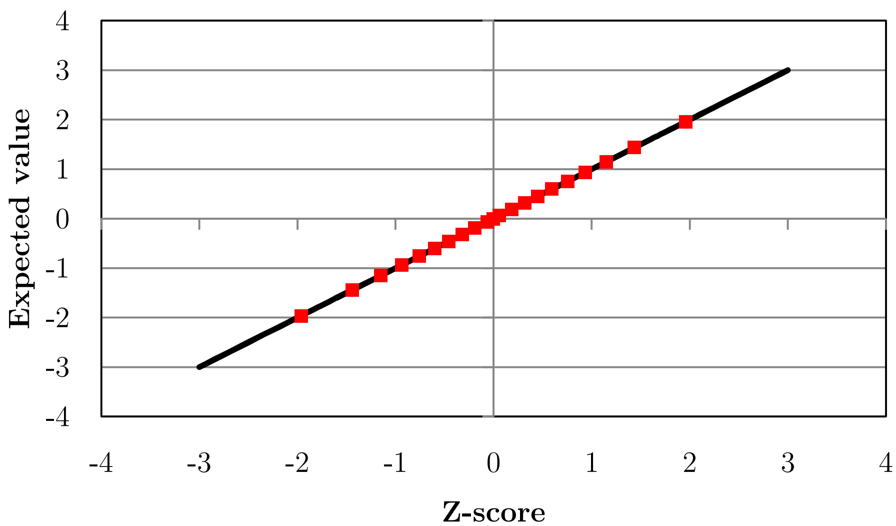

Figure 5-2: Expected value of a standard normal distribution

In the interest of briefness, an example of the process will be shown for the first set of parameter combination in Subsection 4.2.1 at the collapse prevention limit state, i.e., for a mid-rise URM of older construction with large openings, situated in eastern Canada.

For reference, consult Table 4-1. In a population of 20 members, there are 19 intervals to be considered and two half-intervals on each end, for a total of 20 intervals. In other words, there should be 5% of the cumulative density function (CDF) represented between each member and 2.5% at each end. The same should be true of fragility parameters once they are ordered by ascending order in log-format. The expected values for the CP level are shown below in Table 5-1.

Table 5-1: Example of expected Z-score of fragility parameters at CP level

S_a (g) at CP	Expected value of CDF	ln(SA)	Expected Z-score
0.930*	0.025	-0.073	-0.036
1.104	0.075	0.099	0.035
1.167	0.125	0.155	0.134
1.169	0.175	0.156	0.190
1.178	0.225	0.164	0.231
1.216	0.275	0.195	0.266
1.370	0.325	0.314	0.296
1.388	0.375	0.328	0.323
1.401	0.425	0.337	0.349
1.503	0.475	0.407	0.374
1.512	0.525	0.414	0.398
1.545	0.575	0.435	0.422
1.551	0.625	0.439	0.447
1.557	0.675	0.443	0.472
1.600*	0.725	0.470	0.497
1.624*	0.775	0.485	0.525
1.636*	0.825	0.492	0.555
1.656*	0.875	0.504	0.590
1.731	0.925	0.548	0.631
2.247	0.975	0.810	0.687

The last two columns of **Table 5-1** may be respectively plotted against themselves to display the distribution of the selected limit states against the values that should be expected from a log-normal distribution with the same parameters. This is done in Figure 5-3. The coefficient of determination is calculated as per Eq. 5-1, where y_i represents a data point (3rd column of **Table 5-1**), $expected_i$ the expected value of the same point (4th column of **Table 5-1**) and $\bar{y}$ the natural logarithm of the median (1st column of **Table 5-1**).

$$R^2 = 1 - \frac{\sum_{i=1}^{n}(y_i - expected_i)^2}{\sum_{i=1}^{n}(y_i - \bar{y})^2} \tag{5-1}$$

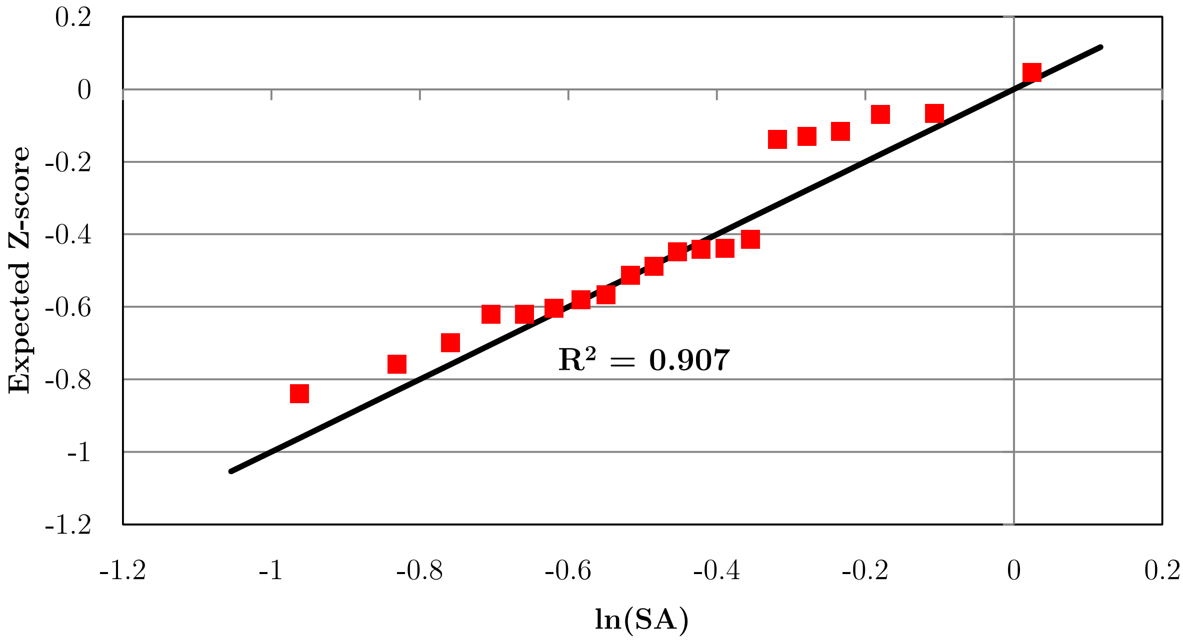

Figure 5-3: Example of expected Z-score of fragility parameters at CP level

In this case, it can be seen that some disagreement exists, stemming mainly from 5 points, each contributing over 10% of the error for a total 78%; these are marked by an asterisk (*) in **Table 5-1**. It can nonetheless be concluded that this is a strong representation of a log-normal distribution even though there may be some room to improve the definition of selected intensities for the collapse prevention. The remaining coefficients of determination are shown below in Table 5-2.

Table 5-2: Coefficients of determination for limit state levels

<table>
<tr><th>URM</th><th>Seismicity</th><th>Code level</th><th>Openings size</th><th>R^2 IO</th><th>R^2 LS</th><th>R^2 CP</th></tr>
<tr><td rowspan="8">Mid-rise</td><td rowspan="4">East</td><td rowspan="2">Pre</td><td>Large</td><td>0.950</td><td>0.930</td><td>0.907</td></tr>
<tr><td>Small</td><td>0.934</td><td>0.965</td><td>0.905</td></tr>
<tr><td rowspan="2">Low</td><td>Large</td><td>0.949</td><td>0.965</td><td>0.963</td></tr>
<tr><td>Small</td><td>0.961</td><td>0.947</td><td>0.988</td></tr>
<tr><td rowspan="4">West</td><td rowspan="2">Pre</td><td>Large</td><td>0.915</td><td>0.973</td><td>0.916</td></tr>
<tr><td>Small</td><td>0.983</td><td>0.936</td><td>0.892</td></tr>
<tr><td rowspan="2">Low</td><td>Large</td><td>0.981</td><td>0.950</td><td>0.953</td></tr>
<tr><td>Small</td><td>0.929</td><td>0.952</td><td>0.976</td></tr>
<tr><td rowspan="4">Low-rise</td><td rowspan="2">East</td><td rowspan="2">Pre</td><td>Large</td><td>0.960</td><td>0.960</td><td>0.960</td></tr>
<tr><td>Small</td><td>0.957</td><td>0.965</td><td>0.956</td></tr>
<tr><td rowspan="2">West</td><td rowspan="2">Pre</td><td>Large</td><td>0.917</td><td>0.971</td><td>0.941</td></tr>
<tr><td>Small</td><td>0.969</td><td>0.966</td><td>0.946</td></tr>
</table>

In general, the coefficients hover well above the 0.90 mark which shows that the log-normal distribution hypothesis is verified. The only coefficient below this threshold, for a mid-rise of older construction and small openings in western Canada, is plotted in Figure 5-4 where it can be seen that four points contribute over half of the error. The overall error remains relatively negligible and the log-normal distribution hypothesis shows to be a good fit for the data.

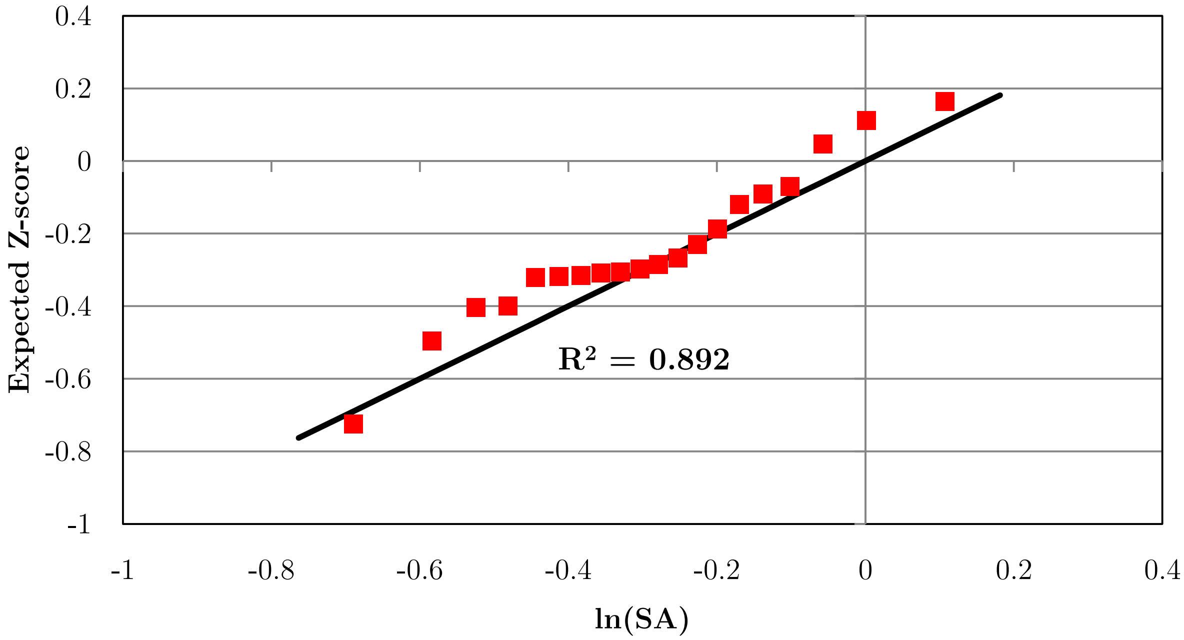

Figure 5-4: Expected Z-score of mid-rise, pre-code, small openings at CP level (W)

5.1.2. Verification of the damage measure

Now that the intensity measure of the limit states have been shown to be statistically sound based on the log-normal distribution, the remaining step consists in verifying that the damage measures considered are also well selected. This step is necessary as the definitions for IO, LS and CP presented in Section 3.4 could not always be exactly met as was previously discussed in Section 4.1. Figures in Section 4.2 show that the immediate occupancy interstorey drift seems to be quite consistent but the data is often scattered for the other two damage measures.

Given that no assumption was made relative to a distribution of the interstorey drift – and none should be expected – it is advantageous to use an estimation of the accuracy of the sample's representativeness of what the population should be. This is usually referred to as the standard error of the mean and is calculated as per Eq. 5-2, where σ is the standard deviation of the sample and n the number of items in the sample.

$$SE = \frac{\sigma}{\sqrt{n}} \tag{5-2}$$

The standard error of the mean is relative to the magnitude of the items within the sample and thus, in order to have a better representation of the impact of the error for all of the damage measures as a whole, it is preferable to express the error as a percentage of the damage measure itself. As with the intensity measures, the median is considered for this task in order to discard effects of any data skewing the mean of the sample. The data presented in Section 4.2 was used to calculate the errors shown in Table 5-3.

Table 5-3: Proportional standard error of the mean for damage measure

URM	Seismicity	Code level	Openings size	***SE*** IO	***SE*** LS	***SE*** CP
Mid-rise	East	Pre	Large	5.4%	4.9%	4.3%
			Small	2.8%	3.9%	5.8%
		Low	Large	3.9%	5.6%	6.5%
			Small	2.6%	5.9%	5.4%
	West	Pre	Large	2.1%	1.8%	5.7%
			Small	1.9%	4.0%	5.2%
		Low	Large	2.0%	5.6%	8.5%*
			Small	2.2%	5.2%	4.9%
Low-rise	East	Pre	Large	1.0%	6.5%	5.2%
			Small	1.2%	3.5%	5.9%
	West	Pre	Large	1.8%	4.6%	6.2%
			Small	1.6%	4.4%	6.3%

As can be seen from Table 5-3, the proportional standard error of the damage measure is very small. The largest of them at 8.5% (marked with an asterisk) is due to the presence of a far-off point of the collapse prevention population which can be seen in Figure 4-17. While this could suggest selecting a different point as limit state so that the standard error would be reduced, it should be noted that the standard error is simply an indication of the accuracy of the damage measure, not a tool used to determine the damage sustained in a structure. The selection of limit states was done based on the structural tools discussed in Section 3.4 and followed the procedure explained in Section 4.1. This type of distribution is not uncommon and can be seen in, among others, Karbassi (2010).

Overall, the errors presented in this subsection confirm that the damage measure provide an accurate depiction of the limit states they represent.

5.2 Observed damage and behaviour

This section briefly examines the damage mechanisms that were observed during the analysis phase of the research. This further serves to confirm that the selected performance levels from Section 3.4 are adequate as the nature of the failures are initiated by shear response first. The typical types of structural damage that can be sustained by URM structures are shown in Figure 5-5.

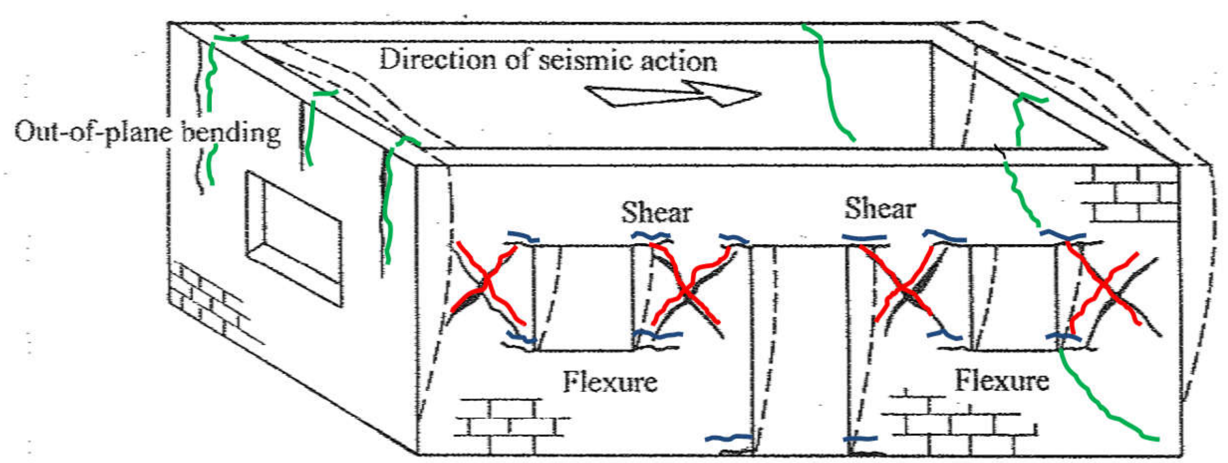

Figure 5-5: Typical failures due to shear (red), bending (blue) and out-of-plane failures (green), from Tomaževič (1999)

5.2.1. In-plane mechanisms

As previously explained, the link between elements in the applied element method is made through non-linear springs which are able to be broken. This allows elements to separate, and the structure may present behaviour such as rocking and sliding that are otherwise difficult to model. Although Figure 5-6 is not to scale, it shows typical cracking patterns observed after the URM model is subjected to a non-critical ground motion. As illustrated earlier in Figure 5-5, horizontal cracks are due to flexure while the diagonal, stair-stepped, cracks are due to shear failure.

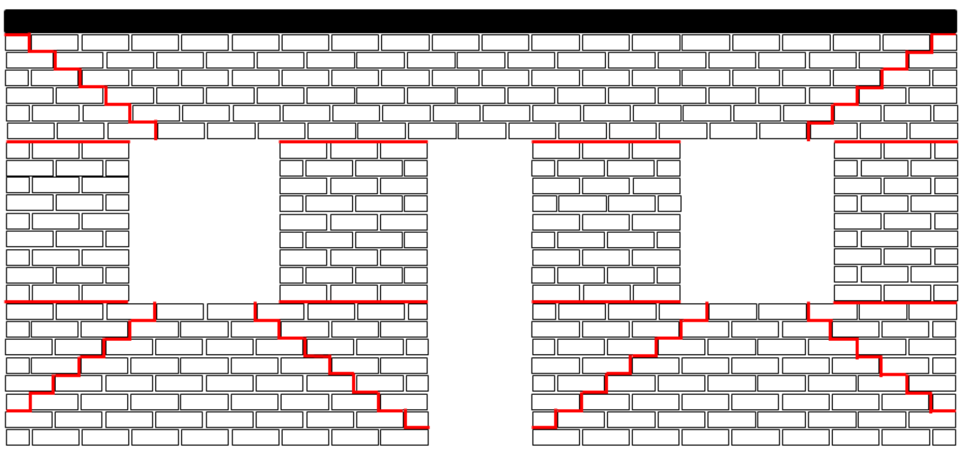

Figure 5-6: Typical crack patterns observed (red) at the end of ground shaking

Shear cracks typically appeared first, weakening the piers and this would eventually lead to the horizontal cracking patterns. Once enough springs were in the non-linear stage, rocking of the piers would occur as shown in Figure 5-7. This was the most visible structural response of the structures, especially for the mid-rise URM. Once the interstorey drift became sufficiently large, excessive stress would accumulate on the rocking toes which could lead to crushing. This typically meant the incoming collapse of the structure. Priestley et al. (2007) explains that while rocking dissipates large amounts of energy (evidenced by a large area of the hysteretic response), the presence of shear cracks leads to stiffness and strength loss and has been shown to result in great damage at interstorey drifts ranging from 0.4 to 0.5%.

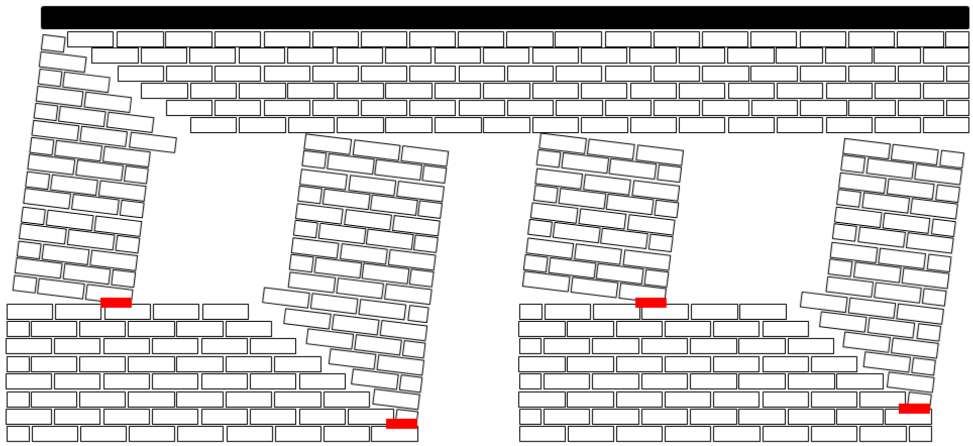

Figure 5-7: Pier rocking and toe crushing (red) observed during ground shaking

When collapse did not occur, residual sliding could be observed as shown in Figure 5-8. This led to permanent damage but not to collapse; the stair-stepped pattern described previously would occur first.

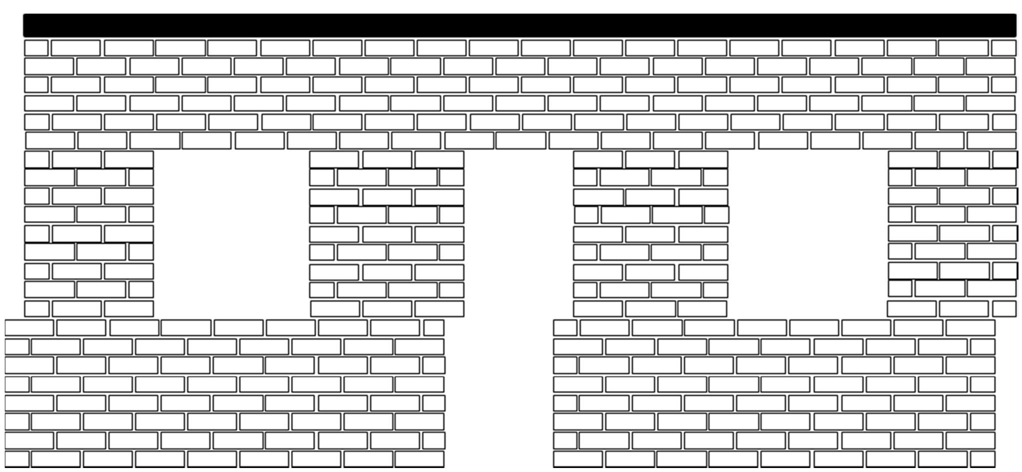

Figure 5-8: Residual sliding observed at the end of ground shaking

5.2.2. Out-of-plane damage

As part of the parameter decisions made in Chapter 3, out-of-plane failures were not meant to occur in the structures as this failure mode, for the most part, is a function of slenderness or the height-to-thickness ratio, $/t$ (ASCE 41, Penner, 2014; Derakhshan et al., 2014; Meisl, 2006). Including wall thickness as a parameter would greatly increase the number of simulations required to develop the overall fragility curves. As previously mentioned, it was instead decided to focus on in-plane failures given that extensive work is being done on out-of-plane failures, such as Penner (2014) and Derakhshan et al. (2014) among others. To this end, a slenderness ratio of 9 was selected for the URM walls as suggested by ASCE 41. This proved effective in developing in-plane fragility curves until the last phase of analysis which consisted of low-code low-rise URM structures. After several simulations, it was noticed that heavy out-of-plane action was occurring in the secondary walls despite the limit recommended by ASCE 41. Such action and its resulting damage are shown in Figure 5-9. The mid-span deflections would become much larger than the interstorey displacements, eventually leading to the collapse of the secondary walls prior to in-plane failures. Due to the relatively low first mode of vibration of the structure, the proximity of the following modes of vibration meant they contributed more to the overall response and thus induced more out-of-plane action. Further readings of the literature led to the work of Penner (2014) who showed that the slenderness limits considered by ASCE 41 could be un-conservative as shown in Figure 5-10. It was subsequently decided to abort this portion of the parametric study as not enough time was available to make the necessary corrections. Furthermore, it also meant that, due to the past construction practices, out-of-plane response would be the most likely reason for structural damage in these types of structures and as a result existing fragility curves for out-of-plane damage already provide the necessary information to assess low-rise URM.

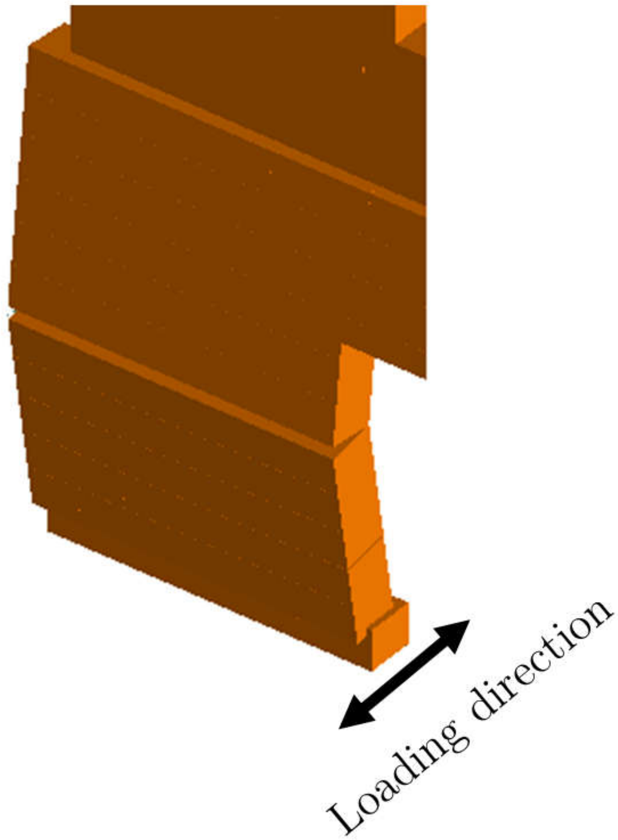

Figure 5-9: Out-of-plane damage of low-code URML

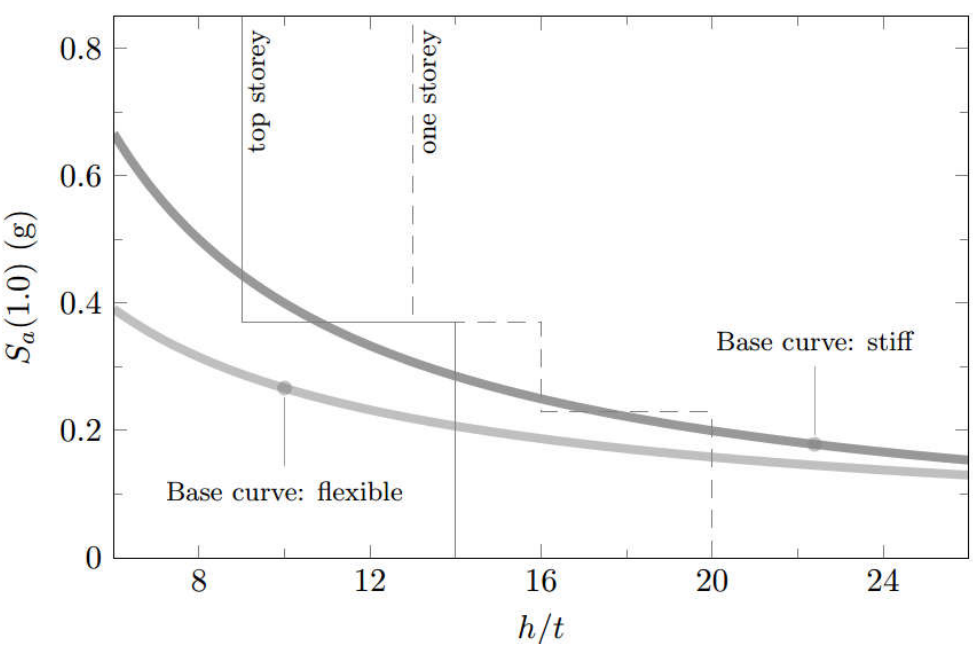

Figure 5-10: Revised slenderness ratios for stiff or flexible diaphragms, from Penner (2014)

5.3 Comparison with existing works

The fragility curves from the present work will be compared with four similar works from the literature in order to explore the differences and similarities that may arise between them.

5.3.1. Karbassi (2010)

As introduced earlier in Section 2.6, this work produced two sets of fragility curves for industrial URM buildings located in Montréal: “long direction” and “short direction”. The main difference between the sets consists in the length (and thus capacity) of the wall. The structure contains large openings in both directions and was built in the early 20th century. As a result, the comparison is done using the fragility curve parameters associated with a pre-code mid-rise URM located in Ottawa and with large openings. The greatest difference between the two sets of fragility curves is the number of storeys of the structures: six vs. three and the effects of this can be observed in Figure 5-11. The immediate occupancy curve for Karbassi (2010) is not as likely to sustain damage; this is a consequence of having a very long wall and thus a high capacity before cracks start propagating. The author’s second set of fragility curves in the “short direction” present the opposite situation as the same structural weight was imposed on a wall with much lower capacity as seen in Figure 5-12.

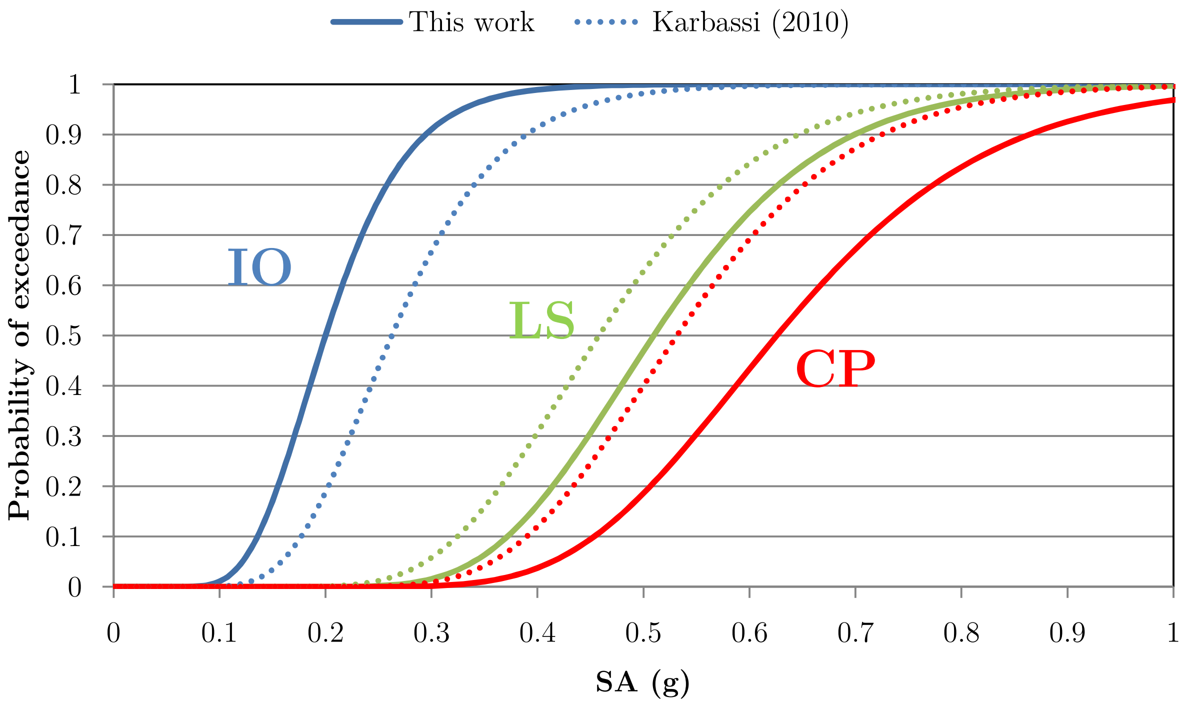

Figure 5-11: Fragility comparison with Karbassi (2010), "long direction"

In both cases, the life safety and collapse prevention levels are, as can be expected, not as fragile as in the current work. This indicates a greater non-linear capacity of a three-storey URM building as it carries a considerably smaller mass – this may be a result of the heavy axial load carried by the author's structure, making critical intensity occur at lower levels. One can also observe that the slope of the fragility curves for the same performance levels are very similar. In other words the deviation is very close and the main difference resides in the "translation" due to the median intensity level. One can conclude that despite their similar behaviours, industrial and residential URM structures present a vast difference in their likelihood to sustain damage during an earthquake.

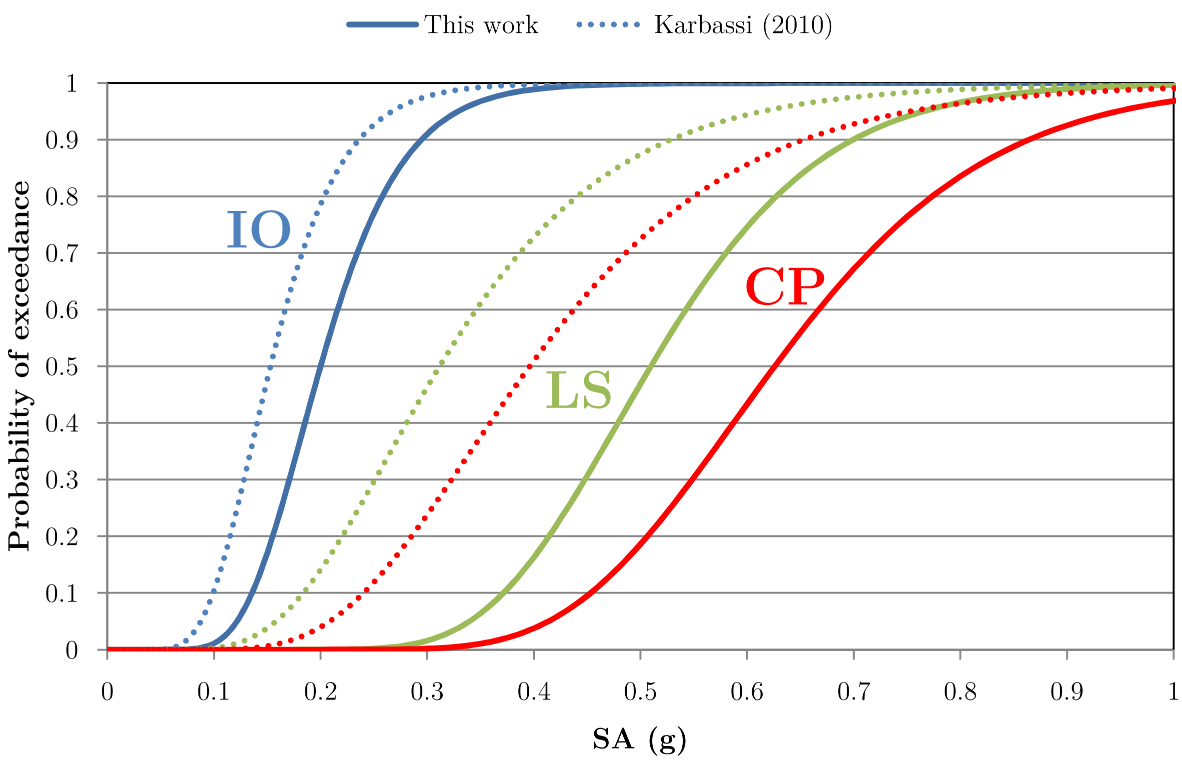

Figure 5-12: Fragility comparison with Karbassi (2010), "short direction"

5.3.2. Park et al. (2008)

Also introduced in Section 2.6, Park et al. (2008) developed three sets of fragility curves for low-rise essential facilities in the central and southern United States with degraded masonry state, featuring large openings. The three sets considered various degrees of connection between the in-plane and out-of-plane walls. This comparison is made with the sets having a sound connection between the walls. Unlike the current research, the authors used limit states to define structural damage. As a result, a direct comparison is difficult and one must resort to approximate comparison of the different damage levels identified. To facilitate the comparison, moderate damage is used as immediate occupancy; extensive damage is used as life safety; and complete damage is used as collapse prevention. The data used from the current work in the comparison is from a pre-code low-rise URM with large openings, situated in Ottawa as shown in Figure 5-13.

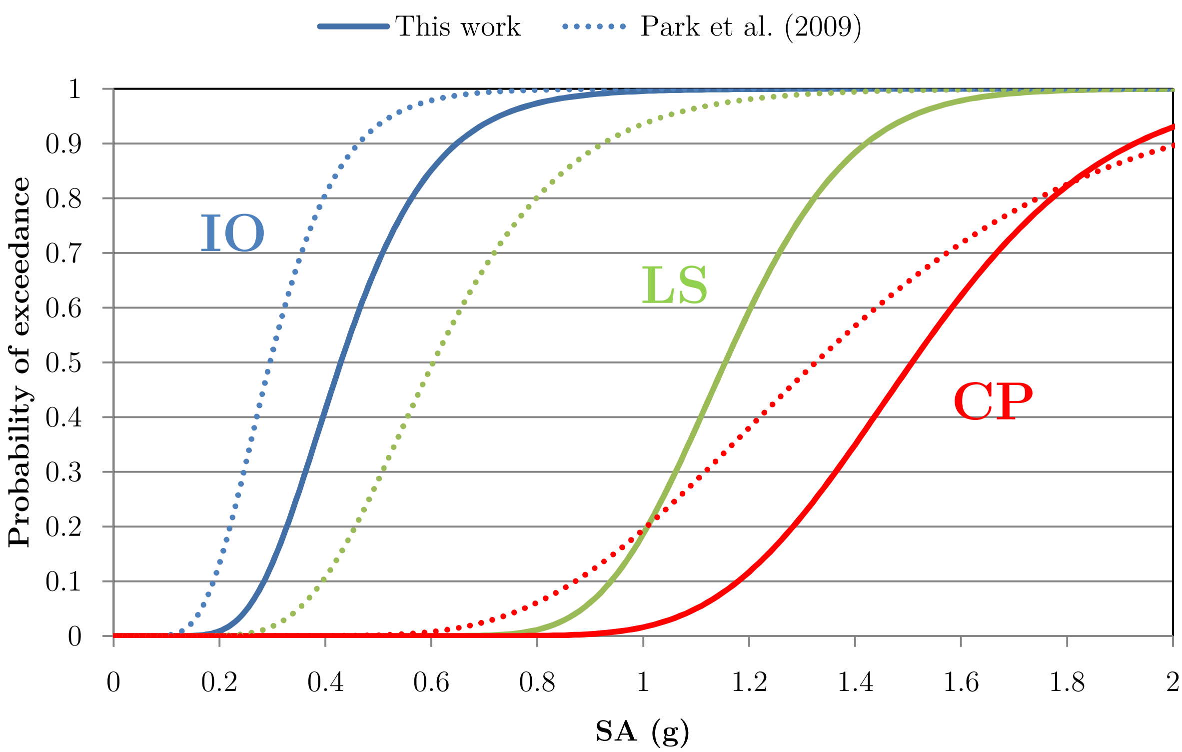

Figure 5-13: Fragility comparison with Park et al. (2008), “case 3”

The immediate occupancy and moderate damage curves are relatively close. The difference can be attributed mainly to the difference in material properties used: the authors considered degraded masonry state as suggested by FEMA 356 (compressive strength of 5.37 MPa). The life safety level is vastly different from the extensive limit state from their definition as 3/7 of the complete damage structural performance level compared to life safety being 3/4 of collapse prevention. It is therefore difficult to conclude anything between these two damage states. A more interesting comparison comes from the collapse prevention and complete damage curves. At higher intensities, there is little difference observable between the two. The observable contrast would be the significantly higher deviation from the authors’ work. One possible explanation for this resides in the approach used to obtain the intensities corresponding to these damage states. The current work used a hunt and fill algorithm with the objective of obtaining high precision on the collapse level, whereas Park et al. (2008) used a fixed intensity interval when scaling up the ground motions, as seen in Figure 5-14. This may have resulted in more uncertainty for the complete damage limit state and associated deviation.

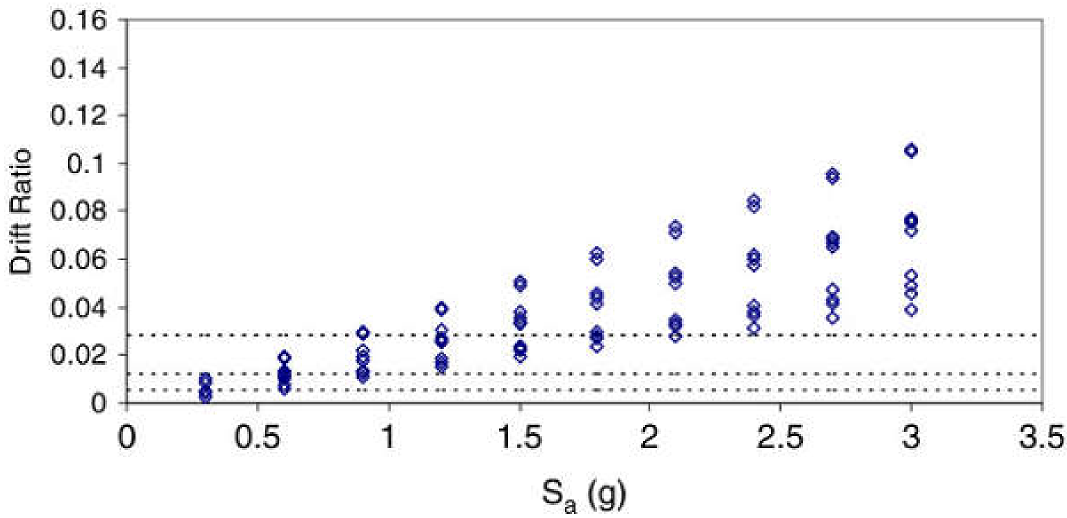

Figure 5-14: Ground motion intensities from Park et al. (2008)

5.3.3. Frankie (2010)

The author considered a database of URM structures in central and eastern United States and was able to generate curves for one to three storey high buildings with varying degrees of construction standards. As with Subsection 5.2.2, the damage states are expressed based on the definitions of Hazus-MH. A URMM from Frankie (2010), having three storeys with the most recent construction material built on competent rock is used. Competent rock is defined by the author as a soil which slightly attenuates the characteristic of ground motions. It is roughly comparable to soil class B as defined by the NBCC. The curves used from the present work represent a recent URMM built in Ottawa with large openings, as illustrated in Figure 5-15. The immediate occupancy level and moderate damage have some distance separating them, indicating that the structures considered are similar although the physical properties of the masonry may differ. On the other hand, the other two damage states vary greatly. The life safety and extensive damage levels are difficult to compare for the same reasons mentioned previously. The medians of the last damage states are far apart as well as the deviations, which greatly affect the slope of the fragility curve. As noted by the author and collaborators (Frankie et al. 2013), the work is done using the capacity spectrum method which does not consider the contribution of out-of-plane walls. They further acknowledge that their contribution may yield higher capacity as was the case with Park et al. (2008). The source and nature of ground motions may also contribute to this discrepancy, given that the primary selection criteria for this research came from spectral acceleration, in comparison with the PGA scaling used by Frankie (2010). As can be observed in Appendix B, several of the ground motions for eastern Canada featured high PGA spikes compared to the rest of the earthquake record. This may be responsible for increasing the required PGA levels, whereas the synthetic ground motions from Frankie (2010) did not exceed 0.275g.

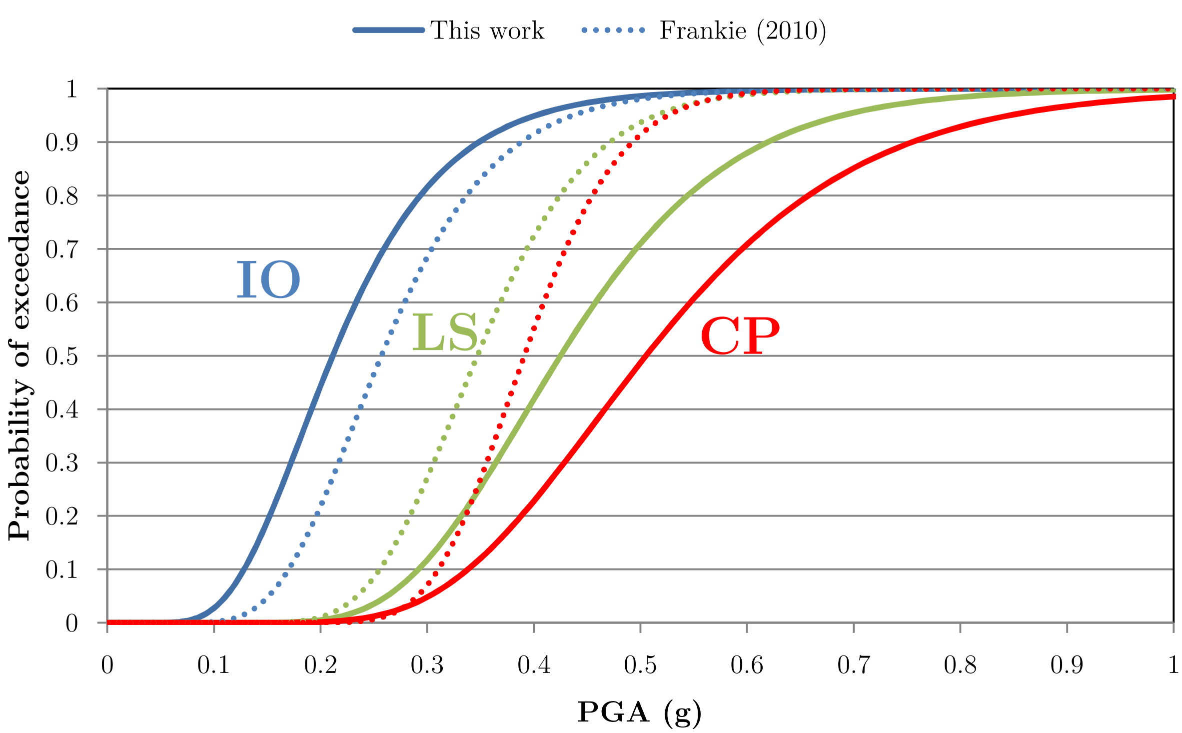

Figure 5-15: Fragility comparison with Frankie (2010), “3-storey uplands”

5.3.4. Hazus-MH

The last comparison presented in this Chapter is from Hazus-MH. As with the two previous Subsections, moderate, extensive and complete damage states are used for comparison. The selected parameters represent a pre-code URMM with large openings in Ottawa. The Hazus-MH parameters represent a similar pre-code URMM. As can be seen in Figure 5-16, the immediate occupancy and moderate damage curves are virtually superposed, differing in deviation more than anything else ($\sigma = 0.492$ and $\sigma = 0.600$, respectively). Once again, the extensive and life-safety curves are difficult to compare for reasons previously mentioned. The collapse prevention and complete damage states are in the same position as the IO and moderate damage: almost identical median (intensity corresponding to 50% probability of exceedance) but their deviations are significantly different ($\sigma = 0.288$ and $\sigma = 0.600$, respectively).

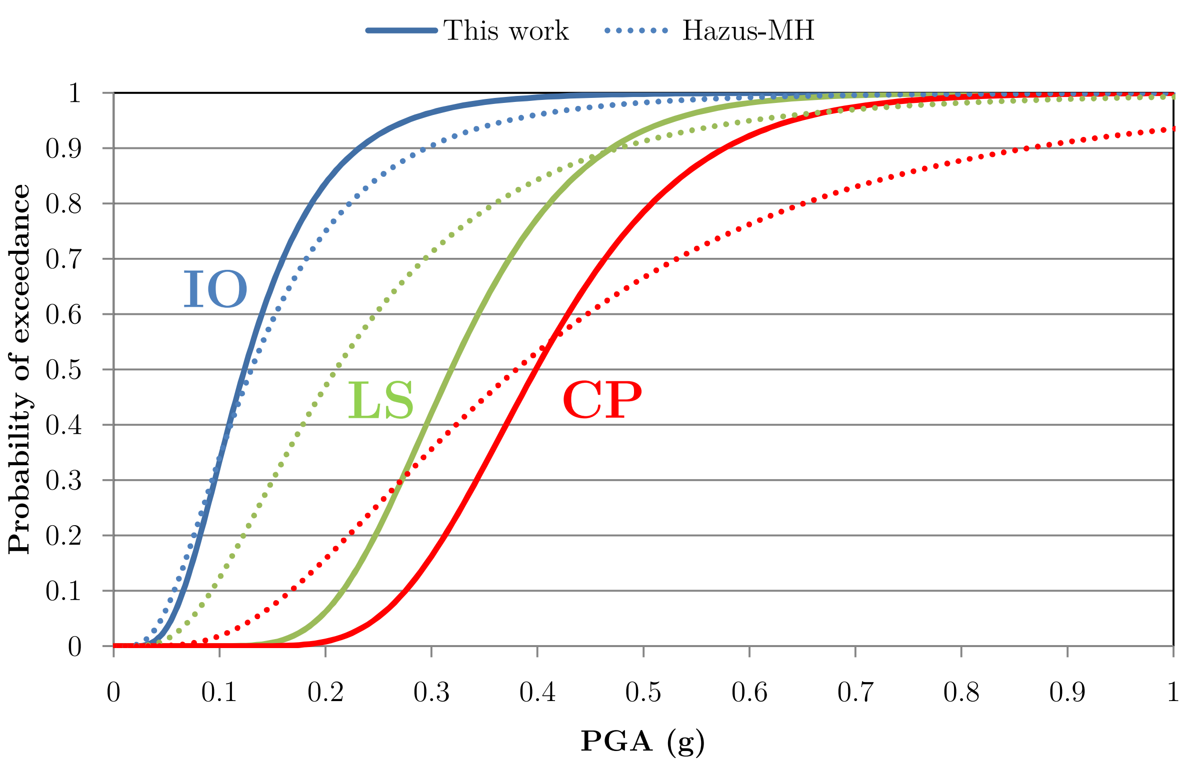

Figure 5-16: Fragility comparison with Hazus-MH (NIBS, 2003a), "URMM pre-code"

As presented in Section 2.6, these fragility curves were generated based on expert opinion and therefore include a relatively large uncertainty as evidenced by the deviation. Barring that distinction, the curves from the present work show strong agreement with those available in the Hazus-MH tool.

5.4 Effect of parameters on building fragility

As indicated in Section 5.2, a significant variability in structural damage can be experienced among different buildings even if they present similar characteristics. This section scrutinizes the effects of parameters that were selected to generate the fragility curves. The effects presented in this section were observed in different combinations of parameters, but in the interest of space, only a few are shown.

5.4.1. Year of construction

As previously detailed, the year of construction of structures was reflected on the models by the degradation of material mechanical properties. Comparing two structures built in different years but otherwise having identical characteristics should indicate that the newer URM to fare better under the same earthquake. Figure 5-17 illustrates this comparison for two such URMM buildings with large openings, built in Ottawa. The first observation that can be made is the significant increase in the capacity of the newer building. An intensity of 0.60g resulted in approximately 50% of probability of exceedance of collapse prevention damage state for the pre-code buildings, as opposed to the low-code structures, which fall below 5% of probability of exceedance. Additionally, the increase in immediate occupancy levels is fairly proportional to the increase in material strength: given that the ratio of mechanical properties is about twofold, the increase in intensity required to generate the same probability of exceedance should be in the vicinity of two. Another interesting observation comes from the increase of the LS and CP levels. The gap separating the two curves is consistent going from pre-code to low-code. This interestingly shows that the definition of the LS state as 75% displacement of the CP level does not directly affect the intensity, as it did for the IO damage state. This is to be expected of non-linear behaviour as the increase in intensity no longer directly relates to an increase in the deformations of buildings.

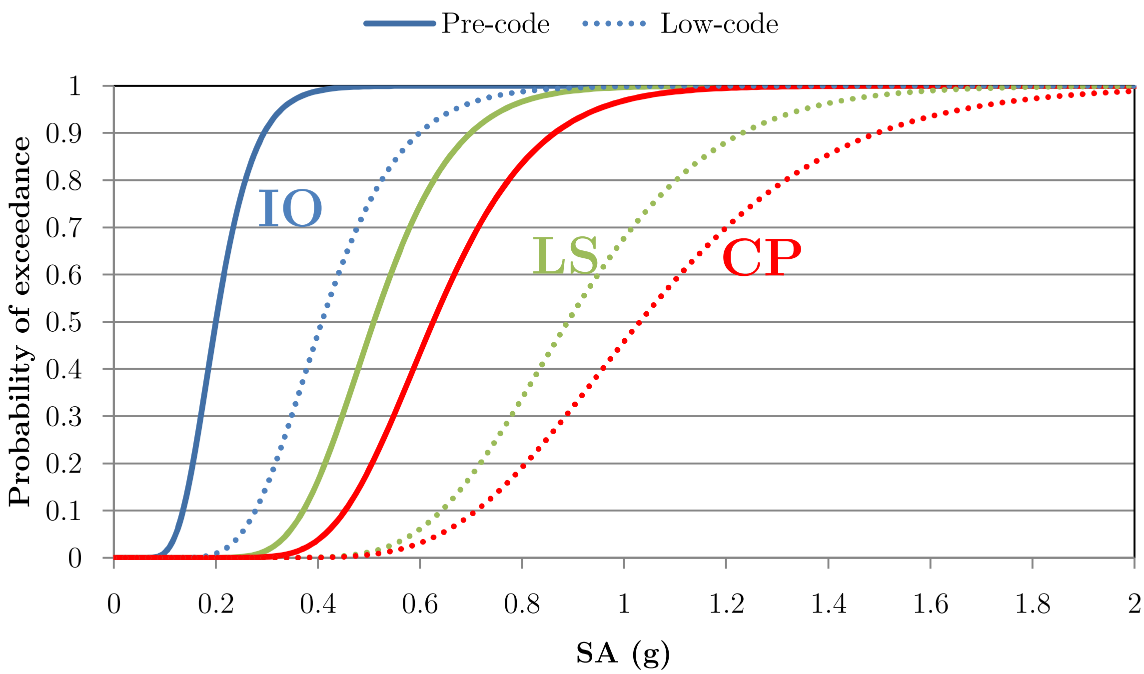

Figure 5-17: Year of construction effect on fragility

Similarly, one can see that the increase in non-linear capacity is greatly affected by the material strength. The gap between the two IO fragility curves is much smaller than that for LS and CP curves. During the analysis phase of the research, it was observed that toe crushing of rocking piers often indicated the collapse of the structure for older masonry (0.4% to 0.6% interstorey drift). Low-code structures featured the same rocking and sliding at similar interstorey drift levels, but toe crushing was observed no sooner than at 0.7% interstorey drift. As a result, greater intensities could be input to take advantage of rocking and sliding piers before a critical intensity would start severely damaging the structure. Unfortunately, time did not permit to explore the effects of intermediate material mechanical properties to better understand the progressive capacity decrease as a function of the age of construction.

5.4.2. Openings size

The amount of openings, their size and their position have a considerable effect on a wall; this is further detailed in Appendix C. Since URM building occupancy is not limited to any specific use, commercial URM structures often have large openings to serve as window displays, which subsequently reduce the capacity of the wall. Figure 5-18 shows the effect of openings on older low-rise URM buildings located in Ottawa. As with the year of construction, smaller openings lead to an increase in capacity. However this increase is generally not as important. The increase is also more important for the non-linear damage states, LS and CP, while the onset of yielding is slightly increased to reflect the enhanced capacity of the wall with smaller openings. There is also an increase in the deviation for the LS and CP levels but this was not observed for every parameter combinations.

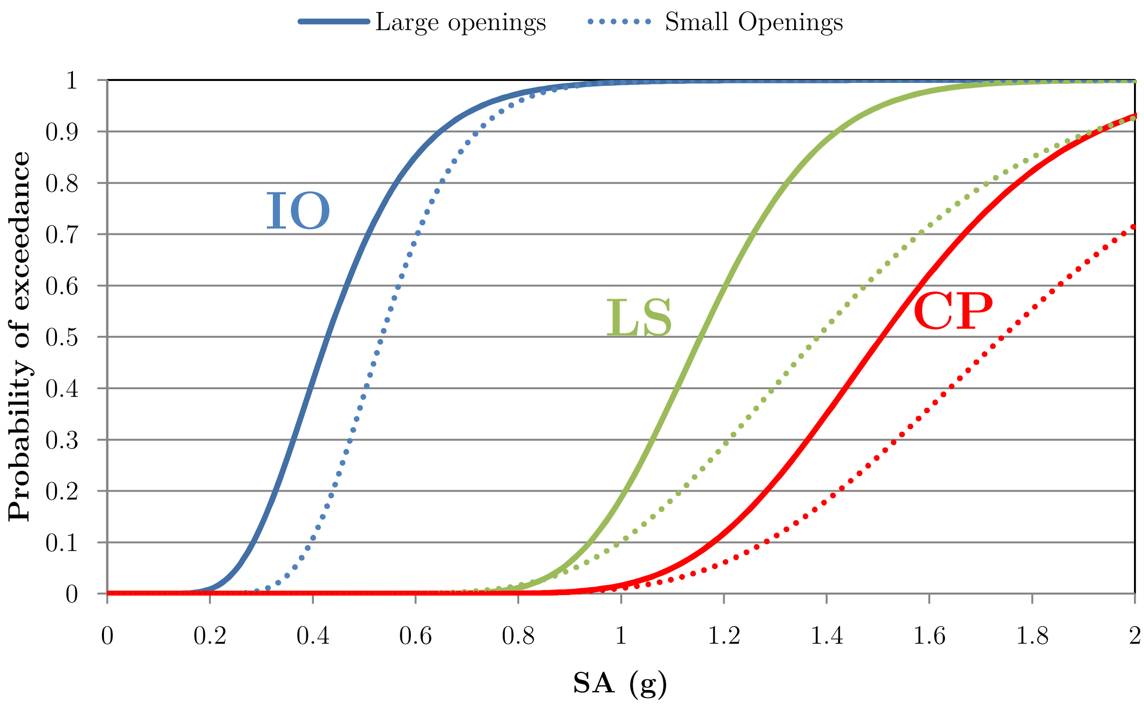

Figure 5-18: Openings effect on fragility

Overall, the effect of openings was found to be significant but less of a factor compared to the age of the structures. Given that URM walls are rarely identical in orthogonal directions, a conservative approach would be to estimate the capacity of the weakest wall and use the fragility curves of structures which closely matches the effective stiffness presented in this thesis.

5.4.3. Number of storeys

The number of storeys is known to affect the fragility of structures and as such, it is common to generate fragility curves for structures of different floor numbers although the difference between one and two storeys is not as prominent as the difference between two and three storeys (Barrantes, 2012; Frankie, 2010; NIBS, 2003a). Figure 5-19 shows the difference between pre-code URML and URMM with large openings in Western Canada. As with the two previous subsections, the gap separating the LS and CP remains relatively constant. Furthermore, the non-linear capacity is much more increased than the yield capacity. This can be explained by the walls being less overburdened from the weight of the above floors, delaying the occurrence of toe crushing. This difference further increased when considering the year of construction, as both the effects described here and those due to the year of construction in Subsection 5.3.1 acted in pair.

The amount of URM structures featuring more than 3 storeys is very small as mentioned in Section 3.1. The amount of work required to generate fragility curves for them is difficult to justify. Should the need arise; seismic assessment of individual structures would prove simpler and more accurate for these structures. Otherwise, a non-conservative approach would be to consider the fragility curves for URMMs presented in this work. For a more conservative approach, the work of Karbassi (2010) may be used for reasons presented in Subsection 5.2.1.

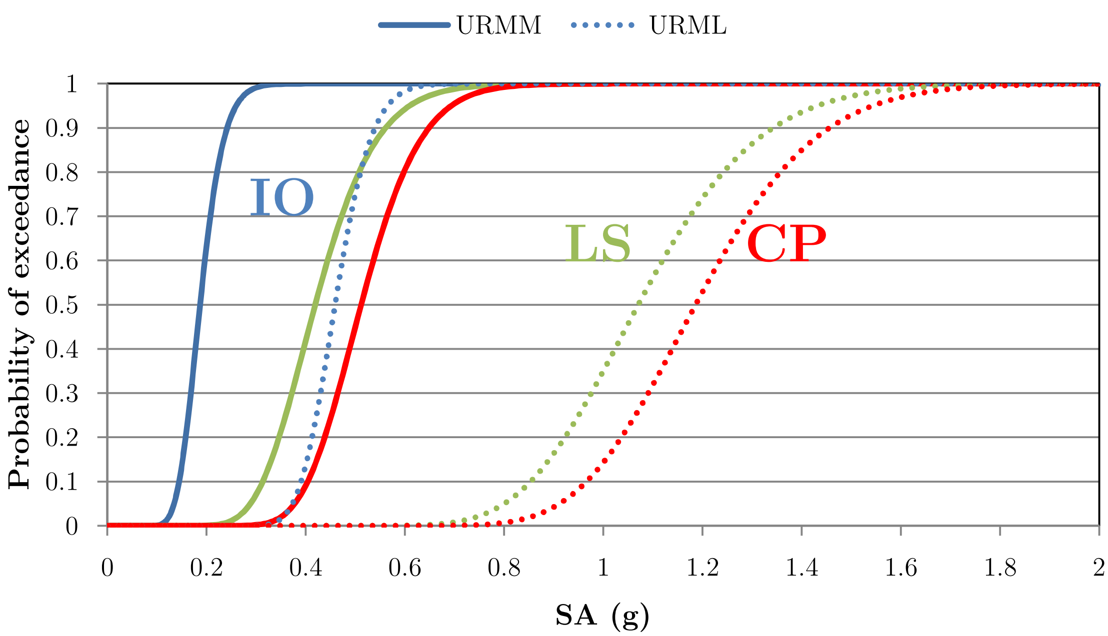

Figure 5-19: Effect of number of storeys on fragility

5.4.4. Geology

The sources of seismicity in Canada are very different in the east and west (Adams and Basham, 1989). The exact source of earthquakes in eastern Canada is still being debated. One of the hypotheses put forward is the weight of the melted glaciers that used to cover North America, causing subsidence and eventual crust rebound as shown in Figure 5-20 (Adams and Basham, 1989). As a result, in the present work different accelerograms were selected from the work of Atkinson (2009) that are representative of the seismicity of the region before being scaled represent the target UHS of an important city in each of those regions. Fragility curves for a pre-code URMM with large openings are shown in Figure 5-21 for both the eastern and western coasts of Canada. The first observation that can be made is that the immediate occupancy level is essentially the same, albeit with some variation in deviation. This should be expected and shows consistency in that the same force is required to reach the yield point of the structure. On the other hand, there is a noticeable reduction in the intensity required to reach the life safety and collapse prevention levels; it is dully noted that the distance between both respective curves is about equal for reasons previously mentioned.

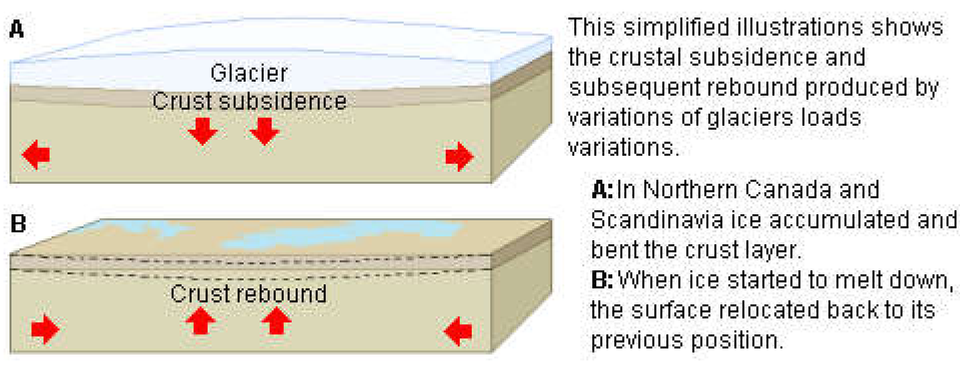

Figure 5-20: Crust rebound due to glaciers, from Wikimedia Foundation by Luis María Benítez

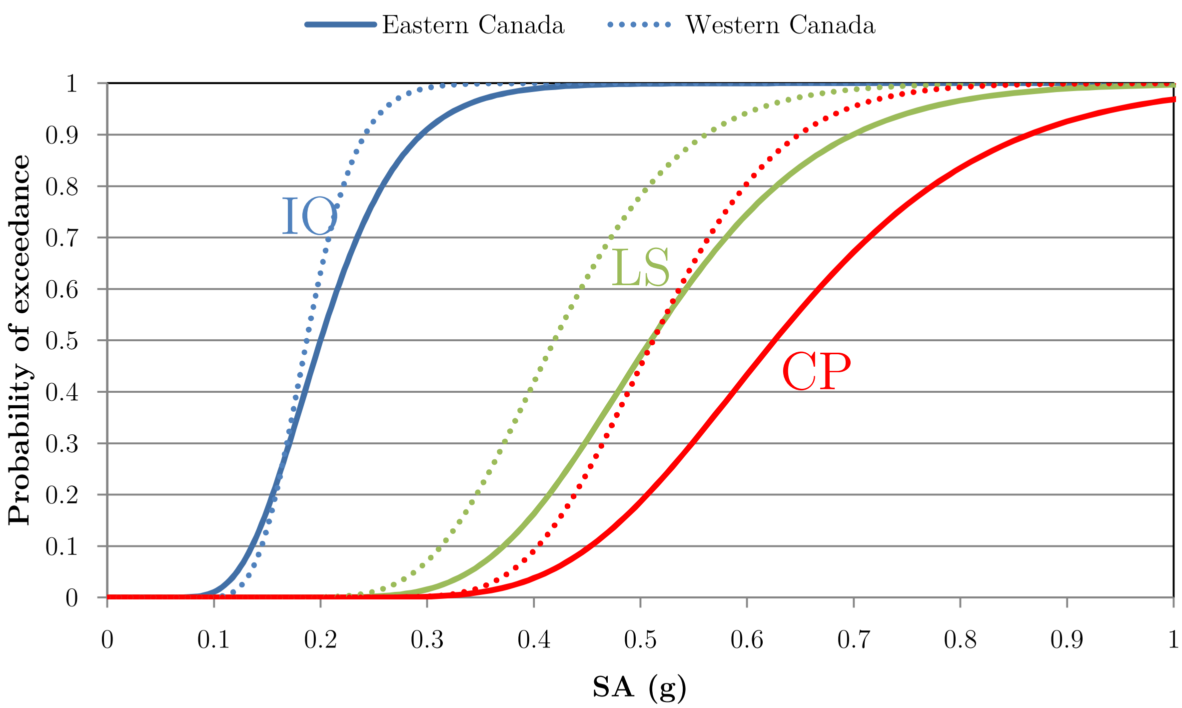

Figure 5-21: Effect of geology on fragility

The ground motions developed by Atkinson (2009) feature several differences when moving from coast to coast as illustrated in Appendix C. Among these, the duration of the earthquakes is typically much longer in the west. This aspect is further investigated in the next Subsection. Atkinson (2009) also provided ground motions at different time intervals to better represent the status of the underlying crust and source of earthquakes. In the east, the shaking is of a higher frequency with a time interval of 0.002 sec, while in the west the time interval is over twice that for the east at 0.005 sec. The input energy resulting from this, sometimes measured as the Arias intensity $I_A = \frac{\pi}{2g}\int_0^T x^2 dt$, would be much greater for earthquakes with larger time intervals and can lead to damage at lower spectral acceleration intensity in the non-linear range.

5.4.5. Earthquake duration

While the fragility curve parameters pertaining to ground motions of various durations are not presented in Chapter 4, the results are examined in order to investigate the effect of the shaking duration on structural fragility. This parameter was not originally intended to be investigated. Furthermore, there is no clear definition of duration groups or sufficient amount of records to generate robust fragility curves.

Longer shaking of ground has shown to be a source of greater damage in structures (Oyarzo-Vera and Chouw, 2008). As mentioned in Subsection 5.3.4, the longer accelerograms in the west resulted in more damage to the structure at equal intensities in the non-linear range. However, this has also been shown to be true in the east. For the pre-code URMM with large openings located in eastern Canada, determined limit states were separated based on their duration such that a set of only the longer earthquakes remained. The fragility curves generated in Chapter 4 with all of the ground motions are used as benchmark. For the sake of comparison, the ground motions issued from sets 7c1 and 7c2 (with a strong motion activity averaging approximately 16s, compared to an average of 5.8s for sets 6c1 and 6c2) are used to generate a new set of fragility curves which clearly showcase the effect of having a longer ground motion sequence. Refer to Appendix B and Table B-1 for more information. As shown in Figure 5-22, the spectral acceleration required to yield the structure remains virtually unchanged whereas the LS and CP limit states fragility curves shift left by a considerable level. This indicates that given a sufficiently long earthquake, lower levels of ground motion intensity may prove sufficient to create severe damage on structures when compared to shorter ground motions.

As concluded by Oyarzo-Vera and Chouw (2008), the longer duration tends to increase the accumulated damage in the non-linear portion. This can be explained by the accumulation of cracks, weakening and softening of the walls which subsequently result in larger deformations even if the shaking is not as intense as that of a shorter earthquake. A good example of this comes from the URMM ground motion E6c1_1 which presents the highest peak ground acceleration of all records at 0.50g as well as shortest ground motion duration. Yet, as Table 4-1 shows, the required spectral acceleration and peak ground accelerations required to obtain the LS and CP damage levels are amongst the highest of the table.

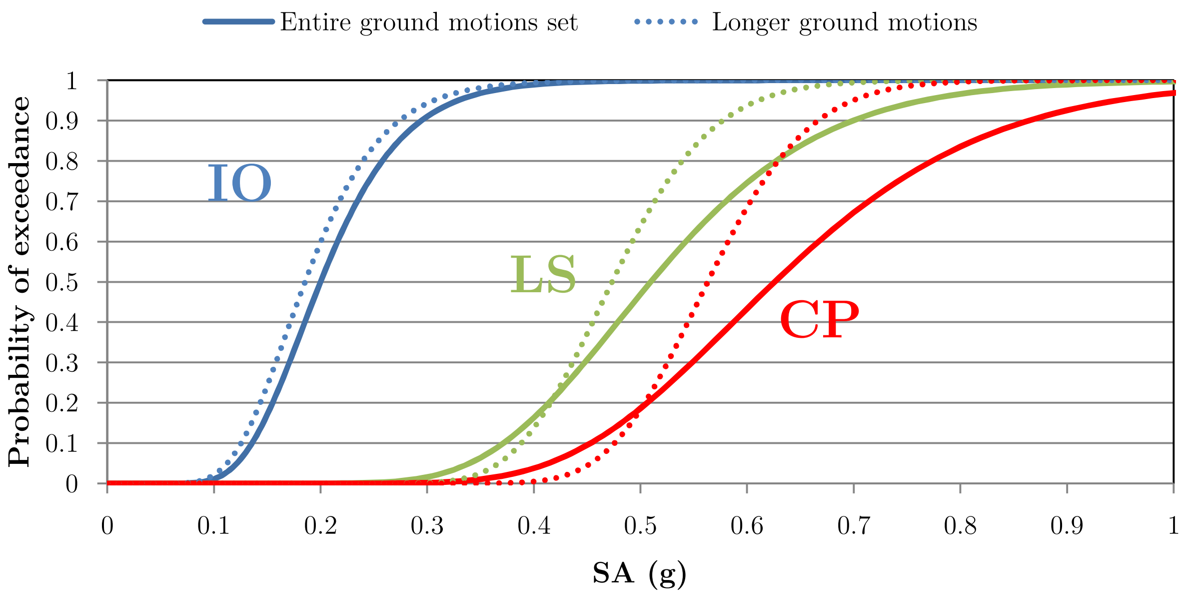

Figure 5-22: Effect of accelerogram length on fragility

5.4.6. Intensity measure

Two intensity measures were used; spectral acceleration and peak ground acceleration. As was previously discussed, the accelerograms used in this work were selected based on a process involving scaling, relative to UHS. This is not to say that one measure is superior to the other but that given the selection method, the deviation of the fragility curves are likely to be smaller when measuring against spectral acceleration. This can be seen in the data from Table 4-13 and by calculating the relative deviation, that is the ratio of the deviation to the median of the limit state. For said data, the ratios for IO, LS and CP are shown in Table 5-4.

Table 5-4: Deviation to median ratio of fragility parameters

Limit state	Spectral acceleration deviation ratio	Peak ground acceleration deviation ratio
Immediate occupancy	0.34	0.83
Life safety	0.28	0.41
Collapse prevention	0.28	0.36

Arguments can be made to show that spectral acceleration is a better indicator as the first mode of vibration tends to govern short structures (e.g. Karbassi, 2010), or that peak ground acceleration provides better information as URMs are sensitive to PGA increases (e.g. Frankie, 2010) or that even another measure such as Arias intensity (e.g. Oyarzo-Vera and Chouw, 2008) provides better relationships. For the sake of convenience and as the information was readily available, it was decided to provide both, in addition to the spectral displacement parameters.

Chapter 6

Summary and Conclusions

6.1 Summary

Seismic assessment of typical URM structures in eastern and western Canada has been conducted by investigating the cities of Ottawa and Vancouver as representative locations of eastern and western Canadian seismicity. The structures considered in the assessment were selected from characteristics obtained from a large building inventory developed by Sawada et al. (2014). The inclusion of that work ensured that the structures considered would be representative of the construction practice in Canada. Twenty synthetic ground motions were used for each location (Ottawa and Vancouver) to conduct this assessment. The accelerograms were carefully selected from a dataset provided by Atkinson (2009) to ensure compatibility with Canadian sources of seismology. A review of literature was conducted to obtain the material properties that represent the conditions of the year of construction. Analytical models were developed using the applied element method which allowed the masonry to show its collapse gradually through typical in-plane failures.

Using the information gathered, incremental dynamic analysis was carried out to determine the response of structures not only at an earthquake of code-level but also for earthquakes of smaller and larger intensities. This analysis was pursued until collapse of the structures so that performance limit states could be adequately determined. Fragility curves were then established for different URM buildings with different characteristics. The fragility curves provided an effective relationship between the intensity of the ground shaking and the likely damage sustained by URM structures. The results were then verified through statistical means and by comparing with other existing fragility curves developed for North America. Finally, the effects of selected parameters were investigated.

6.2 Conclusions

The following conclusions can be drawn from the current research and development project, which resulted in seismic fragility curves for URM buildings in Canada:

- While fragility curves vary with structural and ground motion parameters, the set of curves developed in this investigation, representative of the majority of URM buildings built in Ottawa, provide seismic vulnerability assessment of existing URM buildings in Canada. The fragility curves generated appear to correlate well with others developed for other regions in North America for other URM buildings, with expected differences that can be rationalized based on the characteristics of structural and ground motion parameters considered.
- The verification of the log-normal distribution hypothesis for the fragility curves indicated that the coefficients of determination were almost all well above the 0.9 mark, which shows that the hypothesis is sound. The relative standard error of the mean for the damage measure also showed that the performance level limit states obtained are well defined.
- Both spectral acceleration and peak ground acceleration showed to be valid intensity measures for the fragility curves developed. In the present work, the selection of accelerograms suggested by Atkinson (2009) may have slightly influenced the deviation parameter of the fragility curves based on peak ground acceleration.
- The year of construction showed to have a considerable influence on in-plane fragility: the more recent low-rise structures did not have time to develop

significant in-plane damage before out-of-plane failures occurred. This showed that the ASCE 41 slenderness ratio of 9 is not conservative enough. This observation corroborates well with the findings of Penner (2014). Furthermore, newer constructions featured a considerable increase in non-linear capacity, which reflects the improvements in the construction practice through the years.

- The effect of openings (amount, size and location) had a considerable effect on the vulnerability of older URM buildings, although this effect is not as apparent in newer buildings. This parameter showed considerable variation in the building inventory. Therefore, it is suggested that more variations of this parameter be considered to fully understand its effect.
- The effect of the number of storeys confirmed previous research, in that the additional height and weight contributed to a greater likelihood of damage.
- The nature of earthquakes showed to have a non-negligible effect on the fragility of URM buildings. Longer earthquakes were typically responsible for more damage at equal ground motion intensities. Earthquakes from the west coast of Canada showed a pronounced effect of this phenomenon when compared with those from the east coast. The influence of the duration of earthquakes as a factor is becoming increasingly present in the literature, as confirmed by Oyarzo-Vera and Chouw (2008). On the other hand, the difference in non-linear capacity observed between the eastern and western earthquakes is less understood, and may be attributed to the difference in the seismicity of each region.

6.3 Recommendations for future research

These recommendations are aimed at enhancing the current work either by improving existing weaknesses or by furthering research on the topic.

- Simpler models could be developed and calibrated to the present results. This would speed up further analysis and allow consideration of more parameter combinations (openings effect, year of construction, effect of diaphragm age, effect of slenderness on in-plane capacity);
- Develop in-plane fragility curves for low-rise masonry structures built around 1970 by using an adequate height-to-thickness ratio of the masonry walls;
- Work with a building inventory from Vancouver in order to better assess structures representative of western Canada;
- Incorporate the economical portion of the seismic risk assessment;
- Test some of the more common irregularities such as re-entrant corners of low impact;
- Include buildings arranged in a row to investigate the results of pounding damage;
- Combine in-plane with existing out-of-plane fragility curves in order to develop global fragility curves;
- Extend the work to include non-structural elements such as chimneys, parapets, brick veneers.

References

Abo-El-Ezz, A., Nollet, M.-J., and Nastev, M. (2013). Seismic fragility assessment of low-rise stone masonry buildings. Earthquake Engineering and Engineering Vibration, 12(1), 87-97.

Abrams, D. P. (2001). Performance-based engineering concepts for unreinforced masonry building structures. Prog. Struct. Engng Mater., 3: 48–56. doi: 10.1002/pse.70

Adams, J., and P.W. Basham, (1989). The seismicity and seismotectonics of Canada East of the Cordillera, Geoscience Canada, 16, 3-16

ASI. (2013). Theoretical Manual. Applied Science International. Raleigh, NC.

ASI. (2010a). Modeling Manual. Applied Science International. Raleigh, NC.

ASI. (2010b). Quick Start Guide. Applied Science International. Raleigh, NC.

ASI. (2010c). Results Viewer User Manual. Applied Science International. Raleigh, NC.

ASCE. (2000). Prestandard and commentary for the seismic rehabilitation of buildings. FEMA 356. American Society of Civil Engineers. Reston, Virginia, USA.

ASCE. (2007). Seismic rehabilitation of existing buildings. ASCE 41-06. American Society of Civil Engineers. Reston, Virginia, USA.

ASCE. (2014). Seismic evaluation and retrofit of existing buildings. ASCE 41-13. American Society of Civil Engineers. Reston, Virginia, USA.

Atkinson, G. M. (2009). Earthquake time histories compatible with the 2005 National building code of Canada uniform hazard spectrum. Canadian Journal of Civil Engineering, 36(6), 991-1000.

Atkinson, G. M., and Beresnev, I. A. (1998). Compatible ground-motion time histories for new national seismic hazard maps. Canadian Journal of Civil Engineering, 25(2), 305-318.

Bakeer, T. (2009). Collapse analysis of masonry structures under earthquake actions. Ph. D. Thesis. Technische Universität Dresden. Dresden, Germany.

Barrantes, J.M. (2012). Seismic risk assessment of unreinforced masonry buildings at a territorial scale. Ph.D. Thesis. University of Braunschweig - Institute of Technology. Braunschweig, Germany. University of Florence. Florence, Italy.

Bélec, G., Saatcioglu, M. and Sawada, M. (2015). Seismic assessment of typical unreinforced masonry buildings using non-linear time history analysis. Paper presented at the Proceedings of the 11th Canadian Conference on Earthquake Engineering. July 21-24th, 2015. Victoria, BC.

Beyer, K., and Bommer, J. J. (2007). Selection and scaling of real accelerograms for bi-directional loading: a review of current practice and code provisions. Journal of Earthquake Engineering, 11(S1), 13-45.

Bilgin, H. (2013). Fragility-based assessment of public buildings in turkey. Engineering Structures, 56, 1283-1294.

Bloomberg. (2015, April 28th). Nepal building code author says disaster was waiting to happen. Retrieved from http://bloomberg.com.

Bostrom, A., French, S. P., and Gottlieb, S. J. (Eds.). (2008). Risk assessment, modeling and decision support: Strategic directions (Vol. 14). Springer Science and Business Media.

Bothara, J. K., Dhakal, R. P., and Mander, J. B. (2010). Seismic performance of an unreinforced masonry building: an experimental investigation. Earthquake Engineering and Structural Dynamics, 39(1), 45-68.

Bruneau, M. (1994). Seismic evaluation of unreinforced masonry buildings-a state-of-the-art report. Canadian Journal of Civil Engineering, 21(3), 512-539.

Bruneau, M., and Lamontagne, M. (1994). Damage from 20th century earthquakes in eastern Canada and seismic vulnerability of unreinforced masonry buildings. Canadian Journal of Civil Engineering, 21(4), 643-662.

Brzev, S. (2010). Course E7: Seismic Rehabilitation of Masonry Buildings. [PowerPoint slides], Structural Engineers Association of British Columbia (SEABC), British Columbia, Canada.

Ceran, H. B., and Erberik, M. A. (2013). Effect of out-of-plane behaviour on seismic fragility of masonry buildings in turkey. Bulletin of Earthquake Engineering, 11(5), 1775-1795.

D'Ayala, D., R. Spence, R. Oliveira and Pomonis, A.. (1997). Earthquake loss estimation for Europe's historic town centers. Earthquake Spectra, vol. 13, no 4, p. 773-793.

D'Ayala, D., and Speranza, E. (2003). Definition of collapse mechanisms and seismic vulnerability of historic masonry buildings. Earthquake Spectra, 19(3), 479-509.

Derakhshan, H. (2011). Seismic assessment of out-of-plane loaded unreinforced masonry walls. Ph.D. Thesis. The University of Auckland. Auckland, New Zealand.

Derakhshan, H., Dizhur, D., Griffith, M. C., and Ingham, J. M. (2014). In Situ Out-of-Plane Testing of As-Built and Retrofitted Unreinforced Masonry Walls. Journal of Structural Engineering, 140(6).

Dizhur, D., Lumantarna, R., Ismail, N., Ingham, J. M., and Knox, C. (2010). Performance of unreinforced and retrofitted masonry buildings during the 2010 Darfield earthquake. Bulletin of the New Zealand Society for Earthquake Engineering, 43(4), 321.

Drysdale, R.G., and Hamid, A.A. (2005). Masonry structures: Behavior and design. Mississauga, Ontario: Canadian Masonry Design Centre.

Drysdale, R. G. (2012). The Evolution of the Design and Construction of Masonry Buildings in Canada. Gestão and Tecnologia de Projetos, 7(2), 35-43.

Elsabbagh, A. (2013). Seismic risk assessment of unreinforced masonry buildings using fuzzy based techniques and the regional seismic risk assessment of Ottawa, Ontario. M.A.Sc. Thesis. University of Ottawa. Ottawa, Canada.

Erberik, M. A. (2008). Generation of fragility curves for Turkish masonry buildings considering in-plane failure modes. Earthquake Engineering and Structural Dynamics, 37(3), 387-405.

Erberik, M.A., Ceran, H.B. (2012). Seismic Safety Evaluation of Turkish URM Buildings by Considering Both In-Plane and Out-Of-Plane Behaviour. "Proceedings of the 15th World Conference on Earthquake Engineering"

Frankie, T. M., Gencturk, B., and Elnashai, A. S. (2013). Simulation-based fragility relationships for unreinforced masonry buildings. Journal of Structural Engineering (United States), 139(3), 400-410.

Frankie, T.M. (2010). Simulation-based fragility relationships for unreinforced masonry buildings. M.Sc. Thesis. University of Illinois. Urbana, United States of America.

Ghorbanie-Asl, M. (2007) Performance-based seismic design of building structures. Ph.D. Thesis. Carleton University. Ottawa, Canada.

Grubbs, A. J., Hueste, M. B., and Bracci, J. M. (2007). Seismic Rehabilitation of Wood Diaphragms in Unreinforced Masonry Buildings.

Hill, M., and Rossetto, T. (2008). Comparison of building damage scales and damage descriptions for use in earthquake loss modelling in Europe. Bulletin of Earthquake Engineering, 6(2), 335-365.

Ingham, J. M. (May 2013). Fundamentals of the earthquake response of unreinforced masonry buildings and Lessons re-learned from the Canterbury earthquakes.

Ingham, J. M., and Griffith, M. C. (2011a). The performance of unreinforced masonry buildings in the 2010/2011 Canterbury earthquake swarm. Canterbury Earthquakes Royal Commission of Inquiry, Christchurch.

Ingham, J. M., and Griffith, M. C. (2011b). The performance of earthquake strengthened URM buildings in the Christchurch CBD in the 22 February 2011 earthquake. Canterbury Earthquakes Royal Commission of Inquiry, Christchurch.

Ingham, J. M., Biggs, D. T., and Moon, L. M. (2011). How did unreinforced masonry buildings perform in the February 2011 Christchurch earthquake?. Structural Engineer, 89(6), 14-18.

Ismail, N., Laursen, P. T., Schultz, A. E., and Ingham, J. M. (2011). Cyclic out-of-plane behaviour of post-tensioned clay brick masonry. In The Eleventh North American Masonry Conference.

Kafle, B., Lam, N. T. K., Gad, E. F., and Wilson, J. (2011). Displacement controlled rocking behaviour of rigid objects. Earthquake Engineering and Structural Dynamics, 40(15), 1653-1669.

Karantoni, F., Lyrantzaki, F., Tsionis, G., and Fardis, M. N. (2012, September). Seismic fragility functions of stone masonry buildings. In Proceedings of the 15th world conference on earthquake engineering (pp. 24-28).

Karbassi, A. (2010). Performance-based seismic vulnerability evaluation of existing buildings in old sectors of Quebec. Ph.D. Thesis. École de technologie supérieure - Université du Québec. Montréal, Canada.

Karbassi, A., and Lestuzzi, P. (2012). Fragility analysis of existing unreinforced masonry buildings through a numerical-based methodology. Open Civil Engineering Journal,6(SPEC.ISS.1), 121-130.

Karbassi, A., and Nollet, M.-J. (2013). Performance-based seismic vulnerability evaluation of masonry buildings using applied element method in a nonlinear dynamic-based analytical procedure. Earthquake Spectra, 29(2), 399-426.

Lagomarsino, S., Penna, A., Galasco, A., and Cattari, S. (2013). TREMURI program: An equivalent frame model for the nonlinear seismic analysis of masonry buildings. Engineering Structures, 56, 1787-1799.

Lang, K. (2002). Seismic vulnerability of existing buildings. Ph.D. Thesis. Institute of Structural Engineering - Swiss Federal Institute of Technology. Zurich, Switzerland.

Lazzarini, D.L. (2009). Seismic performance of unreinforced masonry walls retrofitted with post-tensioning tendons. M.A.Sc. Thesis. California Polytechnic State University. San Luis Obispo, United States of America.

Lefebvre, K. (2004). Caractérisation structurale et évaluation de la vulnérabilité sismique des bâtiments historiques en maçonnerie du vieux-Montréal. M.Ing. Dissertation. École de technologie supérieure - Université du Québec. Montréal, Canada.

Lefebvre, K. (2012). Étude du comportement sous charges latérales des ossatures de béton armé avec murs de remplissage de maçonnerie, construites avant les années 1960. Ph.D. Thesis. École de technologie supérieure - Université du Québec. Montréal, Canada.

Lin, L., Naumoski, N., Saatcioglu, M., Foo, S., Booth, E., and Gao, Y. (2013). Selection of seismic excitations for nonlinear analysis of reinforced concrete frame buildings1. Canadian Journal of Civil Engineering, 40(5), 411-426.

Lumantarna, R. (2012). Material Characterisation of New Zealand's clay brick unreinforced masonry buildings (Doctoral dissertation, ResearchSpace@ Auckland).

Lumantarna, R., Biggs, D. T., and Ingham, J. M. (2012a). Compressive, Flexural Bond, and Shear Bond Strengths of In Situ New Zealand Unreinforced Clay Brick Masonry Constructed Using Lime Mortar between the 1880s and 1940s.Journal of Materials in Civil Engineering, 26(4), 559-566.

Lumantarna, R., Biggs, D. T., and Ingham, J. M. (2012b). Uniaxial Compressive Strength and Stiffness of Field-Extracted and Laboratory-Constructed Masonry Prisms. Journal of Materials in Civil Engineering, 26(4), 567-575.

Magenes, G. (2010, July). Earthquake resistant design of masonry structures: rules, backgrounds, latest findings. In Proc. 8th International Masonry Conference, Dresden, Germany (pp. 04-07).

Mebarki, A., Boukri, M., Laribi, A., Farsi, M., Belazougui, M., and Kharchi, F. (2013). Seismic vulnerability: Theory and application to Algerian buildings. Journal of Seismology, 1-13.

Meguro, K. and Tagel-Din, H. (1999). Applied Element Method: A New Efficient Tool for Design of Structure Considering Its Failure Behaviour. In Proc. of the 7th US-Japan Workshop on Earthquake Resistant Design of Lifeline Facilities and Countermeasures against Soil Liquefaction. Washington

Meisl, C.S. (2006). Out-of-plane seismic performance of unreinforced clay brick masonry walls. M.A.Sc. Thesis. The University of British Columbia. Vancouver, Canada.

Mitchell, D., Paultre, P., Tinawi, R., Saatcioglu, M., Tremblay, R., Elwood, K., Adams, J. and DeVall, R. (2010). Evolution of seismic design provisions in the National building code of Canada. Canadian Journal of Civil Engineering, 37(9), 1157-1170.

Mouyiannou, A., Penna, A., Rota, M., Graziotti, F., and Magenes, G. (2014). Implications of cumulated seismic damage on the seismic performance of unreinforced masonry buildings. University of Pavia, Pavia

National Research Council of Canada. (2010). National building code of Canada. Ottawa: Associate Committee on the National Building Code, National Research Council.

NIBS. (1997). Advanced engineering building module. Hazus-MH 2.1. Federal Emergency Management Agency. Redwood City, Washington, D.C., USA.

NIBS. (2003a). Multi-hazard loss estimation methodology: earthquake model. Hazus-MH 2.1, Technical manual. National Institute of Building Science. Washington, D.C., USA.

NIBS. (2003b). Multi-hazard loss estimation methodology: earthquake model. Hazus-MH 2.1, User manual. National Institute of Building Science. Washington, D.C., USA.

NIBS. (2003c). Multi-hazard loss estimation methodology: earthquake model. Hazus-MH MR4, Theoretical manual. National Institute of Building Science. Washington, D.C., USA.

NRCC. (1993). Manual for screening of buildings for seismic investigation. Institute for Research in Construction, National Research Council Canada. Ottawa, Canada.

Onur, T. (2001). Seismic risk assessment in southwestern British Columbia. Ph.D. Thesis. The University of British Columbia. Vancouver, Canada.

OPCM 3431. (2005). “Ulteriori modifiche ed integrazioni all'Ordinanza n.3274 del 20/3/2003, recante ‘Primi elementi in materia di criteri generali per la classificazione sismica del territorio nazionale e di normative tecniche per le costruzioni in zona sismica' " S.O. n.85 alla G.U. n.107 del 10/5/2005.

Pantazopoulou, S. J. (2013). State of the art report for the analysis methods for unreinforced masonry heritage structures and monuments. European center for preparedness and forecasting of earthquakes. URL: ecpfe. oasp. gr/en/node/89.

Paquette, J., and Bruneau, M. (2003). Pseudo-dynamic testing of unreinforced masonry building with flexible diaphragm. Journal of Structural Engineering, 129(6), 708-716.

Paquette, J., and Bruneau, M. (2006). Pseudo-dynamic testing of unreinforced masonry building with flexible diaphragm and comparison with existing procedures. Construction and Building Materials, 20(4), 220-228.

Parisi, F., and Augenti, N. (2012). Uncertainty in seismic capacity of masonry buildings. Buildings, 2(3), 218-230.

Parisi, F., and Augenti, N. (2013). Seismic capacity of irregular unreinforced masonry walls with openings. Earthquake Engineering and Structural Dynamics, 42(1), 101-121.

Park, J., Towashiraporn, P., Craig, J. I., and Goodno, B. J. (2008). Seismic fragility analysis of low-rise unreinforced masonry structures. Engineering Structures, 31(1), 125-137.

Pasticier, L., Amadio, C., and Fragiacomo, M. (2008). Non-linear seismic analysis and vulnerability evaluation of a masonry building by means of the SAP2000 V.10 code. Earthquake Engineering and Structural Dynamics, 37(3), 467-485.

Penner, O. (2014). Out-of-plane dynamic stability of unreinforced masonry walls connected to flexible diaphragms. Ph.D. Thesis. The University of British Columbia. Vancouver, Canada.

Priestley, M. J. N. (2000). Performance based seismic design. Bulletin of the New Zealand Society for Earthquake Engineering, 33(3), 325-346.

Priestley, M.J.N., Calvi, G.M. and Jowalsky, M.J. (2007). Displacement-Based Seismic Design of Structures. IUSS Press, Pavia, 721 pages.

Rainer, J. H., D. E. Allen, and A. M. Jablonski. (1992). Manual for Screening of Buildings for Seismic Investigation. Published by the National Research Council Canada of Canada, Ottawa, Ontario.

Rota, M., Penna, A., and Magenes, G. (2010). A methodology for deriving analytical fragility curves for masonry buildings based on stochastic nonlinear analyses. Engineering Structures, 32(5), 1312-1323.

Sabatino, R., and Rizzano, G. (2011). A simplified approach for the seismic analysis of masonry structures. Open Construction and Building Technology Journal, 5, 97-104.

Sawada, M., Ploeger, S.K., Elsabbagh, A., Saatcioglu, M., Rosetti, E. and Nastev, M. (2014). Integrated desktop/mobile GIS application for building inventory. Geological Survey of Canada. Open File 7345. 35 p. doi:10.4095/293919

Silva, V., Crowley, H., Pinho, R., and Varum, H. (2013). Extending displacement-based earthquake loss assessment (DBELA) for the computation of fragility curves. Engineering Structures, 56, 343-356.

Standards Australia. (1998). Strengthening existing buildings for earthquake. AS 3826:1998. Standards Australia, NSW.

Taghdi, M., Bruneau, M., and Saatcioglu, M. (2000). Analysis and design of low-rise masonry and concrete walls retrofitted using steel strips. Journal of Structural Engineering, 126(9), 1026-1032.

Tarque Ruiz, S.N. (2008). Seismic risk assessment of adobe dwellings. Master’s Thesis. University of Pavia, Pavia, Italy

The Economist. (2015, July 13th). Insurance in Asia: Narrow-minded. Retrieved from http://economist.com.

Tomaževič, M. (1999). Earthquake-Resistant Design of Masonry Buildings. Imperial College Press, London.

Turek, M.E. (2002). In-plane shake-table testing of unreinforced masonry walls strengthened with fibre reinforced-plastics. M.A.Sc. Thesis. The University of British Columbia, Vancouver, Canada.

Ulmi, M., Wagner, C.L., Wojtarowicz, M., Bancroft, J.L., Hastings, N.L., Chow, W., Rivard, J.R., Prieto, J., Journeay, J.M., Struik L.C., and Nastev, M. (2014). Hazus-MH 2.1 Canada User and Technical Manual: Earthquake Module; Geological Survey of Canada, Open File 7474, 245. doi:10.4095/293800

Vamvatsikos, D., and Cornell, C.A. (2002). Incremental dynamic analysis. Earthquake Engineering and Structural Dynamics, 31(3), 491-514.

Ventura, C. E., Finn, W. L., Onur, T., Blanquera, A., and Rezai, M. (2005). Regional seismic risk in British Columbia-classification of buildings and development of damage probability functions. Canadian Journal of Civil Engineering, 32(2), 372-387.

Wijanto, L.S. (2007). Seismic assessment of unreinforced masonry walls. Ph.D. Thesis. University of Canterbury. Christchurch, New Zealand.

Wilson, A. W., Quenneville, P. J. H., and Ingham, J. M. (2011). Assessment of timber floor diaphragms in historic unreinforced masonry buildings. In International conference on structural health assessment of timber structures.

Zardini, M. (2006). Énergie verte Benny Farm : réutilisation / Briques récupérées des bâtiments originaux de 1947, testées en laboratoire pour déterminer leur conformité aux normes actuelles. Vitrine d'une exposition. Montréal : Centre canadien d'architecture.

Appendix A

Model validation

In-plane validation

In order to ensure that the results obtained in this work correlate well with real-world context, a one-storey URM structure (Paquette and Bruneau, 2003) as shown in Figure A-1 was modeled in ELS. The model, seen in Figure A-2, is made of over 6,500 elements to represent as accurately as possible the original structure, including each individual masonry unit. As per the original structure, the west wall is only connected to the rest of the structure through the diaphragm; the authors intentionally left a gap between the out-of-plane and west walls so that it could be analyzed as a stand-alone and further compare the difference when considering or neglecting the contribution of flanges (Paquette and Bruneau, 2003). Given the nature of the present work, it was decided to investigate the east wall which is fully connected to the out-of-plane walls.

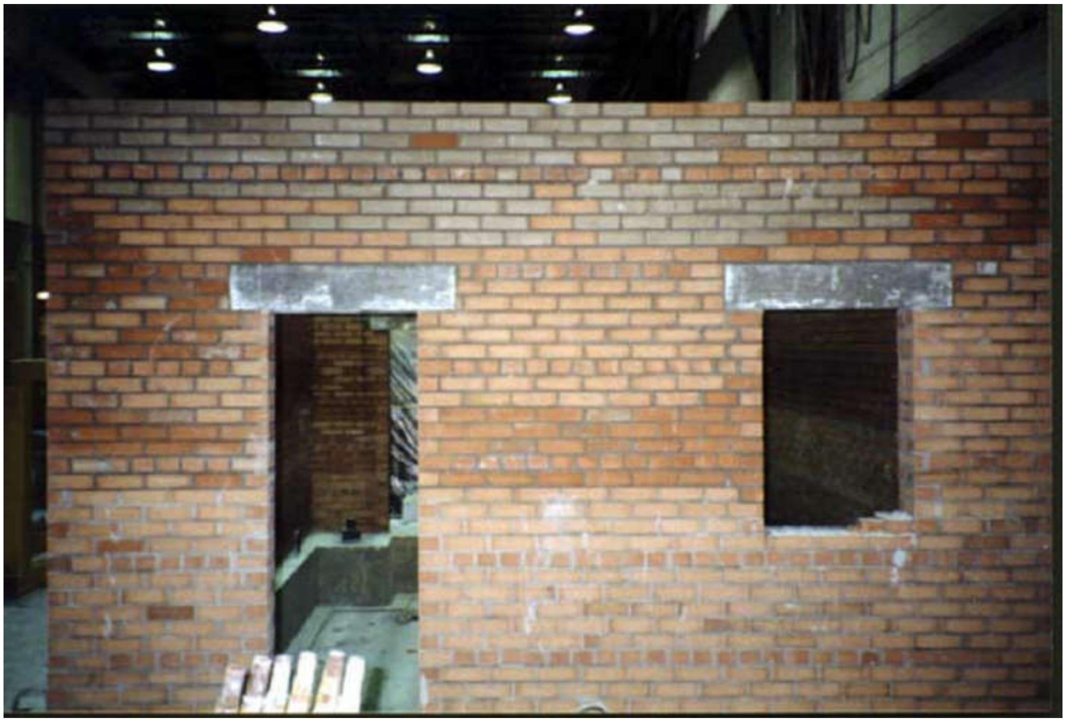

Figure A-1: Test structure (from Paquette and Bruneau, 2006)

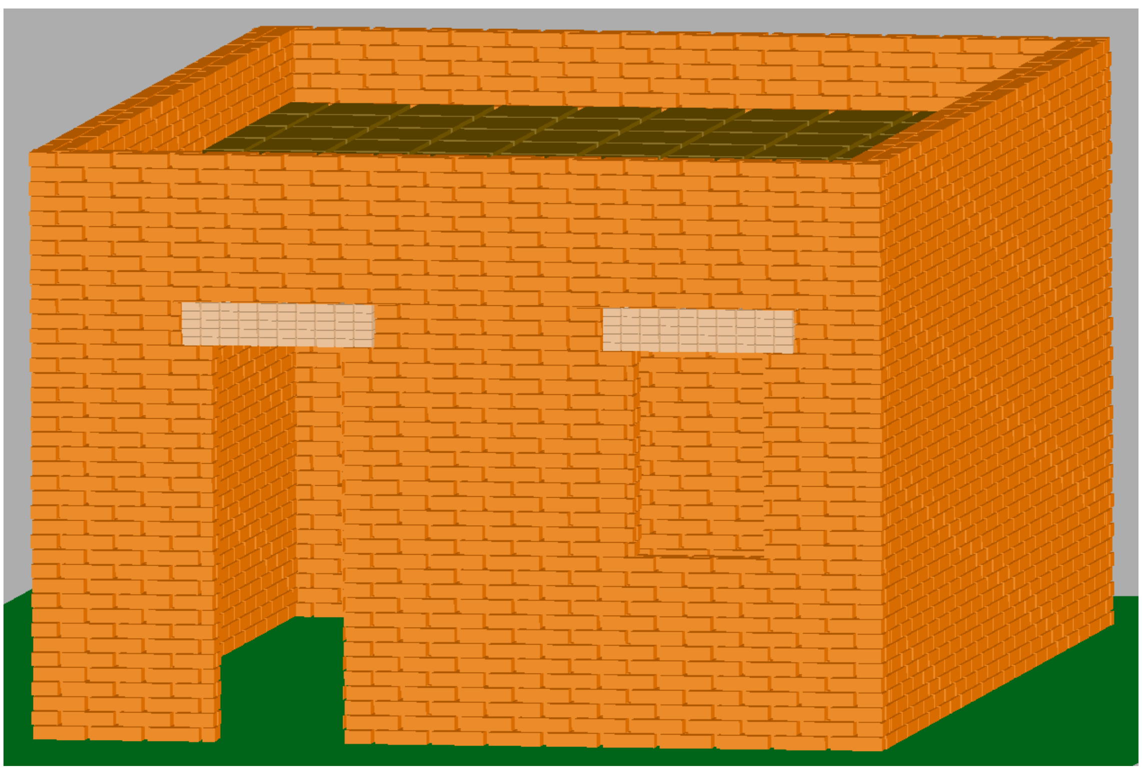

Figure A-2: Analytical model in ELS, east wall focus

Whereas the experimental data was obtained through pseudo-dynamic seismic loading, it was deemed sufficient to compare with a displacement-based force relationship, partly in the interest of time but also since the inelastic behaviour of masonry is the main concern. As a result, the model displays an increased linearly elastic capacity as can be seen in Figure A-3. Similar behaviour was also observed by other model validations using ELS (Karbassi, 2010; ASI, 2013). Nonetheless, it is seen more clearly in Figure A-4 that the initial linear portion in the positive displacement region is related closely to the experimental results.

Looking at the inelastic portion, we observe that the ultimate capacity of the west wall is almost identical: 33.65 kN vs. 33.27 kN and -27.69 kN vs. -26.23 kN when comparing the analytical and experimental results, respectively. In regards to displacement, the positive displacement was reached exactly given that it was set as target; however such was not the case with regards to the negative portion: the model became unstable around -16 mm, which is illustrated by the vertical portion of Figure A-3. On the other hand the experimental test was stopped at -16.5 mm due to instability (Paquette and Bruneau, 2003).

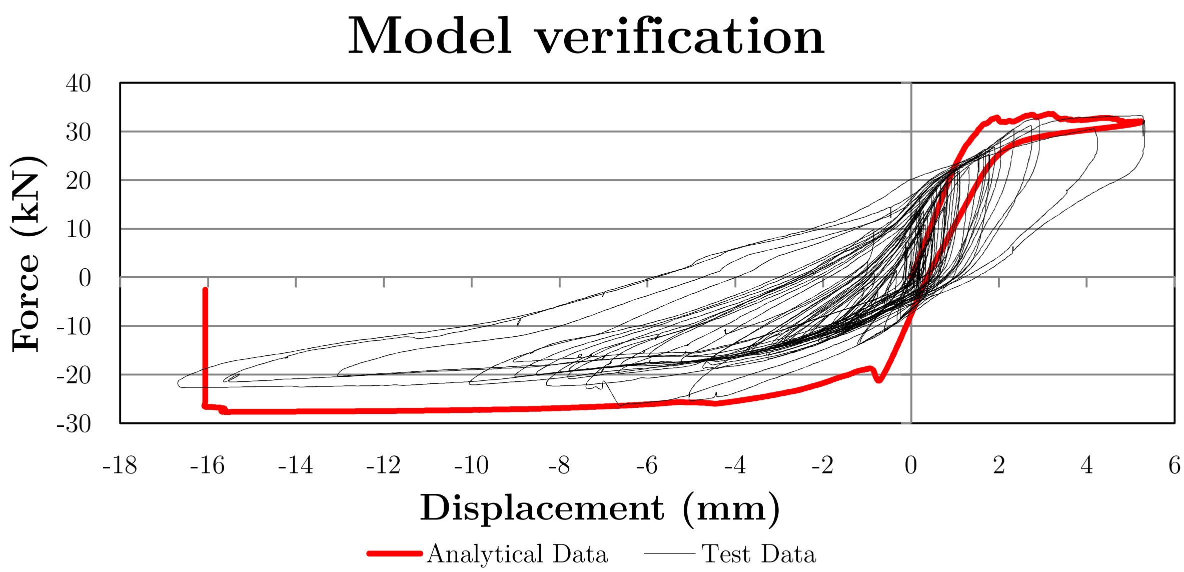

Figure A-3: Comparison of hysteretic loop and displacement-based force relationship

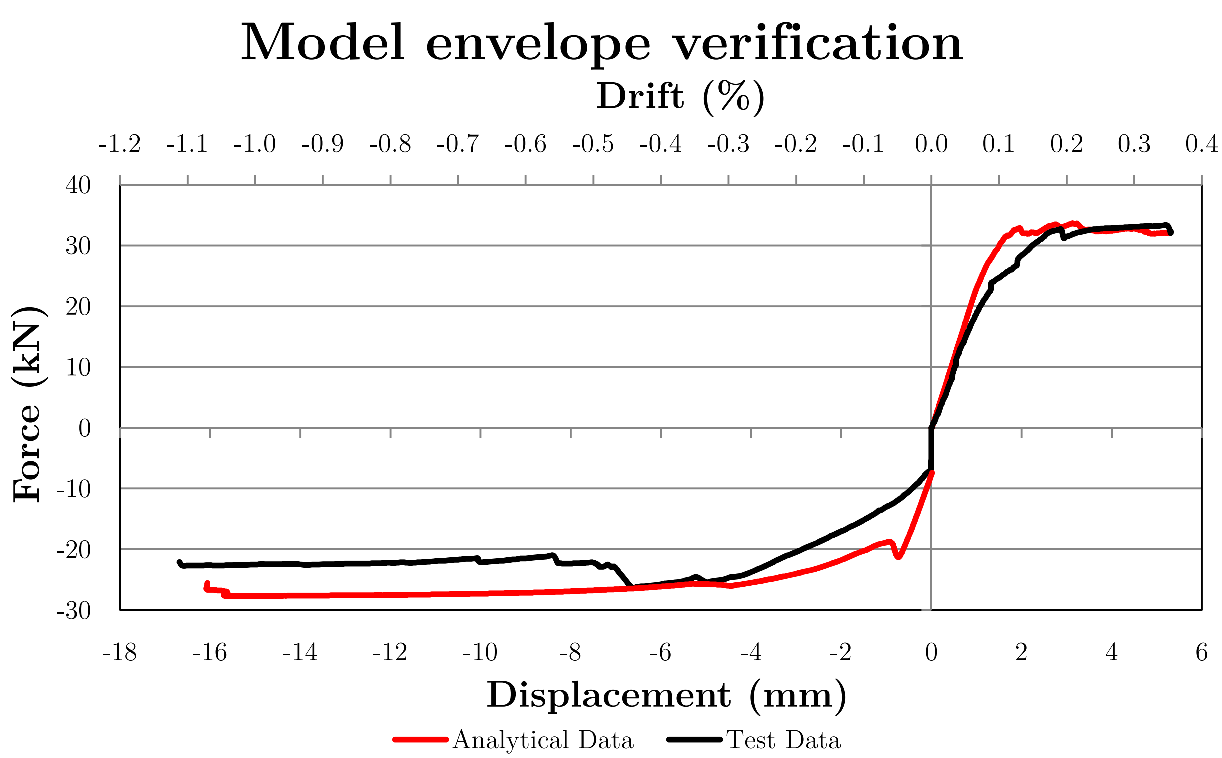

Figure A-4: Comparison of hysteretic loop envelope and displacement-based force relationship

It is worth mentioning that similar behaviour was observed in the analytical model during the negative displacement loading: the door pier (the leftmost portion of Figure A-1) lifted up completely above the door level, rendering its capacity null. In the ELS model, this behaviour occurred at around -1 mm which immediately resulted in a drop of force required to push the structure further, see Figure A-4. This mechanism would later be largely responsible of the instability of the model.

Also worth of note, Figure A-5 shows the six cracking locations observed on the real structure at the end of the test. ELS provides the user with a convenient way to determine likely crack locations, not only by showing which springs have separated but also through showing the principal strains experienced on the elements during positive loading as displayed on Figure A-6. At a strain of 0.10, springs are considered to have ruptured which is clearly seen in the upper part of window pier. The model also predicted quite well the general location of cracks with notably the two cracks of the central pier being remarkably similar.

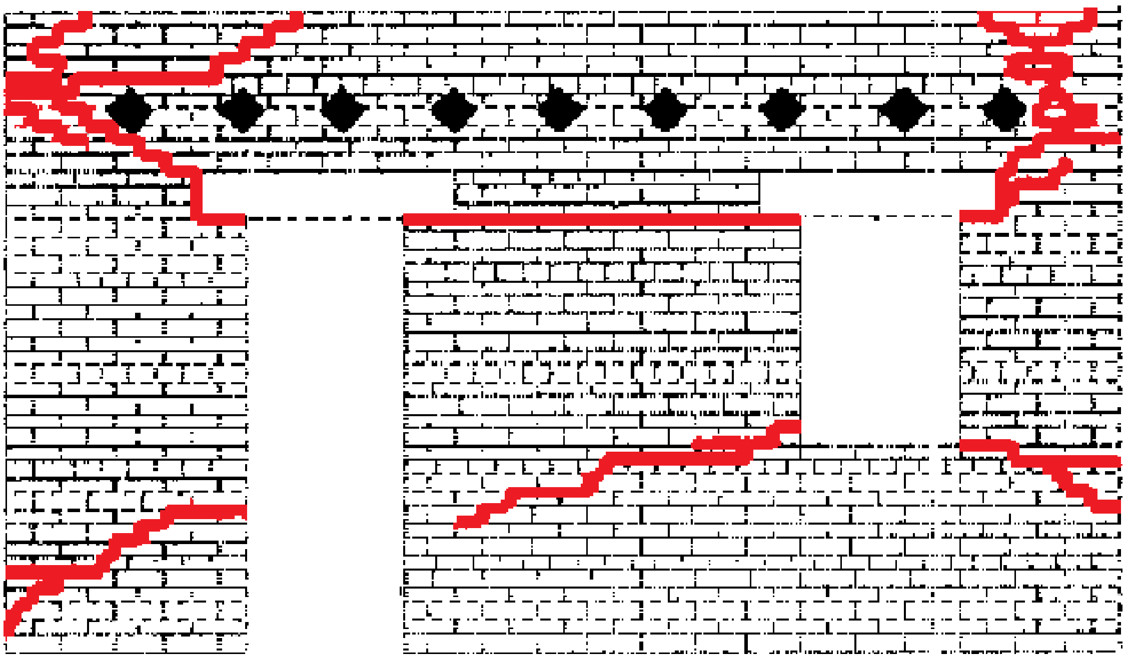

Figure A-5: Experimentally observed cracks on east wall (adapted from Paquette and Bruneau, 2003)

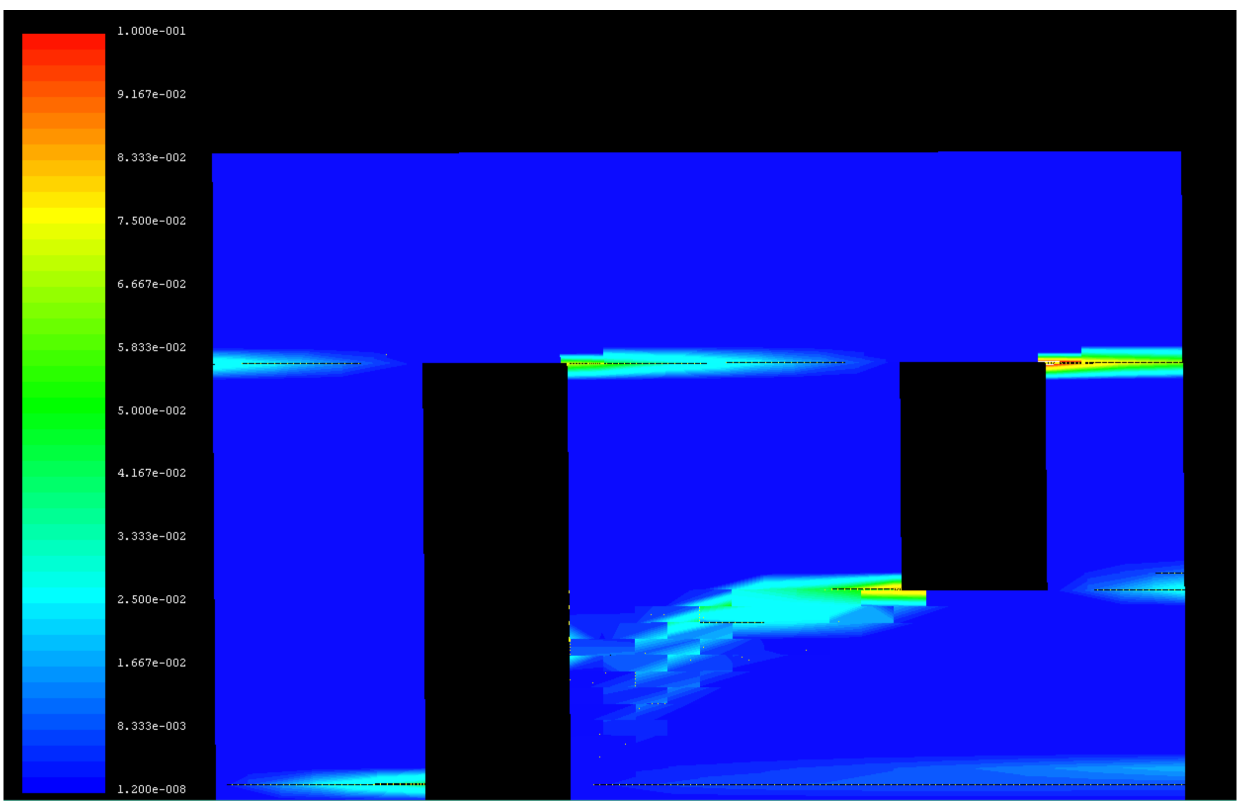

Figure A-6: Location of cracks formed on east wall of ELS model, positive loading

Lastly, the analytical model did not exhibit much activity in the out-of-plane walls, which is consistent with the design criteria aimed at by the authors by designing the building such that rocking failure would occur first (Paquette and Bruneau, 2003).

Considering all of the above, the accuracy of the model appears to be in good agreement with experimental observations for in-plane walls when the out-of-plane action is mitigated.

Out-of-plane validation

A second validation was done based on the work of Ismail et al. (2011) in order to show the out-of-plane accuracy of the model. The authors built several post-tensioned clay brick walls and applied a cyclic uniformly distributed load on them to determine each wall's capacity based on the overburden pressure being applied by the tendon.

While the present work focuses on URM and thus the lack of any reinforcement, a lightly stressed brick wall is representative of URM walls since the latter will be under similar conditions due to the weight coming from the roof, floors and also higher storeys where relevant. In light of this, test wall PTB-01 from Ismail et al. (2011) was modelled and put under cyclic lateral uniformly distributed pressure. The model used weightless elements both on top and bottom of the wall to apply the overburden pressure across the length of the wall. Note that these were hidden and thus not visible in Figure A-7 so that the location of the enlarged tendon would be visible.

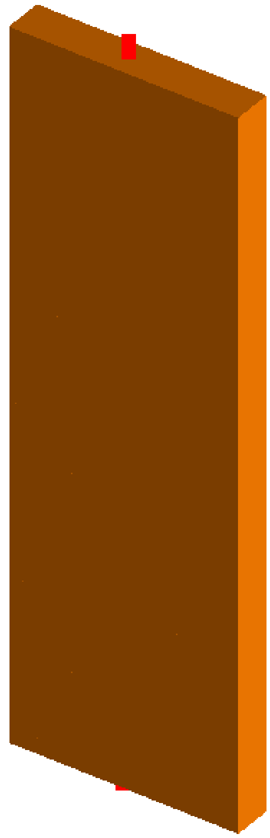

Figure A-7: Wall model showing tendon location

The process proved more challenging than the in-plane validation on account of the out-of-plane behaviour being more sensible to the size of elements used in the model. More precisely, having model elements of equivalent size to clay bricks would yield higher capacity both in terms of strength and displacement of the wall. This is expected due to the applied element method being an energy method and therefore convergence from above is a normal occurrence when increasing the number of elements. Nonetheless, after increasing the number of elements by a factor of ten and running single load and unload scenarios, a thorough cyclic loading test showed the accuracy that can be achieved as Figure A-8 shows. A scaled up deformation of the model as well as the original experiment setup can be seen in Figure A-9.

Looking for explicitly at Figure A-8, we see once again that the initial tangent stiffness is steeper as was also the case in Figure A-3 and Figure A-4. It remains a minor difference given that the experimental initial tangent stiffness is rather steep and the inelastic behaviour starts developing at comparable displacements. The upper limit of the force-displacement envelope is shown to be very accurate with small overshooting in the middle cycles and some undershooting in the last cycle. The hysteretic area is initially quite smaller although the later cycles improve on this fault.

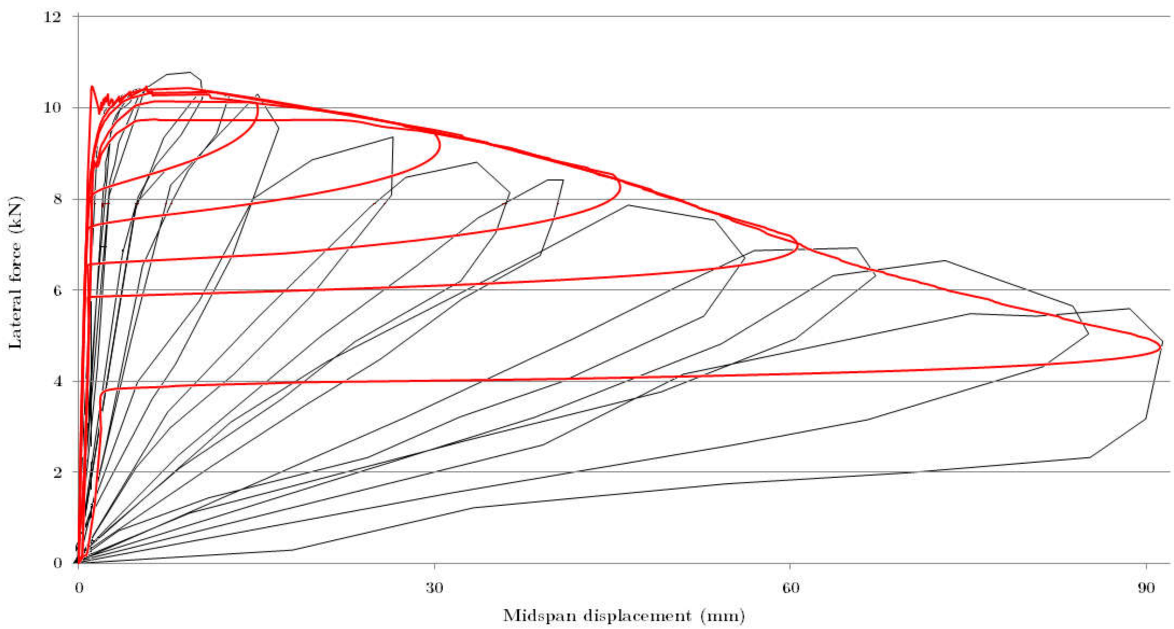

Figure A-8: Force-displacement comparison of experimental (black) and analytical (red) cyclic out-of-plane loading

The greatest fault of the model is the lack of initial stiffness loss: each of the cycles undergo the same path and only exhibit a difference in the required lateral force necessary to resume the inelastic behaviour. This type of behaviour is common in software analysis, for instance the work of Karbassi and Nollet (2013) depicts the same phenomenon.

One can conclude that the in-plane and out-of-plane modeling is adequate and that the results from this work are accurate, if somewhat on the conservative side as can be concluded from these two validations.

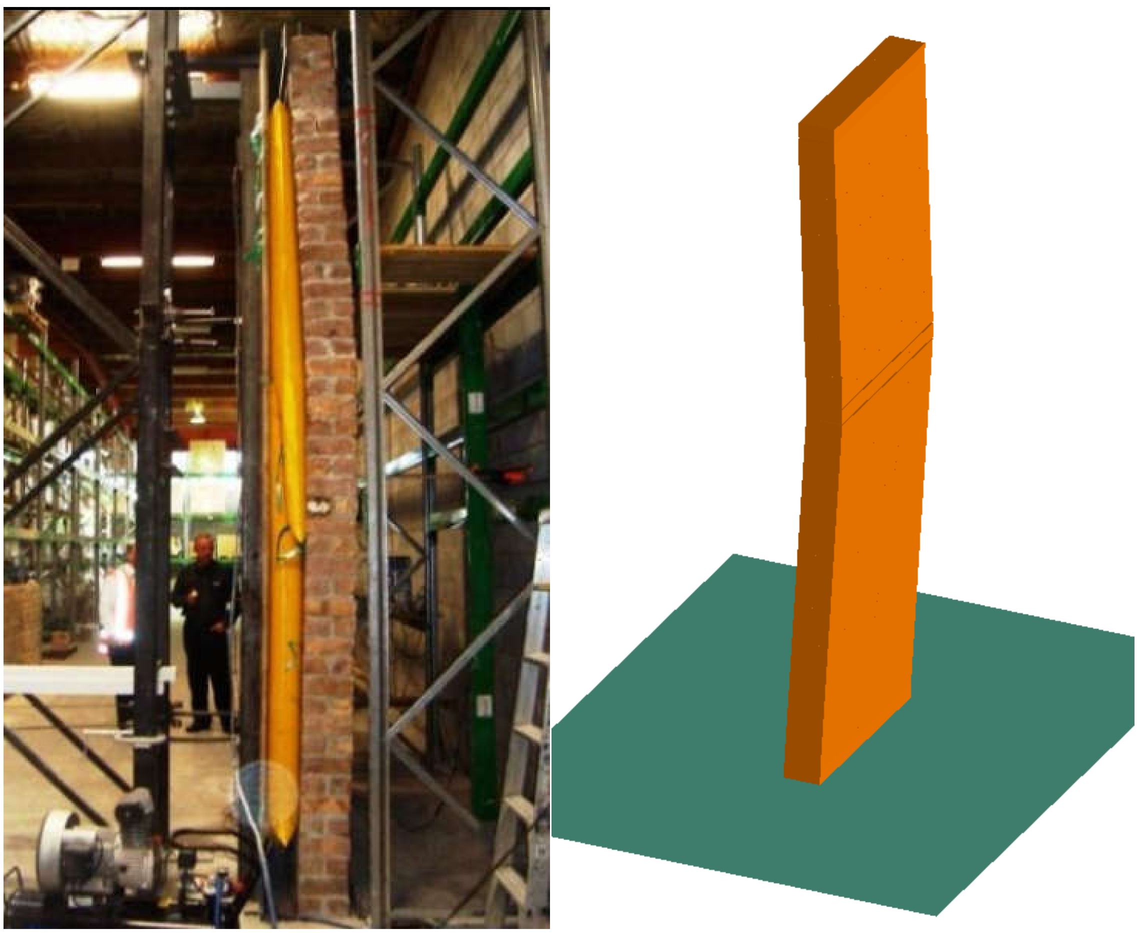

Figure A-9: Midspan deflection of Ismail et al. (2011) experimental setup (left) and analytical model (right)

Appendix B

Accelerograms

For mid-rise URMs eastern accelerogram data, refer to the data in Table B-1.

Table B-1: URMM accelerogram data (E)

	SA (g)				PGA (g)
	Pre-code		Low-code		
Openings	Large	Small	Large	Small	
E6c1_1	0.545	0.587	0.702	0.611	0.502
E6c1_2	0.459	0.607	0.606	0.844	0.369
E6c1_3	0.544	0.772	0.882	0.687	0.460
E6c1_4	0.574	0.585	0.581	0.805	0.362
E6c1_5	0.593	0.584	0.492	0.694	0.432
E6c2_1	0.520	0.513	0.611	0.709	0.313
E6c2_2	0.674	0.583	0.675	0.595	0.289
E6c2_3	0.411	0.646	0.457	0.602	0.311
E6c2_4	0.594	0.501	0.567	0.764	0.324
E6c2_5	0.559	0.516	0.831	0.682	0.310
E7c1_1	0.492	0.679	0.587	0.641	0.293
E7c1_2	0.517	0.620	0.818	0.596	0.306
E7c1_3	0.385	0.581	0.696	0.694	0.305
E7c1_4	0.457	0.662	0.582	0.525	0.332
E7c1_5	0.630	0.708	0.560	0.568	0.348
E7c2_1	0.536	0.589	0.630	0.688	0.282
E7c2_2	0.501	0.578	0.636	0.800	0.339
E7c2_3	0.469	0.526	0.478	0.893	0.276
E7c2_4	0.497	0.582	0.729	0.522	0.339
E7c2_5	0.571	0.639	0.741	0.666	0.297

Accelerograms for the eastern URMM are shown in the following figures.

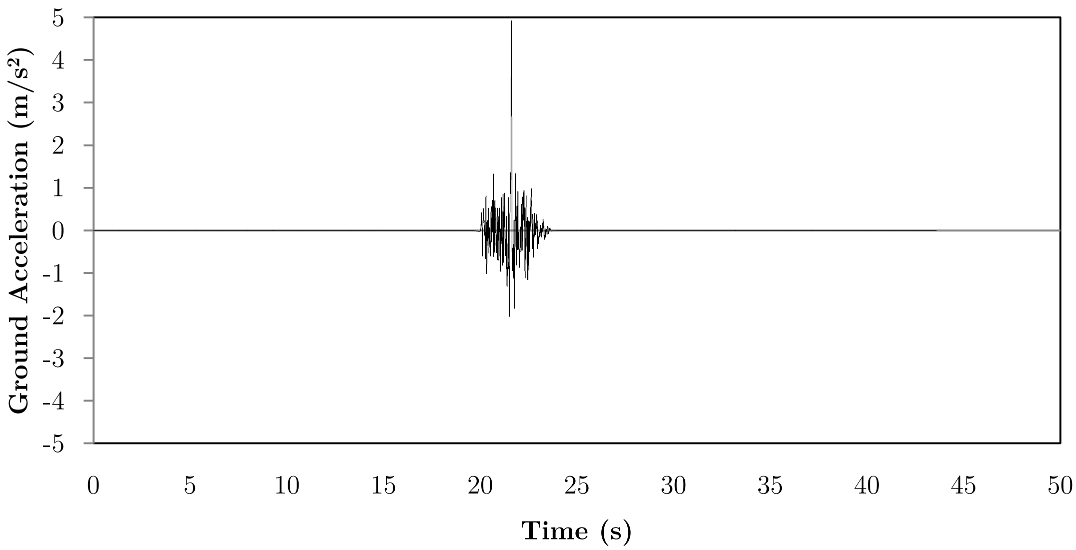

Figure B-1: E6c1_1 accelerogram

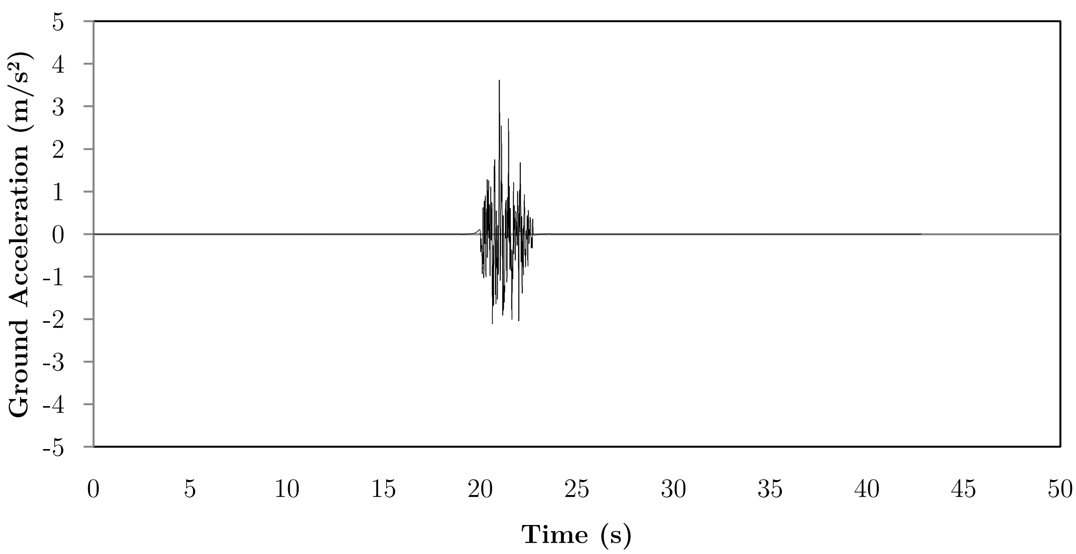

Figure B-2: E6c1_2 accelerogram

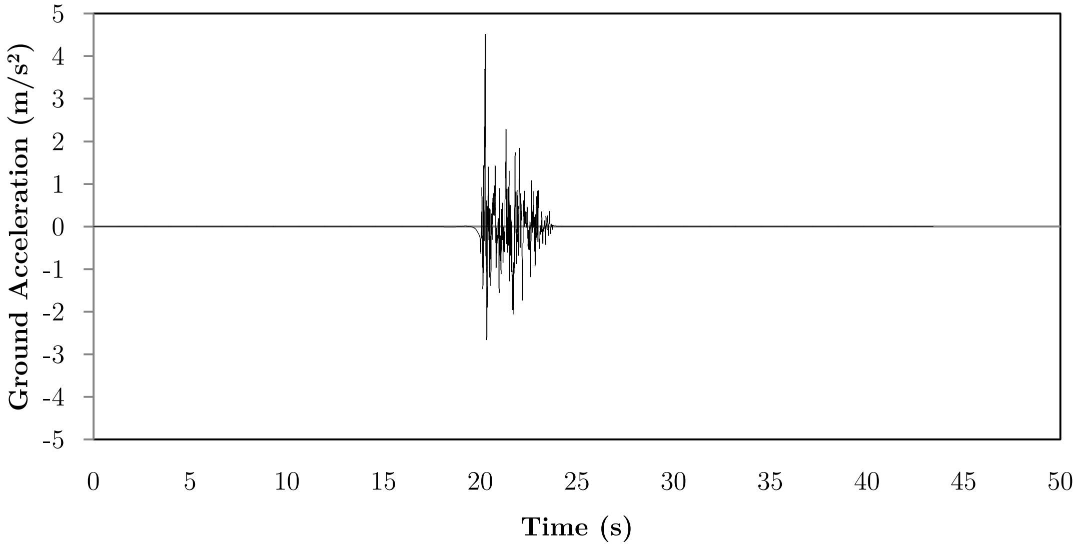

Figure B-3: E6c1_3 accelerogram

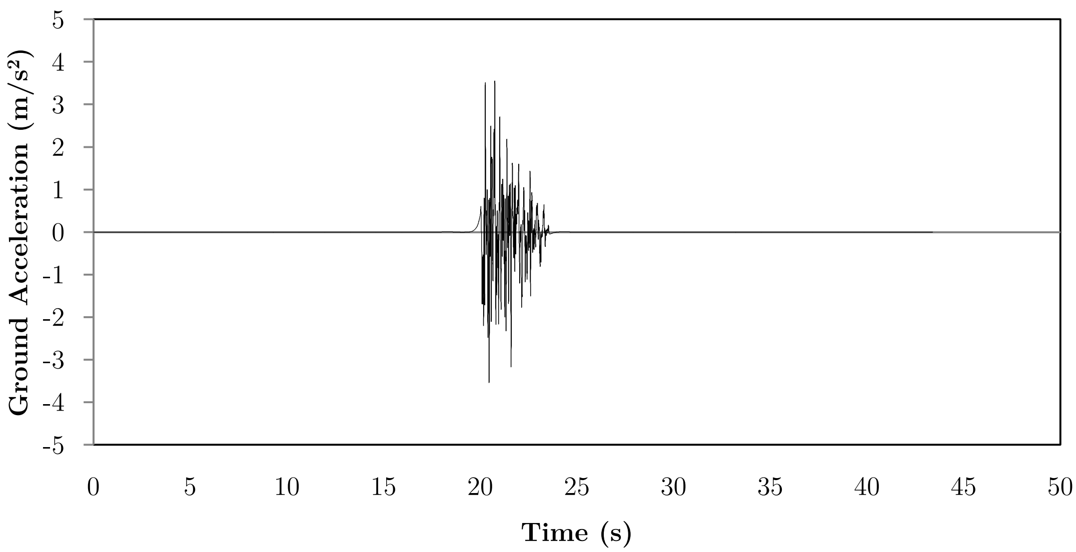

Figure B-4: E6c1_4 accelerogram

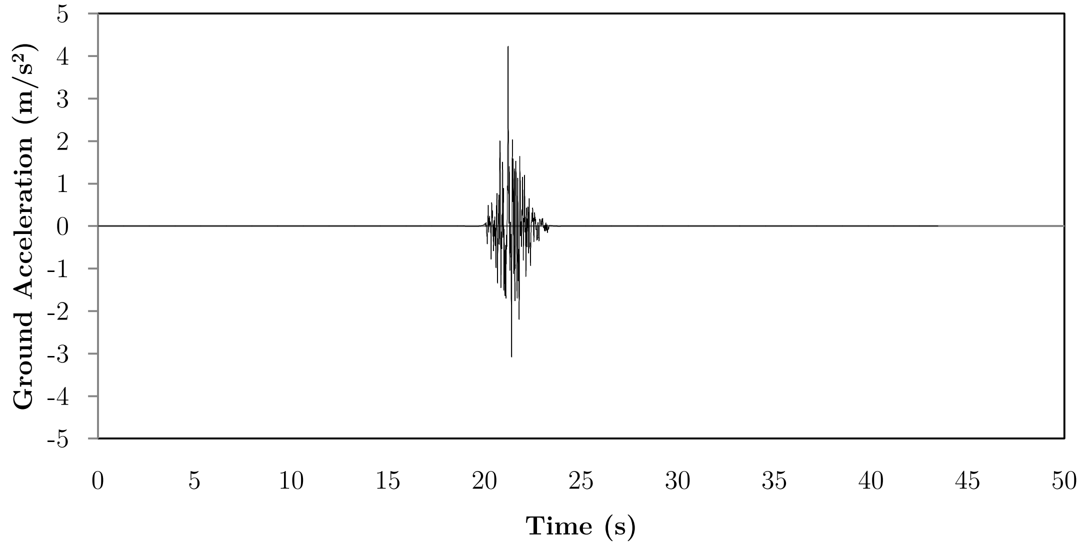

Figure B-5: E6c1_5 accelerogram

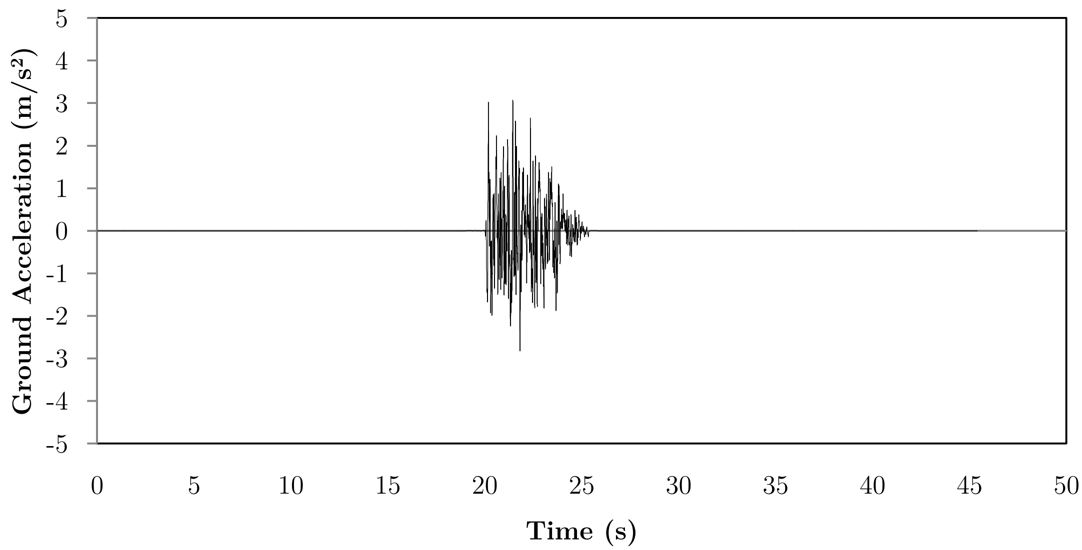

Figure B-6: E6c2_1 accelerogram

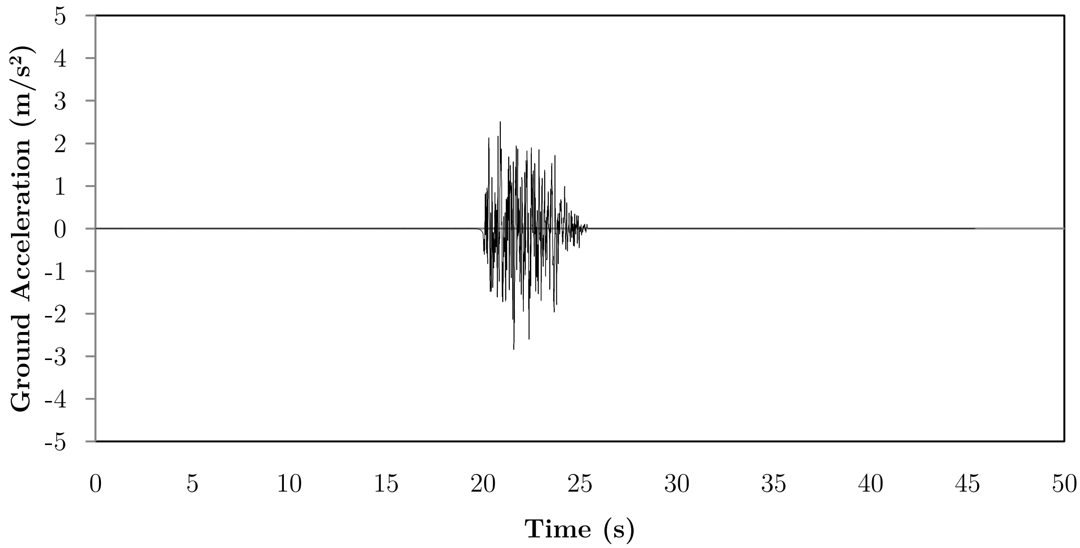

Figure B-7: E6c2_2 accelerogram

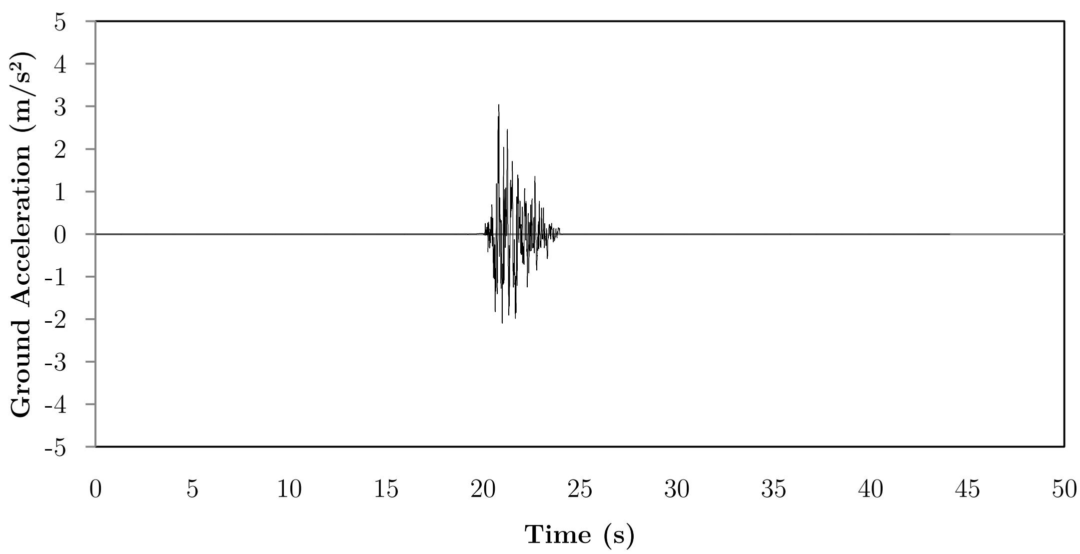

Figure B-8: E6c2_3 accelerogram

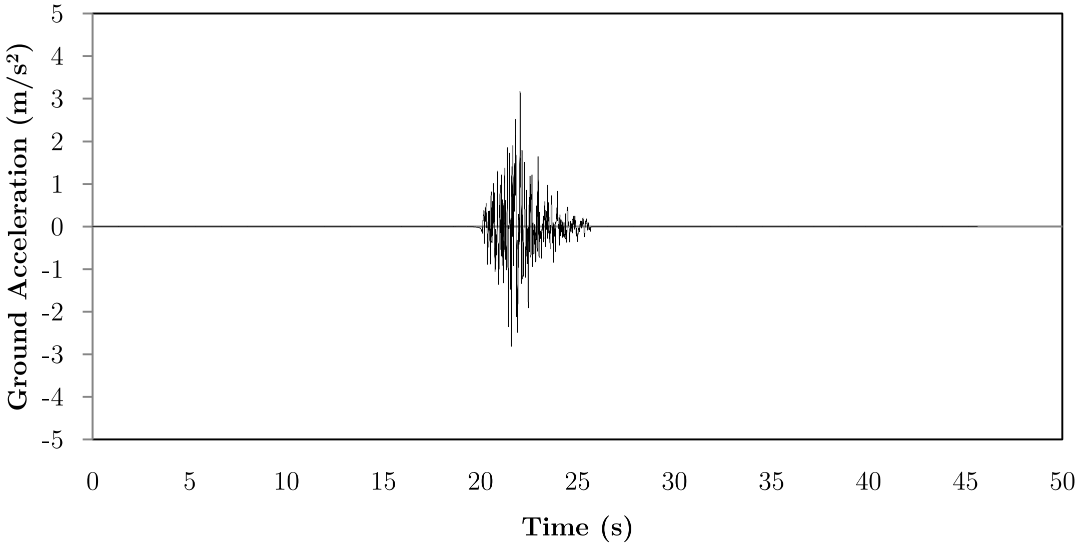

Figure B-9: E6c2_4 accelerogram

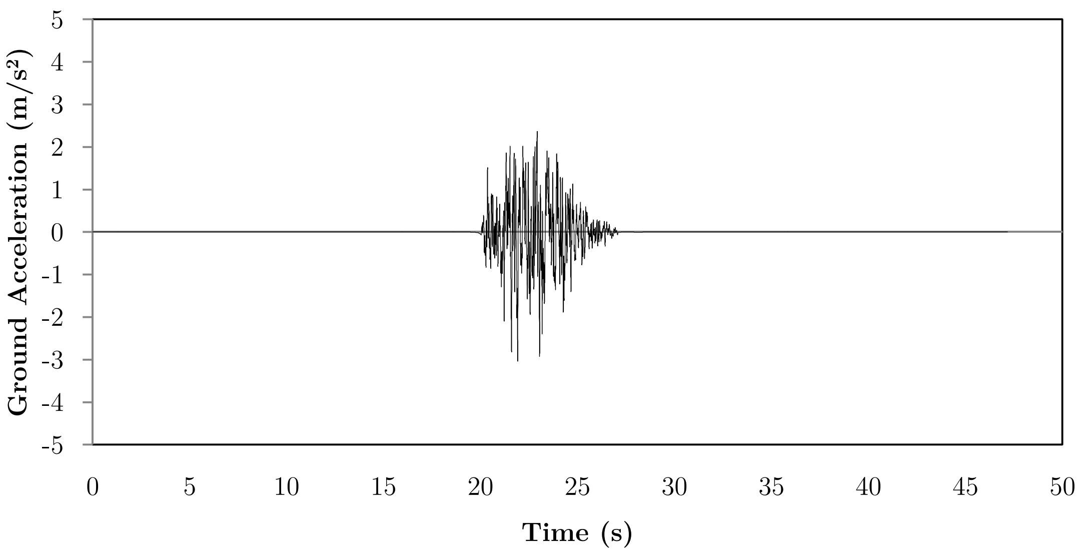

Figure B-10: E6c2_5 accelerogram

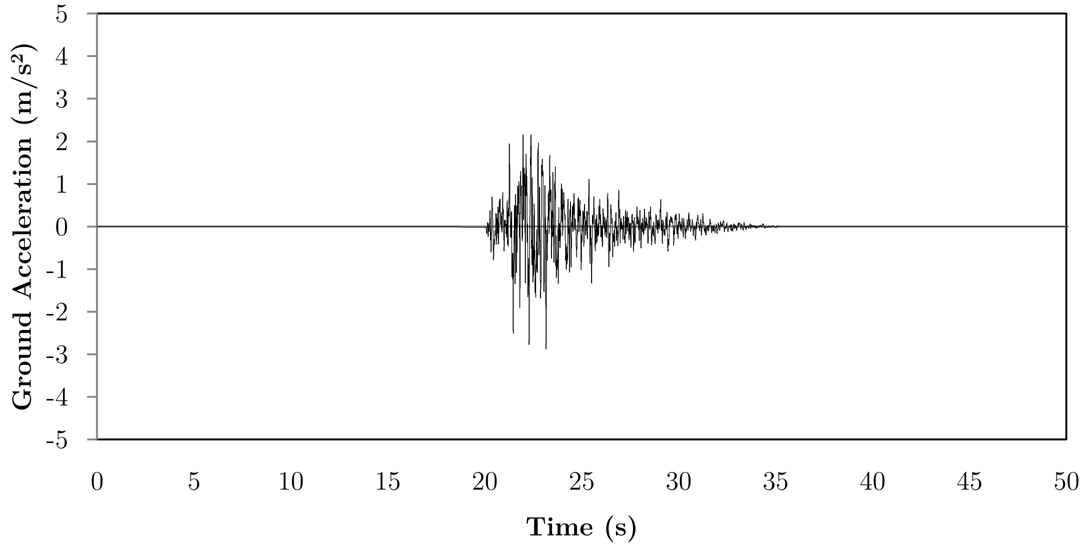

Figure B-11: E7c1_1 accelerogram

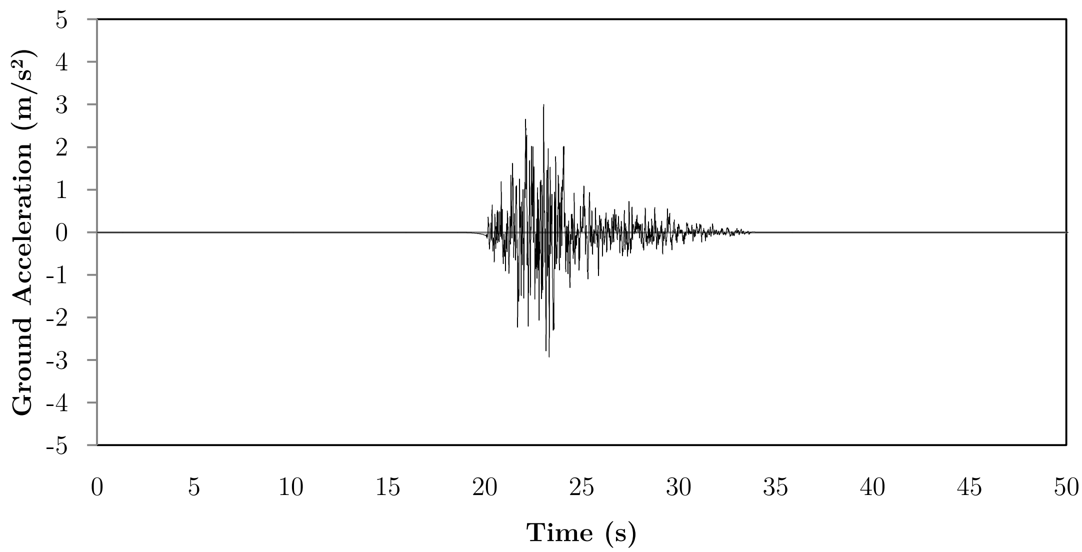

Figure B-12: E7c1_2 accelerogram

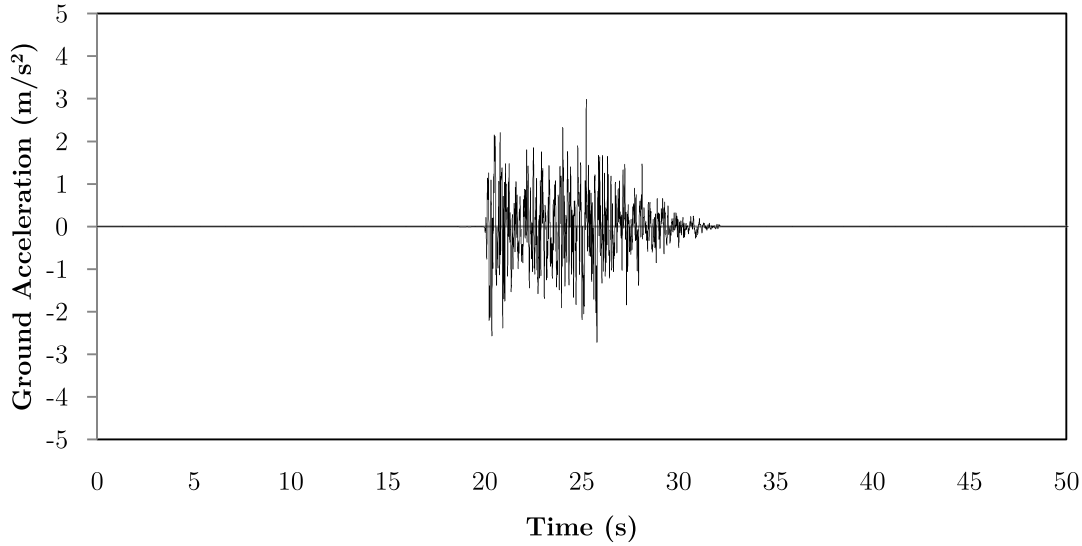

Figure B-13: E7c1_3 accelerogram

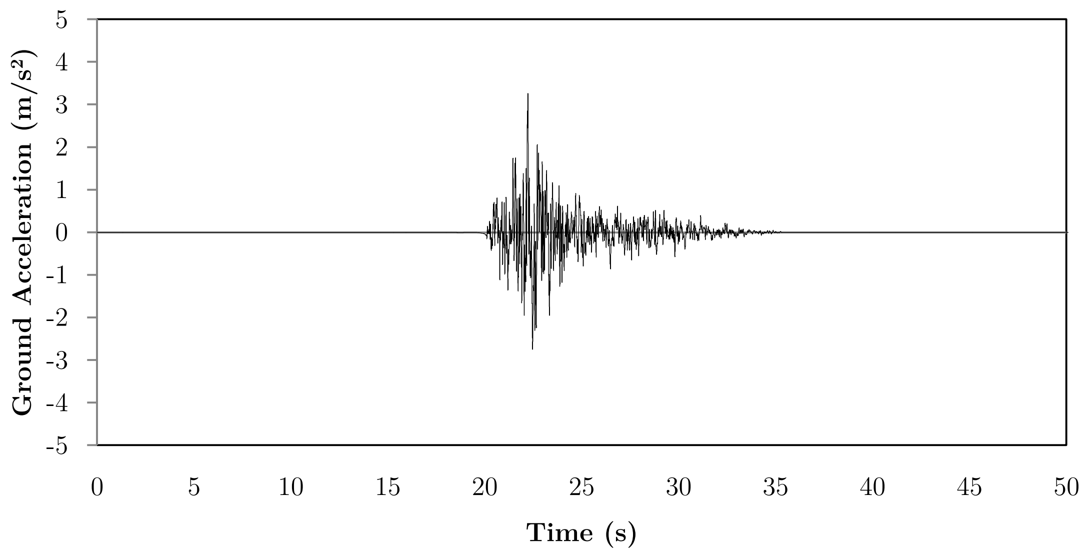

Figure B-14: E7c1_4 accelerogram

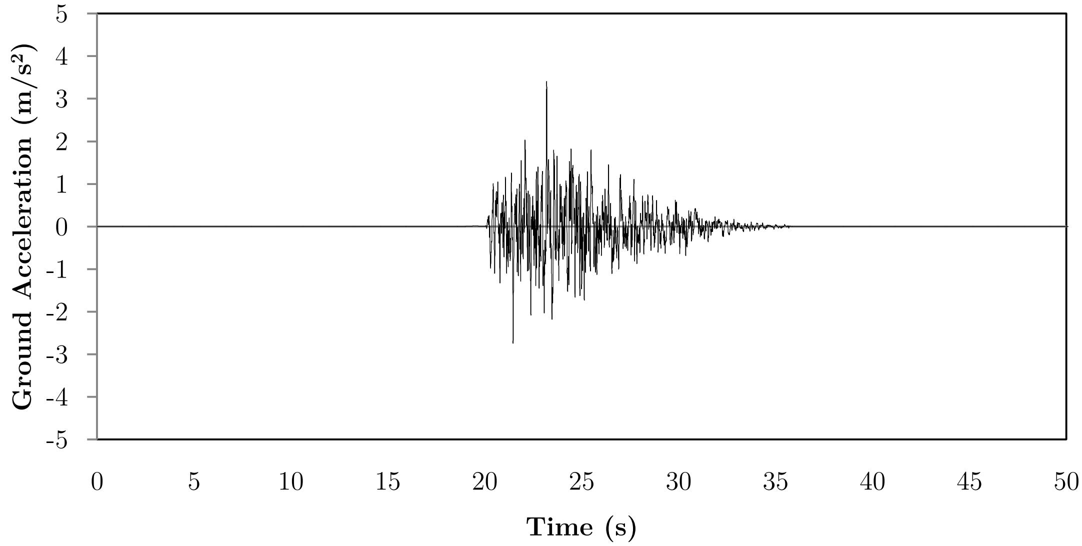

Figure B-15: E7c1_5 accelerogram

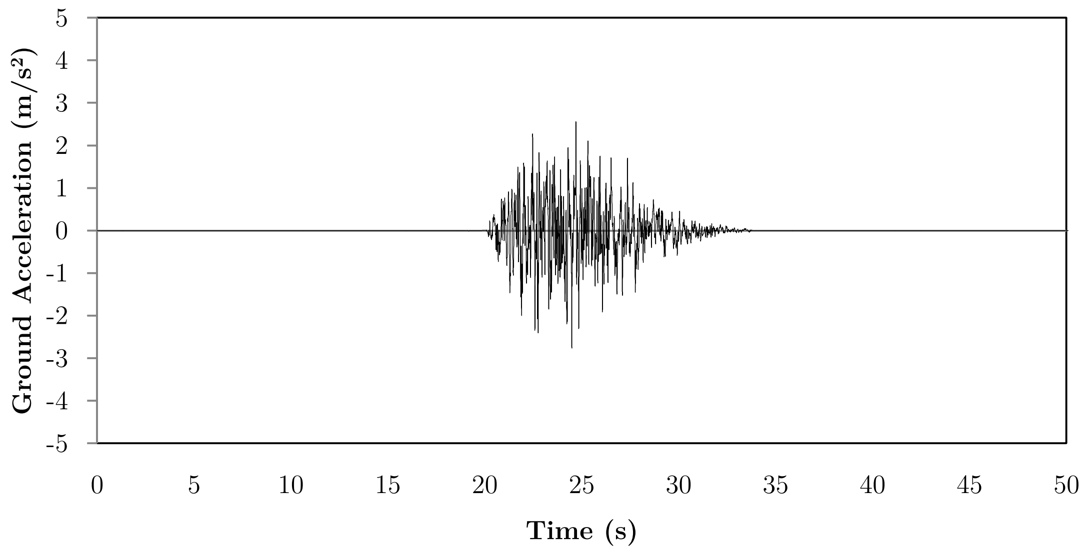

Figure B-16: E7c2_1 accelerogram

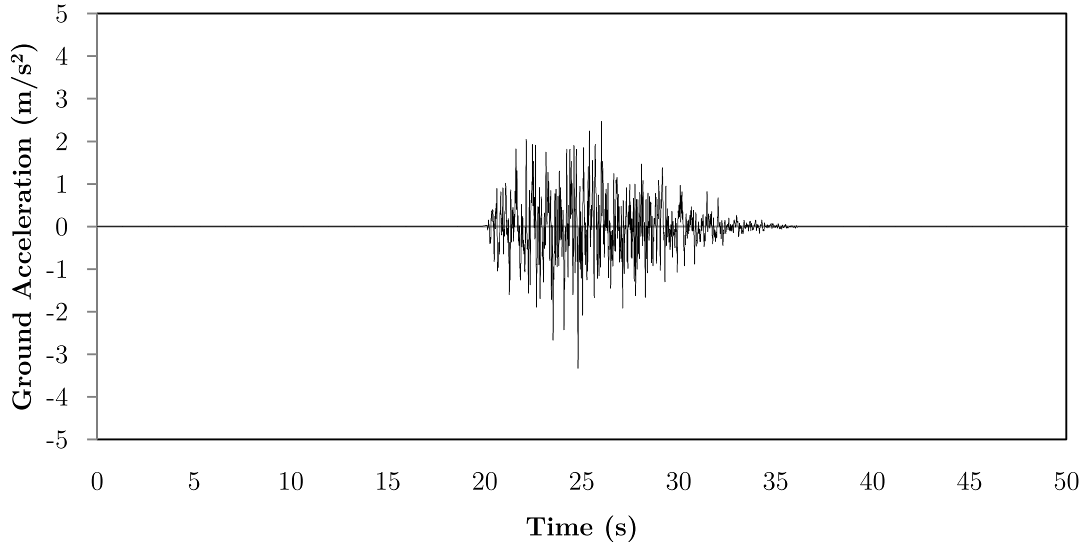

Figure B-17: E7c2_2 accelerogram

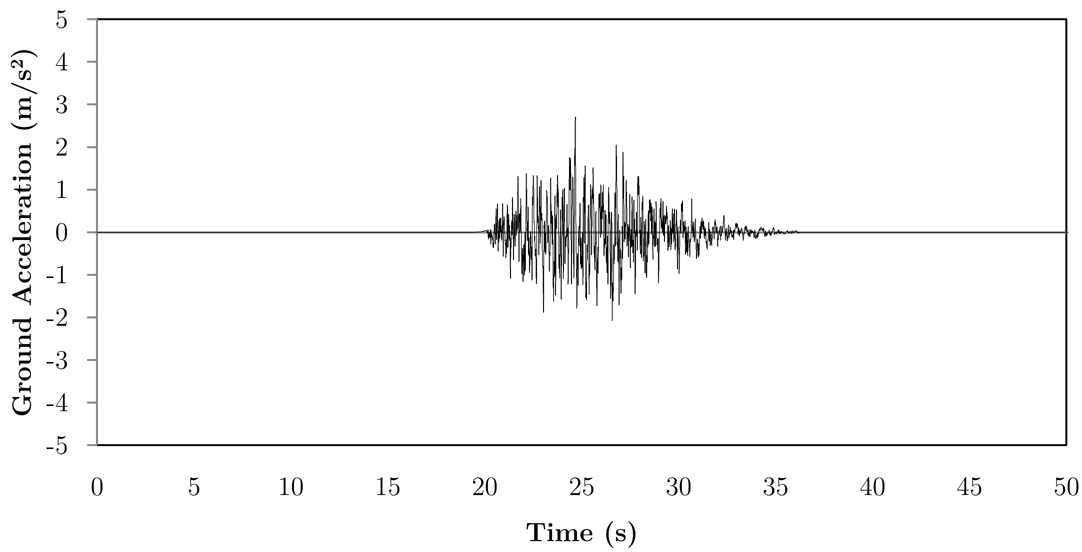

Figure B-18: E7c2_3 accelerogram

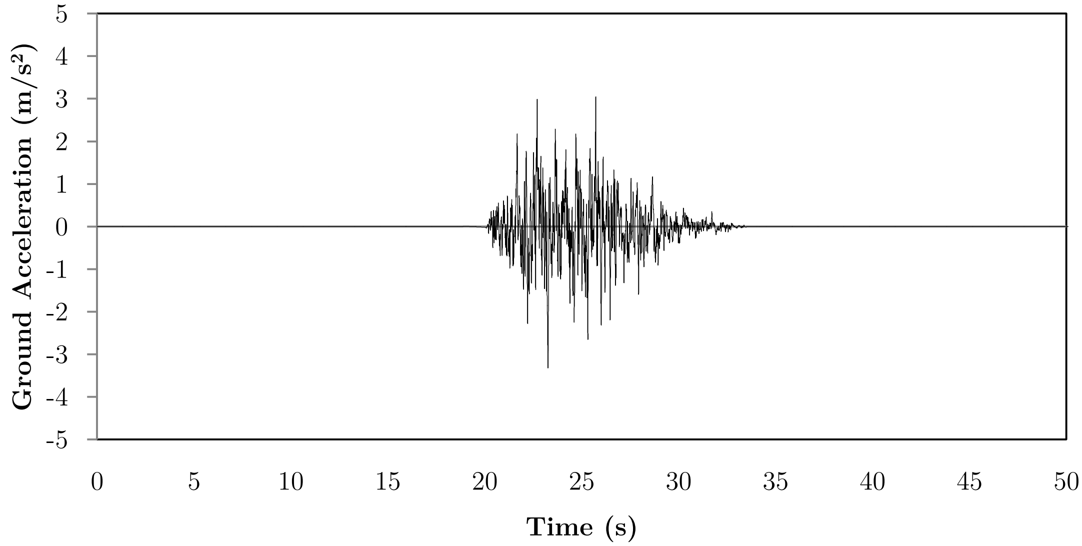

Figure B-19: E7c2_4 accelerogram

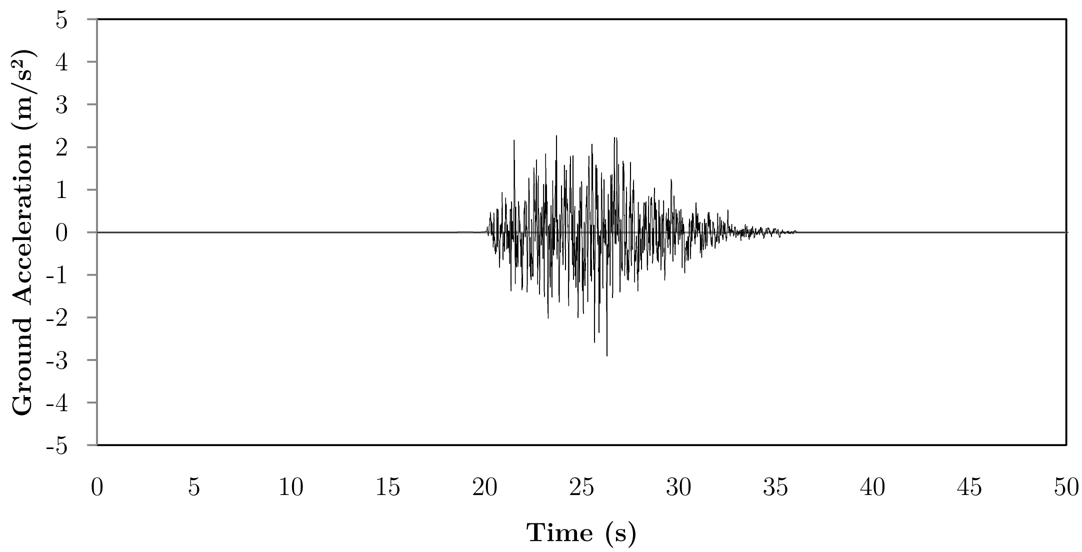

Figure B-20: E7c2_5 accelerogram

For mid-rise URMs western accelerogram data, refer to the data in Table B-2.

Table B-2: URMM accelerogram data (W)

	SA (g)				PGA (g)
	Pre-code		Low-code		
Openings	Large	Small	Large	Small	
W6c1_1	0.837	0.887	0.859	0.971	0.408
W6c1_2	1.035	0.735	0.835	1.190	0.452
W6c1_3	0.737	0.969	0.849	1.014	0.423
W6c1_4	0.758	1.309	1.127	0.878	0.405
W6c1_5	0.832	1.037	0.938	1.025	0.330
W6c2_1	0.949	0.969	0.996	0.876	0.395
W6c2_2	0.868	0.855	0.915	0.885	0.415
W6c2_3	0.826	0.823	1.075	0.970	0.394
W6c2_4	0.870	1.016	0.852	1.061	0.362
W6c2_5	0.799	0.942	0.916	0.934	0.387
W7c1_1	1.115	0.912	0.902	1.029	0.400
W7c1_2	0.827	1.160	1.188	0.911	0.377
W7c1_3	0.847	0.991	0.968	0.852	0.402
W7c1_4	1.064	0.954	0.823	0.745	0.455
W7c1_5	0.788	0.804	1.176	0.804	0.380
W7c2_1	0.729	1.057	0.905	1.045	0.374
W7c2_2	0.853	0.958	0.928	0.915	0.399
W7c2_3	0.954	0.910	0.900	0.836	0.429
W7c2_4	0.974	0.954	0.827	0.851	0.387
W7c2_5	1.005	0.850	0.940	0.968	0.350

Accelerograms for the western URMM are shown in the following figures.

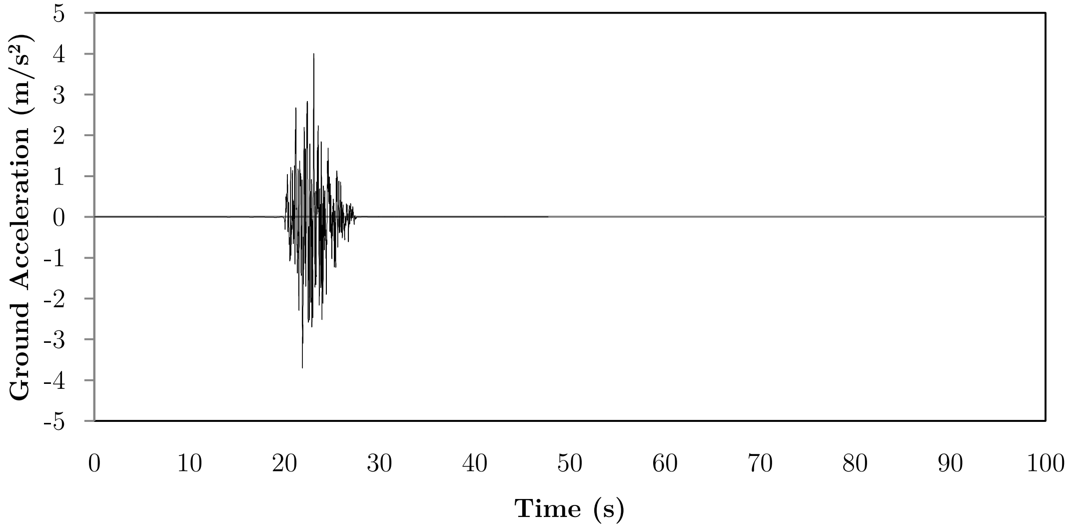

Figure B-21: W6c1_1 accelerogram

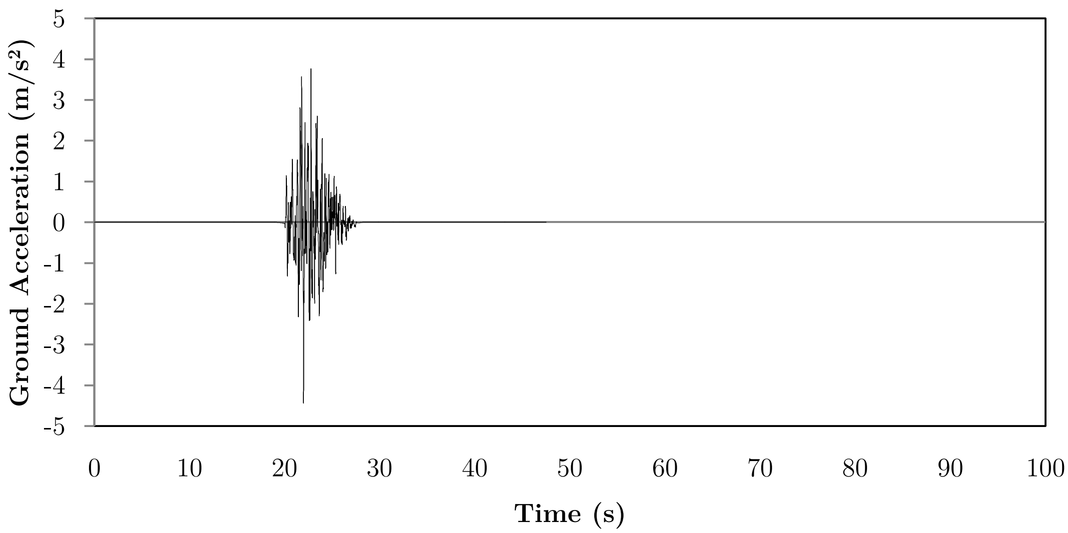

Figure B-22: W6c1_2 accelerogram

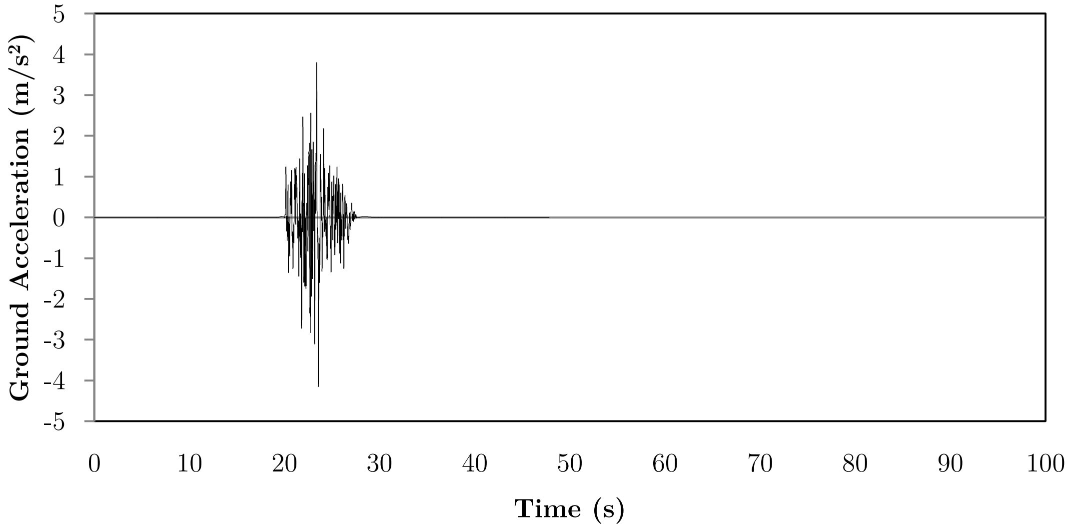

Figure B-23: W6c1_3 accelerogram

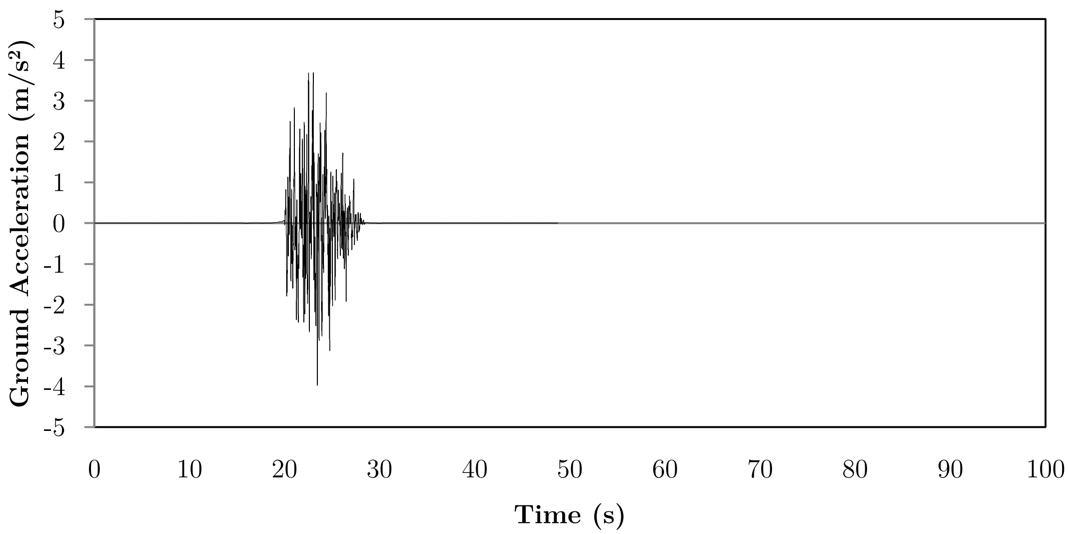

Figure B-24: W6c1_4 accelerogram

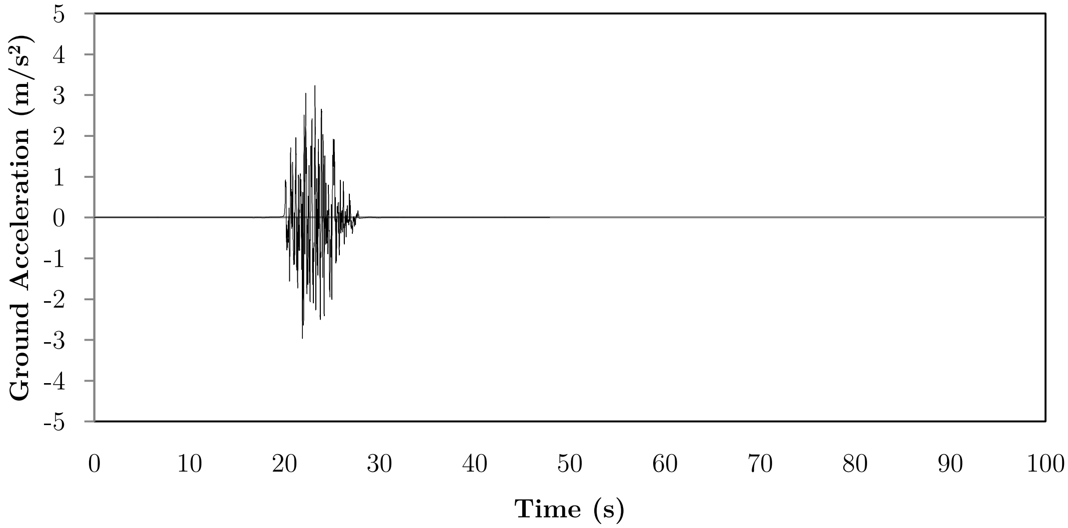

Figure B-25: W6c1_5 accelerogram

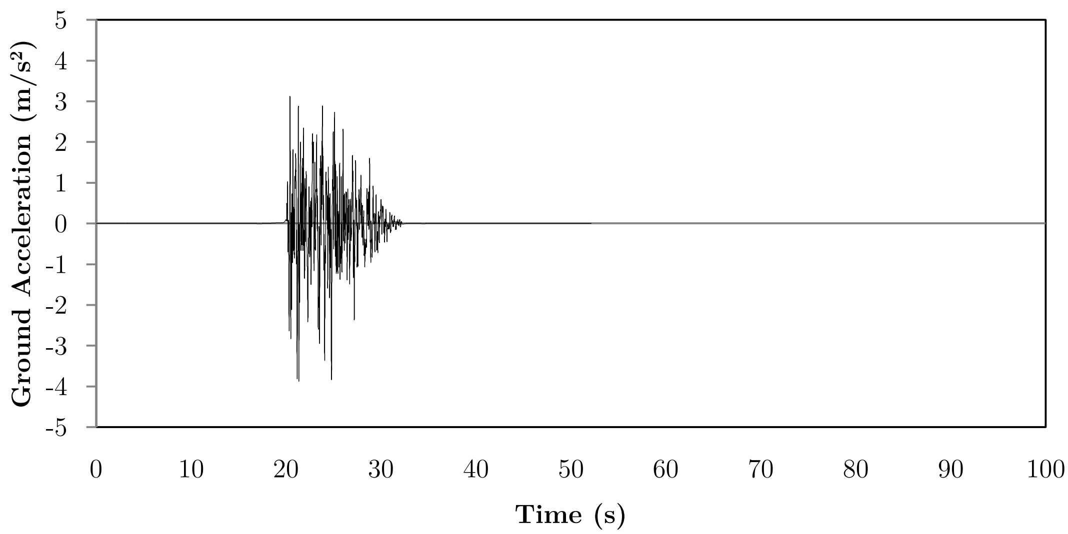

Figure B-26: W6c2_1 accelerogram

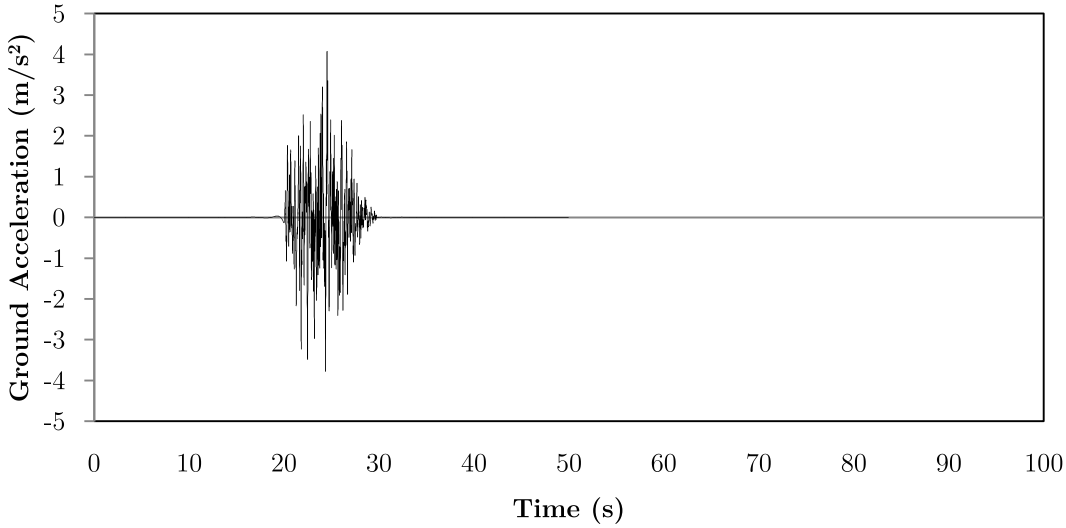

Figure B-27: W6c2_2 accelerogram

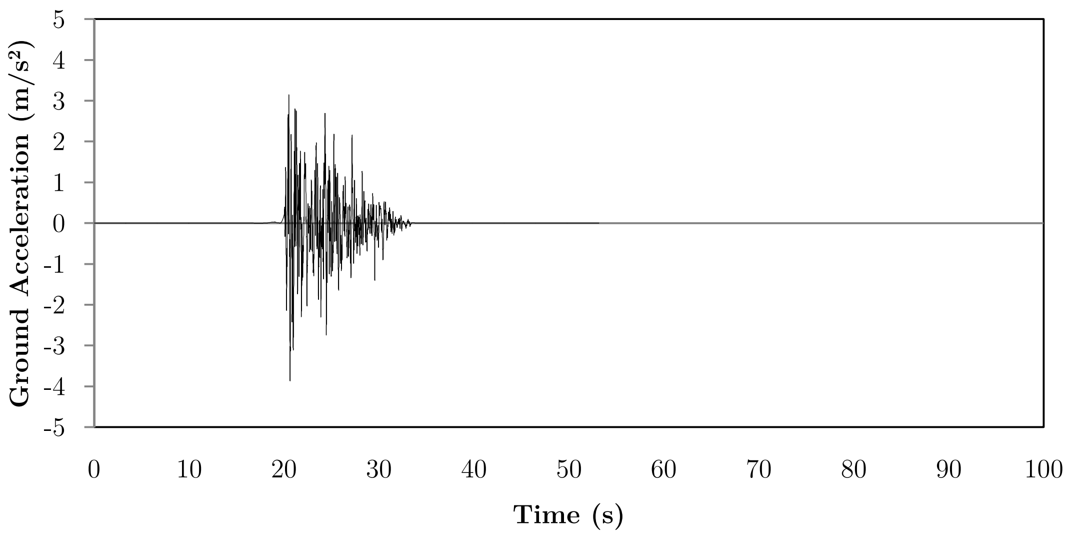

Figure B-28: W6c2_3 accelerogram

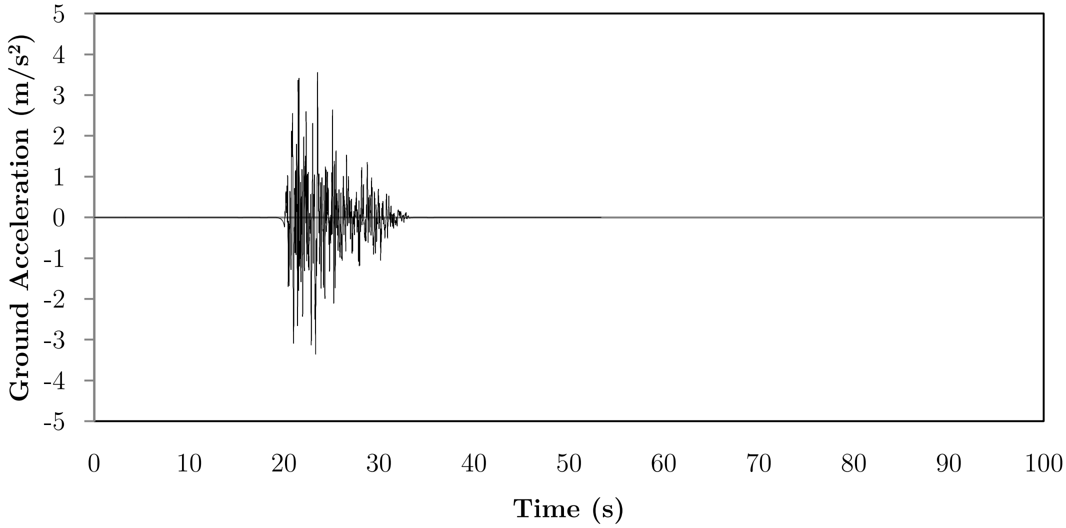

Figure B-29: W6c2_4 accelerogram

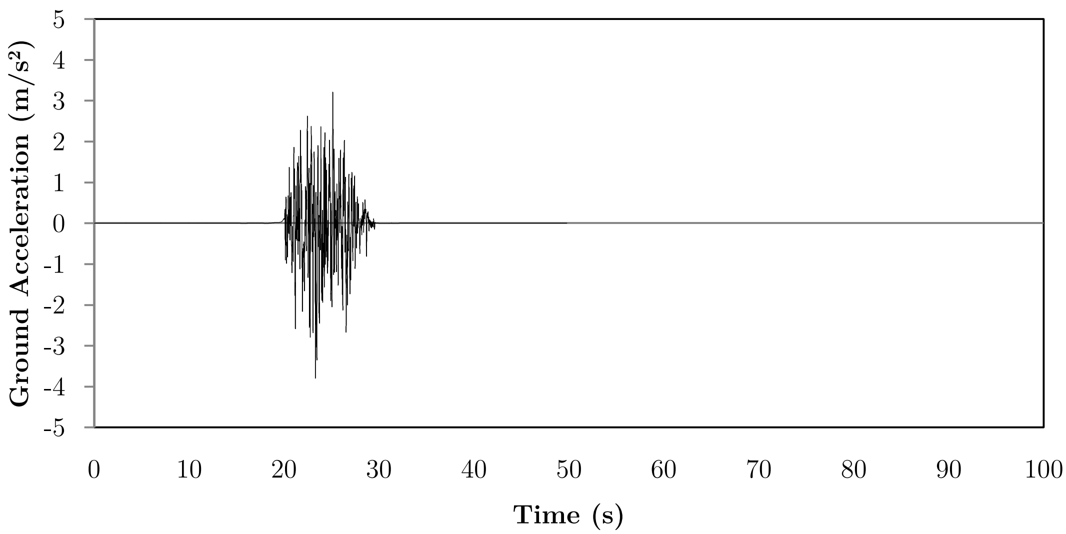

Figure B-30: W6c2_5 accelerogram

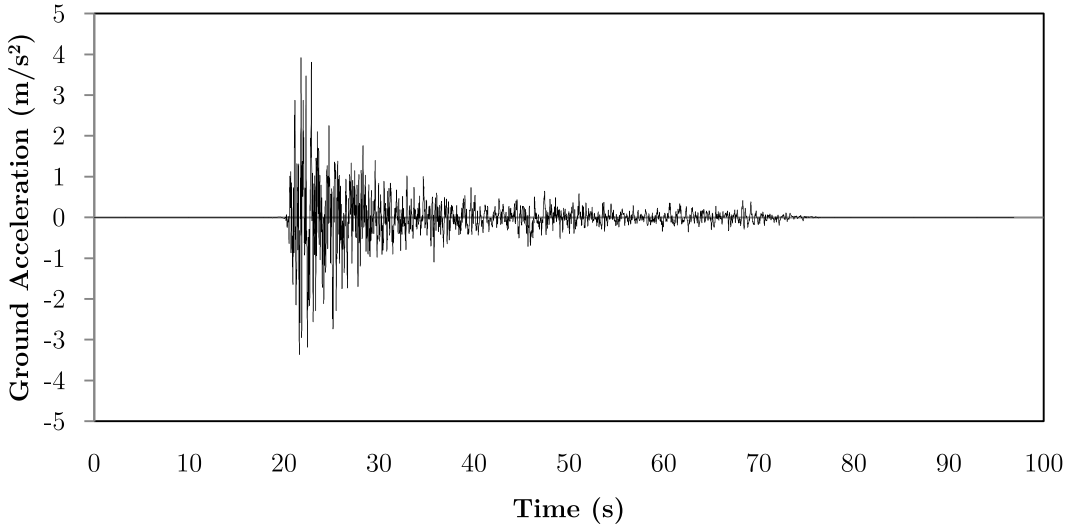

Figure B-31: W7c1_1 accelerogram

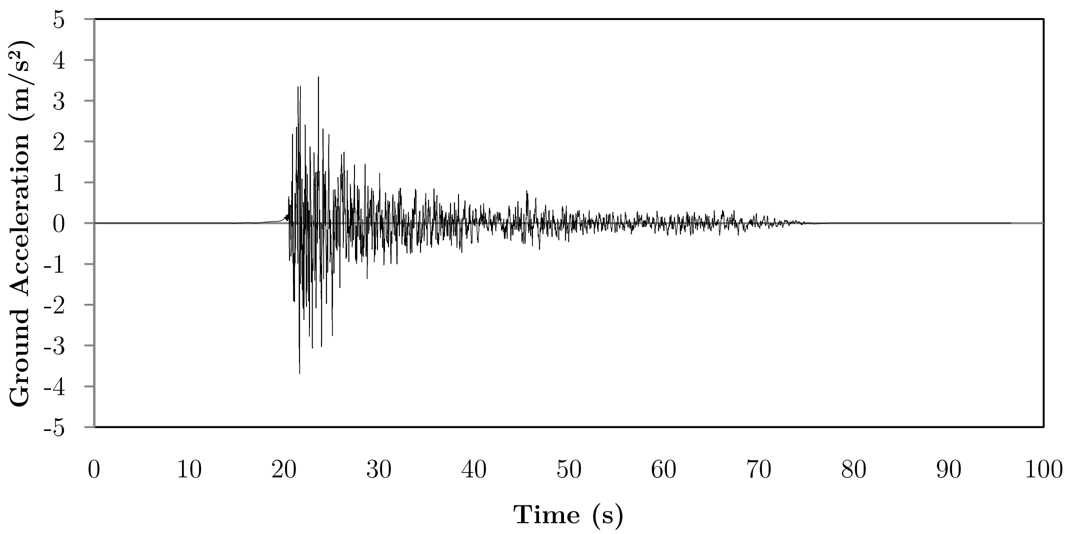

Figure B-32: W7c1_2 accelerogram

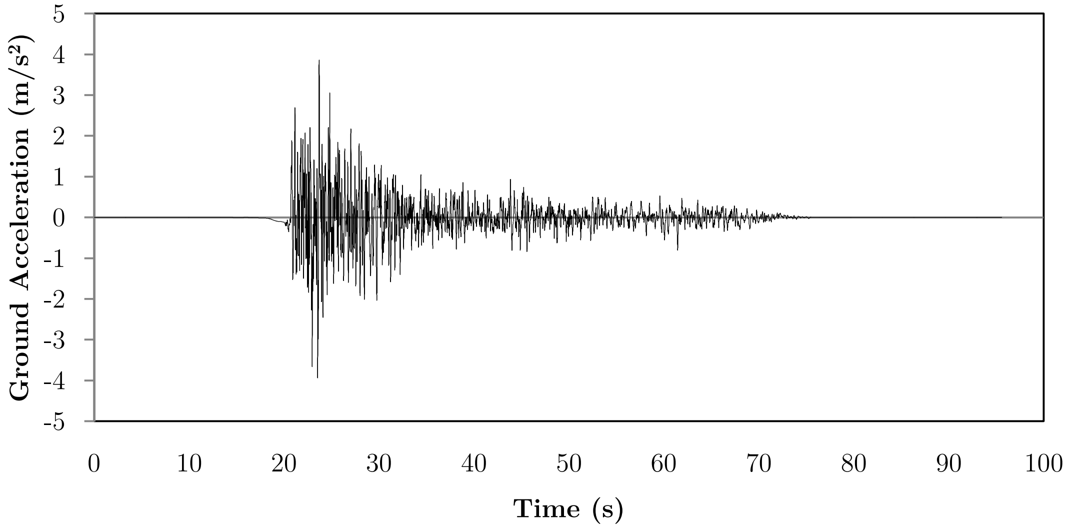

Figure B-33: W7c1_3 accelerogram

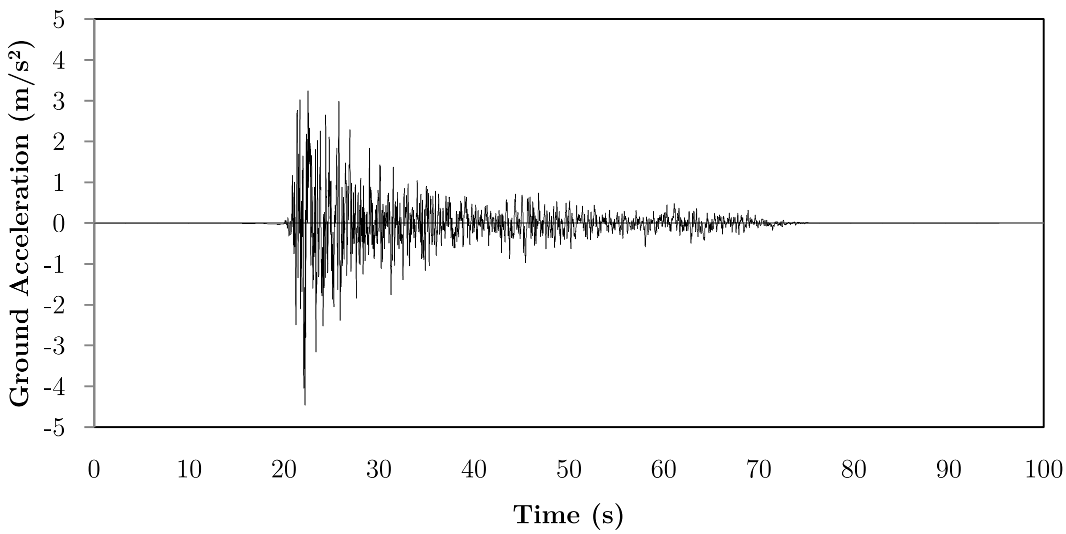

Figure B-34: W7c1_4 accelerogram

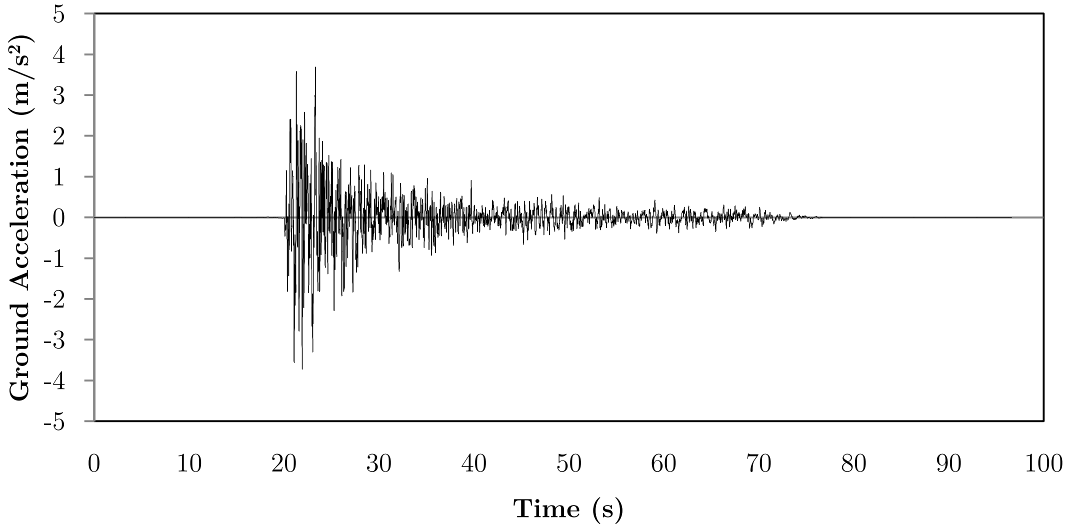

Figure B-35: W7c1_5 accelerogram

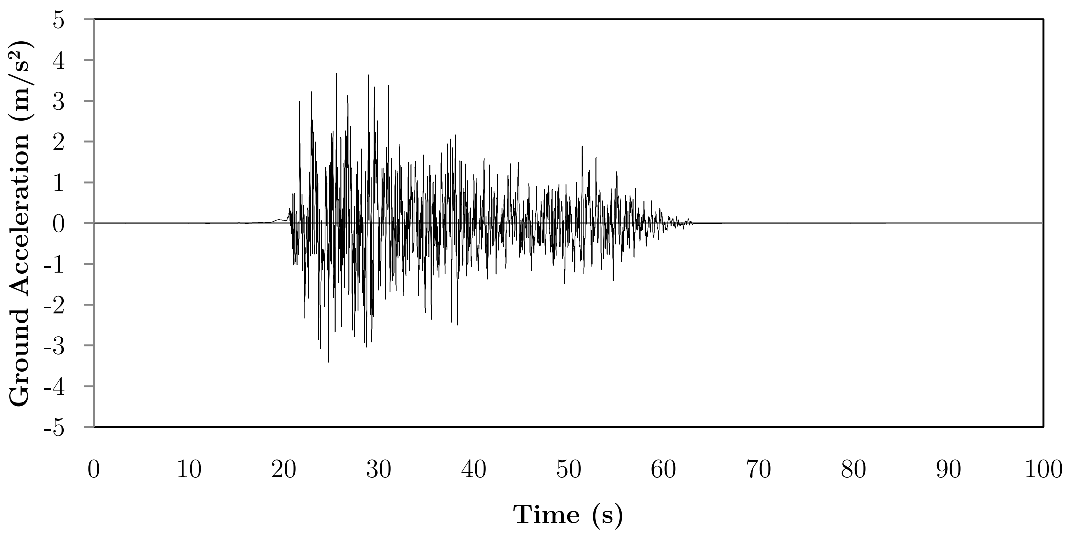

Figure B-36: W7c2_1 accelerogram

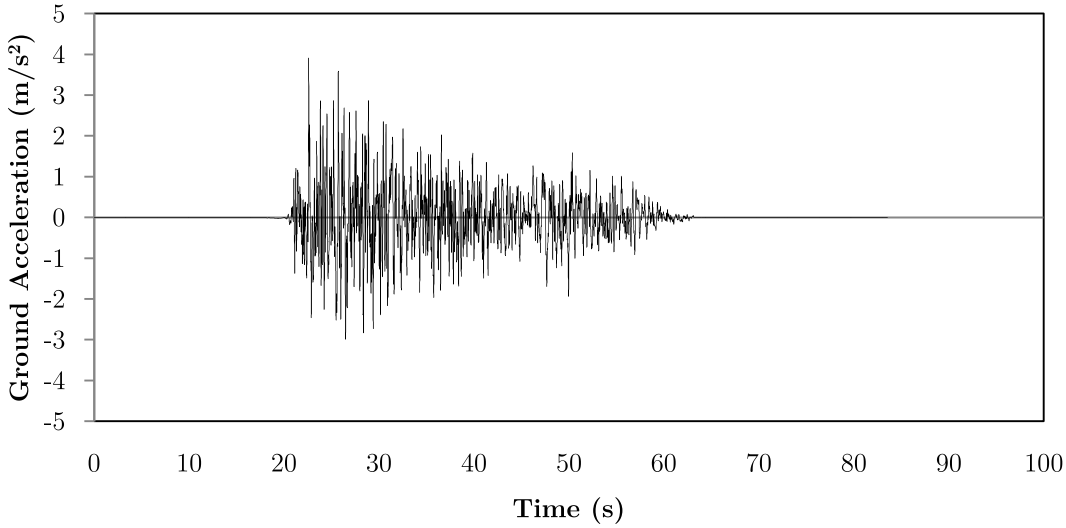

Figure B-37: W7c2_2 accelerogram

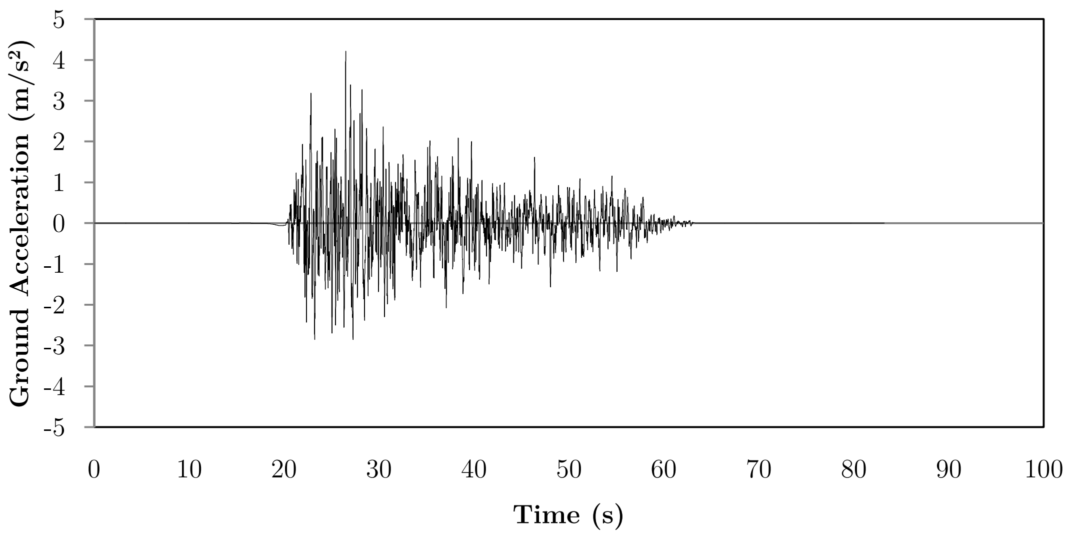

Figure B-38: W7c2_3 accelerogram

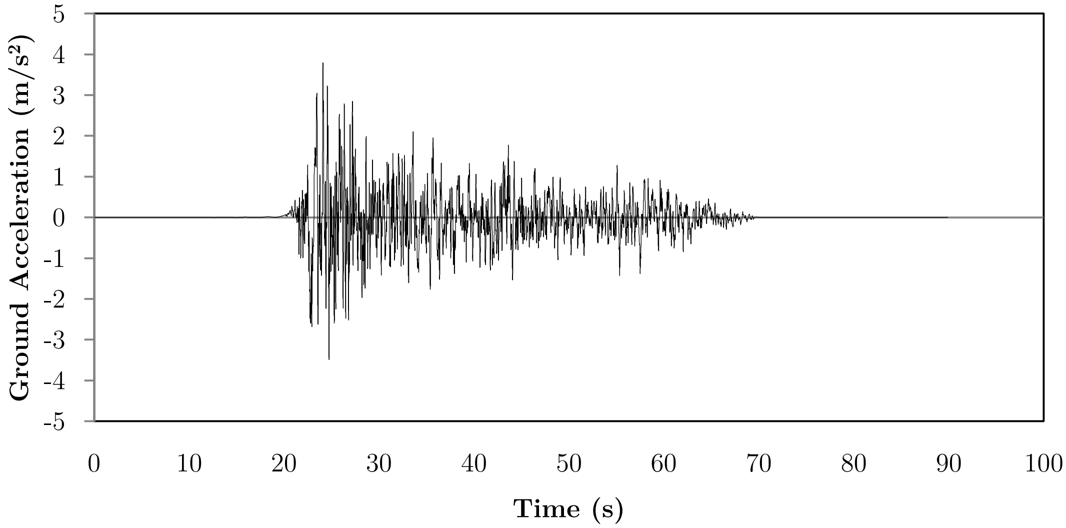

Figure B-39: W7c2_4 accelerogram

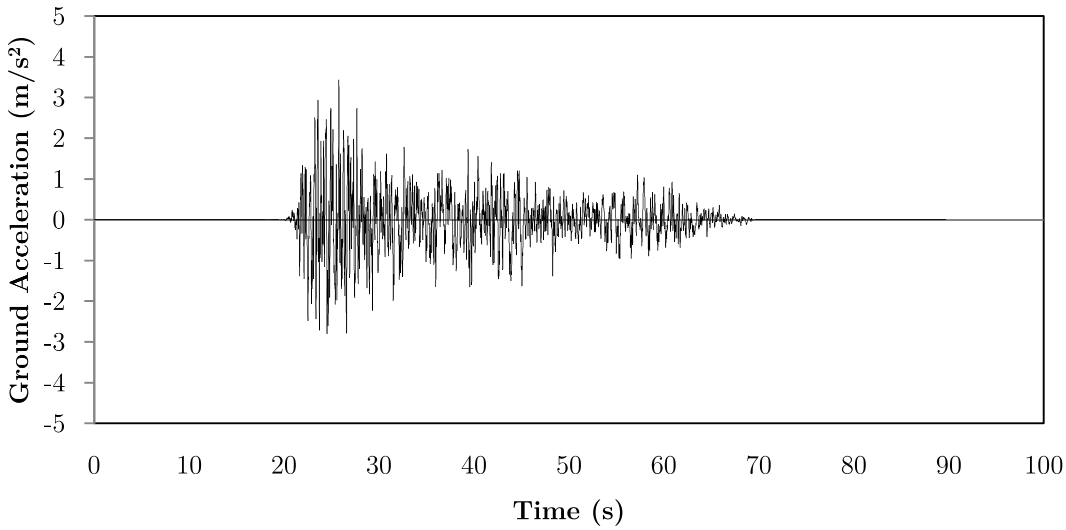

Figure B-40: W7c2_5 accelerogram

For low-rise URMs accelerogram data, refer to the data in Table B-3. As the low-code URML analyses were not completed, the relevant data are left out. In the interest of space and to reduce redundancy seeing as the accelerograms are issued from the same source, the matching accelerogram figures are not shown.

Table B-3: URML accelerogram data

	East			West		
	SA (g)		PGA (g)	SA (g)		PGA (g)
Openings	Large	Small		Large	Small	
x6c1_1	0.649	0.617	0.323	1.220	1.257	0.477
x6c1_2	0.599	0.562	0.460	0.975	0.921	0.454
x6c1_3	0.720	0.617	0.293	0.880	1.042	0.483
x6c1_4	0.666	0.796	0.351	0.963	1.013	0.526
x6c1_5	0.749	0.813	0.302	1.053	1.162	0.521
x6c2_1	0.630	0.554	0.268	1.349	1.254	0.416
x6c2_2	0.634	0.632	0.280	1.018	1.089	0.444
x6c2_3	0.646	0.659	0.289	1.045	0.970	0.436
x6c2_4	0.672	0.691	0.293	0.924	0.989	0.466
x6c2_5	0.584	0.605	0.313	1.058	0.996	0.410
x7c1_1	0.649	0.714	0.311	0.958	1.086	0.424
x7c1_2	0.516	0.528	0.335	0.975	0.979	0.404
x7c1_3	0.655	0.660	0.302	1.024	0.933	0.438
x7c1_4	0.649	0.669	0.295	0.990	0.939	0.441
x7c1_5	0.595	0.585	0.305	0.802	0.785	0.483
x7c2_1	0.615	0.691	0.284	0.913	1.052	0.462
x7c2_2	0.779	0.823	0.255	0.986	0.751	0.485
x7c2_3	0.694	0.659	0.292	1.258	1.135	0.404
x7c2_4	0.579	0.504	0.326	1.071	1.018	0.520
x7c2_5	0.748	0.784	0.333	1.202	1.156	0.417

Appendix C

Effect of openings on stiffness

This appendix covers the means to estimate stiffness of a masonry wall with any opening configuration. The method presented here is adapted from Drysdale and Hamid (2005) but could easily as well be derived from elastic beam theory, Timoshenko beam theory and classical structural analysis. It is usually used to distribute forces to individual piers for design purposes but also gives a good impression of the effects of having openings on the structural capacity of a wall.

Theoretical background

For the given cantilever wall in Figure C-1 with an applied horizontal load P at its top, one can determine the total deflection using the following:

$$\Delta_c = \frac{P\ \ ^3}{3EI} + \frac{1.2P}{GA} \tag{C-1}$$

On the other hand, a similar wall under fixed-fixed conditions will undergo the following deflection:

$$\Delta_{ff} = \frac{P\ \ ^3}{12EI} + \frac{1.2P}{GA} \tag{C-2}$$

In these two equations, is the height of the wall, E is the modulus of elasticity, I is the second moment of area (a function of its width w and thickness t, $wt^3/12$), G is the shear modulus, A is the plan area of the wall (the product of its width w and thickness t), 1.2 is the Timoshenko shear coefficient for rectangles and the coefficients 3 and 12 are issued from the shape of the moment diagrams due to their respective boundary conditions.

Simplifications can be made by replacing I and A by their equivalencies in terms of thickness and width as well as introducing the relation $G = 0.4E$ (refer to Chapter 2). It can also be reasonably assumed that the wall thickness and material capacity are constant. The applied load P can be reduced to unity and thus discarded from the relationships. These coefficients shall be grouped under the term α which transforms eqs. C-1 and C-2 to the simplified expressions below:

$$\Delta_c = \alpha \left(4 \left(\frac{}{w} \right)^3 + 3 \left(\frac{}{w} \right) \right) \tag{C-3}$$

$$\Delta_{ff} = \alpha \left(\left(\frac{}{w} \right)^3 + 3 \left(\frac{}{w} \right) \right) \tag{C-4}$$

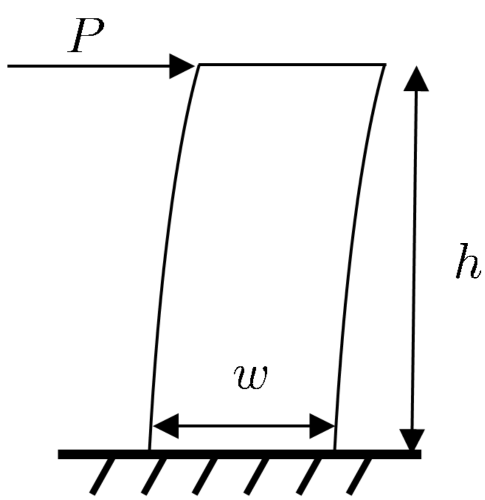

Figure C-1: Cantilever wall dimensions

Recall the definition of stiffness, k, as the slope of the deformation-force relationship of a body: $k = P/\Delta$ or simply $k = 1/\Delta$ by considering unity for the applied load. A common comparison for stiffness is usually made with spring constants where two cases may arise:

springs in parallel (see Figure C-2) or springs in series (see Figure C-3). In the case of parallel springs, compatibility equations demand that displacements in all springs be equal, therefore equivalent stiffness, k_{ep} is given by eq. C-5. On the other hand, springs in series will see their displacements added to each other's, resulting in equivalent stiffness k_{es} given by eq. C-6.

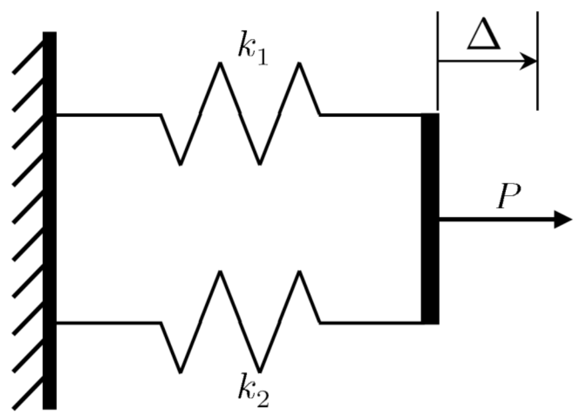

Figure C-2: Springs in parallel

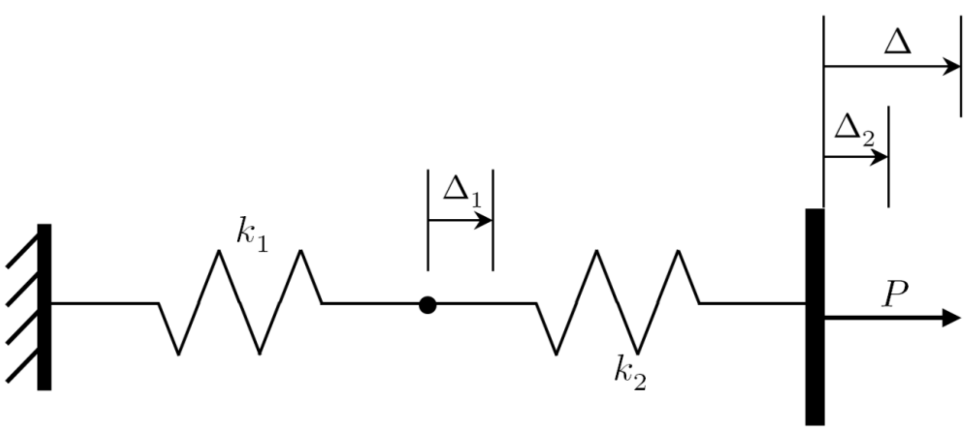

Figure C-3: Springs in series

$$k_{ep} = \frac{1}{\Delta} = \frac{1}{\Delta_1} + \frac{1}{\Delta_2} + \quad + \frac{1}{\Delta_n} = k_1 + k_2 + \quad + k_n \tag{C-5}$$

$$k_{es} = \frac{1}{\Delta} = \frac{1}{\Delta_1 + \Delta_2 + \quad + \Delta_n} = \frac{1}{\frac{1}{k_1} + \frac{1}{k_2} + \quad + \frac{1}{k_n}} \tag{C-6}$$

Openings and effective stiffness

Effective stiffness, K_e, is a measure of the impact of openings on a wall. Consider the two walls in Figure C-4, both identical in dimensions and with a single opening of the same size but placed in different locations. One can appreciate that the stiffness of the large solid portion of the wall from the side opening should yield more stiffness than the combined two solid portions from the central opening.

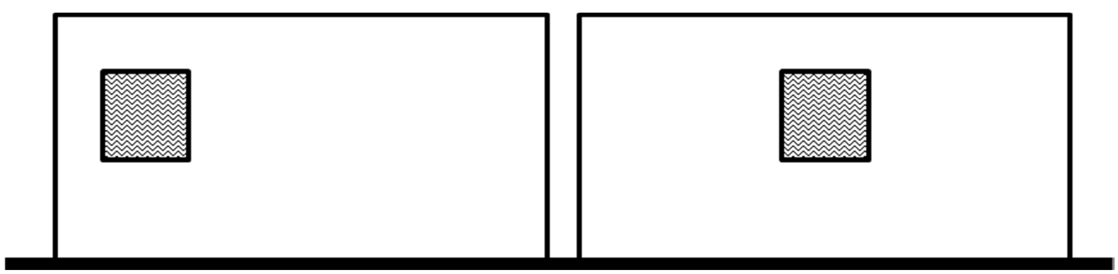

Figure C-4: Effects of opening location on identical walls, side opening (left) and central opening (right)

The effective stiffness looks to provide information on these type of situations by indicating the ratio of the actual stiffness, K_a, to the stiffness which would result from the same wall but without any openings whatsoever, the solid stiffness K_s.

$$K_e = \frac{K_a}{K_s} \tag{C-7}$$

It is possible to plot the effect of an opening's location on the effective stiffness; this is done for an arbitrary wall in Figure C-5. The normalized distance represents how far from the edge the opening is located. For instance, the central opening is at 0.5 normalized distance yielding approximately 0.55 effective stiffness. On the other hand, the side opening would be closer to 0.1 normalized distance for an effective stiffness of approximately 0.75.

When one combines eqs. C-3 and C-4 with eq. C-7, it becomes clear that the term α will vanish and that only the actual width and height of piers must be taken under consideration. This will be called relative stiffness as it is unitless and be expressed as shown next for cantilever relative stiffness k_c and fixed-fixed relative stiffness k_{ff}.

$$k_c = \frac{1}{\left(4\left(\frac{}{w}\right)^3 + 3\left(\frac{}{w}\right)\right)} \tag{C-8}$$

$$k_{ff} = \frac{1}{\left(\left(\frac{}{w}\right)^3 + 3\left(\frac{}{w}\right)\right)} \tag{C-9}$$

This tool is effective regardless of building size: even though a longer/larger wall will undoubtedly have a higher horizontal capacity, it will also carry more load as it is part of a larger structure and therefore attract more seismic forces. Thus, two walls with the same effective stiffness but with different dimensions will likely behave similarly – notwithstanding walls with different failure modes. In any case, Drysdale and Hamid (2005) specify clearly that this is an approximation and that when a user wants a clear portrait of the situation, elastic finite element analysis or similar methods should be conducted to assess the stiffness of the structure, especially in the case of URM.

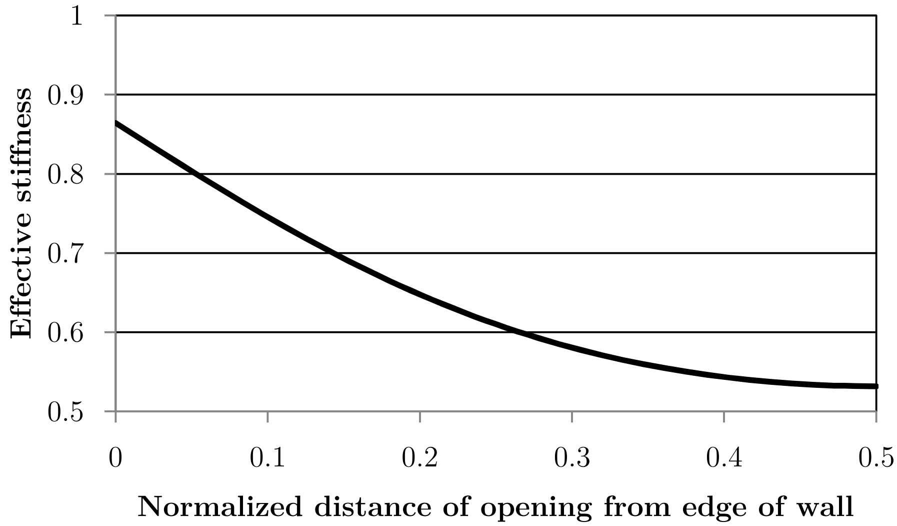

Figure C-5: Effective stiffness as a function of single opening placement

The last remaining issue consists in calculating the stiffness of a wall with openings. As was defined in eqs. C-3 through C-6, piers may be under cantilevered, fixed-fixed boundary conditions as well as in parallel or series arrangement when several of them are present. In practice, a wall will be a combination of piers having some of these different characteristics as shown in Figure C-6.

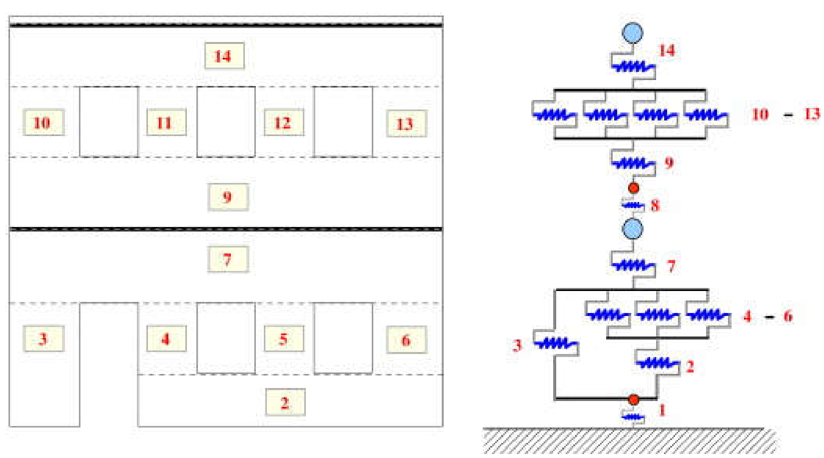

Figure C-6: Springs representation of URM building (from Park et al., 2008)

The more accurate approach in estimating relative stiffness consists in considering a solid pier, removing a solid strip containing the openings and then adding the stiffness of the piers surrounding the openings. The process may require to be repeated when there are multiple openings, starting from the top for each opening that is encountered. Finally, one must consider whether a given pier is more likely to behave under cantilever or fixed-foxed condition. In general, the decision is based on whether a pier connects to something on top of it (fixed-fixed) or not (cantilever). An exception may be considered when a stiff pier connects to an element that is comparatively weak in which case the stiff element will more closely behave like a cantilever. The process can be summarized as follows:

1- Calculate stiffness of the overall solid wall, without openings
2- Calculate the stiffness a strip containing an opening, starting from the top, it will be removed from the total stiffness
3- Repeat steps 1 and 2 starting at the top of the strip that was removed until all openings have been accounted for
4- Once the stiffnesses are known, calculate K as per eq. C-7 while considering pier arrangement as per eqs. C-5 and C-6.

Worked example

Consider the wall in Figure C-7, where dimensions are shown in meters. We will apply the method explained in the previous paragraph to estimate K.

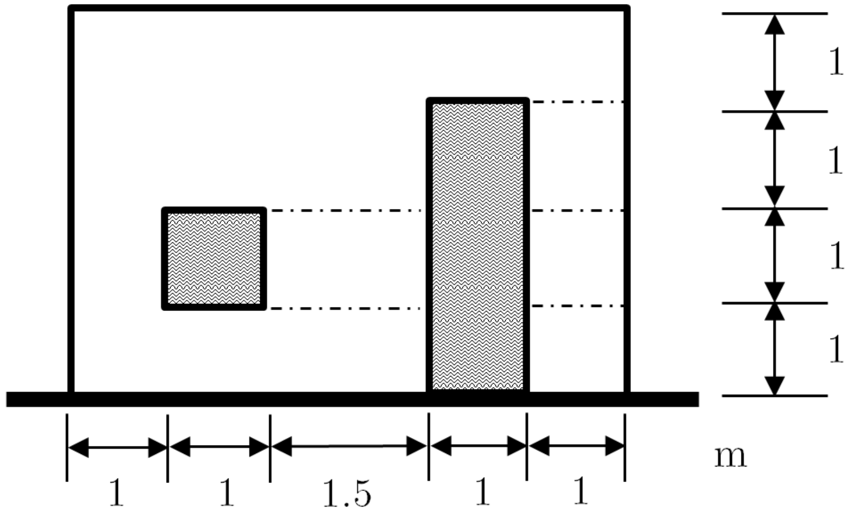

Figure C-7: Wall with openings for evaluation of effective stiffness

First, calculate K_s, that is a solid wall without any openings. This is shown in Figure C-8. Wall sections will be identified within figures when referring to Table C-1 for dimensions, equations and stiffnesses.

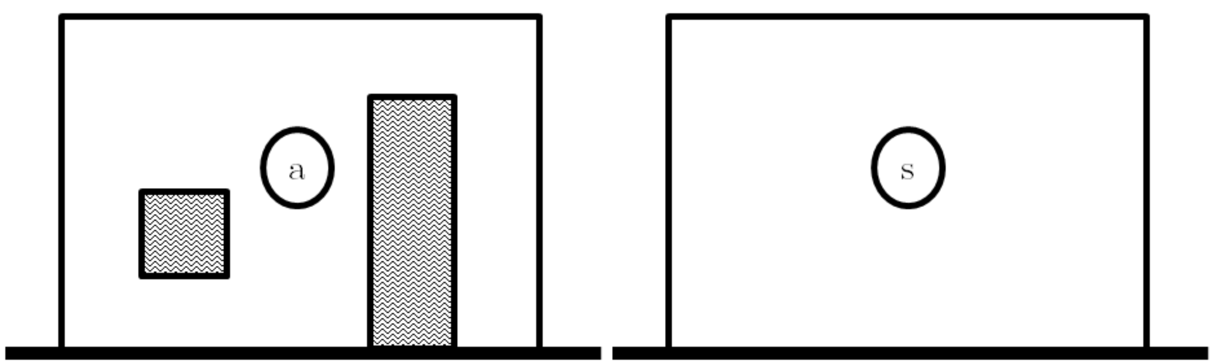

Figure C-8: Solid wall representation

Moving on to step 2, the first strip contains the door opening as shown below in Figure C-9. The strip o1 is considered cantilever as it does not connect to anything above it, it is simply removed from the overall stiffness.

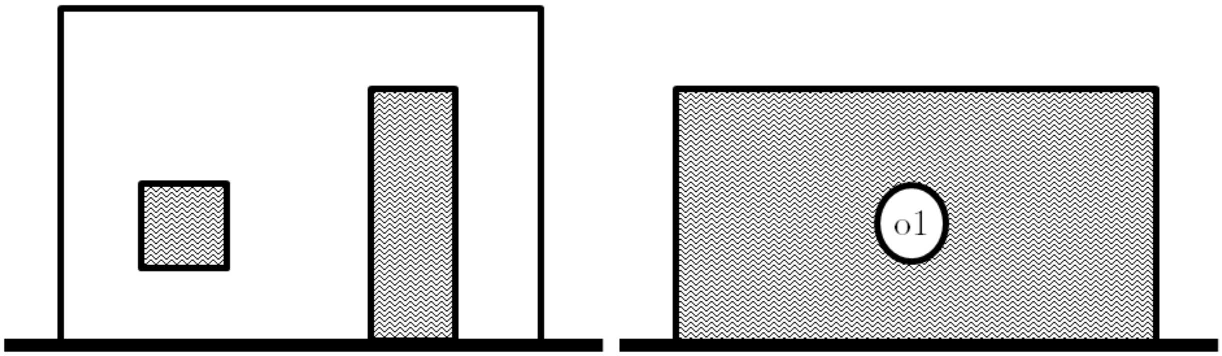

Figure C-9: Opening strip o1

Since there are still openings that have not been accounted for, we repeat step 1. This results in a fixed-fixed pier 1 and cantilever partial pier p1 as shown in Figure C-10. The reasoning behind these boundary conditions is that pier 1 is relatively weak and will connect to the top portion of the wall, being relatively stiff. On the other hand, pier p1 is quite sturdy and connects to a relatively weak portion of the wall above it, thus behaving more like a cantilever. A comparison will be made where all piers were considered as fixed-fixed.

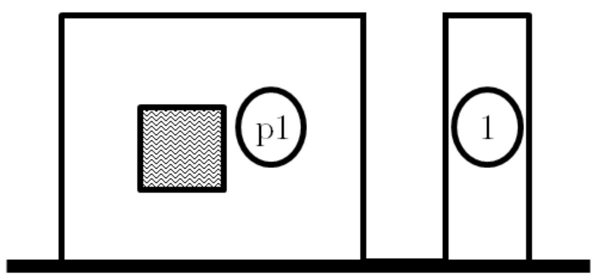

Figure C-10: Partial wall p1 and pier 1

Pier p1's stiffness cannot be directly obtained and steps 1 and 2 must be applied again. A strip can take into account the second opening while still leaving the bottom part of pier p1 within the solid partial wall p1s, removing the necessity of calculating that portion. The process is shown in Figure C-11, below.

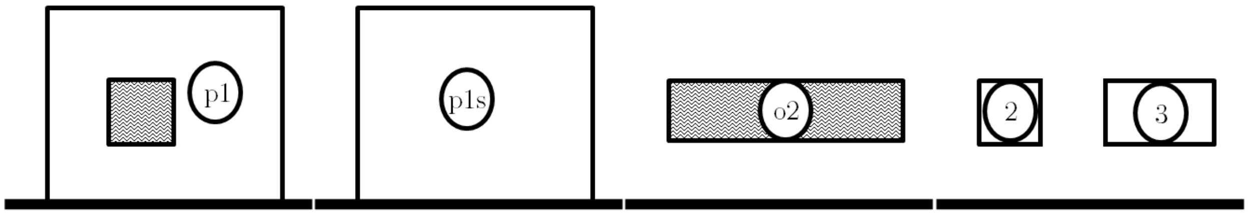

Figure C-11: Remaining pier contributions to be considered

Step 4 consists in correctly combining the calculated stiffnesses. The actual stiffness consists of the solid wall (Figure C-8) from which opening o1 is removed (Figure C-9) while the partial wall p1 and pier 1 are added once correctly combined (Figure C-10) through eq. F-6 as they are in series. It is clear that piers 1 and p1 (p1 & 1) will act in parallel with equal displacements so that they must be considered in parallel as per eq. F-5 and Figure C-2. But in order to do this, the stiffness of p1 must be known.

As a result, the same process is applied on partial wall p1: it consists of solid wall p1s, minus fixed-fixed opening strip o2 to which p2 and p3 (2 & 3) are added once combined with eq. F-6 (refer to Figure C-11). Here again p2 and p3 act in parallel as per eq. F-5 and Figure C-2. The overall process is resumed in Table C-2 and some sample calculations follow. In this case, the effective stiffness of the wall is found to be approximately 0.59; since this is a unitless value, it may be expressed as 59% for clarity. If one were to decide that pier p1 is rather fixed-fixed than cantilever, the resulting effective stiffness would be 77%, which is quite far off the previous result. In the case of uncertainty, it is best practice to refer to an adequate mathematical model to correctly evaluate the wall's effective rigidity.

Table C-1: Piers data for worked example

Pier	Height (m)	Width w (m)	$/w$	Equation	Relative Stiffness (%)
s	4	5.5	0.727	C-8	26.9
o1	3	5.5	0.545	C-8	43.8
1	3	1	3	C-9	2.8
p1s	3	3.5	0.857	C-8	19.6
o2	1	3.5	0.286	C-9	113.6
2	1	1	1	C-9	25.0
3	1	1.5	0.667	C-9	43.5

Table C-2: Combined wall sections for worked example

Piers	Contributing piers (positive)	Openings (negative)	Equation	Relative Stiffness
a	s, p1 & 1	o1	C-6	15.9
p1 & 1	p1, 1	N/A	C-5	20.6
p1	p1s, 2 & 3	o2	C-6	17.9
2 & 3	2, 3	N/A	C-5	68.5

<u>Sample calculations</u>

Piers 2 & 3

$$K_{2\&3} = K_2 + K_3 = 0.250 + 0.435 = 0.685 = 68.5\%$$

Pier 1

$$K_{p1} = \frac{1}{1/K_{1s} + 1/K_{2\&3} \quad 1/K_{o2}} = \frac{1}{1/0.196 + 1/0.685 \quad 1/1.052} = 0.179 = 17.9\%$$

Effective stiffness

$$K_e = \frac{K_a}{K_s} = \frac{0.159}{0.269} = 0.592 = 59.2\%$$